Appendix 5-C

Subsidence Control and Monitoring

Table of Contents

Sections

Subsidence Page 5C-3

Monitoring Page 5C-7

Mitigation of Potential Impacts Page 5C-8

Notification Page 5C-10

Lease U-024316 Page 5C-13

Leases U-38727, U-60148, U-61049, and U-020668 Page 5C-16

Figures

Figure 5C-1 Subsidence Chart Page 5C-5

Figure 5C-2 Subsidence Factor Versus Mining Depth Page 5C-2

Table

Table 5C-1 Estimated Maximum Subsidence Page 5C-6

Attachments

Attachment 1 Analysis of Retreat Mining Pillar Stability

Attachment 2 Modeling of Castlegate Sandstone Escarpment Stability

Attachment 3 Prediction of Surface Deformation Resulting From Longwall Mining Over the Bear Canyon Reserve.

SUBSIDENCE CONTROL AND MONITORING PLAN

SUBSIDENCE

Subsidence can normally be expected to occur over areas where second mining has taken place ~~(pillaring)~~. See R645-301-523 for mining operation. Based on the geologic interruptions within a mine, subsidence becomes very difficult to predict, due to the variable nature of the mining panels. However, Figure 5C-1 will give an estimate of the maximum subsidence from room and pillar mining that may be expected in mine studied in the Western U.S. Maximum subsidence for an average room and pillar panel in the Bear Canyon Mine has been estimated from Figure 5C-1, using the criteria shown in Table 5C-1. For longwall panels, due to their ability to uniformly remove the coal, subsidence predictions are more accurate and there is less surface impacts. An analysis of subsidence effects from longwall mining specific to the Bear Canyon Mine reserves in the Tank seam and Hiawatha seam is included as attachment 3. Attachment 3 mentions additional reserves, these reserves are located in the Blind Canyon. The cumulative affects of subsidence, based on attachment 3 for the Tank and Hiawatha seams, and attachment 1 for the Blind Canyon seam, is shown on Plate 5-3. Subsidence has been estimated based on the number of seams mined in the area and assuming the worst case scenario for mine layout and barrier pillar sizing.

For all subsidence calculations, and in determining the affected area an agle of draw of 22.5° was used. Past experience in this area shows no indication that subsidence would be this drastic, historically mines in the area have experienced an angle of draw of

approximately 15°. Additionally no actual subsidence has been noted from areas pillared as much as 40 years ago, and the subsidence monitoring network initiated in 1987, has shown only minor (0.47 ft max 1992) variations in elevation. Based on this, little, if any, detectable subsidence is expected to become apparent when mining under these depths. Some minor fracturing and an escarpment rock fall have been noted in the adjacent Trail Canyon Mine area, and although these are assumed to be mine-related, they occurred in areas of relatively low cover and unknown outcrop protection. Only minor fracturing has been noted in relation to the Bear Canyon Mine (see Plate 5-3). Based on this and on the environmental friendly design and mining methods being used few surface fractures and escarpment failures are anticipated. The main affect will be a uniform lowering in elevation.

Figure 5C-1 Subsidence Chart

Table 5C-1 Estimated Maximum Subsidence

Coal Seam	Fee and Fed Lease U-024318	Federal Lease U-024316 and U-46484	Federal Lease U-020668 and U-38727	Fee and Federal Lease U-61049	Federal Lease U-61048
BLIND CANYON SEAM Panel Width Average Depth Width/Depth Ratio Seam Thickness Maximum Calculated Subsidence	600 ft. 800 ft. 0.75 9 ft. 5.4 ft.	Mining Questionable	650 ft. 1200 ft 0.54 9 ft. 3.2 ft.	Not Minable	Not Minable
HIAWATHA SEAM Panel Width Average Depth Width/Depth Ratio Seam Thickness Maximum Calculated Subsidence	600 ft. 860 ft. 0.75 5 ft. 3.2 ft.	Mining Questionable	Not Minable	650 ft. 1600 ft. 0.40 14 ft. 5 ft.	650 ft. 1600 ft. 0.40 14 ft. 5 ft.
TANK SEAM Panel Width Average Depth Width/Depth Ratio Seam Thickness Maximum Calculated Subsidence	650 ft. 560 ft. 1.16 8 ft. 5.5 ft.	650 ft. 1,400 ft. 0.46 7 ft. 4.5~~1.9~~ ft.	680 ~~650~~ ft. 3,300 ~~950~~ ft. 0.21 ~~0.68~~ 7.5 ft ~~4.5~~4.1 ft.	760 ft. 4,600 ft. 0.17 7.5ft. 4.5 ft.	Not Minable
Total Calculated Subsidence	**14.1 ft.**	**4.5~~1.9~~ ft.**	**7.7 ~~7.3~~ ft.**	**10 ft.**	**5 ft**

MONITORING

Since subsidence may occur over any underground extraction, a monitoring network was installed in the summer of 1987, and has been monitored since that time. Monitoring stations are steel rebar with aluminum caps, set in concrete so weather, frost heave or wildstock/wildlife will not disturb them. Location of monitoring stations are shown on Plate 5-3.

Ten permanent subsidence monitoring points (SMS-1 thru SMS-5, Con 6, and SMS-7 thru SMS-10) are located on the mine site area. Before expansion into the Federal Lease area U-023416 the subsidence monitoring plan consisted of 3 monitoring points (SMS-1, SMS-2, and SMS-3) in the Bear Canyon Permit Area, a fourth point SMS-4 in the Trail Canyon Permit Area, and a Control Point CON-5, located outside the mining area. SMS-1, SMS-3, and SMS-4 are common to both the Trail Canyon and Bear Canyon Permits. CON-6 and SMS-7 thru SMS-10 were proposed in 1990 and established 22 September 1991. CON-5 became an additional subsidence monitoring point (redesignated SMS-5). The location of all existing and proposed points are shown on Plate 5-3.

15 additional monitoring points were installed on Federal Lease U-024316. These are shown on Plate 5-3 as points 11 through 24. 26 ~~additional~~ points ~~will be~~ were added to Wild Horse Ridge (Nos. 25 through 50) to monitor subsidence on Federal Lease U-020668 and U-38727. 7 points were added in and around Lease U-61049 (Numbers 51-57). Above the first long-wall panel 11 points were established at a spacing of 50 ft

going across the width of the panel (points 25A-K) in order to determine if subsidence is following the predicted pattern. Potential points were also selected above the 2nd and 3rd longwall panels and will continue to be selected above each of the panels one year prior to mining at a spacing of 250 ft as recommended in Attachment 3. The actual spacing and location of these points may change based on the results from points 24A-K, and on the yearly analysis that will be performed. If subsidence occurs as anticipated the spacing of 250 ft will continue. If it does not additional points will be added to determine the behavior, and our subsidence model will be updated. At a minimum 1 point will be placed in each panel as near as possible to the latitudinal and longitudinal centers.

Stations shall be monitored, and evaluated yearly for changes in elevation. This evaluation will include the current year and the previous two years at a minimum. In addition, a field investigation shall be made yearly of the mining area (including escarpment areas), and any obvious subsidence or mine related surface effects will be noted and located on a map. A copy of the results of the subsidence analysis, survey and map will be available for inspection at the office, and a summary of the ~~survey~~ results will be sent to the Division with the Annual Report.

MITIGATION/PROTECTION OF POTENTIAL IMPACTS

~~.11.20025Potential impacts and mitigation efforts are discussed in R645-301-5~~

Mr. Larry Dalton, Resource Analyst Utah Division of Wildlife Resources and the State's foremost authority on potential impacts of subsidence on wildlife, inspected the site in June 1984. The results of that investigation, as well as others, in part are as follows:

Considering the absence of spring, water sources, the negative potential impacts of subsidence within the Bear Canyon Permit Area could easily be offset by potential positive aspects.

On the negative side: Loss of riparian area and/or water sources and state appropriated water rights is of greatest concern, followed by loss of vegetation from methane gas leaking to the surface from an underground works. Considering the lack of riparian area or water sources above the coal seam, this concern is not warranted for most areas. There are two area of concern above Fish Creek in section 19 as shown on Plate 7-4. These areas will be monitored for loss of water as it is being undermined. ~~Secondly~~, In regards to methane gas Co-Op has never encountered methane gas underground so there is little concern relative to potential vegetation loss. , ~~and last,~~ The last concern is the loss of nests due to escarpment failure.

On the positive side: The tension fractures resulting from subsidence along the steep side hills are frequently utilized by big game as movement corridors. The fractures and rubble provide escape cover for a variety of wildlife species as well as additional habitat for burrowing and denning animals. While there is concern over the potential loss of nests as a result of escarpment failure, there is also a potential for additional nesting sites to be created through this gravitational shearing of escarpment surfaces.

PROTECTION

In order to protect water resources and state appropriated water rights from impacts C. W. Mining has designed their mine layout so that areas where these resources

exist with less then 900 feet of overburden between the resource and the coal, the resource will be outside of the affected area. Based on the mining handbook and past history, 900 feet of overburden is sufficient to prevent adverse affects to the resource. Additionally in the areas where perennial streams exist above the affected area (as shown on Plate 7-4) C. W. Mining will increase the monitoring of these areas to a weekly bases one month prior to mining in the area. This weekly monitoring will continue until one month after mining has left the area. Monitoring will then be reduced to once a month for an additional 6 months at which time it will resume its normal schedule. This increased monitoring will include the sites FC-2, FC-3, FC-4, FC-5, and SCC-2 for the right fork of Fish Creek, and FC-1, FC-6, SBC-18, SBC-20, and SBC-21 for the left fork of Fish Creek.

In escarpment failure areas containing raptor nests C. W. Mining will try to time their mining so that it does not occur during the nesting season. If we are unable to do this a physical obstruction such as fencing will be placed over the nesting site to prevent it's use. This would ensure that if a nest was lost no raptors would be lost with it. As of 2005 there were currently 6 raptor nest located inside the affected area. These area discussed in greater detail in Appendix 3L. Anticipated escarpment failure is discussed in greater detail under the applicable lease.

MITIGATION~~NOTIFICATION~~

Notification

During operation, all owners of property within the area that could be impacted by subsidence shall be notified by mail six months prior to mining beneath their property and be informed of:

a. Specific areas mining will take place

b. Dates of underground operations that could cause subsidence in the area.

c. Measures to be taken to prevent and or control adverse surface effects.

Co-Op further commits to the following course of action should subsidence cause any material damage or a reduction in value of structure or land.

a. Restore, rehabilitate, or remove and replace, to the extent technologically and economically feasible, each materially damaged structure, feature or value promptly after the material damage from subsidence is suffered, to the condition it would be in if no subsidence had occurred and restore, to the extent technologically and economically feasible, those surface lands that were reduced in reasonable foreseeable use as a result of such subsidence to a condition capable of supporting before subsidence; or

b. Purchase the damaged structure or feature (except structures or features owned by the person who conducted the underground coal mining activities) for its pre-subsidence fair market value. The person conducting the underground coal mining operation

performed to determine the cause of the failure, and any necessary remedies or protection required. The DOGM and the U.S. Forest Service, Price District Ranger would be notified of such an occurrence. An escarpment stability study is included as attachment 2.

shall promptly, after the material damage or reduction in value or reasonable foreseeable use from subsidence occur, to the extent technologically and economically feasible, restore the purchased structure or the structure owned by the person conduction the underground mining operations, restore those surface lands that were materially damaged or reduced in value or reasonable foreseeable use by such subsidence, to a condition capable and appropriate of supporting the structure, and any other foreseeable uses such surface lands were capable of supporting before mining. Nothing in the paragraph shall be deemed to grant or authorize an exercise of the power of condemnation of the right of eminent domain by any person engaged in underground coal mining activities; or

c. Compensate the owner of any surface structure in the full amount of the diminution in value resulting from subsidence, by purchase prior to mining of a noncancellable premium prepaid insurance policy or other means approved by the Division as assuring before mining begins that payments will occur; identify every person owning an interest in the surface for all damages suffered as a result of the subsidence; and , to the extent technologically and economically feasible, fully restore the land to a condition capable of maintaining reasonably foreseeable uses which it could support before subsidence.

d. The area will be monitored on an annual basis, and field investigation will also be performed at that time. If escarpment failure is observed in areas where no escarpment failure is anticipated, ~~mining will be immediately stopped in the~~An immediate evaluation of the ~~e~~affected area, ~~until a proper evaluation can~~will be

U-024316

Mining is projected within the vicinity of Bear Creek in Federal Lease U-024316. An additional concern over escarpment failure has been raised by the U.S. Forest Service; therefore, the following discussion will address the potential for such failure.

The steep area of Bear Canyon in the S.W. corner of Section 13 is approx 1200 feet above the coal seam (See Plate 6-10). To prevent subsidence to Bear Creek and the adjacent ledges, no retreat mining was conducted East of the in-mine fault paralleling the section line between sections 13 and 14, T.16S., R.7.E. See Plate 3-4C.

This Protection Zone was determined by examining the angles of draw. Figure 5C-2 shows angle of draws plotted against depths for various mines within the general area of the Bear Canyon Mine. Based on this information, an average angle of draw of 22.5° was used.

Plate 5-3 shows the areas which will potentially be affected by subsidence. None of the area within Federal Lease U-024316 is included in this potential area..

Within the lease, pillars were developed on 80' centers minimum. This pillar size was evaluated using the "Analysis of Retreat Mining Pillar Stability (ARMPS)" software, developed by the National Institute for Occupational Health and Safety. A pillar stability factor of 1.54 was determined, which shows the pillar size to be adequate to prevent subsidence of the ledges and Bear Creek. NIOSH research has found that in 94% of all

case studies stability factors greater than 1.5 have provided long-term stability (Mark, 1997), showing that pillars with safety factors above 1.5 are adequate to hold the weight of the overburden, thus preventing subsidence. Monitoring of the ledges for subsidence subsequent to the development on this lease has confirmed that no subsidence has occurred, and no escarpment failures have been observed.

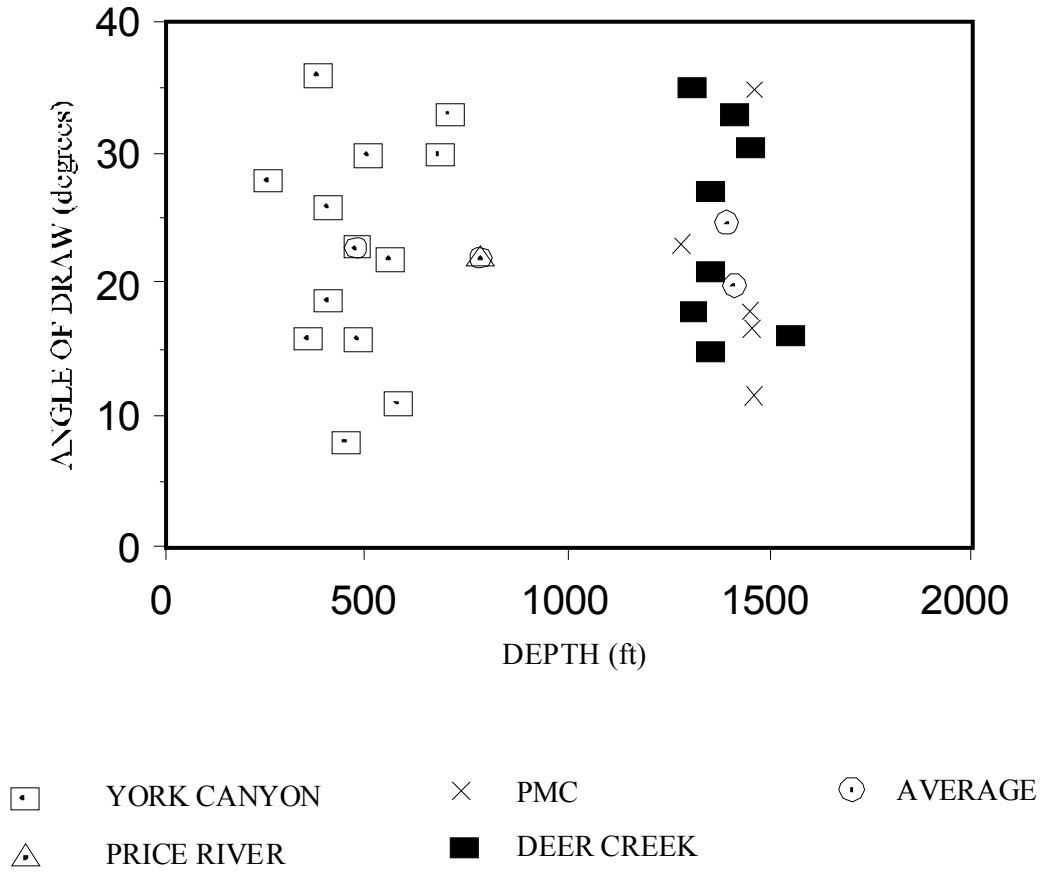

Outcrop protection has been increased to a minimum of 200 feet in the plan (see R645-301-525-300). This is consistent with other mines in the Wasatch Plateau, and with the exception of some longwall operations, has been shown to be effective at preventing escarpment failure near outcrops.

Figure 5C-2

Subsidence Factor Versus Mining Depth

U-38727, U-61048, U-61049, and U-020668

As with Federal Lease U-024316, lease stipulation 13~~12~~ requires mining to be conducted in a manner to prevent hazardous conditions such as potential escarpment failure.

The uppermost escarpment in the Wild Horse Ridge area is the Castlegate sandstone, located approximately 800 ft. above the Tank Seam, and 950 ft. Above the Blind Canyon Seam.

To prevent subsidence to these escarpments in areas where it has been determined escarpment failure would be a hazardous condition, a barrier zone will be left in which no retreat mining will take place. The width of this barrier was determined using an angle of draw of 22.5° (See Figure 5C-2 and attachment 2).

~~or the Tank Seam a minimum barrier of 300' will be maintained in which no retreat mining will take place. For the Blind Canyon Seam, a minimum barrier of 370 feet will be maintained.F~~ Plate 5-3 shows the cumulative anticipated ~~zone which will be affected by~~ subsidence contours, and the Castlegate Sandstone, located ~~outside of this area.~~within the permit area. ~~This zone is also~~Individual seam subsidence contours are shown on Plates 5-1A, 5-1B, and 5-1C to show the relationship between the development and retreat panels. W~~. Therefore, this pillar size will be adequate to prevent subsidence and escarpment failure. Mining on Federal Lease U-024316 has also confirmed that this size is adequate in the Bear Canyon Mine area. for room and pillar retreat mininghere~~

~~panels are shown encroaching on the barrier zone, pillars will be developed and left in place to prevent subsidence. The pillars will be developed on 80' centers minimum. Using the ARMPS software (NIOSH), a minimum pillar stability factor of 1.58 was determined~~

There area two areas within these leases and a third area just outside of the leases where it has been determined that escarpment failure does not present a hazardous condition. The locations of the areas are in the left fork of Fish Creek where it runs through lease U-020668, and U-38782, as well as an area at the top of the left fork of Fish Creek just outside of two portions of lease U-61049, and in the left fork of Bear Creek where it runs through lease U-61049. These areas as well as additional areas of been studied and modeled for rock falls. This study is included as Attachment 2. A summary and discussion of these result are included below. The cross-sections modeled for rock falls are shown on Plate 5-3.

Summary of Rock Fall Anaylsis

Section	Distance to Stream Bed	Maximum Rockfall Distance
A-A'	2,050 ft.	800 ft.
B-B'	1,674 ft.	1,200 ft.
C-C'	2,600 ft.	950 ft.
D-D'	1,980 ft.	650 ft.
E-E'	450 ft.	450 ft. (rock hits bottom of canyon)

Section A-A'

This are is located above the old Bear Canyon #1 and #2 mines. It was used to calibrate the model

Section B-B'

This section is located on the point of Wild Horse Ridge. It was initially selected because it represented the steepest slope within the affected area. However as mining proceeded towards this area it was discovered that there was active burning so mining stopped and never reached this area. This area will however be impacted by natural subsidence resulting from the natural burning of the coal.

Section C-C'

This section is located on Wild Horse Ridge against the left fork of Fish Creek near the south-east end of U-38727. It was selected because secondary mining will take place under this area and also go out past the escarpments. The escarpments in this area range form 0-80 feet. The cross-section was placed where escarpments were the largest and the slope was the steepest. Escarpment failure will occur in this section, however based on models, the failure will not reach the stream channel so no water impacts will occur. There will however be loss of vegetation in the path of the rock fall. This will have minimal aesthetic impacts since there is little vegetation along the slope and also because escarpment failure happens naturally along Fish Creek so any areas would still match the appearance of surrounding areas.

Section D-D'

This section is located on Wild Horse Ridge against the left fork of Fish Creek near the north-east end of U-38727. This section represents the transition area where subsidence contours are beginning to move from under the escarpments to adjacent to the

escarpments, and then away from the escarpments. The escarpments in this area range from 80-160 feet. Any escarpment failure in this area will not reach the stream channel so impacts are the same as section C-C'.

Section E-E'

This area is at the upper portion of the right fork of Fish Creek between the two segments of Lease U-61049. Fish Creek is a box canyon and the escarpments in the area that will be impacted are the stream bed. The escarpments range from 160-240 feet. Since the escarpments are the stream bed any escarpment failure would have an impact on water resources. However the impacts would be quickly dissipated since flow are minimal in this area (10-30 gpm). Little vegetation impact is expected because of the short slope distance and the fact that water has eroded most of the soil in the area leaving exposed rock ledges.

References

Mark, C., and F.E. Chase
Analysis of Retreat Mining Pillar Stability (ARMPS). Paper in Proceedings on New Technology for Ground Control In Retreat Mining, 1997, NIOSH pub. 97-133, pp. 17-34.

ANALYSIS OF RETREAT MINING PILLAR STABILITY (ARMPS)

By Christopher Mark, Ph.D.,[1] and Frank E. Chase[2]

ABSTRACT

The prevention of pillar squeezes, massive pillar collapses, and bumps is critical to safe pillar recovery operations. To help prevent these underground safety problems, the Pittsburgh Research Center has developed the Analysis of Retreat Mining Pillar Stability (ARMPS) computer program. ARMPS calculates stability factors (SF) based on estimates of the loads applied to, and the load-bearing capacities of, pillars during retreat mining. The program can model the significant features of most retreat mining layouts, including angled crosscuts, varied spacings between entries, barrier pillars between the active section and old (side) gobs, and slab cuts in the barriers on retreat. It also features a pillar strength formula that considers the greater strength of rectangular pillars. The program may be used to evaluate bleeder designs, as well as active workings.

A data base of 140 pillar retreat case histories has been collected across the United States to verify the program. It was found that satisfactory conditions were very rare when the ARMPS SF was less than 0.75. Conversely, very few unsatisfactory designs were found where the ARMPS SF was greater than 1.5. Preliminary analyses also indicate that pillar failures are more likely beneath sandstone roof and that the ARMPS SF may be less meaningful when the depth of cover exceeds 230 m (750 ft).

[1]Mining engineer
[2]Geologist
Pittsburgh Research Center, National Institute for Occupational Safety and Health, Pittsburgh, PA.

INTRODUCTION

The use of remote-control continuous miners, extended cuts, and mobile roof supports has increased the productivity of room-and-pillar retreat mining (also referred to as "pillaring," "pillar recovery," "robbing," and "second mining"). In the southern Appalachian coalfields, many mines are choosing room-and-pillar retreat mining because of its lower capital cost and greater flexibility [Blaiklock 1992]. Unfortunately, between 1989 and 1996, 25% of all roof and rib fatalities occurred on pillar recovery sections.

Roof fall accidents are not the only problem associated with retreat mining. Millions of tons of coal are sterilized annually because of pillar squeezes, floor heave, pillar line roof falls, and pillar bumps. Traditional pillar design methods are of little help due to the complex mining geometries and abutment pressures that are present during pillar extraction. The Pittsburgh Research Center has developed the Analysis of Retreat Mining Pillar Stability (ARMPS) computer program to aid in the design of pillar recovery operations. This paper describes the program and presents the findings thus far.

THE ARMPS METHOD

The goal of ARMPS is to help ensure that the pillars developed for future extraction (production pillars) are of adequate size for all anticipated loading conditions. The key is to be able to estimate the magnitudes of the various loads that the pillars might experience throughout the mining process. The formulas used in ARMPS are based on those originally developed for the Analysis of Longwall Pillar Stability (ALPS) method, which is widely used for longwall pillar design [Mark 1992]. ALPS was initially derived from underground measurements of longwall abutment stresses and was later validated by the back-analysis of more than 100 case histories. In ARMPS, the formulas have been extensively modified for the variety of mining geometries typically found in pillar recovery operations.

USER INPUT

The first step in using the ARMPS program is to enter the dimensions of the pillars in the working section, as illustrated in figure 1. The program can accommodate angled crosscuts, varied spacings between the entries, and barrier pillars between the active section and old (side) gob areas. Slabbing of barriers

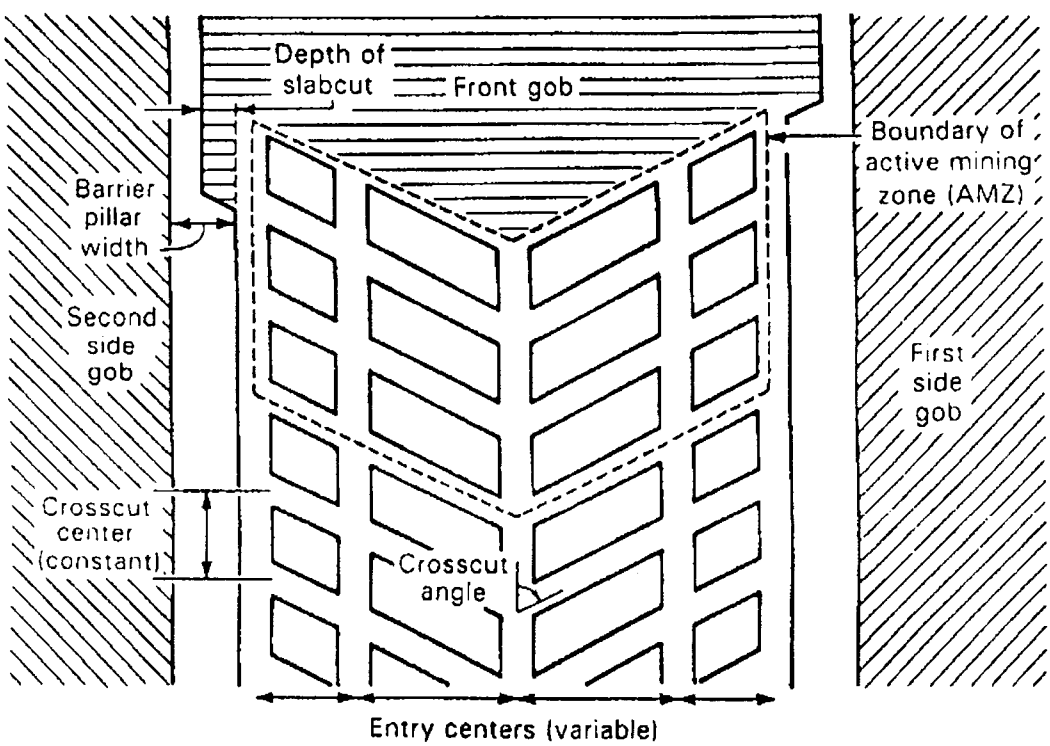

Figure 1.—Section layout parameters used in ARMPS.

on retreat can also be included. Other parameters that must be defined include depth of cover, mining height, entry width, and crosscut spacing. Finally, the user chooses one of four possible *loading conditions* (figure 2). The simplest, loading Condition 1, is development loading only. Loading condition 2 occurs when the active, or "front," panel is being fully retreated and there are no adjacent mined-out areas. The total applied load is the sum of the development loads and the front abutment load. Loading condition 3 occurs where the active mining zone (AMZ) is adjacent to an old (side) gob and the pillars are subjected to development, side abutment, and front abutment loads. Where the pillar line is surrounded by gob on three sides (sometimes referred to as "bottlenecking"), loading condition 4 is used. In every case, the extent of each gob is defined by the user.

ARMPS STABILITY FACTOR FOR THE ACTIVE MINING ZONE

The basic output from the ARMPS program is the stability factor (SF), defined as

$$\text{ARMPS SF} = \text{LBC/LT}, \qquad (1)$$

where LBC = the estimated total load-bearing capacity of the pillars within the AMZ,

and LT = the estimated total load applied to pillars within the AMZ.

Figure 3 illustrates the development and front abutment loads applied to the AMZ.

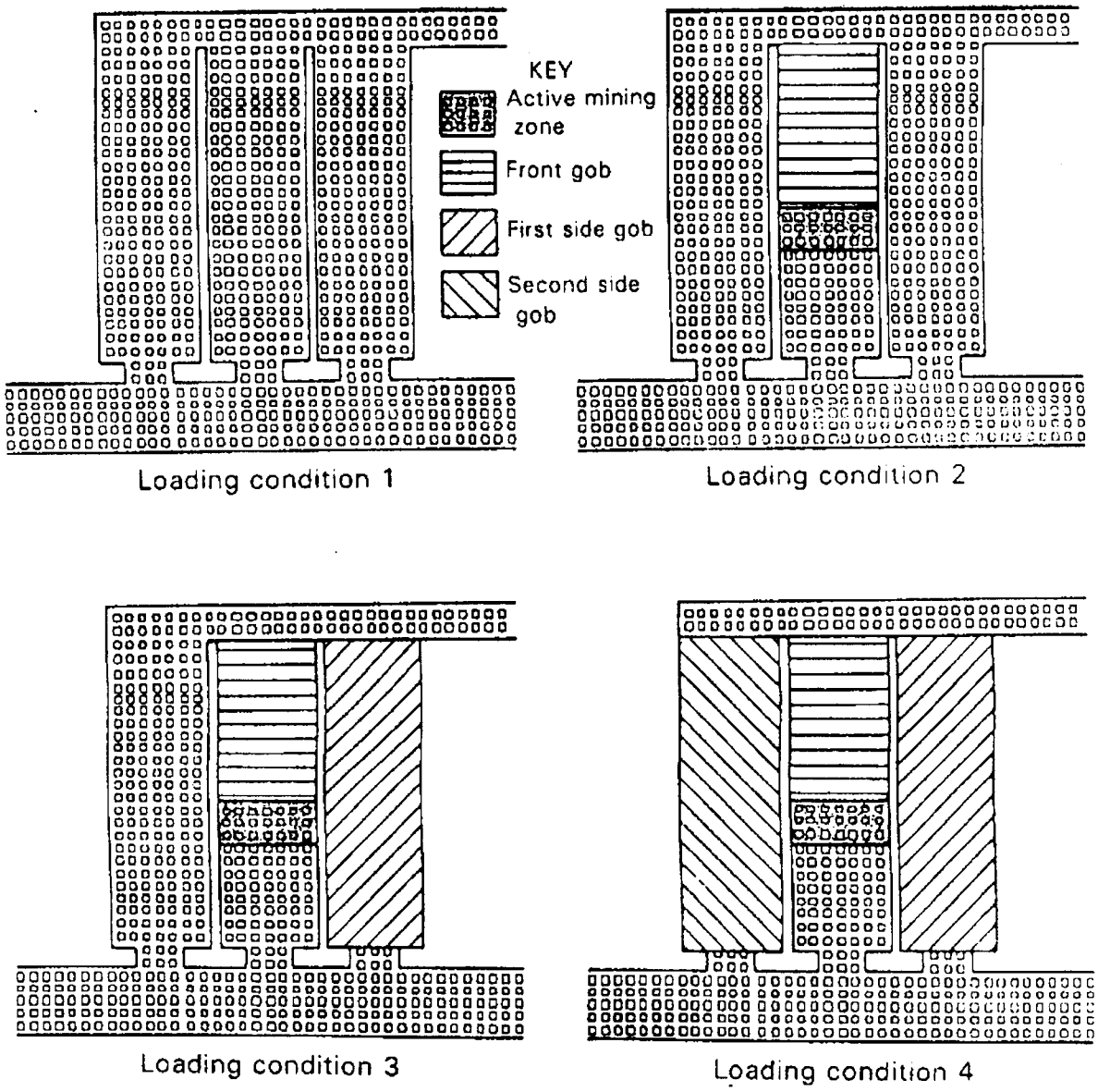

Figure 2.—The four loading conditions that can be evaluated with ARMPS.

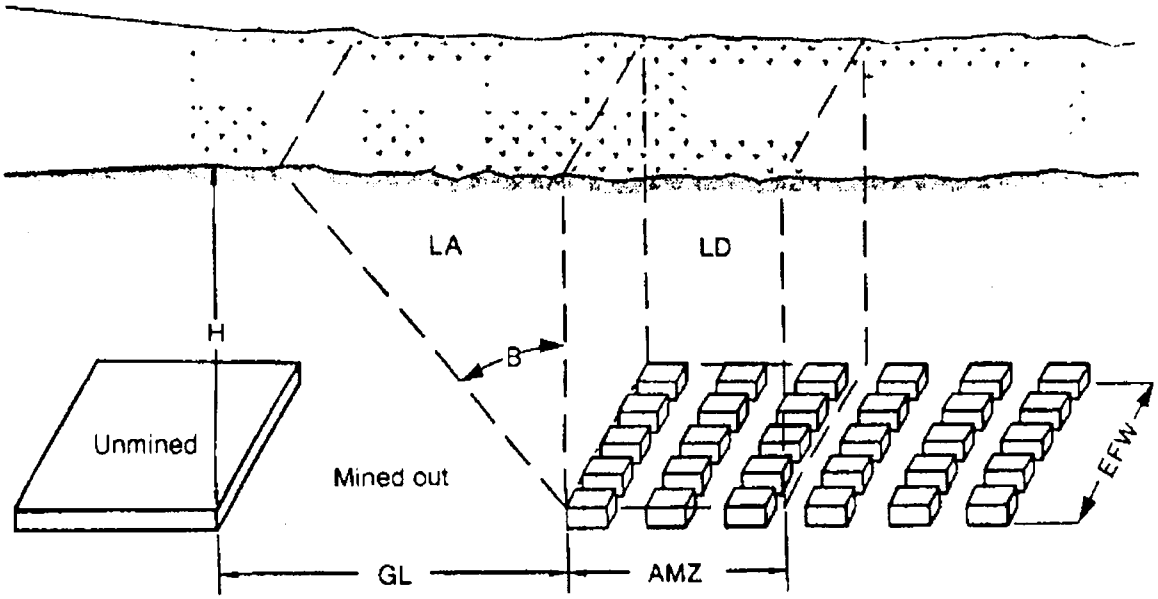

KEY

AMZ	Active mining zone	H	Depth of cover
B	Abutment angle	LA	Abutment load
EFW	Extraction front width	LD	Development load
GL	Mined out area		

Figure 3.—Schematic showing the active mining zone, the development load, and the front abutment load.

The AMZ includes all of the pillars on the extraction front (or "pillar line") and extends outby the pillar line a distance of five times the square root of the depth of cover ($5\sqrt{H}$). This distance was selected because measurements of abutment stress distributions [Mark 1990] show that 90% of the front abutment load falls within its boundaries (figure 4).

ARMPS calculates the SF for the entire AMZ, rather than stability factors for individual pillars, because experience has shown that the pillars within the AMZ typically behave as a *system*. If an individual pillar is overloaded, it will normally transfer its excess load to adjacent pillars. If those pillars are adequately sized, the process ends there. A pillar squeeze occurs only when the adjacent pillars are also undersized. They then fail in turn, resulting in a "domino" of load transfer and pillar failure. The ARMPS SF is therefore a measure of the overall stability of the pillar system.

PILLAR LOAD-BEARING CAPACITY

The load-bearing capacity of the AMZ is calculated by summing the load-bearing capacities of all of the pillars within its boundaries. The strength of an individual pillar (SP) is determined using a new pillar strength formula (the Mark-Bieniawski formula) that considers the effect of pillar length:

$$SP = S_1 [0.64 + (0.54 - 0.18 (w^2/hL))], \qquad (2)$$

where S_1 = in situ coal strength, assumed = 6.2 MPa (900 psi),

w = pillar width,

h = pillar height,

and L = pillar length.

The new pillar strength formula was needed because the pillars used in retreat mining are often much longer than they are wide. The strength of rectangular pillars can be significantly greater than square pillars due to the greater confinement generated within them. The Mark-Bieniawski formula was derived from analyses of the pillar stress distributions implied by empirical pillar strength formulas. A complete discussion of the Mark-Bieniawski formula is included in appendix A of this paper. The in situ coal strength is assumed to be 6.2 MPa (900 psi) in ARMPS; however, this value can be modified by the user.

The load-bearing capacity of the pillars is determined by multiplying their strength by their load-bearing area. When angled crosscuts are employed, the algorithm still calculates accurately each pillar's least dimension, length, and load-bearing area (A_p):

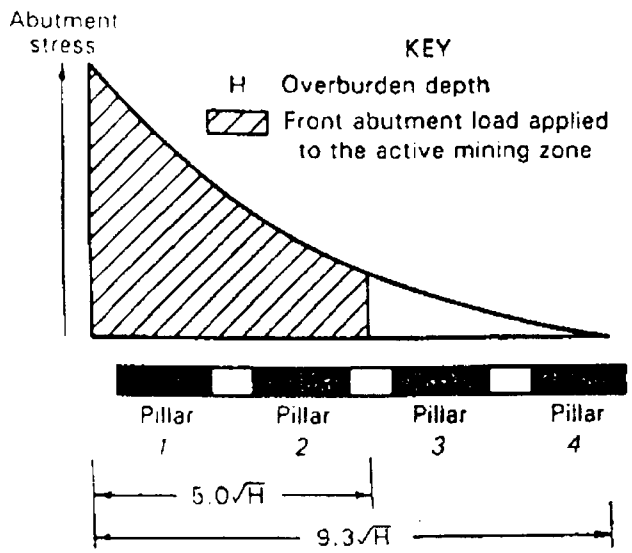

Figure 4.—Distribution of abutment stress, showing that 90% of the abutment falls within the distance of (5√H) from the gob edge.

$$A_p = [(XC)(ECTR) - (XC)(W_e) - (ECTR)(W_e)/(\sin \phi) + (W_e)^2/(\sin \phi)], \quad (3)$$

where XC = center-to-center crosscut spacing,

ECTR = center-to-center entry spacing,

W_e = entry width,

and ϕ = angle between the crosscut and the entry.

The load-bearing capacity of the pillar system is then obtained by summing the capacities of the individual pillars within the AMZ. ARMPS calculates the strength and load-bearing capacity of barrier pillars in the same manner as the panel pillars, except that their length is limited to the breadth of the AMZ.

PILLAR LOADINGS

The loadings applied to the AMZ include development loads, abutment loads, and loads transferred from barrier pillars. Table 1 shows the sources of loads and the loading conditions in which they occur.

Table 1.—Loads applied to the active mining zone in ARMPS

Source of load	Loading condition			
	1	2	3	4
Development	X	X	X	X
Front abutment		X	X	X
Side gob abutments			X	X
Transfer from barriers between active mining zone and side gobs			X	X
Transfer from remnant barriers between front gob and side gobs			X	X

Development loads are due to the weight of the overburden directly above the pillars before any retreat mining takes place. The tributary area theory is used in ARMPS to estimate development loads.

Abutment loads occur as a result of retreat mining and gob formation. They are determined by the depth of cover, the extent of the gobs, the width of the extraction front, and the abutment angles. These parameters are illustrated in two dimensions in figure 5. The abutment angle determines how much load is carried by gob. Measurements of longwall abutment stresses indicated that an abutment angle of 21° is appropriate for normal caving conditions [Mark 1992]. The ARMPS program initializes the abutment angles for all gobs to 21°, however, this can be changed by the user. For example, if it is known that no caving has occurred, then the abutment angle may be set to 90° to simulate zero load transfer to the gob [Chase and Mark 1993].

The abutment stresses are assumed to be distributed following the inverse-square function shown in figure 4. Abutment loads are also applied to barrier pillars; however, if a barrier is too small to carry its share, then some or all of the excess is transferred to the AMZ.

The front abutment load applied to the AMZ is calculated as follows. The volume of the overburden above the mined-out active gob is the depth of cover multiplied by the gob area. The portion of this volume whose weight is carried by the gob is determined by the tangent of the abutment angle, as shown in figure 5. This portion is subtracted, and the remainder is shared between the AMZ and the unmined coal on the other three sides of the gob. It is assumed that barrier pillars (or substantial production pillars) are present on the other three sides of the gob. Load applied to the barriers here may be transferred back to the AMZ if the barriers are removed later in the mining process.

The magnitude of the front abutment load applied to the AMZ is determined by the extent of the extraction zone and the depth of cover. The front abutment is considered fully developed if the gob area is large relative to the depth of cover (figure 6*A*). If only a few rows of pillars have been extracted (figure 6*B*), much of the load will be carried by the back barrier. If the full extraction zone is rather narrow (figure 6*C*), much of the load will be carried by the side barriers.

The side abutment loads are shared by the AMZ and, if it is present, the barrier pillar between the AMZ and the side gob. The inverse-square stress distribution (figure 4) again is used to apportion the load between the barrier and the AMZ. Next, if it is determined that the barriers are overloaded, some additional side abutment load is transferred to the AMZ.

To determine whether a barrier pillar can carry the load applied to it, ARMPS estimates the barrier's SF by dividing its load-bearing capacity by its load. The total load applied to a barrier pillar is the sum of the development load, the front abutment load due to any slabbing, and the side abutment load applied to the barrier. If the SF is greater than 1.5, the barrier is assumed to be stable. When the barrier's SF is between 1.5

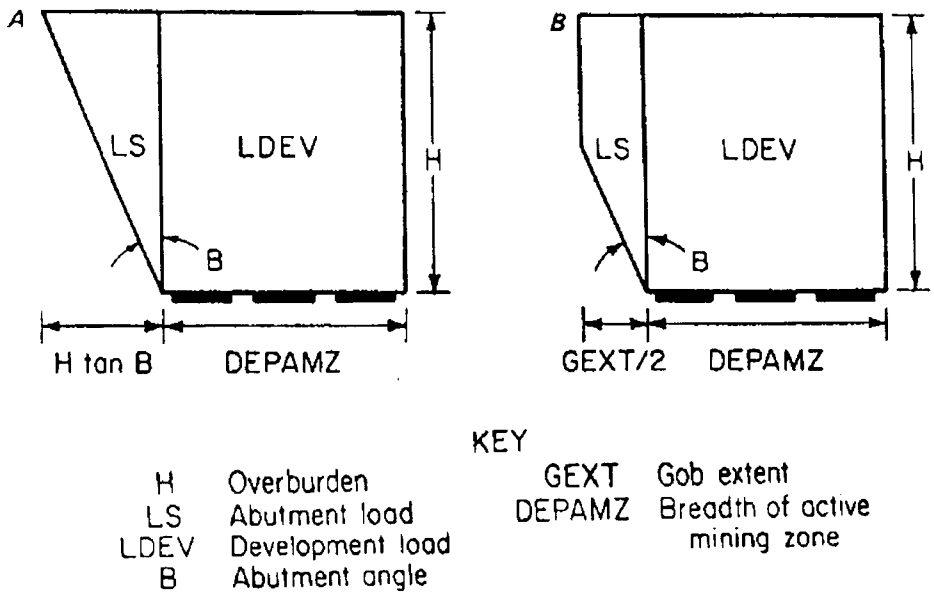

Figure 5.—Schematic showing the abutment load in two dimensions. *A*, supercritical gob; *B*, subcritical gob.

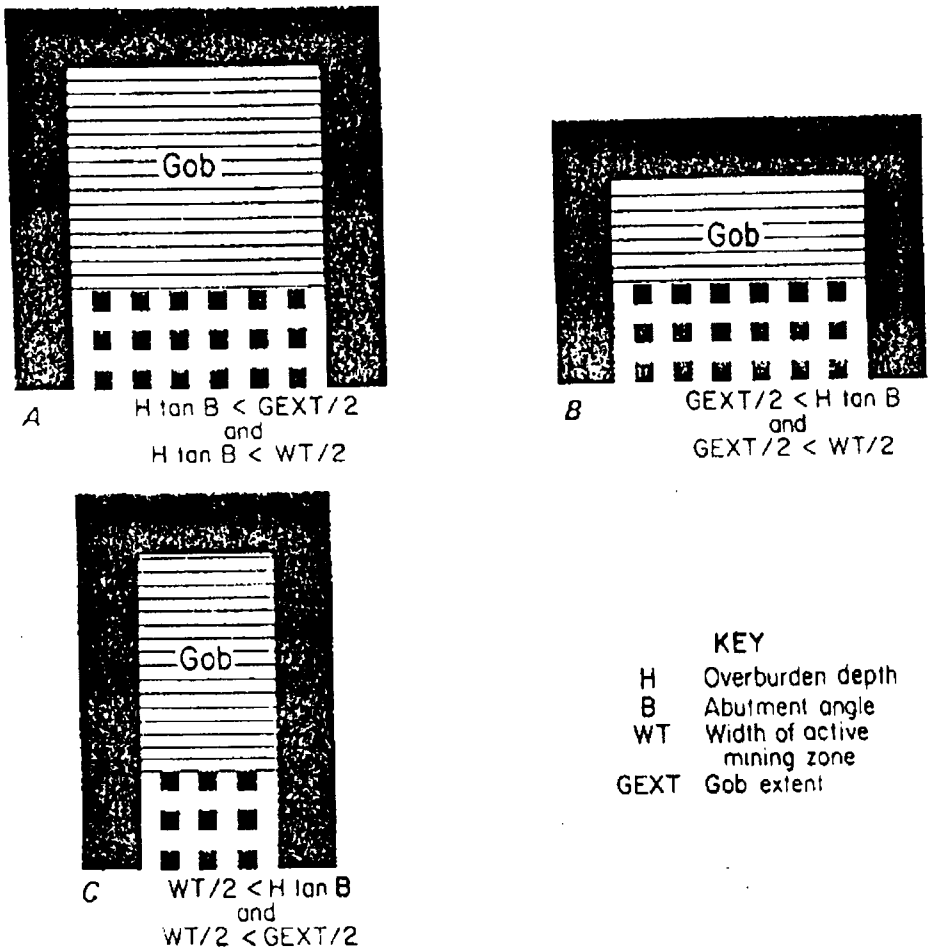

Figure 6.—Illustration of the effect of panel geometry on the front abutment loading in ARMPS. *A*, gob area is supercritical in both width and extent; *B*, gob area is subcritical in extent; *C*, gob area is subcritical in width.

and 0.5, a portion of its abutment load is transferred to the AMZ. If the SF is less than 0.5, all of the additional side abutment load (but not the development or front abutment load) is transferred to the AMZ.

The final sources of load on the AMZ are the remnant barrier pillars inby the pillar line (between the front and side gobs). If the remnant barriers are too small to carry their load, some part of it is returned to the AMZ. The decision to transfer the load and how much is based on the remnant barrier's SF. Slashing of the remnant will also return some abutment load to the AMZ.

Further details on the formulas and calculations used in ARMPS loadings can be found in the "Help" text that accompanies version 4.0 of the program.

VERIFICATION OF THE ARMPS METHOD

The ARMPS method is being verified through back-analysis of pillar recovery case histories. To date, 140 case histories have been obtained from 10 States (see appendix B of this paper). They cover an extensive range of geologic conditions, roof rock cavability characteristics, extraction methods, depths of cover, and pillar geometries. Ground conditions in each case history have been categorized as either satisfactory or unsatisfactory. Pillar failures responsible for unsatisfactory conditions were found to include--

- Pillar squeezes, accompanied by significant entry closure and loss of reserves;
- Sudden collapses of groups of pillars, usually accompanied by airblasts, and/or
- Coal pillar bumps (violent failures of one or more pillars).

As figure 7 shows, pillar failures occurred in 93% of the cases where the ARMPS SF was less than 0.75. Where the ARMPS SF was greater than 1.5, 94% of the designs were satisfactory. SF values ranging from 0.75 to 1.50 form a "gray" area where both successful and unsuccessful cases are found.

Current research has begun to evaluate other factors that may contribute to satisfactory conditions when the ARMPS SF falls between 0.75 and 1.5. These include—

Coal strength: An extensive data base of laboratory tests of the strength of coal was compiled by Mark and Barton [1997]. When compared with the ARMPS data base, no correlation was found between coal strength and pillar strength.

Depth of cover: Figure 8 shows that there is a marked reduction in SF as depth of cover increases. When the depth exceeds 305 m (1,000 ft), the ARMPS SF was below 1.0 for 70% of the satisfactory designs. Highly unsatisfactory conditions have also been encountered under deep cover, which recently led to two fatalities. Pillar design for retreat mining under deep cover remains an important research issue.

Seam height: A plot of seam height against ARMPS SF shows no correlation (figure 9).

Roof geology: A detailed study of pillar performance was conducted at a mining complex in southern West Virginia. More than 50 case histories were collected. Analysis showed that satisfactory conditions were more likely to be encountered under shale roof than massive sandstone roof (figures 10-11). This implies that better caving occurs with shale, resulting in lower pillar loads.

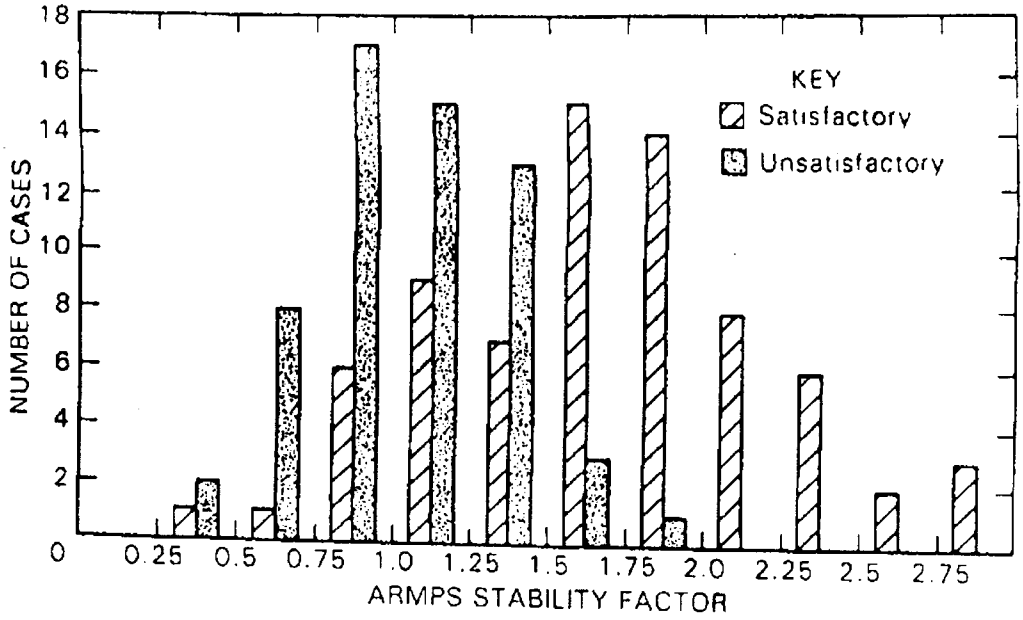

Figure 7.—ARMPS data base.

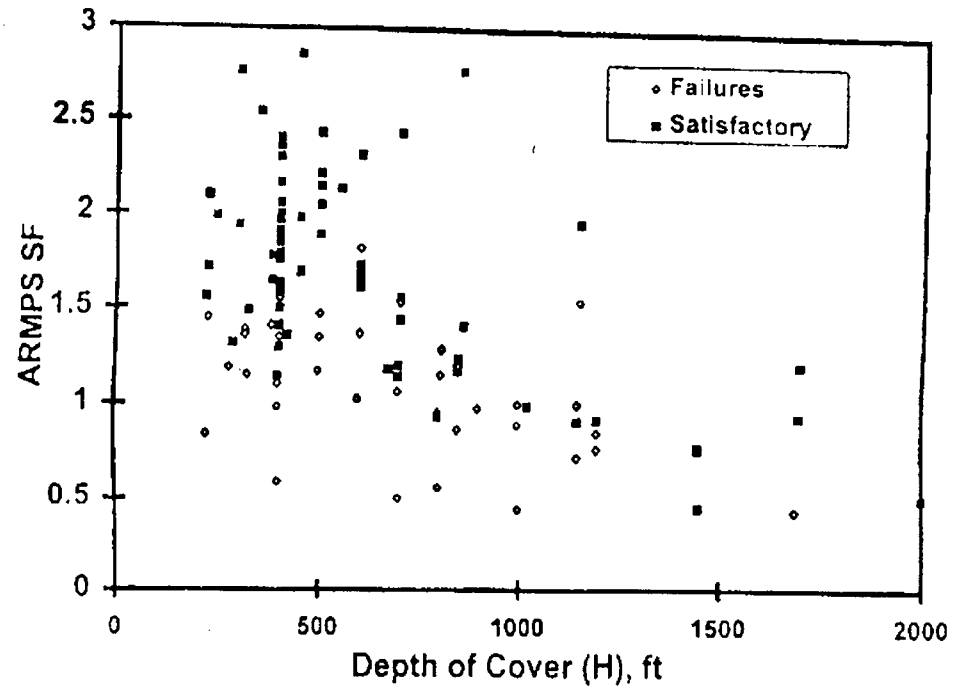

Figure 8.—Relationship between ARMPS SF and depth of cover within the case history data base.

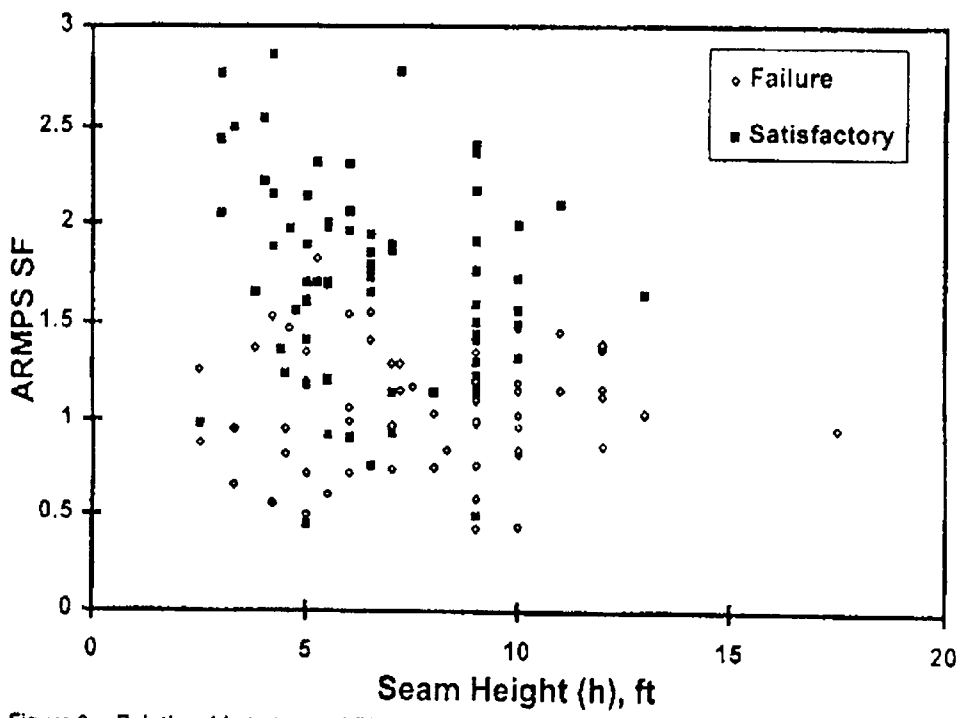

Figure 9.—Relationship between ARMPS SF and seam height within the case history data base.

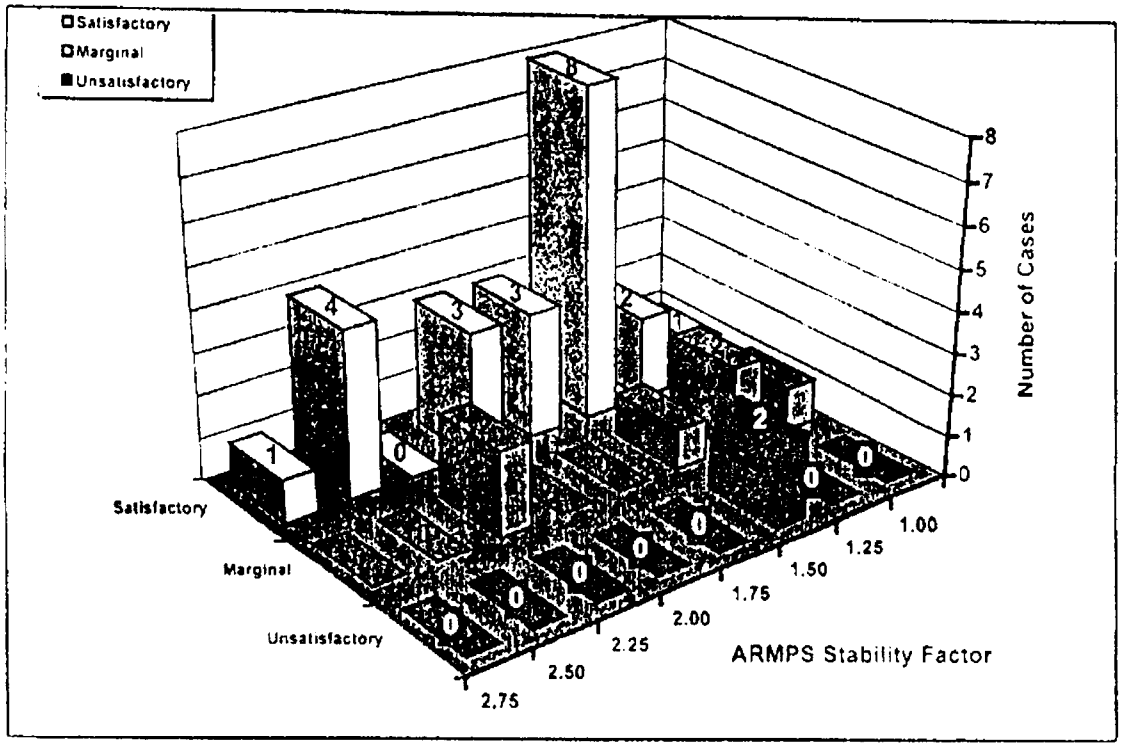

Figure 10.—Shale roof case histories from mining complex in southern West Virginia.

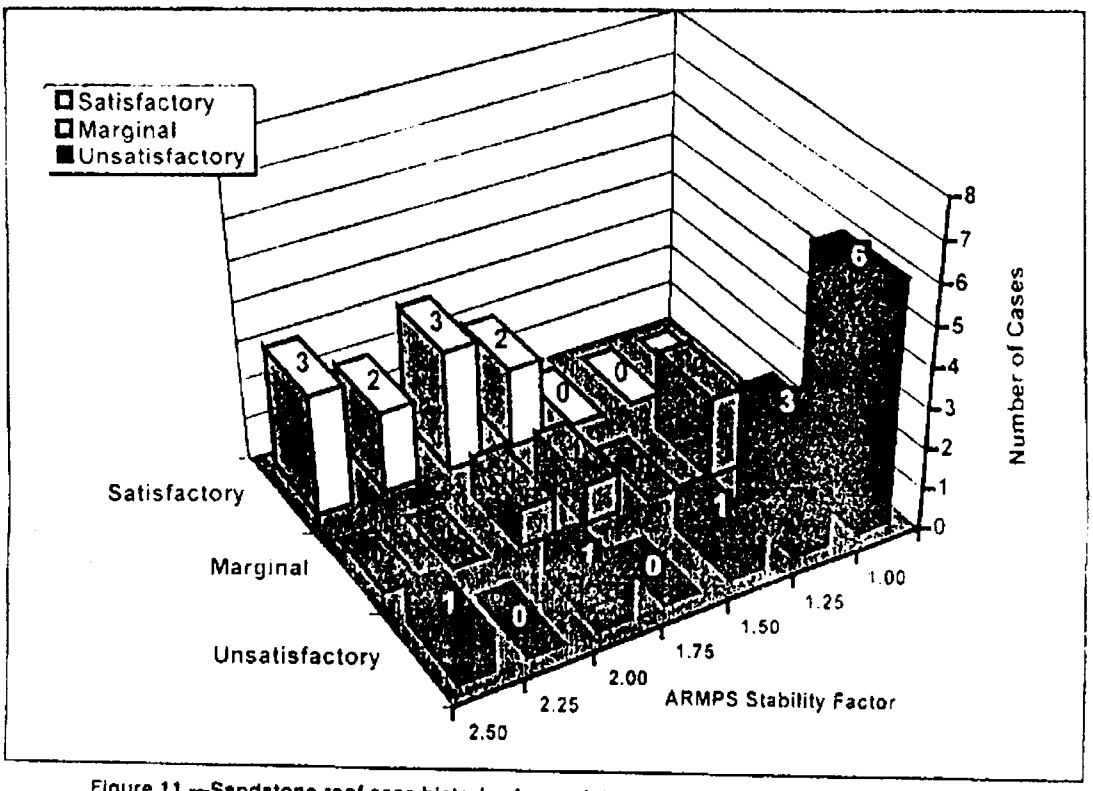

Figure 11.—Sandstone roof case histories from mining complex in southern West Virginia.

GUIDELINES FOR USING ARMPS

ARMPS appears to provide good first approximations of the pillar sizes required to prevent pillar failure during retreat mining. In an operating mine, past experience can be incorporated directly into ARMPS. ARMPS stability factors can be back-calculated for both successful and unsuccessful areas. Once a minimum ARMPS SF has been shown to provide adequate ground conditions, that minimum should be maintained in subsequent areas as changes occur in the depth of cover, coal thickness, or pillar layout. In this manner, ARMPS can be calibrated using site-specific experience.

ARMPS is also well suited for initial feasibility studies where no previous experience is available. Operators may begin with an SF near 1.5, then adjust as they observe pillar performance. ARMPS may also help in optimizing panel designs by identifying pillars that might be needlessly oversized.

ARMPS may be used to analyze a wide variety of mining geometries. For example, most bleeder designs can be analyzed by selecting loading condition 3, then setting the extent of the active gob to zero. The "Help" text included with version 4.0 of the program contains many tips on selecting the proper input parameters when using ARMPS.

In some cases, more detail may be desired than can be provided by ARMPS. Some complex situations, such as multiple-seam interactions, are beyond the capabilities of ARMPS. In these instances, the newly developed LAMODEL [Heasley 1997] may be the appropriate tool to use.

CONCLUSIONS

The ARMPS program has already proven to be a useful aid in planning pillar recovery operations. It is easy to use, and a large number of analyses can be run in a relatively short period. The program is sufficiently flexible to be applicable to a wide variety of mining geometries. If the user desires, it also produces a full range of intermediate calculations in addition to the SF. Many mines throughout the United States and abroad already use ARMPS, and the Mine Safety and Health Administration has also made extensive use of the program.

Current efforts are aimed at improving the interpretation of the ARMPS SF. Although pillar failures seem unlikely when the ARMPS SF is greater than 1.5, there are apparently many cases where SF values as low as 0.75 have been successful. Factors such as roof quality, floor strength, and mining method may determine whether a pillar design succeeds. These factors are now being included in the retreat mining case history data base and will be integrated into future design guidelines.

To obtain a single copy of the ARMPS computer program, version 4.0 for Windows, send three double-sided, high-density diskettes to: Christopher Mark, Ph.D., NIOSH, Pittsburgh Research Center, Cochrans Mills Rd., P.O. Box 18070, Pittsburgh, PA 15236-0070.

REFERENCES

Blaiklock J [1992]. A Kentuckian vote for continuous mining. Mining Magazine *June*:365-366.

Chase FE, Mark C [1993]. Ground control design for pillar extraction. Soc Min Eng AIME preprint 93-282.

Heasley KA [1997]. A new laminated overburden model for coal mine design. In: Mark C, Tuchman RJ, comp. Proceedings: New Technology for Ground Control in Retreat Mining. Pittsburgh, PA: U.S. Department of Health and Human Services, Public Health Service, Centers for Disease Control, National Institute for Occupational Safety and Health, IC 9446.

Mark C [1990]. Pillar design methods for longwall mining. Pittsburgh, PA: U.S. Department of the Interior, Bureau of Mines, IC 9247.

Mark C [1992]. Analysis of longwall pillar stability (ALPS): an update. In: Iannacchione AT, Mark C, Repsher RC, Tuchman RJ, Jones CC, comp. Proceedings of the Workshop on Coal Pillar Mechanics and Design. Pittsburgh, PA: U.S. Department of the Interior, Bureau of Mines, IC 9315, pp. 238-249.

Mark C, Barton TM [1997]. Pillar design and coal strength. In: Mark C, Tuchman RJ, comp. Proceedings: New Technology for Ground Control in Retreat Mining. Pittsburgh, PA: U.S. Department of Health and Human Services, Public Health Service, Centers for Disease Control, National Institute for Occupational Safety and Health, IC 9446.

APPENDIX A.—DERIVATION OF THE MARK-BIENIAWSKI PILLAR STRENGTH FORMULA

Early versions of the ARMPS program, following the ALPS program, used the Bieniawski formula to estimate pillar strength [Bieniawski 1992]:

$$S_p = S_i\,[0.64 + (0.36\ w/h)], \qquad \text{(A-1)}$$

where S_p = pillar strength,

S_i = in situ coal strength,

w = pillar width (or least plan dimension),

and h = pillar height.

The Bieniawski formula was originally developed in the 1960's from in situ testing of large-scale coal specimens. The specimen strengths were determined as the ultimate load-bearing capacity divided by the area. Bieniawski recognized that the formula underestimated the strength of rectangular pillars, however, because all of the specimens were square, there was no obvious way of estimating a "pillar length" effect.

It has been recognized that a major disadvantage of empirical formulas, like that of Bieniawski, is that they treat the pillar as a single structural element. In reality, the stress within even a relatively small pillar is highly nonuniform. Tests conducted by Wagner [1974] demonstrated this quite dramatically (figure A-1).

Modern *mechanics-based* approaches to coal pillars begin with stress distribution. Perhaps the best known is the approach proposed by Wilson [1973, 1983]. Wilson derived an expression for the vertical stress gradient within the yield zone, which he then integrated over the area of the pillar (figure A-2) to determine the ultimate pillar resistance (R). The "pillar strength" is simply the ultimate pillar resistance divided by the pillar area. Numerical models also provide stress distribution profiles, although not normally in the form of an equation. Mechanics-based approaches can be used to evaluate any pillar shape, because the stresses within the pillar are determined by laws that are independent of overall pillar geometry.

Although empirical formulas do not explicitly consider the effect of internal pillar mechanics, it is apparent that they imply a nonuniform stress distribution because of the shape effect. Once the implied stress gradient has been derived, the length effect can be readily determined. The derivation has been published previously [Mark et al. 1988; Mark and Iannacchione 1992] and is summarized below.

First, three assumptions are implicit in Wilson's and other analytical formulations.

1. The stress within the yield zone of a given pillar is a continuous function of the distance from the nearest rib.

2. The stress gradient within the yield zone of a given pillar does not change with time or load (i.e., the yielded coal is perfectly plastic).

3. The stress distribution is symmetric with respect to the center of the pillar.

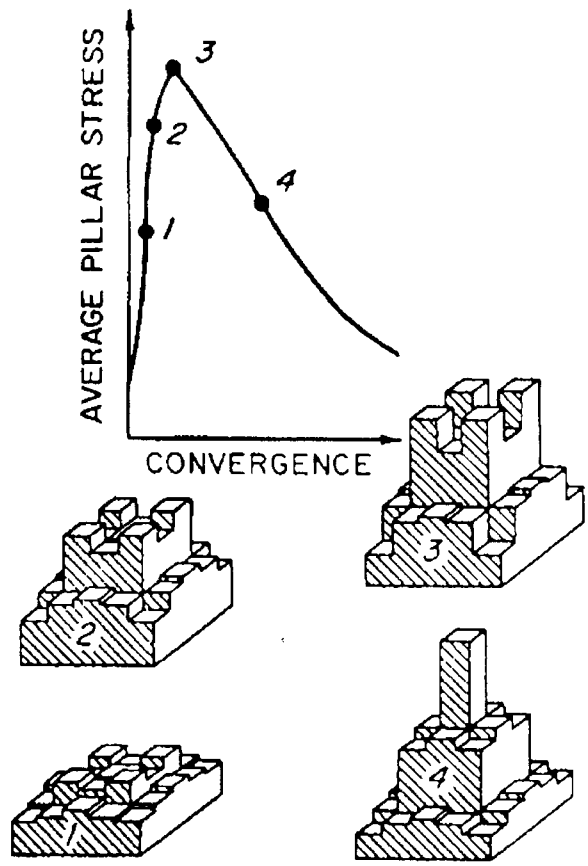

Figure A-1.—Pillar stress profiles measured in small coal pillars (after Wagner [1974]).

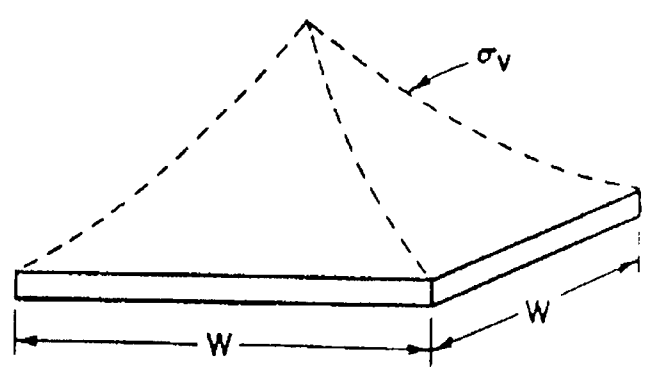

Figure A-2.—Determination of pillar load-bearing capacity as the integral of the pillar stress distribution.

The next step in the derivation is to calculate the ultimate resistance of a square pillar. Using the Bieniawski formula:

$$R = S_1 \left(0.64 + 0.36 \frac{w}{h}\right) w^2. \qquad \text{(A-2)}$$

Then, the increase in pillar resistance dR due to an increase in cross-sectional area $dA = 2w\ dw$ (figure A-3*A*) may be calculated by taking the derivative of equation A-2 with respect to w:

$$dR = S_1 \left(1.28 + 1.08 \frac{w^2}{h}\right) dw. \qquad \text{(A-3)}$$

In the next step, the assumption that the vertical pillar stress is a continuous function of the rib distance (x) is applied. It may be seen (figure A-3*B*) that

$$dR = 4 \int_0^{\frac{w}{2}} \sigma_v\ dx\ dw. \qquad \text{(A-4)}$$

Equating A-3 and A-4 and simplifying, we have

$$S_1 = \left(0.32\ w + 0.27 \frac{w^2}{h}\right) = \int_0^{\frac{w}{2}} \sigma_v\ dx. \qquad \text{(A-5)}$$

The function that satisfies equation A-5 is

$$\sigma_v = S_1 \left(0.64 + 2.16 \frac{x}{h}\right). \qquad \text{(A-6)}$$

Equation A-6 is the stress gradient in the yield zone predicted by the Bieniawski formula. Stress gradients have also been derived for several other common empirical pillar strength formulas [Mark and Iannacchione 1992].

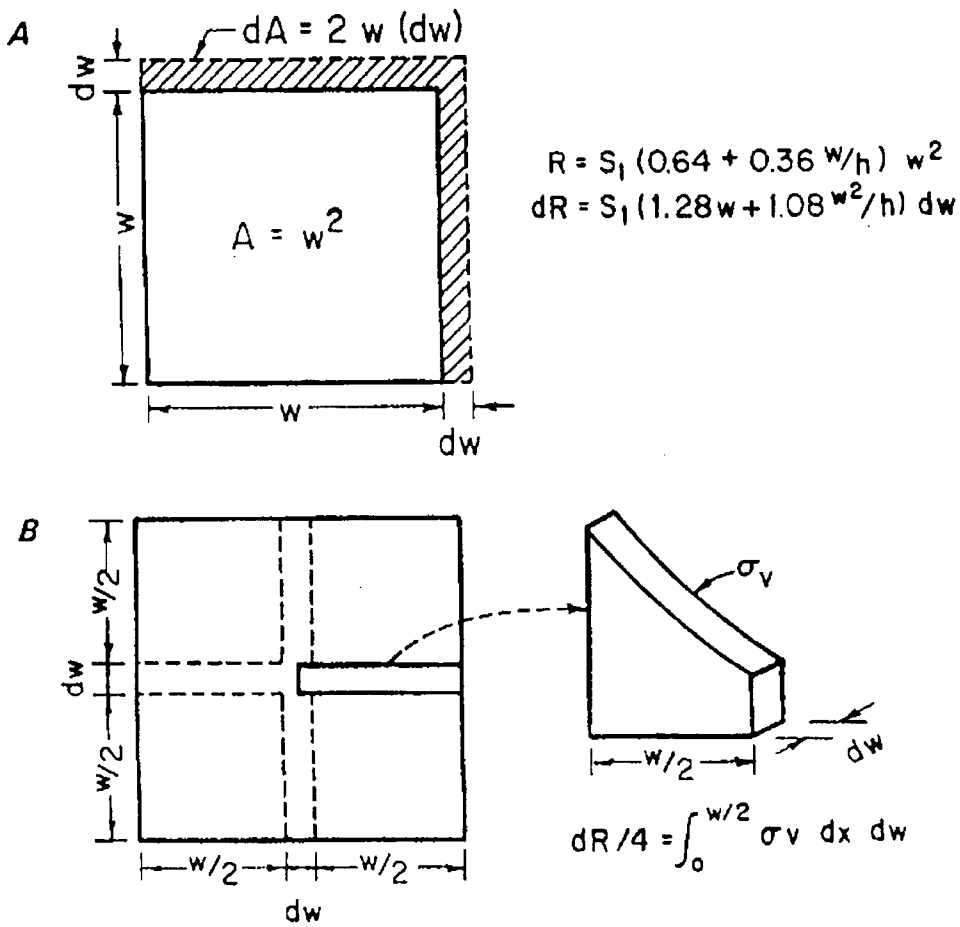

Figure A-3.—Determination of pillar stress gradients from a pillar strength formula. *A*, calculation of dR directly from the formula; *B*, calculation of dR in terms of the vertical stress gradient.

To determine the load-bearing capacity of any pillar shape, it is now only necessary to integrate equation A-6 over the load-bearing area of the pillar. For example, the load-bearing capacity of an extremely long strip pillar (R_s) is

$$R_s = 2L\int_0^{\frac{w}{2}} S_1\left(0.64 + 2.16\frac{x}{h}\right) dx. \qquad \text{(A-7)}$$

Solving:

$$R_s = (Lw)\, S_1\left(0.64 + 0.54\frac{w}{h}\right). \qquad \text{(A-8)}$$

Dividing by the pillar area (Lw) yields the strength of a strip pillar (S_s):

$$S_s = S_1\left(0.64 + 0.54\frac{w}{h}\right). \qquad \text{(A-9)}$$

Equation A-9 implies that a strip pillar's strength can approach 150% that of a square pillar, but that the strength difference is reduced as the w/h ratio is reduced.

The ultimate load carried by a rectangular pillar is equivalent to the load carried by a square pillar of width w plus a section of a strip pillar of length (L - w), as shown in figure A-4. Combining equations A-6 and A-9, the ultimate load carried by a rectangular pillar (R_r) is

$$R_r = S_1\left\{\left[w^2\left(0.64 + 0.36\frac{w}{h}\right)\right] + \left[(w(L-w))\left(0.64 + 0.54\frac{w}{h}\right)\right]\right\}. \qquad \text{(A-10)}$$

Simplifying:

$$R_r = S_1\left[0.64\,wL + 0.54\left(w^2\frac{L}{h}\right) - 0.18\left(\frac{w^3}{H}\right)\right]. \qquad \text{(A-11)}$$

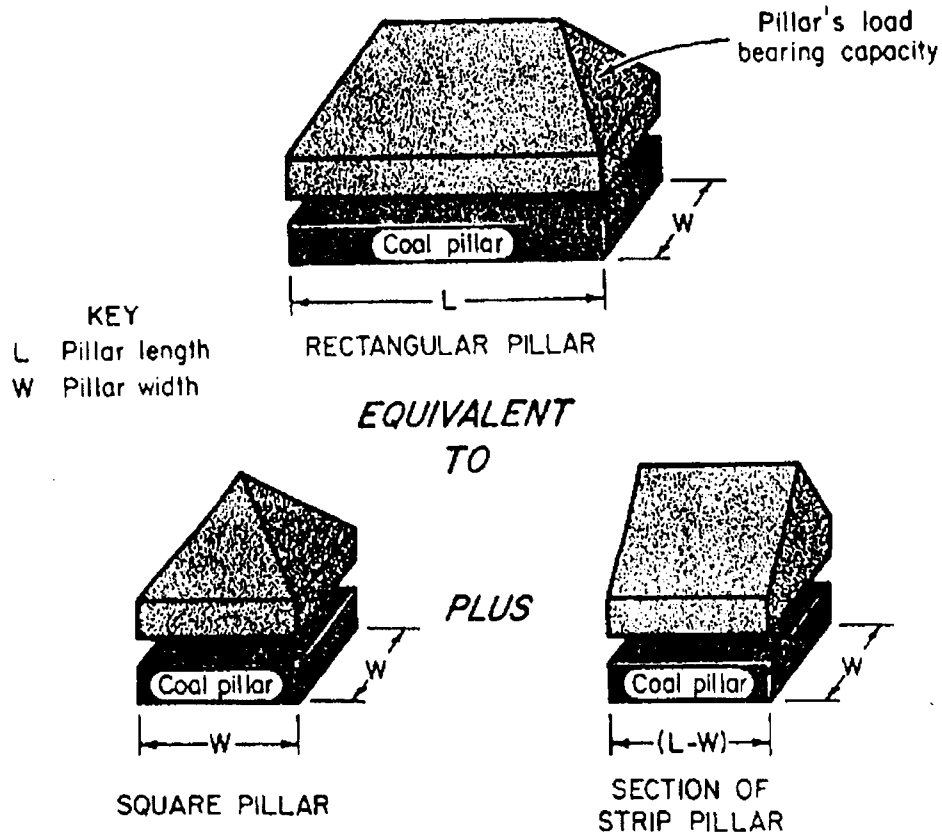

Figure A-4.—Pillar stress distributions for square, strip, and rectangular pillars.

Dividing by the load-bearing area (wL), the Mark-Bieniawski formula is obtained:

$$S_p = S_1 \left[0.64 + 0.54 \left(\frac{w}{H} \right) - 0.18 \frac{w^2}{Lh} \right]. \qquad \text{(A-12)}$$

Equation A-12 indicates that the increase in strength in a rectangular pillar depends on both (w/h) and (w/L). Table A-1 compares the pillar strengths determined by the Mark-Bieniawski formula with those obtained from the Bieniawski formula.

Table A-1.—Pillar strength from the Mark-Bieniawski formula, assuming the strength of a square pillar (original Bieniawski formula) as unity

Pillar L/w	Pillar w/h				
	1	2	4	10	20
1.5	1.06	1.09	1.12	1.14	1.16
2.0	1.09	1.13	1.18	1.21	1.23
4.0	1.14	1.23	1.32	1.41	1.45
10.0	1.16	1.25	1.34	1.42	1.46

REFERENCES

Bieniawski ZT [1992]. A method revisited: coal pillar strength formula based on field investigations. In: Iannacchione AT, Mark C, Repsher RC, Tuchman RJ, Jones CC, comp. Proceedings of the Workshop on Coal Pillar Mechanics and Design. Pittsburgh, PA: U.S. Department of the Interior, Bureau of Mines. IC 9315. pp. 158-165.

Mark C, Iannacchione AT [1992]. Coal pillar mechanics: theoretical models and field measurements compared. In: Iannacchione AT, Mark C, Repsher RC, Tuchman RJ, Jones CC, comp. Proceedings of the Workshop on Coal Pillar Mechanics and Design. Pittsburgh, PA: U.S. Department of the Interior, Bureau of Mines. IC 9315. pp. 78-93.

Mark C, Listak JM, Bieniawski ZT [1988]. Yielding coal pillars—field measurements and analysis of design methods. In: Proceedings of the 29th U.S. Symposium on Rock Mechanics. Minneapolis, MN: University of Minnesota. pp. 261-270.

Wagner H [1974]. Determination of the complete load-deformation characteristics of coal pillars. In: Proceedings of the 3rd International Society for Rock Mechanics Congress. Denver, CO: pp. 1076-1081.

Wilson AH [1973]. An hypothesis concerning pillar stability. Min Eng (London) *133*(141):409-417.

Wilson AH [1983]. The stability of underground workings in the soft rocks of the coal measures. Intl J Rock Mech Min Sci *1*:91-187.

APPENDIX B.—ARMPS CASE HISTORY DATA BASE

Table B-1.—Unsatisfactory pillar retreat case histories

State and coal seam	ARMPS SF	Seam thickness, m (ft)	Depth, m (ft)	Loading condition
Alabama:				
Blue Creek	1.54	1.8 (6.0)	350 (1,150)	2
Blue Creek	0.99	1.8 (6.0)	350 (1,150)	3
Colorado:				
Cameo	0.74	2.1 (7.0)	90 (300)	1
D	1.20	2.7 (9.0)	260 (850)	2
D	0.99	2.7 (9.0)	305 (1,000)	3
Kentucky:				
Harlan	1.16	3.7 (12)	285 (940)	1
Harlan	0.96	2.1 (7.0)	305 (1,000)	1
Harlan	0.86	3.7 (12)	260 (850)	2
Harlan	1.12	3.7 (12)	325 (1,070)	1
Hazard No. 4	0.44	3.0 (10)	305 (1,000)	4
Hazard No. 4	0.56	1.3 (4.2)	245 (800)	3
Hazard No. 4	0.50	1.5 (5.0)	215 (700)	3
Lower Elkhorn (No. 2 Gas)	1.03	4.0 (13.0)	245 (800)	1
Lower Elkhorn (No. 2 Gas)	1.02	4.0 (13.0)	185 (600)	3
Ohio:				
Lower Freeport	1.20	1.5 (5.0)	215 (700)	1
Mahoning	0.66	1.0 (3.3)	75 (250)	1
Mahoning	0.95	1.0 (3.3)	75 (250)	1
Pennsylvania:				
Lower Kittanning	1.41	2.0 (6.5)	115 (380)	2
Lower Kittanning	1.55	2.0 (6.5)	120 (400)	2
Lower Kittanning	1.29	2.1 (7.0)	75 (250)	1
Pittsburgh	0.97	2.1 (7.0)	275 (900)	3
Pittsburgh	1.17	2.3 (7.5)	150 (500)	3
Pittsburgh	1.29	2.2 (7.2)	245 (810)	4
Pittsburgh	1.15	2.2 (7.2)	245 (810)	4
Sewickley	1.82	1.6 (5.25)	185 (600)	3
Tennessee:				
Beach Grove	1.26	0.8 (2.5)	315 (1,025)	1
Beach Grove	0.88	0.8 (2.5)	305 (1,000)	3
Utah:				
Blind Canton	0.84	2.5 (8.3)	365 (1,200)	3
Gilson	0.76	2.7 (9.0)	365 (1,200)	3
Gilson	0.43	2.7 (9.0)	515 (1,690)	3
Lower O'Connor	0.95	5.3 (17.5)	170 (550)	1
Virginia:				
Blair	1.37	1.2 (3.8)	185 (600)	3
Glamorgan	1.06	1.8 (6.0)	215 (700)	3
Jawbone	1.53	1.3 (4.2)	215 (700)	3
Jawbone	1.47	1.4 (4.6)	150 (500)	3
Pocahontas No. 3	0.61	1.7 (5.5)	520 (1,700)	1
Pocahontas No. 3	1.35	1.5 (5.0)	150 (500)	3
Pocahontas No. 4	1.03	2.4 (8.0)	90 (300)	1
West Virginia:				
Beckley	0.72	1.8 (6.0)	350 (1,150)	4
Coalburg	0.75	2.4 (8.0)	90 (300)	1
Coalburg	0.59	2.7 (9.0)	120 (400)	NAp
Coalburg	0.98	2.7 (9.0)	120 (400)	NAp
Coalburg	1.10	2.7 (9.0)	120 (400)	NAp
Coalburg	1.35	2.7 (9.0)	120 (400)	NAp

See explanatory notes at end of table.

Table B-1.—Unsatisfactory pillar retreat case histories—Continued

State and coal seam	ARMPS SF	Seam thickness, m (ft)	Depth, m (ft)	Loading condition
West Virginia —Continued				
Dorothy	1.36	3.7 (12.0)	95 (315)	3
Dorothy	1.37	3.7 (12.0)	95 (315)	2
Dorothy (Winifrede)	1.15	3.4 (11.0)	70 (225)	1
Dorothy (Winifrede)	1.45	3.4 (11.0)	70 (225)	4
Dorothy (Winifrede)	1.39	3.7 (12.0)	95 (315)	2
Dorothy (Winifrede)	1.02	3.0 (10.0)	55 (175)	1
Dorothy (Winifrede)	1.15	3.0 (10.0)	100 (325)	2
No 2 Gas	0.95	1.4 (4.5)	245 (800)	4
Stockton	0.84	3.0 (10.0)	70 (225)	2
Stockton	0.96	3.0 (10.0)	75 (240)	1
Stockton	0.82	3.0 (10.0)	75 (245)	1
Stockton	1.47	3.0 (10.0)	85 (280)	1
Stockton	1.19	3.0 (10.0)	85 (280)	2
([1])	0.72	1.5 (5.0)	120 (400)	1
([1])	0.82	1.4 (4.5)	115 (375)	1

NAp Not applicable.

[1]Not provided by original reference.

Table B-2.—Satisfactory pillar retreat case histories

State and coal seam	ARMPS SF	Seam thickness, m (ft)	Depth, m (ft)	Loading condition
Alabama:				
Blue Creek	1.96	1.8 (6.0)	350 (1,150)	2
Colorado:				
Cameo	1.86	2.1 (7.0)	120 (400)	3
Cameo	1.14	2.1 (7.0)	215 (700)	2
Cameo	0.93	2.1 (7.0)	245 (800)	3
D	1.23	2.7 (9.0)	260 (850)	2
D	1.44	2.7 (9.0)	215 (700)	2
Illinois:				
Herrin No. 6	1.14	2.4 (8.0)	215 (700)	3
Kentucky:				
Harlan	1.94	2.0 (6.5)	90 (300)	3
Hazard No. 4	1.36	1.3 (4.4)	130 (420)	3
Kellioka	1.41	1.5 (5.0)	260 (860)	2
Kellioka	1.18	1.5 (5.0)	205 (675)	3
Kellioka	0.45	1.5 (5.0)	440 (1,450)	3
Kellioka	1.61	1.5 (5.0)	185 (600)	3
Lower Elkhorn (No. 6 Gas)	1.64	4.0 (13.0)	120 (400)	3
Pond Creek	1.20	1.7 (5.5)	215 (700)	2
Pond Creek	1.70	1.7 (5.5)	135 (450)	3
Pond Creek	2.0	1.7 (5.5)	120 (400)	2
Pond Creek	1.98	1.7 (5.5)	135 (450)	3
Pond Creek	1.69	1.7 (5.5)	135 (450)	2
Ohio:				
Lower Freeport	1.60	1.5 (5.0)	170 (550)	1
Lower Freeport	1.70	1.5 (5.0)	170 (550)	1
Mahoning	2.50	1.0 (3.3)	75 (250)	1
Pennsylvania:				
Lower Freeport	2.06	1.8 (6.0)	120 (400)	3
Lower Kittanning	1.65	2.0 (6.5)	115 (380)	3
Lower Kittanning	1.78	2.0 (6.5)	115 (380)	3
Lower Kittanning	1.79	2.0 (6.5)	120 (400)	3
Lower Kittanning	1.85	2.0 (6.5)	120 (400)	2
Lower Kittanning	2.14	1.5 (5.0)	170 (550)	3
Pittsburgh	1.89	2.1 (7.0)	150 (500)	3
Pittsburgh	2.78	2.2 (7.2)	260 (855)	2
Sewickley	1.70	1.6 (5.25)	185 (600)	3
Sewickley	2.32	1.6 (5.25)	185 (600)	2
Upper Freeport	1.88	1.3 (4.2)	65 (210)	1
Tennessee:				
Beach Grove	0.98	0.8 (2.5)	315 (1,025)	2
Utah:				
Gilson	0.50	2.7 (9.0)	610 (2,000)	2
Virginia:				
Blair	1.65	1.2 (3.8)	185 (600)	3
Glamorgan	2.31	1.8 (6.0)	120 (400)	3
Jawbone	2.86	1.3 (4.2)	135 (450)	2
Jawbone	2.15	1.3 (4.2)	150 (500)	3
Jawbone	1.97	1.4 (4.6)	120 (400)	3
Mossy-Haggy	2.05	0.9 (3.0)	150 (500)	3
Pocahontas No. 3	0.92	1.7 (5.5)	520 (1,700)	2
Pocahontas No. 3	1.21	1.7 (5.5)	520 (1,700)	3
Pocahontas No. 3	1.89	1.5 (5.0)	150 (500)	2
Pocahontas No. 4	0.91	1.8 (6.0)	365 (1,200)	3
Pocahontas No. 4	2.77	0.9 (3.0)	90 (300)	2
Pocahontas No. 4	0.76	2.0 (6.5)	440 (1,450)	3
Red Ash	2.44	0.9 (3.0)	150 (500)	2
Red Ash	2.44	0.9 (3.0)	215 (700)	3
Tiller	2.22	1.2 (4.0)	150 (500)	3

See explanatory notes at end of table.

Table B-2.—Satisfactory pillar retreat case histories—Continued

State and coal seam	ARMPS SF	Seam thickness, m (ft)	Depth, m (ft)	Loading condition
West Virginia:				
Beckley	0.90	1.8 (6.0)	350 (1,150)	4
Beckley	1.17	2.7 (9.0)	260 (850)	4
Coalburg	1.14	2.7 (9.0)	120 (400)	NAp
Coalburg	1.30	2.7 (9.0)	120 (400)	NAp
Coalburg	1.41	2.7 (9.0)	120 (400)	NAp
Coalburg	1.50	2.7 (9.0)	120 (400)	NAp
Coalburg	1.59	2.7 (9.0)	120 (400)	NAp
Coalburg	1.76	2.7 (9.0)	120 (400)	NAp
Coalburg	1.91	2.7 (9.0)	120 (400)	NAp
Coalburg	2.17	2.7 (9.0)	120 (400)	NAp
Coalburg	2.37	2.7 (9.0)	120 (400)	NAp
Coalburg	2.41	2.7 (9.0)	120 (400)	NAp
Dorothy (Winifrede)	2.10	3.4 (11.0)	70 (225)	2
Dorothy (Winifrede)	1.32	3.0 (10.0)	85 (285)	2
Dorothy (Winifrede)	1.49	3.0 (10.0)	100 (325)	2
Dorothy (Winifrede)	1.72	3.0 (10.0)	70 (225)	2
Fire Creek	1.24	1.4 (4.5)	260 (850)	2
Lower Winifrede	1.73	2.0 (6.5)	185 (600)	2
Peerless	1.56	1.4 (4.75)	215 (700)	2
Sewell	2.55	1.2 (4.0)	105 (350)	2
Stockton	1.56	3.0 (10.0)	65 (220)	2
Stockton	1.99	3.0 (10.0)	75 (245)	2

NAp Not applicable.

MODELING OF CASTLEGATE SANDSTONE ESCARPMENT STABILITY

Prepared for

C.W. MINING COMPANY

Huntington, Utah

July 2001

By

MALEKI TECHNOLOGIES INC.
Consulting Mining & Geotechnical Engineers
South 5608 Magnolia
Spokane, WA 99223
(509) 448-7911
maleki.tech@worldnet.att.net

1. INTRODUCTION

This report with attachments was prepared in response to a request by C.W. Mining Co. that Maleki Technologies, Inc. (MTI), complete an analysis of the stability of the Castlegate Sandstone escarpment for two-seam mining in the Wild Horse Ridge reserves. The specific objectives and the scope of work were outlined by C.W. Mining and consisted of : (1) evaluate surface subsidence and the stability of the Castlegate Sandstone escarpments and (2) analyze the distances that unstable material may travel after mining.

C.W. Mining Co has used the room-and-pillar technique to extract three-seam reserves in coal fields on the Wasatch Plateau near Huntington, Utah (figure 1). These seams are located toward the base of the Blackhawk Formation and consist of the Tank, Blind Canyon, and Hiawatha. Within the present two-seam mining area (to the west of Bear Canyon), the Tank Seam and the Blind Canyon Seam are locally mined in descending and ascending order. Mining has taken place in conjunction with geotechnical monitoring in two panels in each seam (Maleki and others 1999, 2000). Because ground conditions between the present mining areas and the Wild Horse Ridge reserve are similar, existing data were used to estimate potential recovery and associated ground movement in the Wild Horse Ridge reserve. In addition, longwall mining experience and geotechnical data regarding mining in the vicinity of escarpments near mines operated by Energy West are available (Jones 1994; Maleki and others 2000). Attachment A contains technical papers dealing with geotechnical and escarpment assessments in the C.W. Mining and neighboring mines.

During the last decade, Energy West Mining Co., government agencies, academia, and MTI have directed a significant amount of research to developing predictive tools for assessing the stability of the Castlegate Sandstone escarpment. These studies were initiated to satisfy needs for escarpment stability and resource recovery. Escarpment instability is associated with the release of rocks from the escarpment face onto slopes below the escarpment. The government agencies responsible for the administration and protection of nonmineral resources in the area (U.S. Forest Service; Fish and Wildlife Service; Utah Division of Wildlife Resources; Utah Division of Oil, Gas, and Mining) are interested in the impact of escarpment failure on animal and plant life and public safety, The Bureau of Land Management (BLM), which administers and leases mineral resources, is responsible for ensuring that mining companies maximize resource recovery. Thus, the optimum goal has become one of meeting the requirement of resource recovery while minimizing mining impacts on the surrounding environment.

To achieve this goal, interested parties have recently focused on development of a predictive statistical technique so that the economic benefits of mining can be analyzed against the probability of escarpment failure and its influence on the surrounding environment. In cooperation with Energy West engineers, MTI has been developing this statistical model to assess the impacts of longwall mining on Corncob Wash and Newberry Canyon while characterizing escarpment conditions along Rilda Canyon reserves in detail. The model will be fine tuned after mining in Rilda Canyon is complete in the near future (appendix A). C.W. Mining's experience with room-and-pillar techniques will complement the existing escarpment stability database by allowing an evaluation of both longwall and room-and-pillar mining methods.

To evaluate escarpment stability in C.W. Mining operations, we have expanded the existing models for Energy West mines to typical sections in the Wild Horse Ridge while accounting for differences in geologic and mining conditions. Two known factors that are different in the Wild Horse Ridge reserve area are (1) use of room-and-pillar mining to the south near most of the escarpments instead of longwall mining and (2) the shorter distance between the sandstone escarpments and the Tank Seam. Room-and-pillar mining is associated with 50% less subsidence and thus is beneficial to escarpment stability. The shorter distance between the Tank Seam and the Castlegate Sandstone is detrimental. Overall, these two factors cancel out and the existing models and data from neighboring mines are judged to be applicable for this preliminary evaluation until more detailed monitoring data become available.

To the south where escarpments of interest to this study are exposed (figure 2), C.W. Mining is planning to extract the Tank and Blind Canyon seams using the room-and-pillar mining technique in a descending order. Two-seam longwall mining is planned to the north for the extraction of the Tank and Hiawatha seams. This longwall area is not overlain by Castlegate escarpments in most areas, excepting reserves within the initial four longwall panels. The escarpment study area consists of the eastern side of Bear Canyon and the areas located near the Left Fork of Fish Creek.

In response to a request by C.W. Mining, MTI has used its models and comparative analysis techniques to address escarpment stability along the Wild Horse Ridge study area for permitting purposes. C.W. Mining has the ultimate responsibility for analyzing and mitigating any safety issues related to escarpment instability. MTI does not offer any expressed or implied warranty with regard to public safety for any option selected and implemented by C.W. Mining for controlling ground movements.

The scope of this work consists of (1) a review of the geotechnical framework for the Wild Horse Ridge reserve, (2) a review of subsidence characteristics for two-seam reserves in western U.S. mines, (3) an evaluation of escarpment stability, and (4) estimates of the distances rocks travel.

Following the introduction, conclusions and recommendations are given in section 2, and the geotechnical framework for the C.W. Mining reserve is analyzed in section 3. Section 4 presents a description of subsidence characteristics in western U.S. mines and identifies typical subsidence factors and the angle of draw for C.W. Mining's geologic conditions. The stability of the Castlegate Sandstone escarpment is evaluated in section 5, and possible rock travel distances are discussed in section 6. Travel distances are estimated along a cross section of interest using the Colorado Rock Fall Simulation program and site-specific data from failures at Energy West and C.W. Mining operations.

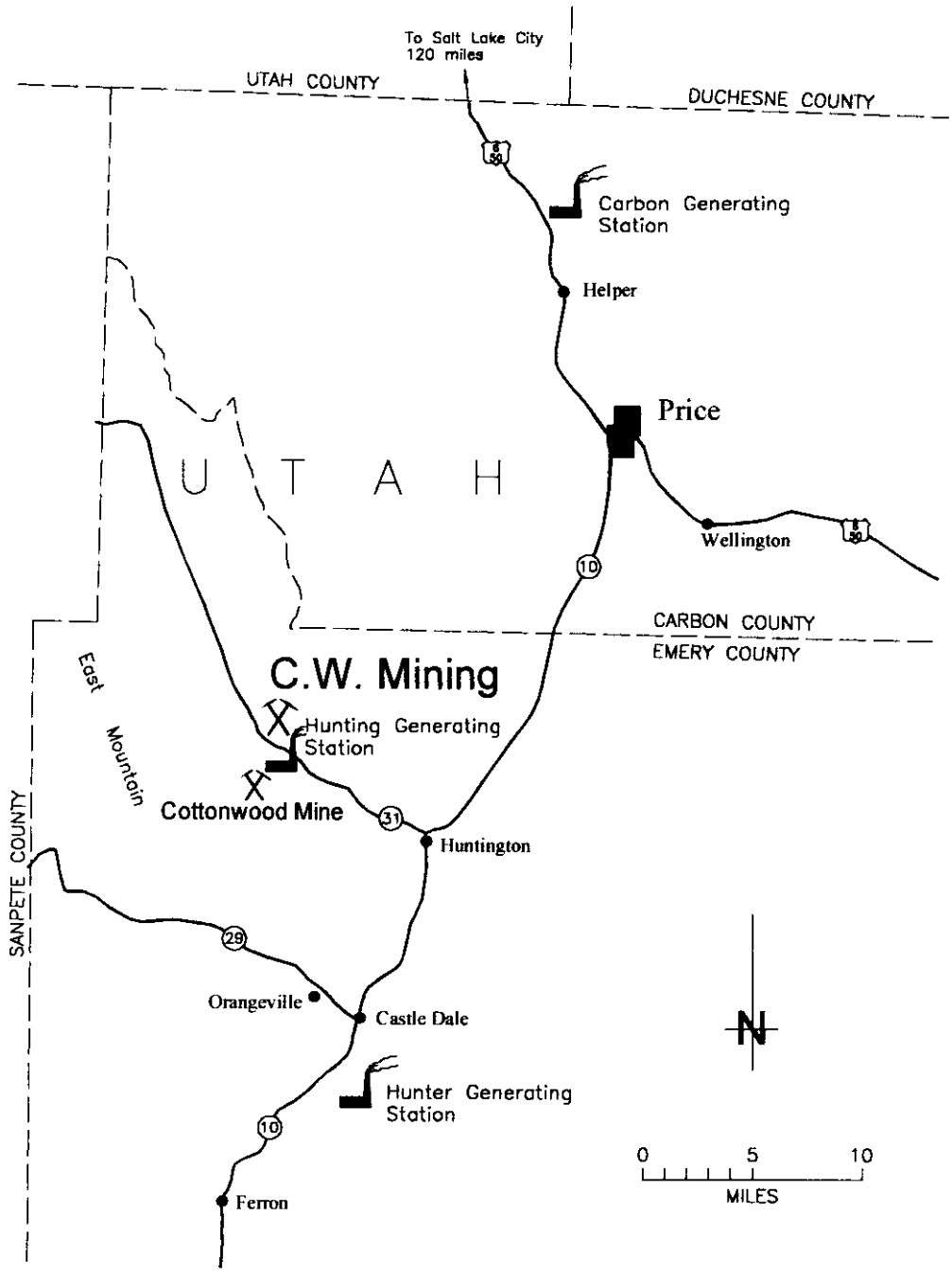

Figure 1. Project location map.

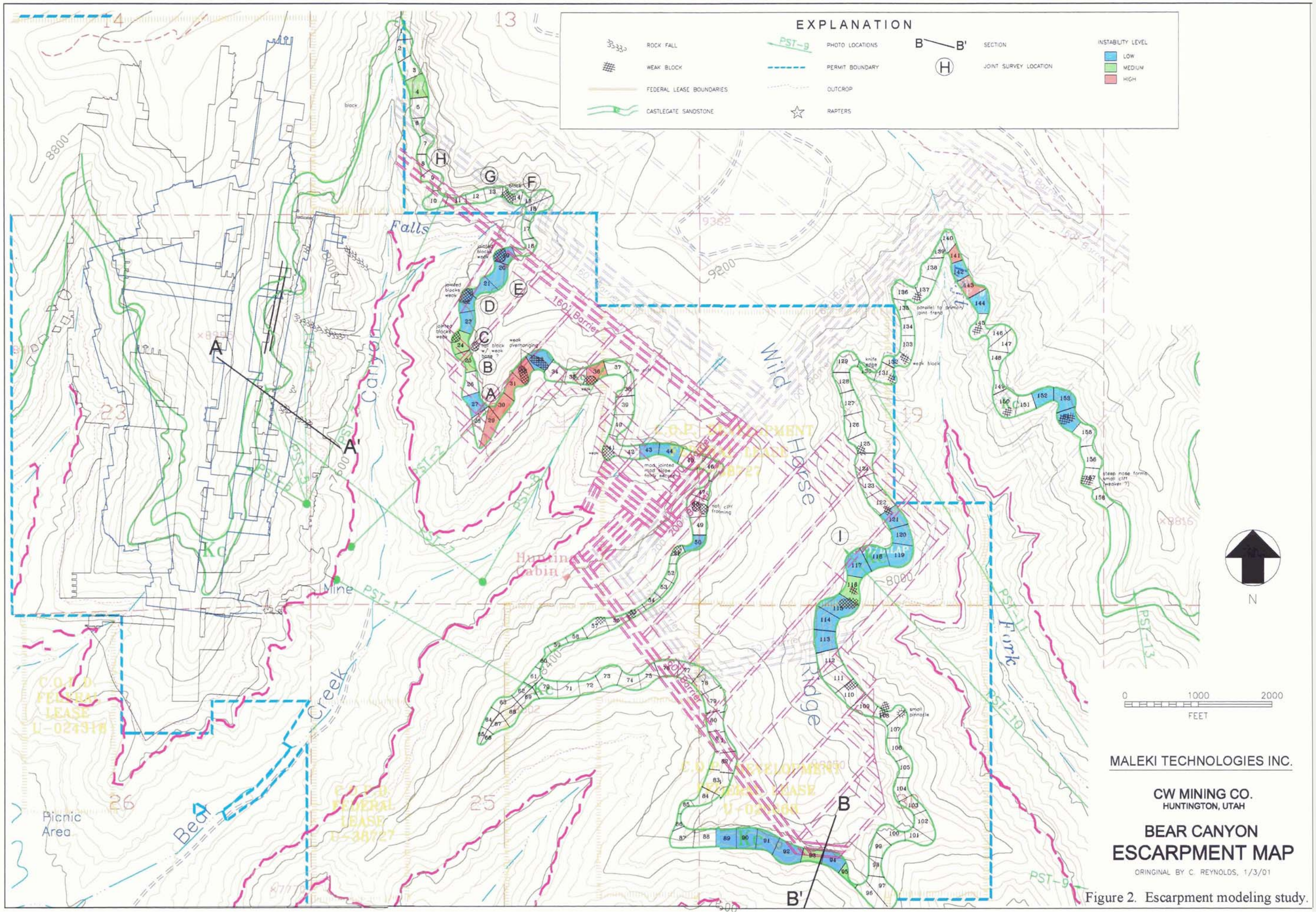

Figure 2. Escarpment modeling study.

2.0 SUMMARY AND CONCLUSIONS

In response to a request by C.W. Mining, MTI evaluated escarpment stability along the Wild Horse Ridge study area using the Rockrisk computer program. Travel distances along a cross section of interest were estimated using rock fall simulation programs and experience in the area. To assess escarpment stability, the area of interest was divided into 158 study cells. For each cell, escarpment and canyon geometries were characterized using base maps provided by C.W. Mining and field observations. An instability index was calculated using the Rockrisk computer program and decades of experience in the mine area.

Three instability levels indicating overall low to medium volumes of spalling are identified in figure 2. These instability levels are—

- Low (not likely to have significant spalling)
- Medium (likely to have spalling)
- High (very likely to have significant spalling).

Rock fall simulations along cross sections of interest are in general agreement with observations of mining-induced rock travel distances of 800 ft in the neighboring canyons. Maximum rock travel distances, however, vary according to canyon slope and frictional and rebound properties of rock blocks.

It is recommended that escarpment stability be monitored selectively, depending on safety and environmental needs. The data from such monitoring will also be important for verifying the assumptions of this study and for enhancing model capabilities when predicting the stability of the Castlegate Sandstone escarpment during multiple-seam room-and-pillar mining.

3.0 GEOTECHNICAL FRAMEWORK

3.1 Stratigraphy

The three coal seams of economic interest belong to the Blackhawk Formation, which is overlain by the Castlegate Sandstone and underlain by the Star Point Sandstone and the Mancos Shale (figure 3). Minable seams are the Tank and Blind Canyon to the south and the Tank and Hiawatha to the north of the Wild Horse Ridge reserves. These seams average 8, 11, and 6 to 8 ft in the study area .

The overlying, cliff-forming Castlegate Sandstone is a massive cross-bedded unit. It contains intermittent thin interbeds of shale, pebble conglomerate, and mudstone. Based on corehole data, this unit is 170 to 250 ft thick in the area; however, the actual exposed thickness is much less locally (as low as 50 ft). The exposed thickness of the Castlegate Sandstone escarpment is directly related to the stability of the escarpment and the volume of displaced rocks (Maleki and others 2000). The Price River Formation consists of numerous beds of cross-bedded sandstones with occasional interbeds of shale, pebble conglomerate, and mudstone.

The Blackhawk Formation is composed of interbedded deltaic mudstone and siltstone and is less resistant to weathering than the neighboring units. It is characterized by alternating slope- and cliff-forming units. This unit is approximately 750 ft thick.

The Star Point Sandstone consists of thick cliff-forming sandstone units separated by shales. It is light colored and is approximately 350 ft thick in the Wild Horse Ridge area. The Mancos Shale is a blue-grey color marine shale approximately 1,000 ft thick and is soft and well weathered.

3.2 Jointing

A 2-day geologic field mapping trip was conducted by MTI during the course of this study. The objective was to (1) characterize joint orientations in the study area and (2) estimate the exposed thickness of the Castlegate Sandstone. The latter was important in improving the historical data collected by Dwelling regarding the Castlegate Sandstone unit shown on the base map provided by C.W. Mining. During field mapping to the east, C.W. engineering staff collected data regarding the location and amount of failed rocks on the slopes to the west of Bear Canyon over the existing mine. Attachment B is a photographic record of the Castlegate Sandstone escarpment, and figure 2 shows the location of joint measurements (A to I).

The joint patterns at the Castlegate Sandstone horizon are similar across the study area. Joint trends are thought to coincide generally with joints found in the overlying Price River and underlying Blackhawk formations and are consistent with measurements collected on the Wasatch Plateau (Maleki 1988; Maleki and others 1999). Joints were typically within a few degrees from vertical. Three general orientations were identified (table 1).

NORTH HORN FORMATION	Interbedded sandstone, siltstone and mudstone with increasing proportions of limestone upwards in the formation.
PRICE RIVER FORMATION	Trough cross-stratified sandstone with subordinate amounts of pebble conglomerate and mudstone.
CASTLEGATE SANDSTONE	Trough cross-stratified fluvial sandstone.
BLACKHAWK FORMATION	Interbedded deltaic mudstone, siltstone, and economic coal seams.
TANK COAL SEAM	
BLIND CANYON COAL SEAM	
HIAWATHA COAL SEAM	
STARPOINT SANDSTONE	Massive, cliff forming marine sandstone.
MANCOS SHALE	Massive marine shale.

Figure 3. Typical stratigraphic column.

The most pronounced (primary) joint trend typically ranges between N10°E to N20°E (N15°E average). There may be a few degrees of counterclockwise rotation in this joint set as one moves to the east because measurements greater than N20°E were noted only on the west side of Wild Horse Ridge, and measurements less than N10°E were noted only on the east side of the ridge.

A less pronounced, secondary joint system trending S80°E to S90°E was also observed. This trend appeared to be generally consistent across the study area. The only variation in this trend was noted at location 1, but the data are too limited and inclusive.

A third joint set was noted having a N50°E to N55°E trend. This set was only observed in the east near Fish Creek Canyon. Spacing on this set is estimated to be greater than 10 ft due to its lack of occurrence or expression.

Apparent joint spacing appears to be controlled by confining stress. In outcrop, the primary and secondary joints are more apparent and appear more closely spaced at or near the points than in the head of drainages. Rocks in place often exhibit jointing at 10 to 15 ft spacings, but more broken rocks nearly always showed more closely spaced joints.

Table 1. Measured joint orientation and spacing for the Castlegate Sandstone within the Wild Horse Ridge reserve.

Location	Joint set 1	Set 1 spacing, ft	Joint set 2	Set 2 spacing, ft	Joint set 3
A	N16°-25°E	3-6	S75°-85°W	12	
B	N10°-17°E	3-6			
C	N15°-20° E	10-20 subordinated joints at 3			
D	N18°E	5	N85°-90°E	10	
E	N17°-28°E	3-8	S87°E		
F	N18°E	6-8	S82°E	7	
G	N15°E	2-6	S85°E	6-10	
H	N15°-23°E	1-6			
I	N13°-21°E	2-10	S77°-87°E	3-5	N52°E

2.3 Stress Field

Researchers from the former U.S. Bureau of Mines (USBM) and private industry have made a number of stress measurements in mines on the Wasatch Plateau. There are two stress measurements in proximity of C.W. Mining's operations (Maleki and others 1986). These measurements confirm that the far-field stress field is unremarkable. The horizontal stress is moderate and is less than 50% of the vertical stress magnitude. We anticipate a similar stress field at C.W. Mining operations based on observations of the lack of stress-induced stability problems (such as cutters) and an analysis of measurements in the existing reserve (Maleki and others 2000).

3.4 Mechanical Properties

Site-specific geologic and rock mechanics data are limited, although MTI has collected large amounts of information from adjacent properties. The available information on the values for mechanical properties for Blind Canyon coal measure rocks within the existing reserve is summarized in table 2. This data are in general agreement with rock testing results from East Mountain. Jones (1994) reports the results of rock testing and notes uniaxial compressive strengths ranging from 6,000 to 12,000 psi for sandstones and 12,000 to 16,000 psi for shales (mudstones). Similar to the rocks on the C.W. Mining property, the East Mountain units are generally stiff with Young's modulus ranging from 1.6 to 3.4 million psi.

Table 2. Laboratory mechanical properties test results from core testing

Rock type	Uniaxial compressive strength, psi	Young's modulus, million psi	Poisson's ratio
Coal	2,000-3,000	0.4 to 0.45	0.3 to 0.4
Shale	15,000 - 17,000	3 to 4	0.2 to 0.4
Sandstone	7,000-12,000	3 to 4	0.3 to 0.4

4.0 SUBSIDENCE CHARACTERISTICS

4.1 Subsidence Mechanisms

Surface subsidence occurs as a result of downward rock mass movement resulting from closure and collapse of mined-out excavations. Surface subsidence processes result in both vertical and horizontal displacement of rocks. Three major mechanisms of surface subsidence are associated with mining: formation of sinkholes, uniform settling, and formation of troughs. For the C.W. Mining plans using either high-extraction longwall mining or room-and-pillar mining with retreat, we expect trough subsidence.

Trough subsidence is characterized by the formation of a basin. Continuous fracturing from the mine to the surface usually does not occur, and there is much less abrupt surface fracturing than occurs during sinkhole subsidence. Trough subsidence creates an elliptical shape in plan view and extends over large areas, typically from hundreds to thousands of feet in breadth.

There are three subsidence phases associated with trough subsidence. These are shown in figure 4.

- The *subcritical phase* occurs immediately in the beginning when movement is in a small area at the center of the basin.

- The *critical phase* occurs as the basin area expands when the maximum extent of the downward movement is reached at the center. The critical excavation width is generally larger than 1.4 times the overburden thickness and is influenced by position and strength of competent layers within the overburden.

- The *supercritical phase* occurs as the basin develops a flat bottom. In this phase, the basin area continues to increase with the cave area, but subsidence will remain at the maximum extent attained in the critical phase.

Thus, the surface response to longwall mining activity, shown in figure 4, begins with the subcritical phase, then progresses to the critical phase, and finally to the supercritical phase. The subsidence process first shows effects on the surface as the upper strata bend. Tension (expansion) causes near-surface fractures to open and new ones to be created. Figure 4 shows how the middle portion of the excavation expands as subsidence continues, going through a cycle of first tension and then compression, which closes tension cracks. The tighter and more uniform the cave, the better the fracturing and closing process. Final subsidence shows an excavation with the middle portions lower in elevation, but back to a near-original state. Areas on the edge of the excavation basin are subjected to tensile strains.

Various geologic and mining factors affect the extent and magnitude of vertical displacements. The subsidence factor (ratio of total subsidence to mining height) depends on the bulking characteristics of overburden rocks. The angle of draw identifies the limits of vertical displacement beyond the excavation boundaries (figure 4).

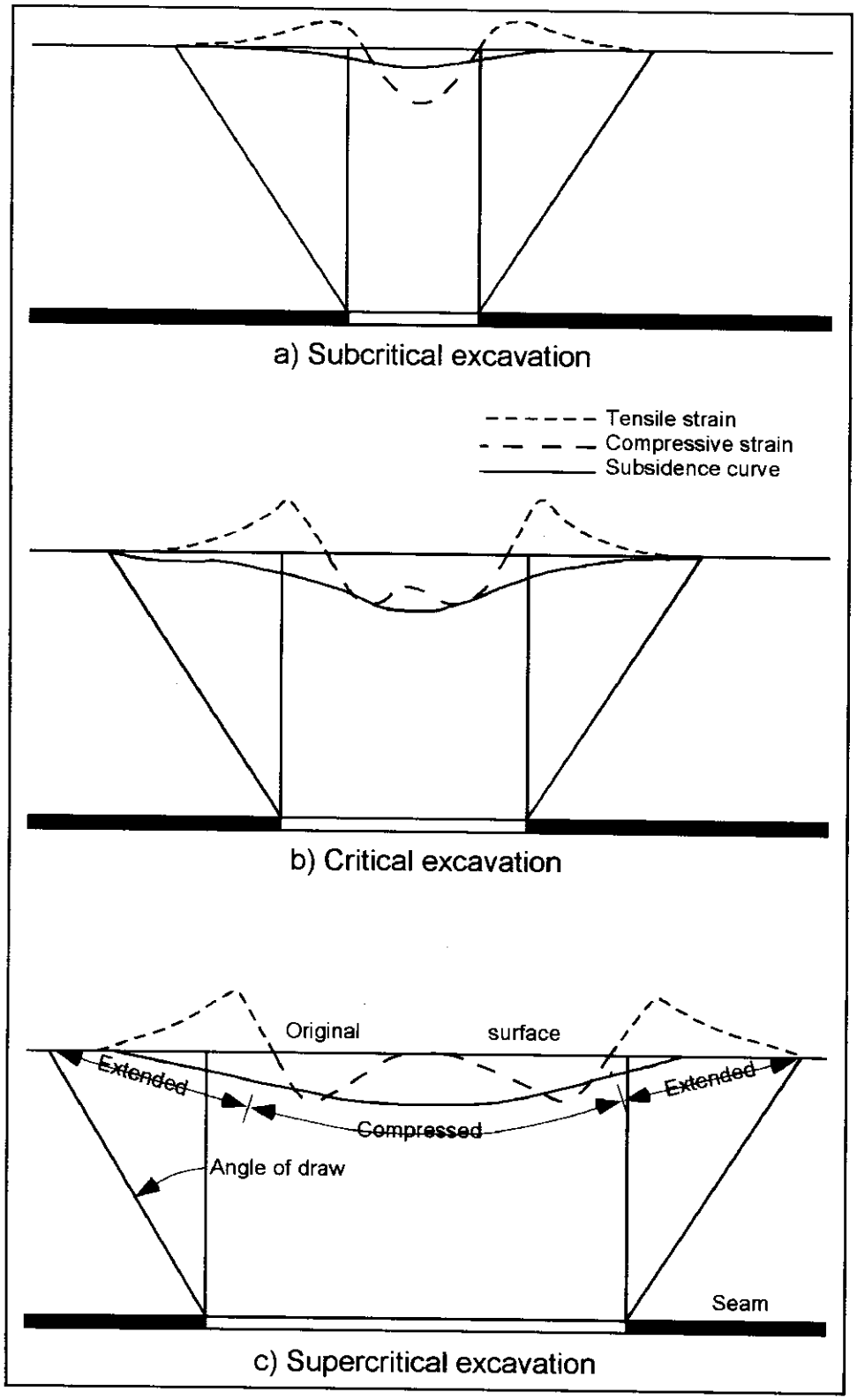

Figure 4. Schematic presentation of subsidence stages as extraction width is increased.

The best estimates for the extent and magnitude of subsidence for the two-seam mining conditions at C.W. Mining can be obtained by reviewing the results of long-term monitoring in Utah. The USBM implemented a comprehensive subsidence study over Energy West's two-seam longwall reserve from 1978 to 1989. The study monitored surface movements over four Blind Canyon and six Hiawatha panels. The study addressed angle of draw, subsidence factors for single and multiple-seam mining, and critical width. Similar to the Wild Horse Canyon reserve, the mining area was bounded by faults. Maximum subsidence was 68% to 72% of the extraction height for single- and two-seam mining conditions, respectively. This is in general agreement with other measurements in Utah that show a subsidence factor of 70%. The angle of draw ranged between 25° to 30° for single- and two-seam mining conditions, respectively. This reported maximum angle of draw is higher than average values for Energy West and other Utah operations (22.5° to 25°, Fejes 1985), but is significantly lower than values reported by the British National Coal Board (NCB) (1975).

Surface subsidence is expected to be limited to an angle of draw of 25° at the Wild Horse Ridge reserve. Maximum subsidence will occur toward the center of the mining area and will range from 5.6 to 13.3 ft for single- and two-seam longwall mining, respectively. For the room-and-pillar mining method, however, maximum subsidence can be much smaller because stumps and pillars are typically left in the gob for ground control purposes. Measurements by researchers from the USBM indicated lower subsidence factors (0.3 to 0.4) (Jones and Kohli 1995; Magers 1993). Applying this subsidence factor to C.W. Mining conditions will result in maximum movement of 2.8 to 6.6 ft under single- and two-seam mining conditions.

Standard subsidence engineering parameters, such as angle of draw and subsidence factor, are useful for estimating expected deformation and for comparing expected ground behavior in different mines under flat topography. An angle of draw of 15° has been used in some situations by the BLM as a simple criterion for balancing the need for resource recovery and protection of sandstone escarpments in Utah mines. Considering the variations in topography over Utah coal mines, the angle of influence is a better indicator of escarpment stability given the geologic and geometric conditions in Utah (Maleki and others 2000) (attachment A). This angle measures the position of the escarpment with respect to full-extraction mining limits (figure 5).

4.2 Rock Movement Associated with Escarpment Instability

Full-extraction mining at the Wild Horse Ridge will reach the supercritical phase with tensile strains forming over the boundaries of mining blocks. For escarpment edges that are near-parallel to panel boundaries and/or joint orientations, instability may result because of the formation of tension cracks at the surface and shear failure at the bottom interface with the Blackhawk Formation. This process contributes to lateral translation of the escarpment, depending on the location of the escarpment with respect to mining limits, escarpment shape (convex or concave), effective height of the escarpment, and the slope of the canyon (Maleki and others 2000). Instability of the escarpment results in release of rocks from the escarpment face onto slopes below the escarpment. The travel distance is influenced by the size of the rocks, surface geometry, and roughness conditions. Travel distances can be calculated using rock fall simulation programs and/or measurements from similar ground.

Two sources provide information on the actual distance traveled by rock on the failure of the Castlegate Sandstone escarpment: (1) extensive measurements taken at Energy West's longwall

operations and (2) limited measurements taken near the existing room-and-pillar retreat mining areas to the west of Bear Canyon. Measurements at the Energy West operations indicate that travel distances were approximately 800 ft (Semborski 2000), a distance that is in agreement with estimations at C.W. Mining. In contrast to the Energy West experience, however, the volume of failed rocks is significantly less at the C.W. Mining reserves. This assertion is made based on inspection of escarpment stability along Bear Canyon by C.W. engineering and MTI staff (figure 2) after the completion of mining in the Blind Canyon and Tank seams. Similar to the Energy West experience, instability is confined mostly to concave areas, but the volume of failed rocks is lower.

An estimate of the volume of failed rocks was obtained by C.W. Mining staff using field observations over the existing mine. Estimated volumes for 100-ft-long study cells are between 1 to 10,000 ft^3. This volume reflects changes resulting from mining the Tank Seam. Many areas have been fully undermined in two seams without significant impact on escarpment stability. The lower bench of the Castlegate Sandstone (20 ft high) experienced skin failure during extraction of the Tank Seam. The diameter of the failed rock averaged 2 ft and ranged from 6 in to 6 ft in diameter.

Following are factors that favor the stability of the Castlegate escarpment at the Wild Horse Ridge reserves.

- The mine layout is oriented 45° from the direction of major joints, a factor that is favorable to escarpment stability. This is because mining can activate movements along preexisting joints if they are parallel to panel orientations, particularly at shallow depths.

- The Blind Canyon Seam is significantly thinner than in the existing mine (11 ft on average in comparison to 16 ft). The lower total extraction results in lower subsidence, lower tensile strains, and less potential for escarpment instabilities.

- The planned use of the room-and-pillar mining method near most of the escarpments is beneficial because this method is associated with approximately 50% lower subsidence than full extraction longwall mining (subsidence factor of 0.3-0.4 in comparison to 0.7). The lower subsidence translates into lower surface strain and thus less potential for escapement instability. However since the Tank Seam is located closer to the Castlegate Sandstone, overall, we expect slightly less deformation than calculated for similar conditions in the Energy West longwall operations mining the Blind Canyon Seam.

- The exposed thickness of the Castlegate Sandstone is lower (50 to 200 ft), particularly near Fish Creek Canyon, in comparison to full exposure at neighboring mines.

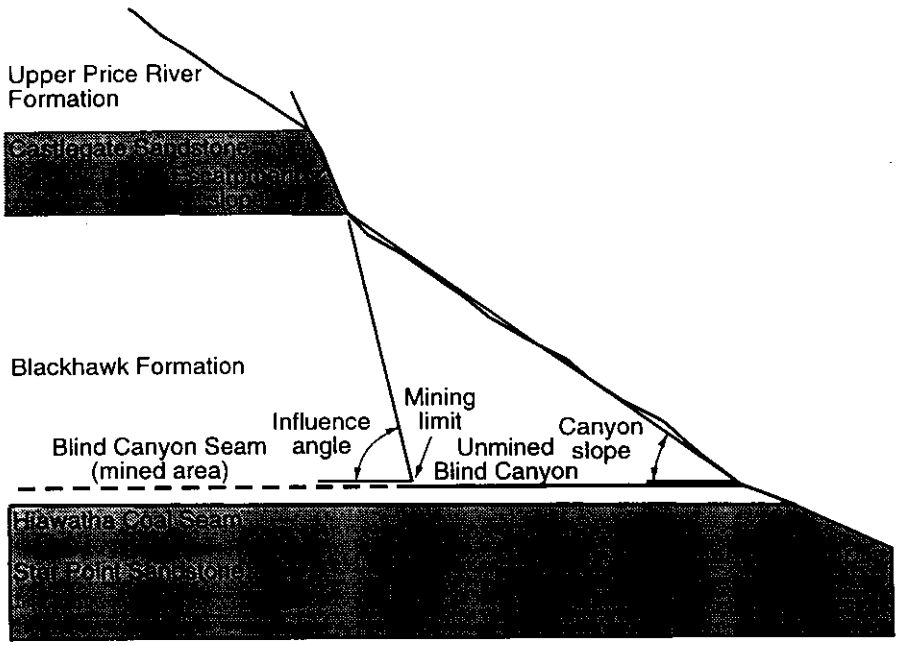

Figure 5. Schematic presentation of pertinent geologic and geometric factors.

5.0 CASTLEGATE SANDSTONE STABILITY

Based on principles of subsidence engineering, geologic investigations, and data available from escapement monitoring on the Wasatch Plateau, we expect ground reactions to two-seam room-and-pillar mining in the C.W. Mining reserves to be similar to the mechanisms studied in the neighboring Energy West mines. Thus, to evaluate Castlegate escarpment stability, we use the model developed for the Energy West operations while using site-specific geologic and geometric conditions obtained for the Wild Horse Ridge reserve.

In this section, we will briefly review the development of this statistical model, identify important variables that influence escarpment stability, and finally, use the model to estimate the potential for escarpment instability in the Wild Horse Reserve study area.

5.1 The Escarpment Stability Model

MTI has used multiple-regression analysis techniques and a wealth of data collected over many years on geology, mining, and escarpment stability to develop this model. An index related to the volume of failed rocks (called the failure index) is used as the response variable after several other factors were considered, including measurements of surface deformation and frequency of mining-induced surface fractures. Geologic and geometric variables were obtained along miles of escarpment exposure at 70 study locations. Regression analysis of data for the first 29 study locations, which had been fully undermined, showed that surface topography (or the shape of the escarpment) played a critical role in influencing escarpment stability.

More recent regression analysis of data from 70 study locations identified several other important geologic and mining factors that influence the stability of the sandstone escarpment. These are—

- Thickness of the Castlegate sandstone
- Angle of mining influence (measuring the position of the escarpment ledge in comparison to full-extraction mining limits), and
- Canyon slope.

The failure index is higher at locations where the canyon slope is steeper (figure 5), the Castlegate exposed thickness is higher, and full extraction is completed beneath and beyond the escarpments. It is interesting to note that joint characteristics are not an influencing factor where an area is fully subsided.

5.2 Escarpment Instability Level

To characterize geologic and mining factors along the Wild Horse Reserve study area, we used field estimates of exposed escarpment thickness, inspected available borehole logs, and used multilayer maps prepared by the C.W. Mining staff (figure 2). The Castlegate escarpment was divided into 158 study cells, each approximately 200 ft wide.

To evaluate escarpment stability, we calculated the failure index for each study cell, given canyon slope, thickness of exposed escarpment, and influence of mining angles. Attachment C presents a

histogram frequency diagram for these parameters. Results were summarized in figure 2 in terms of three instability levels:

- Low (not likely to have significant spalling),
- Medium (likely to have spalling), and
- High (very likely to have significant spalling).

Considering the accuracy that can be achieved for calculating geologic and geometric factors using existing overlays and field observations, the proposed instability levels provide a convenient means of assessing the potential and severity of escarpment instability. The areas identified as highly unstable will benefit from monitoring. Monitoring should also be considered at other areas, depending on functional requirements for the canyon and safety and environmental concerns. For instance, we recommend limited monitoring near study cells 78-79 because of a lack of in-depth geotechnical data, among other factors.

6.0 SIMULATED TRAVEL DISTANCES

In section 3.2, we provided a discussion of travel distances for failed rocks using experience from both existing (west Bear Canyon) and neighboring mines. In this section, we will provide estimates of travel distances by using the Colorado Rock Fall Simulation program. For this, we will use the program (1) to simulate rock movements along an existing failure path (section A-A', west Bear Canyon) for calibration of the model and (2) to estimate travel distances along a selected location in the southern Wild Horse Ridge reserve area (cross section B-B', figure 2).

6.1 Background, Colorado Rock Fall Simulation Program

The Colorado Department of Transportation in collaboration with the Colorado School of Mines developed a computer program (CRSP) for simulating rock movement along slopes and canyons. The program is based on detailed observations of rock falls, as well as considerations of the kinematics of a rolling block. To estimate a statistical distribution of travel distances, the program uses canyon profile, rebound, and friction characteristics of the canyon floor and the kinematic energy of a selected number of rocks rolling down the canyon.

The program has been extensively used by the Colorado Department of Transportation, as well as by Energy West, with good success. Based on extensive simulations and back-analyses of travel distances at the Energy West operations, it is possible to estimate travel distances reliably for similar conditions at the neighboring C.W. Mining operations. To calculate travel distances, one needs to divide the travel path into segments, each having specific frictional and rebound characteristics. To get a range of possible travel distances, the program simulates movements of a number of rock blocks and creates a histogram of travel distances, velocities, and rebound heights at any specific analysis point. The size of a rock block is an important parameter and can be easily estimated by using either joint spacing at the source or by measuring the maximum size of rock that has traveled down failed slopes.

6.2 Simulated Rock Movements

Figures 6 and 7 present the results for west Bear Canyon and Wild Horse Ridge locations A-A' and B-B', respectively. Attachment D includes additional information regarding travel distances, block velocity, and rebound heights. These simulations are based on 25 spherical rock blocks 6 ft in diameter. This diameter was selected conservatively, considering both the actual spacing of joints at the source and observed sizes of rolled blocks along the west Bear Canyon location (.5 to 6 ft).

Figure 6 is in general agreement with observations of travel distances, considering the accuracy of topographic data near section A-A'. This section consists of nine mostly gently dipping segments, and thus the calculated travel distances are limited to 770 ft from the source (Castlegate Sandstone). The estimated travel distances are larger for steeper canyon slopes at the location of B-B', which can reach a maximum distance of 1,200 ft from the base of the Castlegate Sandstone. Figure 7 presents rock travel trajectories along the 13 segments forming this profile.

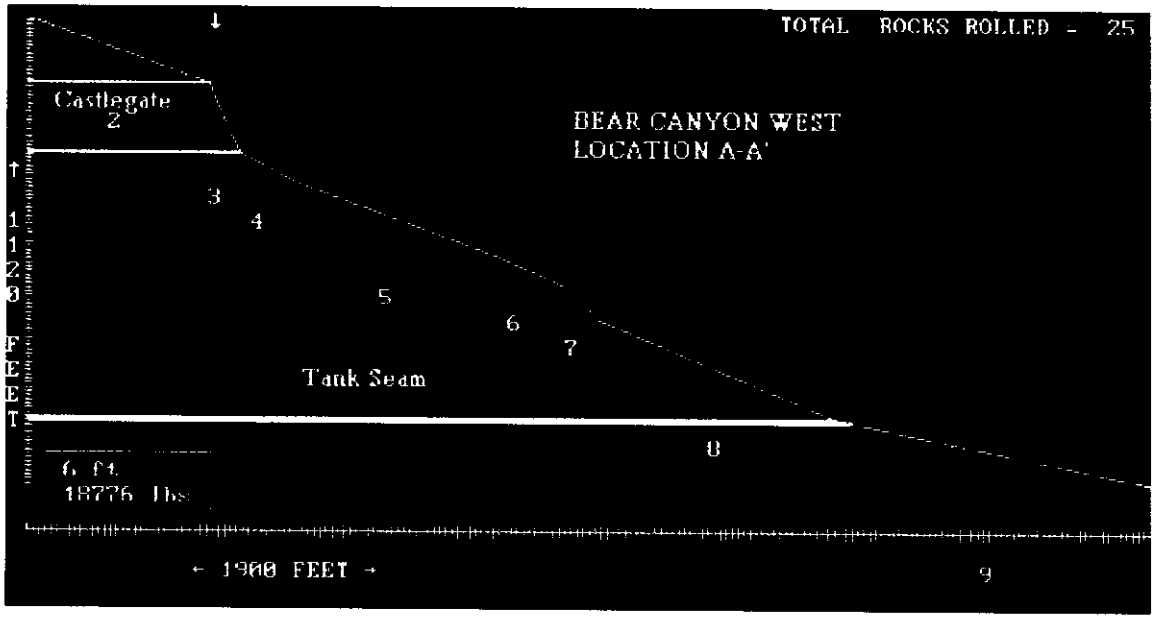

Figure 6. Simulated rock travel distances and trajectories for section A-A' (figure 2).

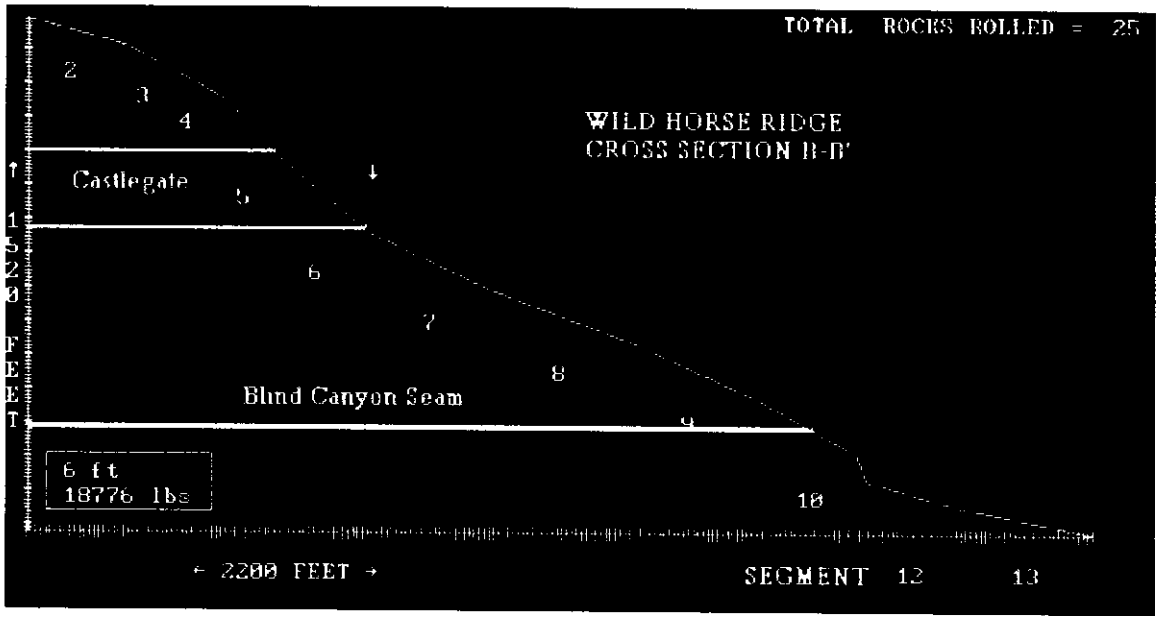

Figure 7. Simulated rock travel distances and trajectories for section B-B' (figure 2).

References

Jones R.E., 1994, Investigation of Sandstone Escarpment Stability in the Vicinity of Longwall Mining Operations. M.S. thesis, Department of Mining Engineering, University of Utah.

Jones, T.Z., and K.K. Kohli, 1995, Subsidence Over a Room-and Pillar Panel in Southern West Virginia. USBM contract # JO328010.

King, R., 1980. Evaluation of Surface Subsidence and Horizontal Strain at York Canyon Mine, New Mexico. M.S. thesis, Colorado School of Mines.

Maleki, H., 1988, Ground Response to Longwall Mining--A Case Study of Two-Entry Yield Pillar Evolution in Weak Rock. *Colorado School of Mines Quarterly*, vol. 83, no. 3.

Maleki H., K. Fleck, C. Semborski, and C Pollastro, 2000, Development of a Statistical Technique for Assessing Sandstone Escarpment Stability. 19th International Conf. On Ground Control, WV University, 2000.

Maleki, H., J. Owens, W. Howie, 1999, An Overview of Geomechanics Safety Research on Mobile Roof Supports. 17th Intern. System Safety Conf., Aug. 16-21, 1999, Orlando, FL.

Magers, J, A., 1993, Surface Subsidence Over a Room-and-Pillar Mine in the Western United States. U.S. Bur. Mines IC 9347.

National Coal Board (NCB), 1975. The National Coal Board's Subsidence Engineering Handbook.

Semborski, C, 2000, personal communications.

Shea-Albine ,1992, Effects of Longwall Subsidence on Escarpment Stability. Proc., 3rd Workshop on Surface Subsidence Due To Underground Mining. WV University.

SPSS, 1995. Statistical Packages for the Social Sciences, Chicago, IL.

ATTACHMENT A

COPIES OF PERTINENT PUBLICATIONS

19th CONFERENCE ON GROUND CONTROL IN MINING

DEVELOPMENT OF A STATISTICAL TECHNIQUE FOR ASSESSING SANDSTONE ESCARPMENT STABILITY

Hamid Maleki, Principal
Maleki Technologies, Inc.
Spokane, WA

Kenneth Fleck
Chuck Semborski
Carl Pollastro
Larry LaFrentz
Energy West Mining Company, Huntington, Utah

ABSTRACT

During the last decade, a significant amount of research has been conducted by Energy West Mining Company, government agencies, academia, and consulting companies to develop predictive tools for assessing the stability of the Castlegate Sandstone, which is found approximately 250 m above multiple-seam coal reserves. Energy West Mining uses longwall mining techniques in its operations near Huntington, Utah, and these studies were initiated to satisfy requirements for maintaining the stability of the Castlegate Sandstone and resource recovery.

In this study, the authors have used multiple-regression analysis techniques and a wealth of data collected over many years on geology, mining, and escarpment stability. The volume of failed rocks is used as the response variable after several other factors were considered, including measurement of surface deformation and frequency of mining-induced surface fractures. Geologic and geometric variables were obtained along 3.7 km of escarpment exposure at 130 study locations. Regression analysis of data for the first 29 study locations, which had been fully undermined, showed that surface topography played a critical role in influencing escarpment stability. Preliminary regression analysis results from 70 study locations identified several other important geologic and mining factors that influence the stability of the sandstone escarpment. These are canyon slope, sandstone thickness, and mining influence angle.

INTRODUCTION

This paper presents progress being made in developing a predictive statistical model as a tool for assessing the stability of escarpments in the vicinity of Energy West's longwall operations near Huntington, Utah. Such models are ideal for probabilistic risk analysis so that the economic benefits of extracting coal reserves can be compared to the likelihood of escarpment instability.

There are two methods routinely used by engineers and researchers to help predict what conditions will be in the future: statistical and computational. Starfield and Cundall (1) identify rock mechanics problems as "data-limited," that is, one seldom knows enough about a rock mass to use computational methods unambiguously. These methods, however, are extremely useful for studying failure mechanisms and testing different hypotheses about the cause of failure. Statistical methods, on the other hand, are uniquely capable of being applied where there are good data, but a limited understanding of certain phenomena, such as the mechanism of escarpment failure (toppling, pure translation, or a combination of these and other mechanisms).

Various investigators from both the U.S. government and universities have used computational techniques for analyzing surface subsidence and escarpment failure mechanisms. The results are in general agreement with studies in the Sydney Basin of Australia (2). A combination of two-dimensional, boundary-element (3), finite-element (4) and discrete-element formulations was used in the U.S. studies. To overcome the limitations of using small-strain, continuum finite-element methods, a hybrid approach was used. In this approach, finite-element deformation was imposed on a detailed discrete-element model of the escarpment and the mudstone foundation and incorporated both horizontal slip planes and vertical joints (5). Researchers from the U.S. Bureau of Mines (6) also completed a few preliminary three-dimensional, finite-element modeling studies. While successful in analyzing failure patterns and mechanisms, these studies have clearly identified the limitations of numerical modeling techniques in matching measured surface deformation because of the data-limited nature of these modeling efforts.

Statistical and semi-analytical techniques have been used alternatively for many rock mechanics problems where there are good data but limited understanding of some natural phenomena, such as rock bursts (7), creep (8), and ground support (9-10). Australian researchers (11) have used the results of comprehensive field investigations with other data analysis techniques to identify the influence of individual factors (such as horizontal movements and cliff heights) on cliff stability. Multivariate statistical evaluations of these results are awaiting additional investigation.

The technical approach in this study consisted of incorporating and digitizing data on geology, mining, and escarpment stability collected over many years in several mining areas into a statistical model. This model is being used by mine personnel for routine assessments of escarpment stability in new mining areas even as new data are being incorporated to enhance model predictions. Model input consists of geologic and mining conditions, including escarpment geometry, orientation of joints with respect to the escarpment, joint density, joint continuity, and mining influence angle.

The authors implemented the first phase of the study during 1997, collecting detailed geologic and mining factors at 29 study locations, each 30 m wide. Phase 1 consisted of (1) characterization of geologic, mining, and response variables in the study area and (2) analysis of patterns seen in the data and identification of important variables through the use of multilinear regression models. In the Corncob Wash study area, which is the primary focus of this paper (figure 1), the 1,000-m-long escarpment exposure provided the opportunity to observe surface effects and evaluate factors that contributed to escarpment instability after mining had been completed. In the Rilda Canyon study area, premining conditions were characterized in detail, and postmining conditions will be observed in the near future as both the Blind Canyon and the Hiawatha seams are mined.

During the second phase of the project, post-mining conditions at 41 study locations in the South Newberry study area were characterized along the 1,200-m-long escarpment. Additional analyses are planned when mining in the Rilda Canyon is complete (phase 3).

CHARACTERIZATION OF GEOLOGIC, MINING, AND RESPONSE VARIABLES

The first step in developing predictive statistical models was to create suitable numerical values that expressed geologic and mining conditions in the study area (figure 1). The second step was to reduce the number of independent variables by combining some existing variables into new categories and identifying highly correlated independent variables. Reducing the number of variables is needed when there are too many variables to relate to the number of data points. The presence of highly correlatable variables influ-

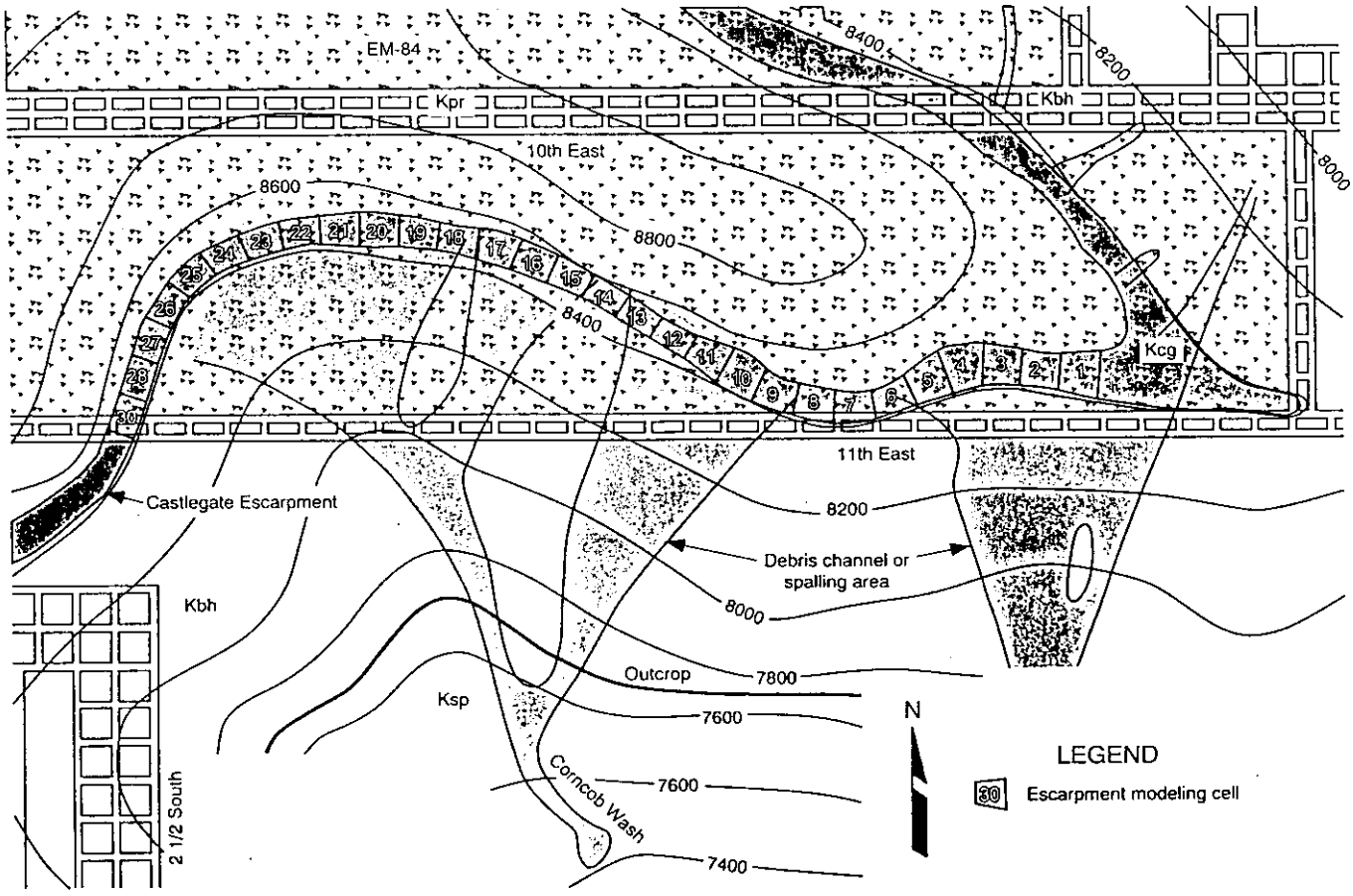

Figure 1. Corncob Wash study area

ences what procedures are selected for multiple-regression analyses. The third step was to develop a multivariate regression model and identify significant factors that contribute to escarpment stability.

The study areas were partitioned into cells approximately 30 m wide. This resulted in 29 cells for the Corncob Wash study area and 41 cells in the South Newberry area. The authors estimated geologic, mining, and response variables for individual cells based on field mapping, examination of borehole logs, and aerial photographs obtained before and after mining. Table 1 presents statistical information, including mean and standard deviation for the first 29 cells in the Corncob Wash study area.

Most variables are self explanatory. A brief description of some of the variables (in italics) is given below.

- *Joint sets 1 and 2* are the primary and secondary persistent joint sets mapped in each area.

- The *angle between joint sets and an escarpment* can influence escarpment stability, a hypothesis that is based on observations of subsidence-related fracturing in the western United States (12). Using this hypothesis, an escarpment may have a higher probability of failure where the angle between joints and the escarpment (or mining boundaries) is small (0° to 30°).

- The *excavation width-to-depth ratio* is similar to a subsidence engineering term (13) that relates the total width of an excavation to the average depth of cover over the panel of interest. This ratio measures changes in subsidence mode as excavations are widened during mining of successive panels. As the ratio approaches 1.4, a supercritical subsidence stage is reached.

- Based on a review of mining maps and experience in Newberry Canyon (4-5), *escarpment shape* (convex or concave) appears to influence escarpment stability and thus is included as a geologic variable. Observations in Newberry Canyon by researchers from the University of Utah indicate that virtually all of the failures occurred in a concave portion of the escarpment. A hypothesis was that natural erosion of the escarpment took place at a faster rate at these locations as a result of greater premining joint density (5).

Table 1. Population statistics for the Corncob Wash study area

Variable	Mean	Standard deviation
A. Geologic:		
Angle between joint set 1* and escarpment, deg	27	27
Angle between joint set 1 and longwall face, deg	61	24
Angle between joint set 2* and escarpment, deg	57	26
Angle between joint set 2 and longwall face, deg	19	12
Joint set 1 spacing, m	9.5	12
Joint set 2 spacing, m	9.5	14
Horizontal continuity for joint set 1, m	6.4	6.5
Horizontal continuity for joint set 2, m	8.5	7.6
Vertical continuity for joint set 1, m	4	3.6
Vertical continuity for joint set 2, m	2.4	0.8
Joint set 1 and escarpment index	1.1	1.7
Joint set 1 and longwall index	1.2	1.8
Joint set 2 and escarpment index	0.2	0.8
Joint set 2 and longwall index	0.4	1.2
Joint set 1 index	3.9	5.2
Joint set 2 index	0.9	1.0
Erosion under escarpment index	0.1	0.3
Escarpment shape index	0.9	0.3
Canyon slope, percent	80	9
Escarpment slope, percent	218	45
Thickness of Castlegate Sandstone, m	76	6.4
Seam-to-sandstone distance, m	237.8	5.5
B. Mining:		
Influence angle, deg	71	11
Excavation width-to-depth ratio	2.5	0.6
C. Response:		
Failure index	1.4	0.8

- The *influence angle* is defined as the angle from a horizontal plane and a line from the mining limit to the base of the Castlegate escarpment (figure 2). This angle is 90° where the escarpment is directly above the mining limit and over 90° in areas outside the mining limit.

Several indexes were created to combine joint data from various data sets into a single variable

- The *joint set I and escarpment* index (or INJSiE) took values 0 to 4, depending on the amount of deviation between a joint set and the escarpment (figure 3).

- The *joint set I and face* index (or INJSiF) took values 0 to 4, depending on the amount of deviation between a joint set and a longwall face.

- The *joint set I* index is a cumulative measure of joint orientation and block size —

  INJSiE + INJSiF + horizontal continuity × vertical continuity ÷ spacing^2 where INJSiE = the joint set I and escarpment index and INJSiF = the joint set I and face index.

- The *erosion under escarpment* index equals values of 1 and 0, depending whether the area under the escarpment at the particular cell is eroded or not.

- The *escarpment shape* index equals values of 1 and 0 for concave and convex escarpment geometries.

- The *failure* index equals values of 0, 1, and 2, depending on the estimated volume of failed material within the cell of interest. The failure index was selected from among other response variables, including tensile cracking and vertical and horizontal movement on the surface, because it best describes the stability of the escarpment and can be estimated for each cell. The failure index is used as a dependent variable in regression analyses.

TRENDS IN DATA AND IMPORTANT VARIABLES

Because there are many variables that could influence the stability of the escarpment (table 1), it is important to study trends in the data and use prudent statistical procedures that take into account the interrelationships among independent variables. To study these relationships, a bivariate correlation matrix was constructed to measure the linear correlation among geologic, mining, and response variables. The correlation matrix includes correlation coefficient, number of data points, and two-tailed significance tests. The correlation coefficient (r) indicates the strength of linear relationships between any pair of variables.

Based on a review of the correlation matrix, the authors found fair correlation between the failure index variable and several independent variables, as well as among some independent variables. For example, the correlation coefficients between the failure index variable and the escarpment shape and influence angle variable are 0.58 and -0.48, respectively. However, escarpment shape and influence angle happen to have fair correlation as well (correlation coefficient equals -0.48). Thus, there is an interrelationship among the independent variables that can be taken into account using step-wise inclusion of these independent variables while conducting multiple-regression analyses (7).

To identify important factors that contribute to escarpment stability, a multiple-regression analysis was used. Escarpment stability was estimated using the failure index as the dependent variable. The multilinear regression procedure consisted of entering independent variables one at a time into the equation using a forward selection method (14). In this method, a variable is entered into the equation using the largest correlation with the dependant variable. If a variable fails to meet entry requirements, it is not included in the equation. If the first variable meets the criteria, the second variable with the highest partial correlation is

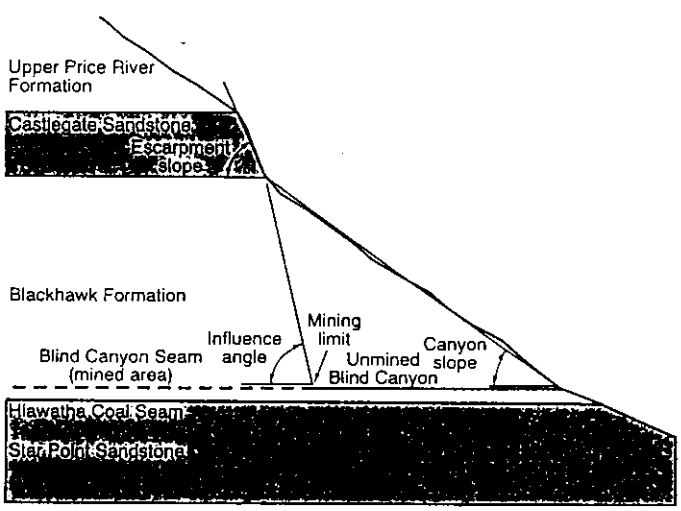

Figure 2. Mining and escarpment geometry

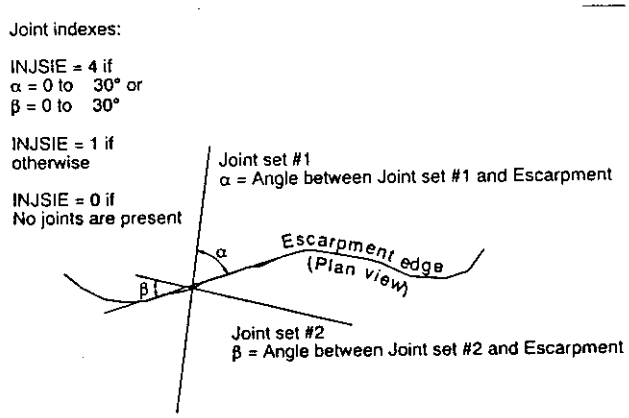

Figure 3. Escarpment geometry and geological discontinuities

then selected and tested for entering into the equation. This procedure is very good when there are hidden relationships among the variables. The multiple correlation coefficient, R, which is a measure of goodness-of-fit, for the last step is 0.68.

Based on an examination of standardized regression coefficients for the first 29 cells, the following variables best explain variations in the failure index.

- *Escarpment shape* index. The lower the escarpment shape index, the smaller the failure index. This is in agreement with experience in Corncob Wash and other areas where convex areas have historically remained stable when undermined.

- *Joint set 2 and escarpment* index. This is the only geologic variable that contributes to goodness-of-fit in a mathematical sense. Because there are very few secondary joints mapped in the Corncob Wash study area, it is not clear to the authors how relevant this factor is to escapement stability.

New data from the South Newberry Canyon have recently become available and were incorporated in the model during phase 2. Preliminary results using a total of 70 cells have identified several other important mining and geologic factors, including *canyon slope*, *thickness of Castlegate Sandstone*, and *mining influence angle*. The failure index is higher at locations where the canyon slope is steeper, the Castlegate escarpment is thicker, and full extraction is completed beneath the escarpments.

CONCLUSIONS

Based on the regression model and observations of escarpment behavior prior and after longwall mining, the authors have identified important factors influencing escarpment stability. It is shown that surface topography (escarpment shape) played a critical role in influencing escarpment stability and that convex escarpment geometries remained stable after the area had been undermined. Work is in progress to enhance existing models by including data from other study areas that have different geologic, geometric, and stability conditions. Preliminary results from a new study area (South Newberry) have identified several other important factors, including canyon slope, thickness of the Castlegate Sandstone, and mining influence angle.

REFERENCES

1. Starfield and Cundall 1988. Towards a Methodology for Rock Mechanics Modeling. *Inter. J. Rock Mech. Min. Sci.*, v. 25, no. 3, pp. 99-106.

2. Pells, P.J., J.C. Braybrook, J. Mong, and G. Kotze, 1987. Cliff Line Collapse Associated with Mining Activities. Slope Stability and Stabilization. Balkema.

3. Ahola, M., 1990. Geomechanical Evaluation of Escarpments Subjected to Mining-Induced Subsidence. *Rock Mechanics Contributions and Challenges: Proceedings of the 31st U.S. Symposium*, ed. by W. A. Hustrulid and G. A. Johnson (CO Sch. Mines, Golden, CO, June 18-20, 1990). Balkema, pp. 129-136.

4. Jones R.E., W.G. Pariseau, V. Payne, and G. Takenaka. 1990. Sandstone Escarpment Stability in the Vicinity of Longwall Mining Operations. *Rock Mechanics Contributions and Challenges: Proceedings of the 31st U.S. Symposium*, ed. by W. A. Hustrulid and G. A. Johnson (CO Sch. Mines, Golden, CO, June 18-20, 1990). Balkema, pp. 555-562.

5. Jones, R.E., 1994. Investigation of Sandstone Escarpment Stability in the Vicinity of Longwall Mining Operations. MS thesis, Dept. of Mining Engineering, University of Utah, Salt Lake City, UT.

6. Shea-Albine, V., 1992. Effects of Longwall Subsidence on Escarpment Stability. Proc., 3rd Workshop on Surface Subsidence Due To Underground Mining. WV Univ

7. Maleki, H., and B. White, 1997. Geotechnical Factors Influencing Violent Failure in U.S. Mines. *International Symposium on Rock Support: Applied Solutions for Underground Structures*, ed. by E. Broch, A. Myrvang, and G. Stjern (Lillehammer, Norway, June 22-25, 1997). Pp. 208-221.

8. Maleki, H., and L. Chaturvedi, 1997. Prediction of Room Closure and Stability of Panel 1 in the Waste Isolation Pilot Plant. Presentation, ISRM Int. Symp. and 36th U.S. Rock Mech. Symp., June 29-July 2, 1997. Abstract, paper 186, *Int. J. Rock Mech. Min. Sci. & Geomech. Abstr* 34:3-4: (Available on CD-ROM.)

9. Parson, P., and D. Dahl, 1971. A Study of Causes for Roof Instability in the Pittsburgh Coal Seam. Proceedings of the 7th Canadian Rock Mechanics Symposium (Edmonton, AB, Mar. 1971). Mines Branch, Dept. of Energy, Mines, and Research, Ottawa, ON, pp.

10. Maleki, H., and J. Owens, 2000. Application of Computational and Statistical Techniques to the Evaluation of Mobile Roof Support. University of Arizona, 10th Inter. Conf. of Ass. of Computer Meth. and Advances in Geomechanics.

11. Kay, D.R., and J.P. Carter, 1992. Effects of Subsidence on Steep Topography and Cliff Lines. *11th International Conference on Ground Control in Mining, Proceedings*, ed. by N. I. Aziz and S. S. Pend (Univ. Wollongong, Wollongong, Aust., July 7-10, 1992). Australasian Instit. of Min. and Metall., Wollongong, NSW, Aust., pp. 483-490.

12. King, R., 1980. Evaluation of Surface Subsidence and Horizontal Strain at York Canyon Mine, New Mexico. MS thesis, Colorado School of Mines, Golden, CO.

13. National Coal Board, 1975. *The National Coal Board's Subsidence Engineering Handbook.*

14. SPSS, 1995. *Statistical Packages for the Social Sciences*, Chicago, IL.

20th International Conference on Ground Control in Mining

FIELD EVALUATION OF MOBILE ROOF SUPPORT TECHNOLOGIES

FINAL

Hamid Maleki
Maleki Technologies, Inc., Spokane, WA

John Owens
Spokane Research Laboratory, National Institute for Occupational Safety and Health, Spokane, WA

Marc Endicott
J. H. Fletcher & Co., Huntington, WV

Abstract

This study presents a historic overview of the role of mobile roof support (MRS) technologies in improving stability and worker safety and presents the results of recent field evaluations of the MRS load rate monitoring device and other remote deformation-monitoring techniques. Field studies were implemented at two sites in cooperation among researchers from the National Institute for Occupational Safety and Health (NIOSH), Maleki Technologies, Inc., and J. H. Fletcher & Co. The objective of the field programs were to (1) study the interaction between MRS's and coal mine strata and (2) develop and test suitable monitoring systems for assessing roof and pillar stability. An MRS consists of a roof canopy, four hydraulic cylinders, a caving shield canopy, and associated electromechanical systems mounted on crawler tracks. The machines are controlled by radio from a remote location and operate on self-contained power units. Typically, MRS's have capacities of 5,340 and 7,120 kN (600 and 800 tons). In comparison to posts, an MRS is capable of maintaining the yield load after significant amounts of roof-floor deformation. Because the mining cycle is accelerated, MRS's help reduce the potential for time-dependent roof falls.

MRS performance has been monitored in the laboratory under controlled static loading conditions and in the field under deep, two-seam mining conditions. Laboratory studies have quantified support capacity and system stiffness as a function of machine height. Field investigations have focused on determination of optimum operating conditions and development of warning systems that indicate excessive load on the machine and/or impending roof-pillar stability problems. Analyses of field data show that roof instabilities are influenced by (1) pillar failure, (2) pillar yielding, (3) mine seismicity, (4) geologic structures, and (5) panel layout designs and mining practice. Pillar yielding and failure (unloading) and seismicity can be conveniently monitored by the load rate monitoring device, but for consistent detection of roof falls, additional deformation measurements directly within the cuts are needed.

INTRODUCTION

Room-and-pillar mining is one of the oldest methods used for the extraction of tabular ore bodies. In this method, a series of rooms are driven on advance using continuous miners and shuttle cars while the roof is bolted a short distance behind the face. During the retreat, the same equipment is used to mine the pillars, which allows roof rocks to cave behind the face. To control the cave line, a series of secondary support systems are installed as mining continues within the pillars.

The room-and-pillar mining method is at a disadvantage when compared to other mining techniques, such as longwall mining. Because of economies of scale, productivity using room-and-pillar mining is significantly lower. The longwall method is also much safer because the retreat is completed under the protection of self-advancing hydraulic support systems at the face. However, during the last two decades, federal laboratories, mining companies, equipment manufacturers, and geomechanics consultants have cooperated to improve the understanding of strata mechanics and develop a remotely controlled, self-advancing support system called a mobile roof support (MRS). This cooperation has resulted in improvements in the safety and productivity of room-and-pillar retreat operations.

Figures 1 and 2 illustrate generic panel layouts and pillar extraction sequences for two typical room-and-pillar retreat systems. The first is three-entry access and retreat to one side, while the second is nine-entry access with full retreat within the panel. In the first system, mining starts by driving a three-entry panel access to the boundaries of the room-and-pillar panel. A three-entry system using narrow rib pillars is developed to the side and retreated. After pulling one row of pillars, another row is driven into the solid coal block, and the sequence is repeated until the panel coal is extracted. Pillar recovery operations consist of splitting the pillars and fenders. Figure 1*A* presents the mine layout at four stages of pillar recovery. Figure 1*B* shows the sequence of the pillar cuts, typical position of posts, and the location of unmined stumps for the extraction of a pillar using the split-and-fender method.

In the second system, a nine-entry access is developed on advance to the panel boundaries. The pillars are then extracted until the entire panel is mined. Figure 2*A* presents a panel layout and the location of MRS's at three intermediate stages of pillar recovery using the "Christmas tree" method. Figure 2*A* shows the sequence of cuts taken from two pillars where MRS's are used as secondary support. Many variations in these two panel layouts and excavation sequences are

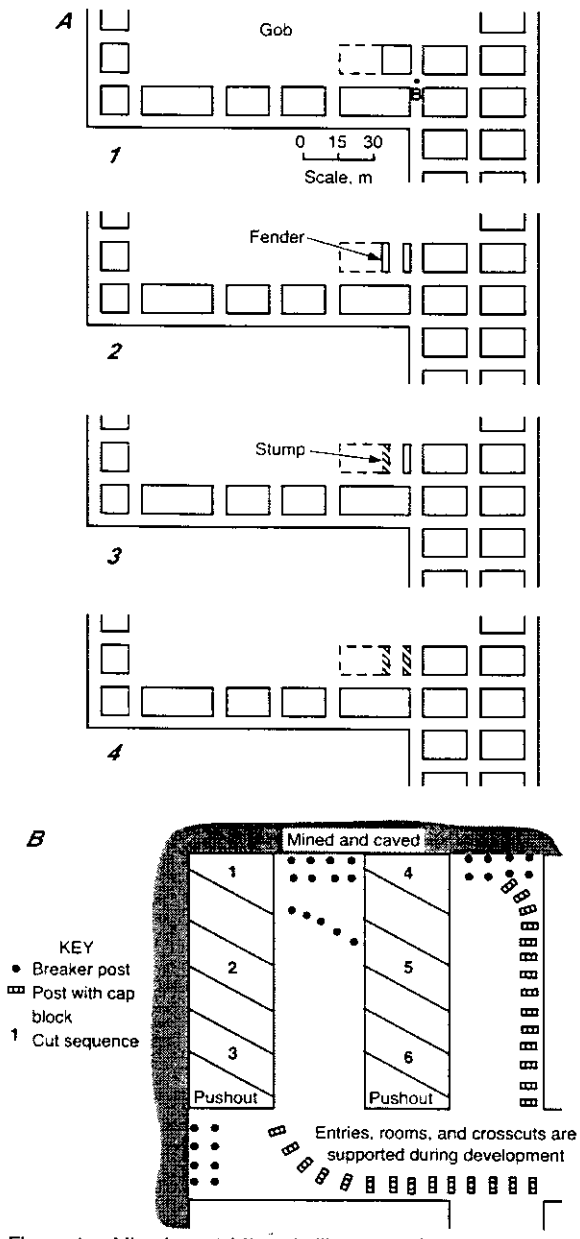

Figure 1.—Mine layout (*A*) and pillar extraction sequence (*B*) using split-and-fender method with posts.

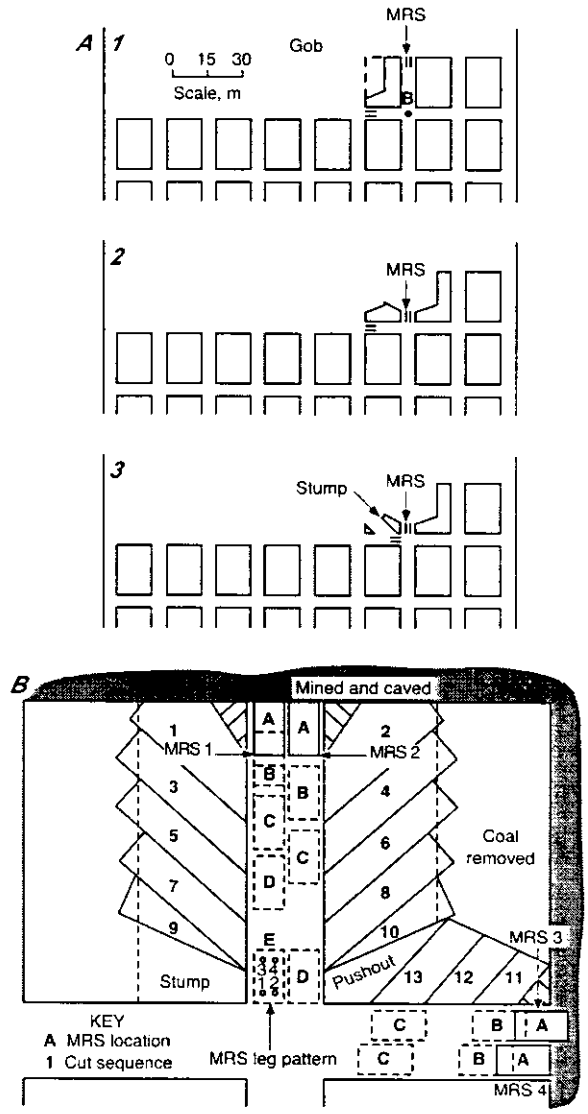

Figure 2.—Mine layout (*A*) and pillar extraction sequence (*B*) using Christmas tree method with MRS's as support.

practiced in U.S. coal mines. New applications of the three-entry system involve use of MRS's instead of posts and eliminates fenders completely.

After completing an analysis of the hazards of room-and-pillar retreat mining systems, it became apparent to the authors that safety could be significantly improved by considerations of (1) human factors, (2) remotely controlled MRS's, (3) mine layout designs, and (4) ground monitoring systems. A significant effort was directed to studying the above factors both in the laboratory and in the field. Recent geomechanics field evaluations focused on identifying failure mechanisms and critical levels of load and movement rates that are indicative of impending stability problems.

HUMAN FACTORS

Several human factors considerations were identified during an earlier geomechanics field study (Maleki 1981) in which the main objective was to identify causes of roof stability problems and develop practical monitoring techniques for detecting these problems (Maleki and McVey 1988). These factors were (1) the number of people required at the face, (2) the amount of time required to work at the cave line, (3) poor footing in entries, which influenced timely escape during a roof fall, (4) worker reaction at the time of a roof fall, and (5) the judgment-based methods used by miners to evaluate the stability of the roof and determine the optimum time for retrieving miners and equipment.

A large crew is required for conventional room-and-pillar retreat operations because posts must be delivered, cut to size, and installed. Each installation takes approximately 20 minutes and requires two to three workers. Debris on a mine floor can accumulate quickly and create poor footing. Miners must judge roof stability continually on

the basis of observations of primary and secondary support behavior (bending of roof plates, crushing of posts, etc.). In the study mine, when the roof caved prematurely and trapped a miner in a cab, other miners rushed to help. A second rock fall could have resulted in serious injury to rescuers (Maleki 1981). This could have easily happened, considering that many posts had already been broken and some had been knocked down during the first fall.

DEVELOPMENT AND TESTING OF MRS

To improve the safety of room-and-pillar retreat systems, a two-step solution was proposed. First, the mechanics of strata behavior was studied through extensive field measurements, and practical techniques for assessing roof behavior were developed. Second, a prototype of a remotely controlled roof support system was developed to eliminate the need to install posts near the gob. The machine was equipped with a dozer blade so that floor debris could be cleaned routinely, which allowed easier travel and escape. The prototype unit was developed by the U.S. Bureau of Mines in cooperation with an equipment manufacturer and a mining company (Thompson and Frederick 1986).

Commercial units have since been developed by U.S. and Austrian manufacturers and are being used on two continents. The commercial MRS units are more rugged and have higher capacities (5,340 to 7,120 kN [600 to 800 tons]) (Wilson 1991; Howe 1998) than the prototype. They consist of a roof canopy, four hydraulic cylinders, a caving shield canopy, and associated electro-mechanical systems mounted on crawler tracks. The system has radio control and self-contained power units. Because of their greater mobility and because they allow higher resource recovery, they are currently being used in 36 U.S. coal mines, as well as a number of Australian mines (Shepherd and Lewandowski 1992; Habenicht 1988).

MRS performance has been monitored both in the laboratory and in the field by NIOSH and MTI personnel. Laboratory investigations focused on an evaluation of support stiffness and load-carrying capacity under controlled static loading conditions. The study quantified system stiffness as a function of machine height for both two- and three-stage hydraulic cylinders (Barczak and Gearhart 1997, 1998). The advantage of the three-stage cylinder design is greater operating range, but a disadvantage is reduced support stiffness. Each unit has the load-bearing capacity of six posts and the stiffness of two hardwood posts (Barczak and Gearhart 1997). The study also identified inaccuracies in hydraulic cylinder pressure measurements of roof loads when the bottom cylinder stages were fully extended.

The mechanics of load transfer from pairs of MRS's to the mine strata was analyzed using laboratory results, boundary-element modeling, and analytical solutions. The results showed that MRS's support roof rocks near the machines, but do not have the capacity to control overall roof-floor convergence and overall stress distributions because the MRS's are considerably less stiff than coal-measure rocks. In comparison to posts, however, an MRS is capable of maintaining the yield load after significant amounts of roof-floor deformation. Because the mining cycle is accelerated, MRS's help reduce the potential for time-dependent roof falls.

To study the influence of pairs of MRS's on the mine roof, the authors used analytical solutions for two pairs of MRS's positioned 5.5 m (18 ft) apart (figure 3) (Maleki and Owens 1998). Results

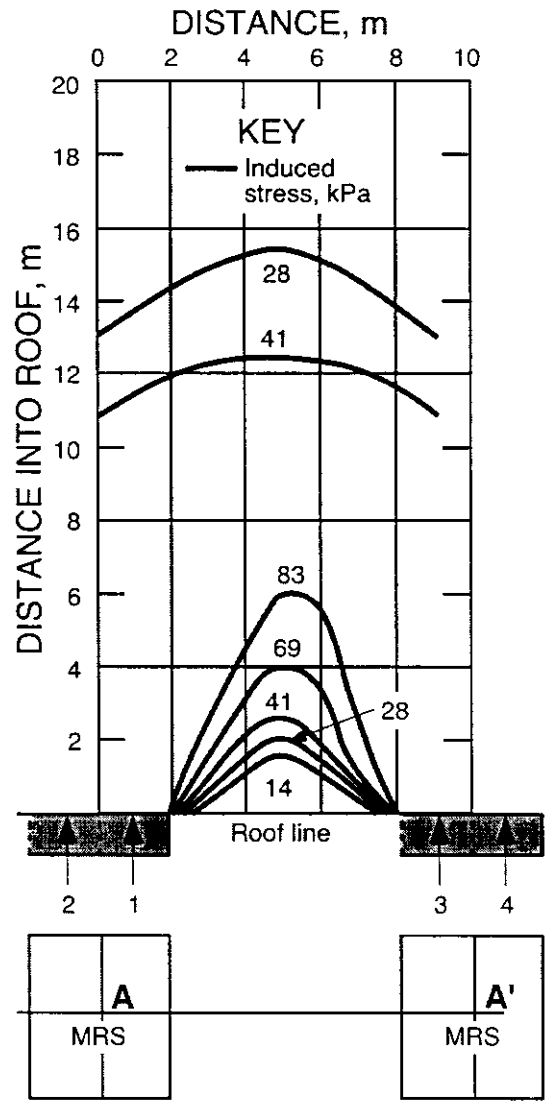

Figure 3.—Stress isobars along A-A' for two pairs of MRS's at 5.5-m spacings.

showed that MRS's form a pressure arch in the immediate roof that reduces the potential for roof falls in the space confined by the MRS's. This is beneficial for protecting a continuous miner when it is operating within this space. It was also found that higher MRS capacities and setting pressures are useful for stabilizing the upper strata, but may contribute to differential loading on the immediate roof, failure of mechanical bolts, and reduction in the stability of the immediate roof.

Early field evaluations focused on a comparison of ground movements in two room-and-pillar retreat sections using the split-and-fender method with posts (figure 1) and the Christmas tree method with MRS's as the secondary support system (figure 2). In addition, the history of hydraulic pressure was analyzed for all four MRS legs (Hay et al. 1995). Deformation measurements indicated generally higher strata movement at the intersections in the section using the Christmas tree method. Because of differences in geologic conditions and mining practices, it was not possible to make a direct comparison. We recommended that numerical modeling of these geometries address mine layout designs while keeping geologic conditions constant.

PANEL LAYOUT DESIGN

Early field studies identified the importance of mine layout designs and revealed the dangers of overconfidence concerning the ability of MRS's to support the entire area. Such overconfidence contributed to workers choosing unsafe operating locations. Thus it became apparent to the authors that to improve stability, layout designs that control convergence and stress should be developed. To illustrate this point, boundary-element analyses were completed in which stress distributions were calculated in both single and multiple seams. These analyses were also helpful in tailoring the type of monitoring required to assess changes in the stability of the mining system.

The first study compared stress distribution and convergence patterns for two pillar recovery plans: split-and-fender and Christmas tree. Model input was based on extensive laboratory and field measurements in one mine (Maleki 1981), and modeling procedures were based on a methodology developed for coal mine excavations (Maleki 1990; Maleki and Owens 1998). The analyses were completed for a typical depth of 305 m (1,000 ft).

Figure 4 presents the calculated roof-floor convergence for a point in the intersection for two pillar recovery methods (point B in figures 1A and 2A) and provides guidance for selecting monitoring systems. Note that calculated deformation significantly increases within a mining step, which is associated with the failure of fenders and stumps. MRS's will therefore experience an increase in both vertical and lateral support loading as fenders fail. Since fender failure induces differential movement in the mine roof, a roof fall may be triggered. Such a roof fall may be sensed through monitoring either roof movements or possibly MRS leg pressures. The change in convergence that occurs as a result of failure of the fenders is large enough to cause a change in leg pressure and can be conveniently detected by the load rate device. Obviously, changes in convergence and roof movements may best be directly detected by monitoring roof-floor movements (Maleki 1981) if inadequacies in measuring the hydraulic leg pressures of the MRS's are suspected.

Roof-floor convergence is at least 10% higher using the Christmas tree method, as illustrated in figure 4. To control convergence, a stump is left in the model (figure 2). Further improvements in stability and convergence can be achieved by changing the size of the stumps and pillars left behind while considering site-specific structural conditions (i.e., using engineered mine layouts and extraction designs).

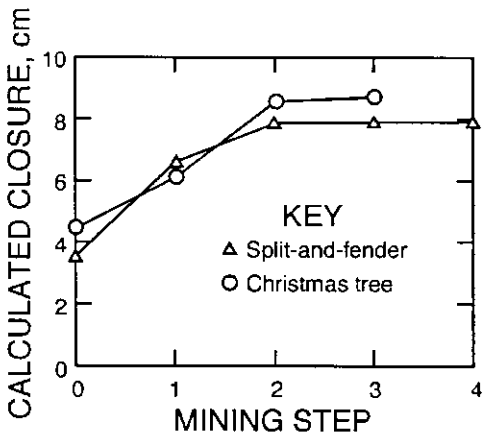

Figure 4.—Calculated closure for split-and-fender and Christmas tree methods at location B.

MRS's are used often when mining difficult reserves, such as where there are earlier workings in adjacent seams. In a second study in a cooperating mine described here, numerical modeling techniques and field data were used to show how two-seam layouts influence stability and support response. The mine uses the room-and-pillar technique to extract three-seam reserves in coal fields on the Wasatch Plateau near Huntington, Utah. These seams are located toward the base of the Blackhawk Formation and consist of the Tank, Blind Canyon, and Hiawatha. The Tank Seam is presently being mined in an area partially undermined by the Blind Canyon Seam, approximately 85 m (280 ft) below. Thus, mining layout and pillar pulling plans are complex. The test site in the Tank Seam is located in a graben bordered to the east and west by two major faults (figure 5). North-south-trending joints are common in the section and influenced by mining and caving process during extraction of the Blind Canyon Seam.

Figure 6 presents Tank Seam mining geometry and vertical stress distributions over a portion of the two-seam mining areas during the extraction of pillar 2. A stress profile was also prepared (figure 7) along an east-west cross section positioned toward the middle of the modeled area (away from the active face in the 1st North Mains). Modeled geometry in the Blind Canyon Seam was limited to the fully retreated 2nd East panel. This panel lies directly under the 1st Main North, but shifts some 24 m (80 ft) toward the east and so the last (most westerly) row of 1st North Mains pillars is not undermined. Modeled areas in the Tank Seam include a fully retreated room-and-pillar panel to the western boundary of the model (top of the page) and a 43-m- (140-ft-) wide barrier pillar between this gob and the 1st North Mains (figure 5)

Results indicate a nonuniform stress distribution over the 1st North Mains. Pillar stresses increase to the west across the 1st North Mains. Maximum stresses are concentrated over the last row of pillars (row 8) and the barrier pillar. This is in agreement with underground observations indicating large amounts of rib spalling and floor heave near pillar 8 in contrast with little (unnoticeable) movement to the east. This two-seam mining geometry created an opportunity to assess machine performance in the field under these two different loading conditions.

Based on this and other multi step stress analyses, it became apparent that pillar stresses exceeded pillar strength [21 MPa (3,000 psi)] (Maleki 1992) when approximately half a pillar was extracted. At this time, the pillar exceeded yield loads and was approaching the post-failure regime. Seismicity noticeably increased. Pillar unloading resulted in increased roof-floor convergence and load transfer to the MRS units nearby. This process was associated with an increase in the rate of loading on the MRS's. Roof falls may be triggered by additional movement, particularly if smooth joints are present.

DEVELOPMENT OF GROUND MONITORING SYSTEMS

During field tests in underground mines, the authors identified three factors that might adversely influence worker safety in an MRS section.

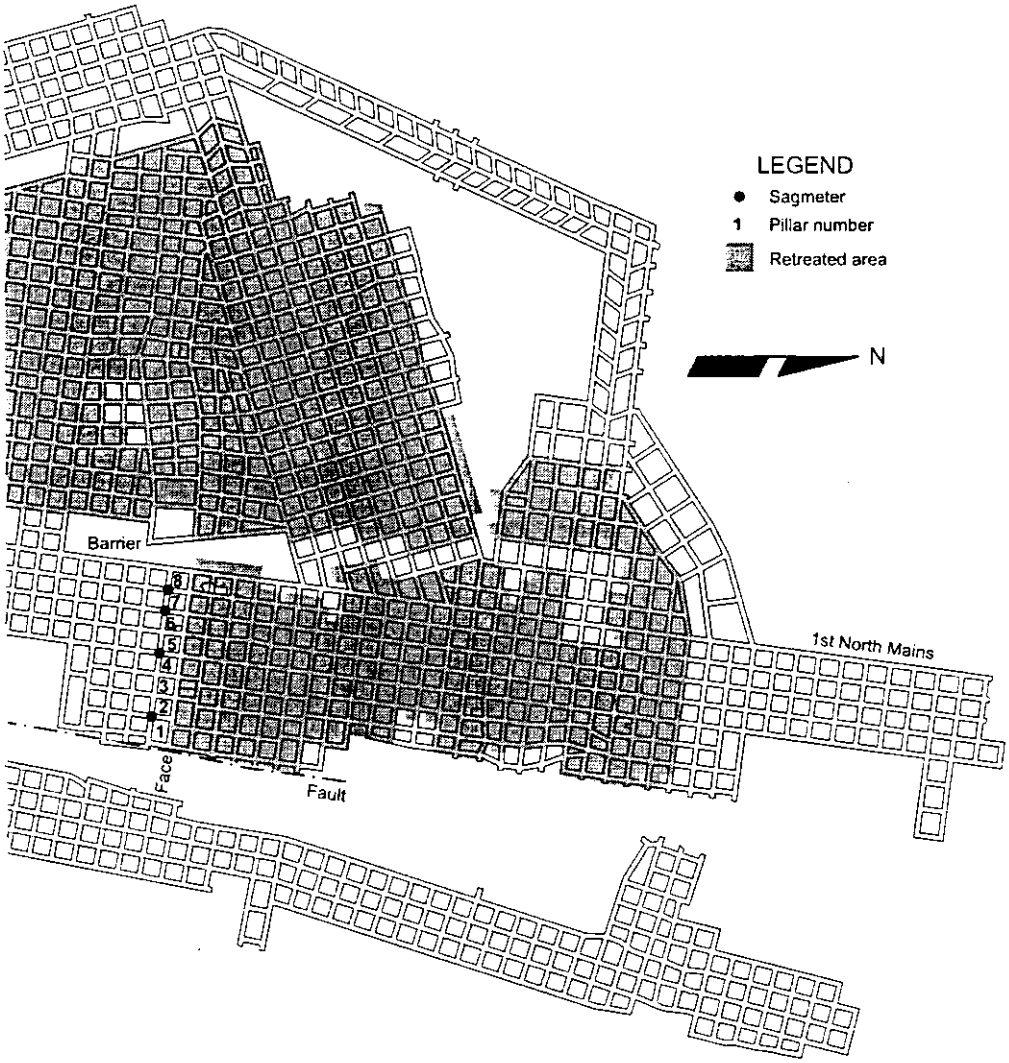

Figure 5.—Mining geometry and monitoring locations in Tank Seam.

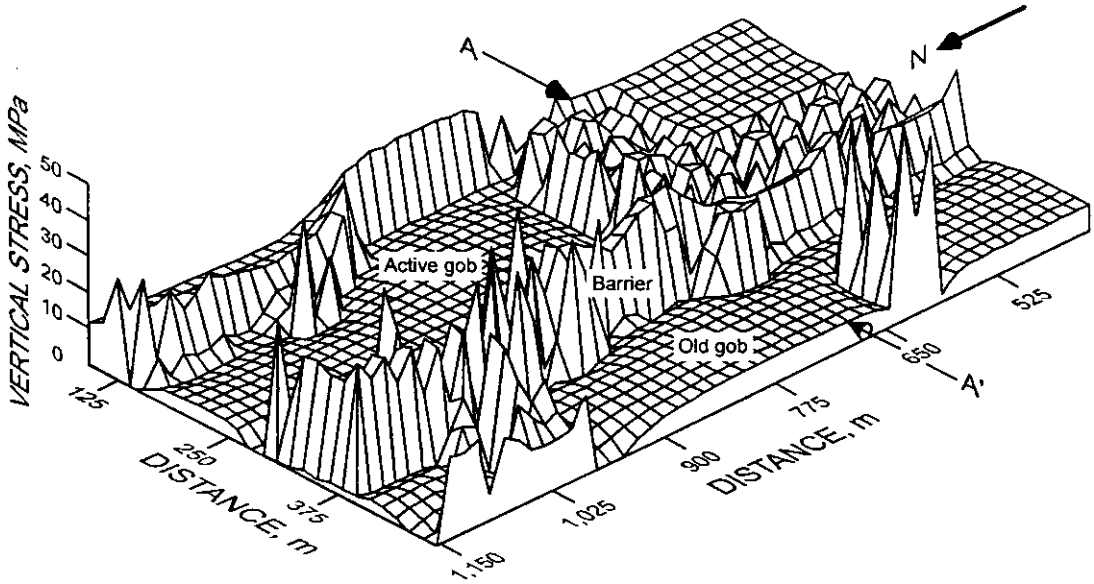

Figure 6.—Vertical stress distribution on the Tank Seam.

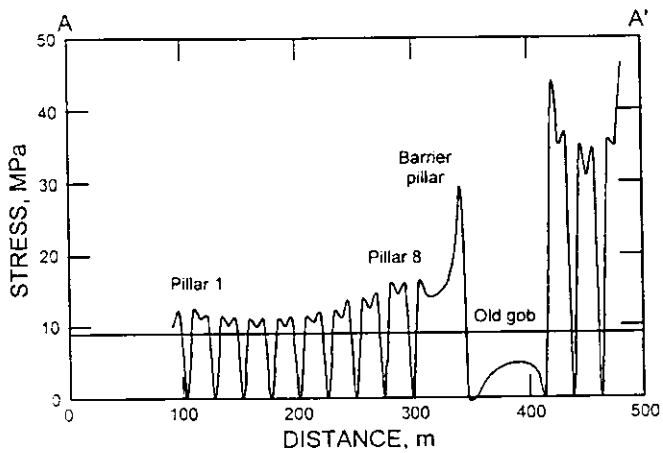

Figure 7.—Vertical stress profile along section A-A'.

- Elimination of posts reduced a worker's ability to assess roof conditions.
- Overconfidence in the ability of MRS's to support the entire area caused some miners to chose unsafe operating positions.
- Use of MRS's on a routine basis under adverse geologic and mining conditions to recover reserves that were otherwise unminable.

It became apparent to the authors that there was a need to develop a warning system that would alert workers to unstable roof conditions so that miners and equipment could be removed before a roof fall occurred. Two monitoring methods were chosen on the basis of mine measurements and numerical modeling considerations. These were load-rate monitoring on the hydraulic legs of MRS's and remote monitoring of roof movements using a theodolite. A reliable warning system needs to combine both ground deformation and load-rate data. Theodolite and spads have been effectively used for the remote measurement of roof movements and for the detection of roof falls in room-and-pillar operations (Maleki 1981). In this application, marked spads are installed in the area of interest during pillar recovery and ground movements are remotely monitored using a theodolite (or transit). By measuring the change in vertical angle, the rate of roof movement is calculated.

A load rate monitoring device was developed by NIOSH that monitors dynamic loading rates on an MRS in real time and displays warning signals. Hydraulic supports such as the MRS provide little or no discernible audible or visual indications of impending roof stability problems. In MRS retreat mining sections, miners rely on the hydraulic gauges on the MRS's to determine when to cease operations and leave the area of the active mining face before a roof fall. An imminent roof failure is sometimes preceded by a rapid increase in pressure on the dial gauges. However, these gauges are difficult to read, requiring miners to approach the MRS to monitor the gauges, which in turn requires them to be close to the active mining face, an area susceptible to roof falls, and in a location with a lot of equipment activity. As a result, miners do not check the pressure gauges often. Monitoring the rate of loading on MRS legs was shown to provide warnings about major events, such as failures of fenders and pillars. These events often trigger roof falls.

With the cooperation of the MRS manufacturer, J. H. Fletcher & Co., the device was installed and tested on MRS's in the laboratory and in the field. The system is MSHA permissible and operates as an integral part of the MRS. Research continues in analyzing the data from recent field installation and in identifying critical loading parameters associated with roof and/or pillar stability problems. Necessary calibration can be done prior to installation or periodically as mine conditions change, but need not be done by operating personnel at the mine. The operating parameters for the system are set by connecting the system to a laptop computer via an RS-232 null modem cable with the communication terminal emulator acting as the laptop client program. This allows a trained user to change the parameters for triggering the various load rate indicator devices easily to suit conditions at the mine.

FAILURE MECHANISMS AND MONITORING RESULTS

MRS performance was monitored during the extraction of one row of pillars. Hydraulic leg pressures were collected on all four MRS's using Campbell Scientific[1] data acquisition systems. Two loading rates are used to analyze the loading history of MRS's: (1) Instantaneous loading rate calculated by taking measurements every 2 sec and (2) average loading rates calculated by taking measurements following an acceleration in loading rates up to a period of 1 hour. The instantaneous rate is highly variable but useful when addressing seismically induced events. The average loading rate is more suitable for addressing overall changes in pillar stability.

Three time windows were selected to analyze failure mechanisms and machine response to applied load during pillar extraction. Mining geometry, MRS location, load histories, and roof fall locations are illustrated in figures 8, 9, and 10.

Pillar Failure Mechanism

Monitoring results during the extraction of the second half of pillar 1 clearly show the influence of fender failure and deterioration in roof stability. No roof falls occurred within the mining areas of interest while mining pillar 1 (figure 8). However, three roof falls occurred near the outside boundary of the excavation. These falls took place during and after extraction of cuts 11 and 12 when pillar failure was in progress as the effective pillar area was reduced. Maximum yield load was achieved on MRS 4 during excavation of the pushout cut, completing the pillar failure process. The instantaneous measured rates varied from 280 to 450 kPa/sec (40 to 65 psi/sec) during these events. Average load rates varied between 75 to 105 kN/min (17,000 to 24,000 lb/min) during this process.

Pillar Yielding Mechanism and Geologic Structure

Figure 9 presents mining geometry and roof fall locations during the extraction of pillar 2. Two roof falls occurred while completing approximately 50% extraction in the pillar. The first was outside of areas of active mining during mining cut 12. The second roof fall buried the continuous miner during mining of cut 14; this roof fall was structurally controlled by north-south-trending joints. At this time, the effective area of the pillar was reduced by approximately 50%, and thus the pillar approached yielding and the post-failure regime. This assertion is made based on stress analyses (figure 6) and loading

[1]Mention of specific products and manufacturers does not imply endorsement by the National Institute for Occupational Safety and Health.

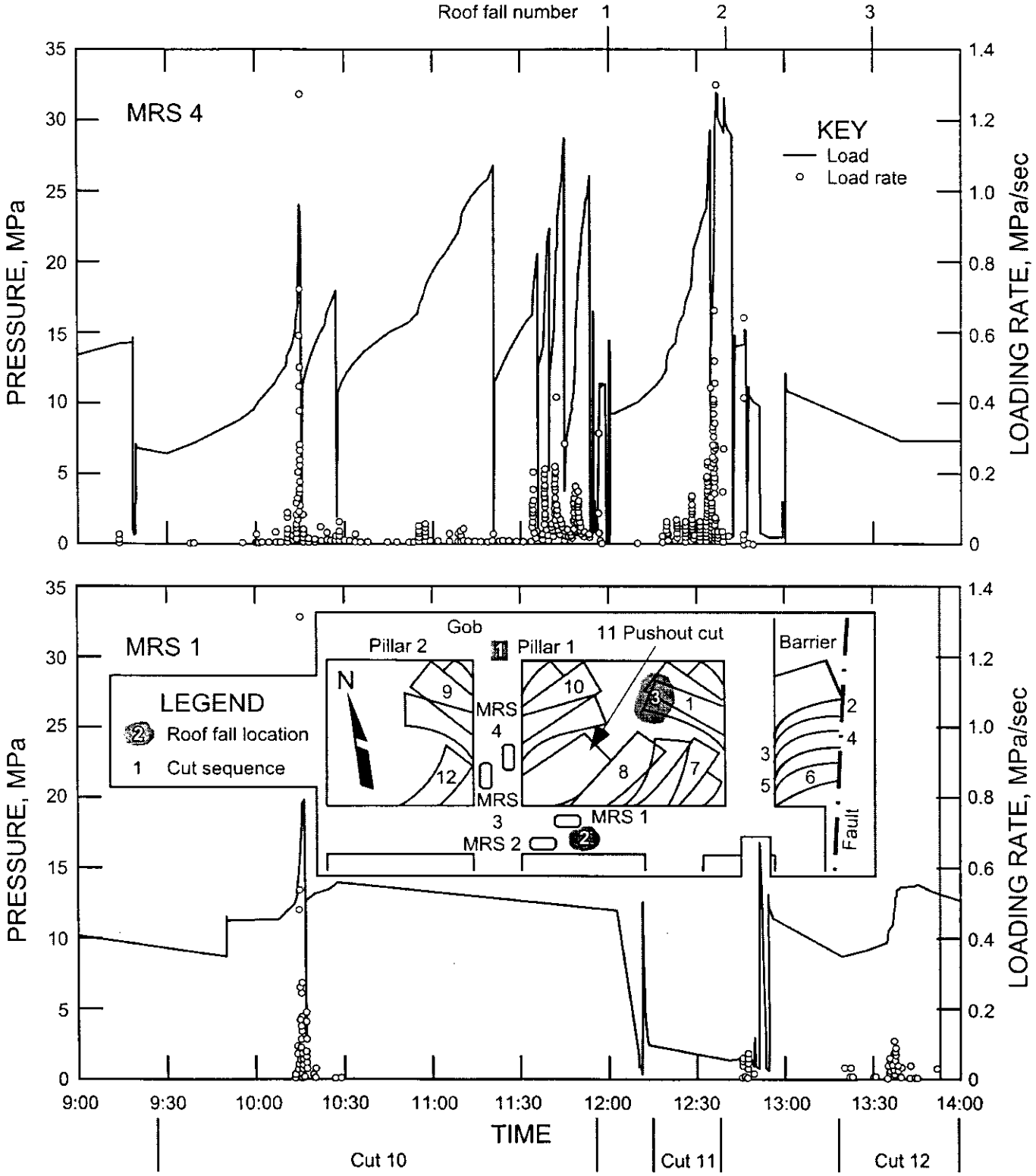

Figure 8.—Load history for MRS's 1 and 4 while completing extraction of pillar 1.

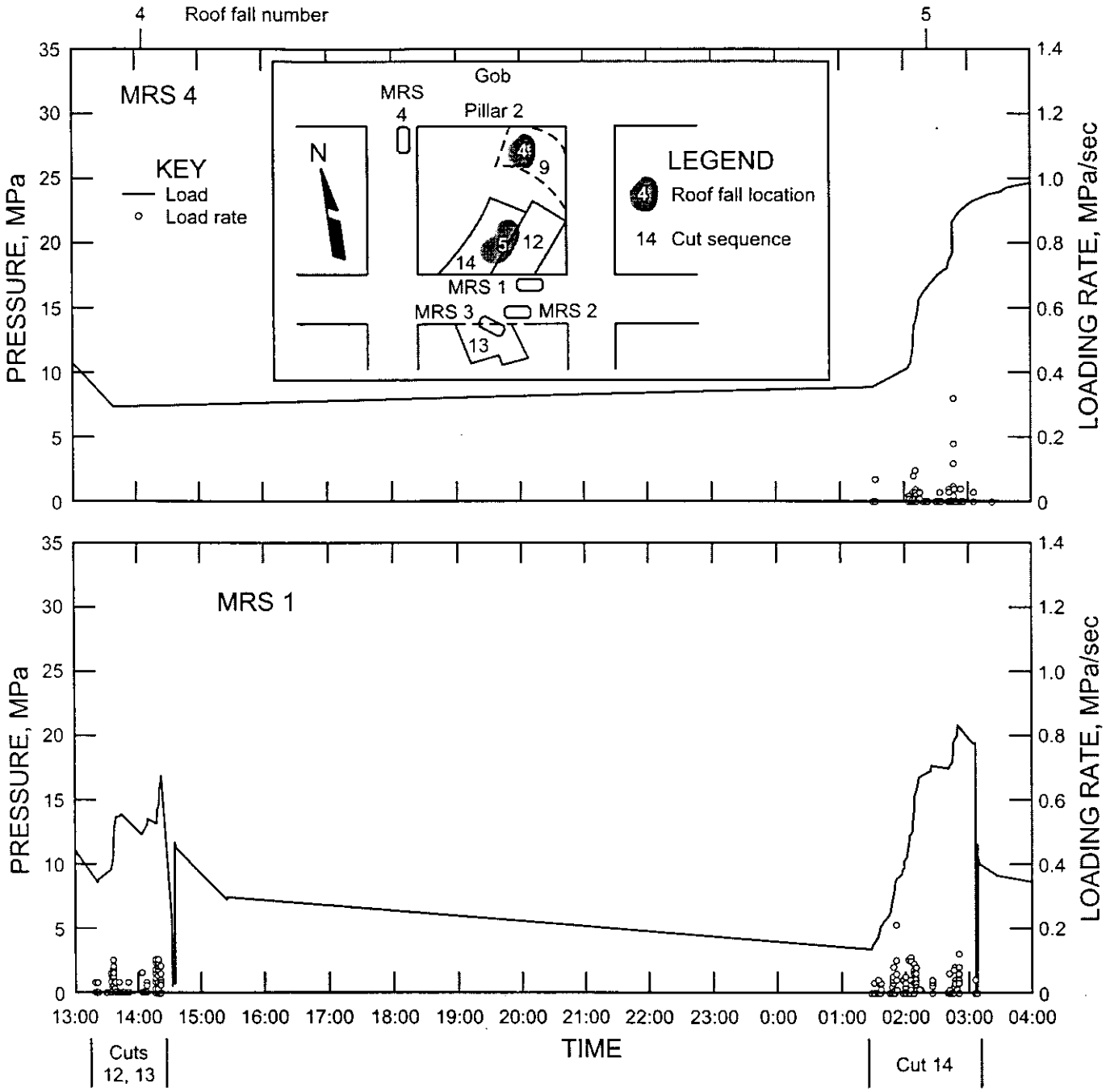

Figure 9.—Load history for MRS's 1 and 4 while completing extraction of pillar 2.

patterns on MRS's 1 and 4 (figure 9). Three minutes prior to this roof fall, load on both MRS 1 and 4 increased to approximately 21 MPa (3,000 psi) and instantaneous load rates varied from 120 to 200 kPa/sec (18 to 29 psi/sec) with an average load rate of 670 kN/min (15,000 lbf/min). In comparison to events for pillar 1, both load and load rates were lower because pillar 2 still provided sufficient resistance to limit roof-floor convergence. We suspect that pillar 2 was in a post-failure load deformation stage because there was a gradual load increase on MRS 4 during equipment recovery operations. At the termination of recovery operations, load was approaching 28 MPa (4,000 psi). Pillar yielding thus appear to have triggered movements in roof blocks outlined by preexisting joints.

Seismically Triggered Roof Falls

Figure 10 presents mining geometry and roof fall location during the extraction of pillar 8 and the barrier pillar. At this location, only MRS's 3 and 4 were used. One roof fall, a block of rock 1 by 1 by 3.7 m (3.3 by 3.3 by 12 ft), occurred during the extraction of cut 6. The block was structurally controlled by north-south-trending joints. At the time of failure, loads were moderate on both MRS 3 and 4 of about 21 MPa (3,000 psi) and instantaneous load rates were generally small, 76 kPa/sec (11 psi/sec) with average load rate of 36 kN/min (8,000 lbf/min). A large, instantaneous increase in the load rate of 390 kPa/sec (56 psi/sec) was measured on MRS 3 shortly before the block

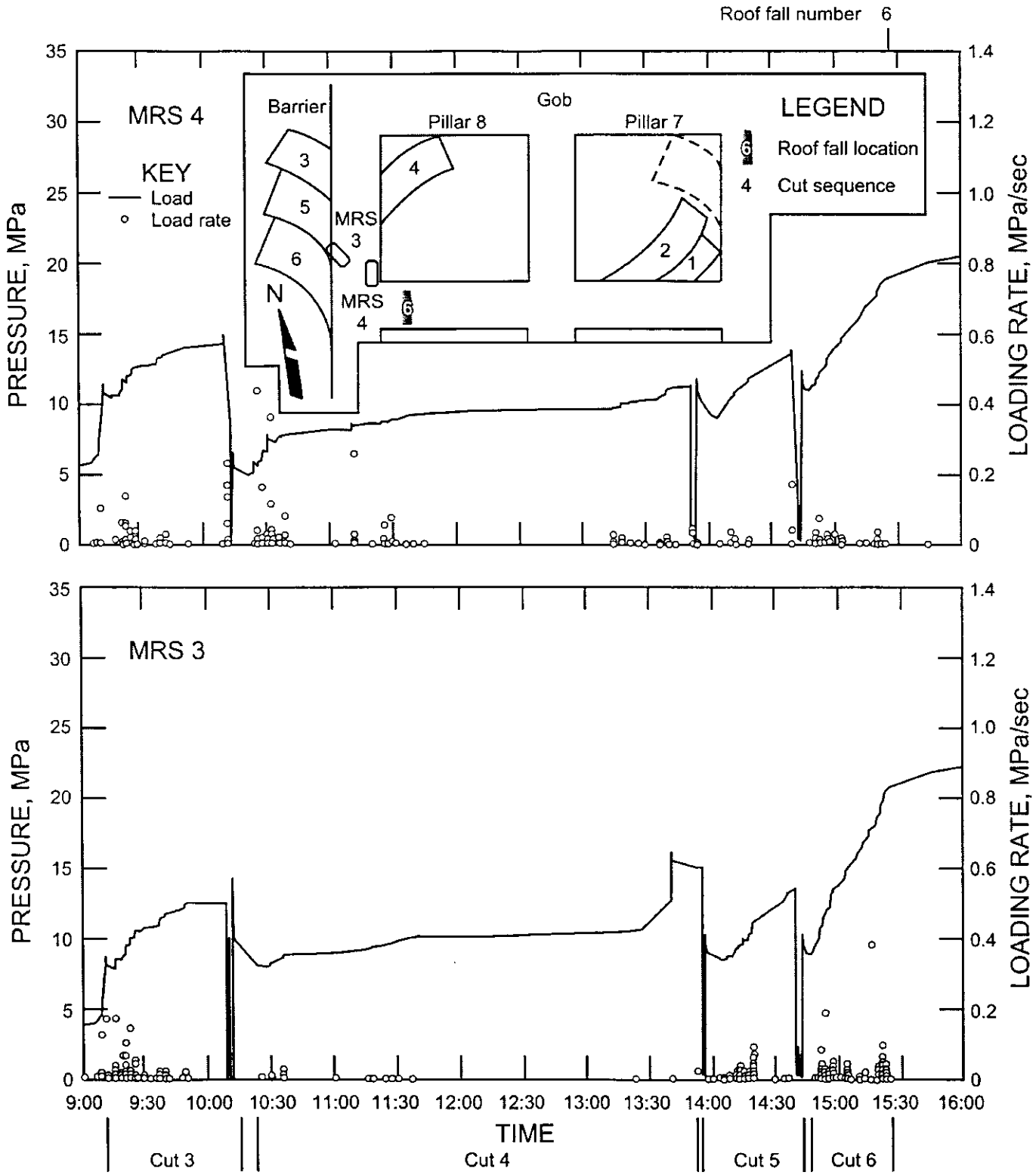

Figure 10.—Load history for MRS's 3 and 4 while extracting pillar 8 and barrier pillar.

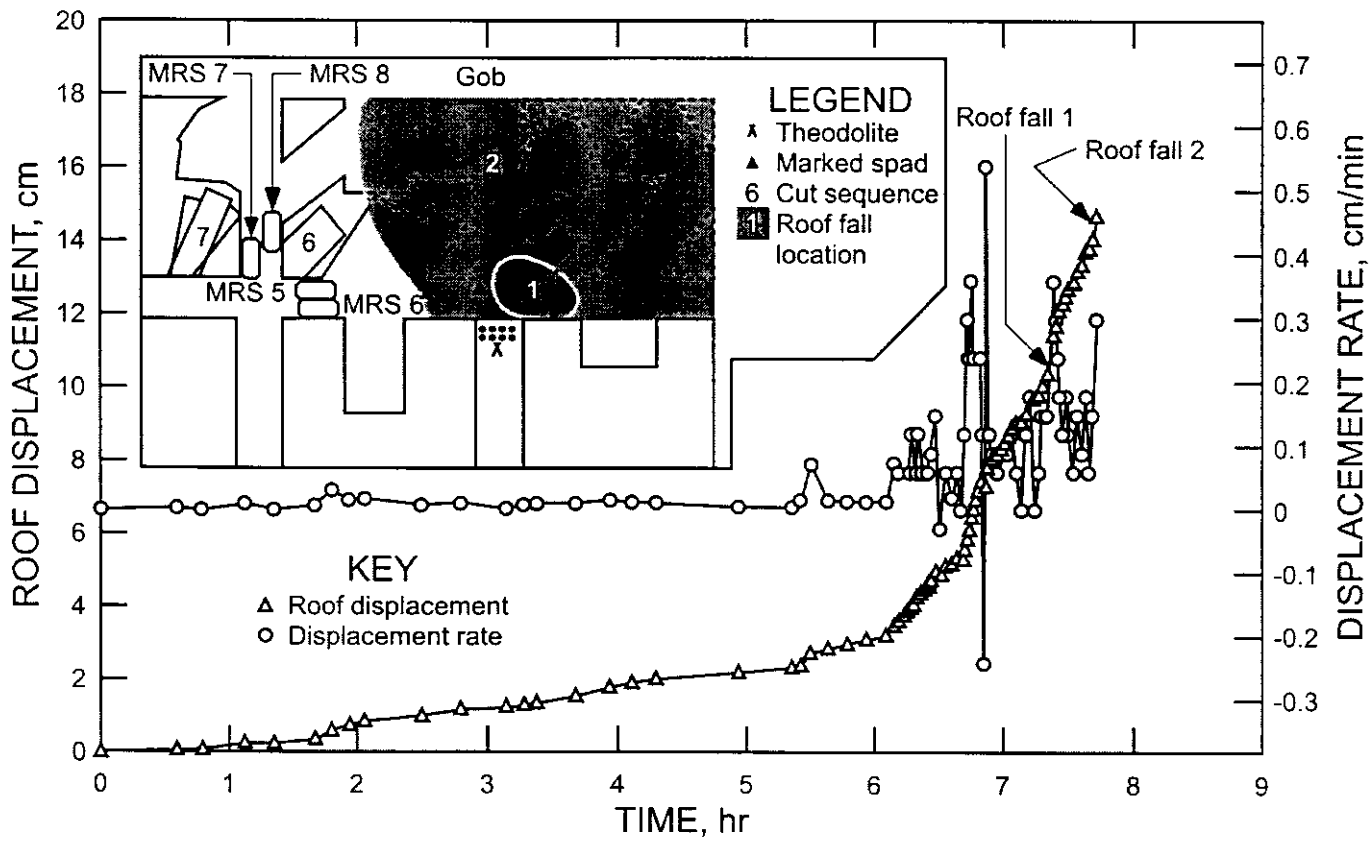

Figure 11.—Roof displacement history prior to major roof falls.

fell. The authors suspect preexisting structures to have contributed to this roof fall, which was triggered by higher-than-normal mine seismicity in this high-stress area.

Typical Deformation Monitoring Results

Reliable detection of impending stability problems requires monitoring both loading patterns on MRS's and roof movements. This is illustrated by presenting a roof deformation and major caving history approximately 30.5 m (100 ft) behind the face using a theodolite and marked spads at the study mine in the Blind Canyon Seam (figure 11). Note an increase in roof deformation and roof deformation rate prior to two roof falls. The deformation rate exceeded a critical rate of 0.5 cm/min (0.2 in/min) approximately 30 min prior to roof fall 1. This critical rate is in close agreement with other measurements of convergence in four other U.S. coal mines (Maleki 1981; Maleki 1988; Maleki et al. 1999). The second roof fall was associated with seismicity that was registered as spikes in the loading patterns on four MRS's.

CONCLUSIONS AND RECOMMENDED WORK

To eliminate setting and handling posts and reduce the number of miners required to work near the cave line and at other dangerous locations, a remotely controlled MRS has been developed and tested in the field. Optimum use of MRS's depends on careful panel designs, mine orientation, and primary support designs geared to expected geologic and stress conditions (Maleki and Owens 2001). MRS's have a limited zone of influence around them and thus can best be utilized in combination with other MRS's and in conjunction with ground monitoring systems.

An integrated ground monitoring system was tested in which the simplicity of deformation measurements were combined with more elaborate load rate monitoring on MRS leg cylinders. Analyses of field data show that roof instabilities are influenced by four mechanisms: (1) pillar failure, (2) pillar yielding, (3) mine seismicity, and (4) geologic structures. Pillar yielding and failure (unloading) and seismicity can be conveniently monitored by the load rate monitoring device, but to detect impending roof falls, additional deformation measurements directly within the cuts are needed.

Preliminary results show that roof falls occur when roof movements accelerate, reaching critical limits of 0.5 cm/min (0.2 in/min). Using average loading rates on MRS's at the study mine, there is a high potential for roof-pillar failure when the MRS loading rate increases beyond 44 kN/min (10,000 lbf/min). At such high loading rates, it is considered very likely for an MRS and/or the continuous miner to be buried during either mining or relocating the MRS. Between 22 to 44 kN/min (5,000-10,000 lbf/min), stability problems are still likely to pose some risk to equipment and worker safety. Structurally controlled instabilities play a bigger role at the lower end of this range, depending on mine seismicity, geology, and operating conditions. Below 22 kN/min (5,000 lbf/min), the likelihood of pillar stability problems is very low, and overall stability can be controlled through prudent support and excavation techniques.

Research continues in testing and evaluating MRS performance

under dynamic loading conditions. The focus of future ground control research is to quantify and verify critical loading parameters that are indicative of impending stability problems under different geologic conditions.

REFERENCES

Barczak, T., and D. Gearhart, 1997. Full-Scale Performance Evaluation of Mobile Roof Supports. Paper in *Proceedings of 16th International Conference on Ground Control in Mining*, ed. by S. S. Peng and C. T. Holland (Morgantown, WV, Aug. 5-7, 1997). Dept. of Mining Engineering, WV Univ., pp. 211-220.

Barczak, T., and D. Gearhart, 1998. Performance and Safety Considerations of Hydraulic Support Systems. Paper in *Proceedings, 17th International Conference on Ground Control in Mining*, ed. by S. S. Peng (Morgantown, WV, Aug. 4-6, 1998). Dept. of Mining Engineering, WV Univ., pp. 176-186.

Habenicht, H., 1988. The Alpine Breaker Line Support (ABLS): A Means to Promote Full Extraction. Paper in *3rd International Conference on Innovative Mining Systems*, ed. by J. M. White (Rolla, MO, Nov. 2-4, 1987). MO Univ., pp. 22-29.

Hay, K., S. Signer, M. King, and J. Owens, 1995. Monitoring Mobile Roof Supports. Paper in *Proceedings of 14th International Conference on Ground Control in Mining*, ed. by S. S. Peng (Morgantown, WV, Aug. 1-3, 1995). Dept. of Mining Engineering, WV Univ., pp. 55-62.

Howe, L., 1998. A Decade of Mobile Roof Support Application in the United States. Paper in *Proceedings, 17th International Conference on Ground Control in Mining*, ed. by S. S. Peng (Morgantown, WV, Aug. 4-6, 1998). Dept. of Mining Engineering, WV Univ., pp 187-201.

Maleki, H., 1981. Coal Mine Ground Control. Ph.D. dissertation, Colorado School of Mines, Golden, CO, 432 pp.

Maleki, H., 1988. Detection of Stability Problems by Monitoring the Rate of Movement. *Coal Age*, Dec., pp. 34-38.

Maleki, H., 1990. Development of Numerical Modeling Procedures for Coal Mine Stability Evaluations. Paper in *Rock Mechanics Contributions and Challenges: Proceedings of the 31st U.S. Symposium*, ed. by W. A. Hustrulid and G. A. Johnson (Golden, CO, June 18-20, 1990). Balkema, pp. 85-92.

Maleki, H., 1992. In Situ Pillar Strength and Failure Mechanisms for U.S. Coal Seams. Paper in *Proceedings of the Workshop on Coal Pillar Mechanics and Design*, comp. by A. T. Iannacchione, C. Mark, R. C. Repshar, R. J. Tuchman, and C. C. Jones (Santa Fe, NM, June 7, 1992). U.S. Bur. Mines Inform. Circular 9315, pp. 73-77.

Maleki, H., and R. McVey, 1988. Detection of Roof Instability by Monitoring the Rate of Roof Movements. U.S. Bur. Mines Rep. Invest. 9170, 12 pp.

Maleki, H., and J. Owens, 1998. Analysis of the Interaction Between Mobile Roof Supports and Mine Strata. Paper in *Design and Construction in Mining, Petroleum, and Civil Engineering: Proceedings of the Fifth South American Congress on Rock Mechanics and Second Brazilian Conference in Rock Mechanics-SAR Rocks 98*, ed. by L. A. da Silva, E. F. de Quadros, and H. H. S. Conçalves (Santos, São Paulo, Brazil, Nov. 22-25, 1998). Univ. de São Paulo, Escola Politécnica, pp. 287-293.

Maleki, H., and J. Owens, 1999. An Overview of Geomechanics Safety Research on Mobile Roof Supports. In *System Safety at the Dawn of a New Mellennium. Proceedings, 17th International System Safety Conference* (Orlando, FL, Aug 16-21, 1999). System Safety Society, Unionville, VA, pp. 554-563.

Maleki, H., and J. Owens, 2001. Application of Computational and Statistical Techniques to an Evaluation of Mobile Roof Supports. Paper in *Computer Methods and Advances in Geomechanics: Proceedings of the Tenth International Conference on Computer Methods and Advances in Geomechanics*, ed. by Chandra S. Desai, Tribikram Kundu, Satya Harpalani, Dinshaw Contractor, and John Kemeny (Tucson, AZ, Jan. 7-12, 2001). Balkema, pp. 1705- 1711.

Shepherd, J., and T. Lewandowski, 1992. Modified Wongawilli Extraction with Mobile Breaker Line Supports: Preliminary Geomechanics. *Australian Coal Journal*, no. 38, pp. 41-47.

Thompson, R., and J. Frederick, 1986. Design and Field Testing of Mobile Roof Support for Retreat Mining. Paper in *Proceedings, 5th Conference on Ground Control in Mining*, ed. by A. W. Khair and S. S. Peng (Morgantown, WV, June 11-13, 1986). Dept. of Mining Engineering, WV Univ., pp. 73-78.

Wilson, H. G., 1991. Mobile Roof Support for Retreat Mining. Paper in *10th International Conference on Ground Control in Mining, Proceedings*, ed. by S. S. Peng (Morgantown, WV, June 10-12, 1991). Dept. of Mining Engineering, WV Univ., pp. 103-114.

ATTACHMENT B

PHOTOGRAPHS OF CASTLEGATE ESCARPMENT CONDITIONS

Legend

Following 13 pages present typical conditions photographed from positions 1 to 13 (figure 2)

MALEKI TECHNOLOGIES, INC.

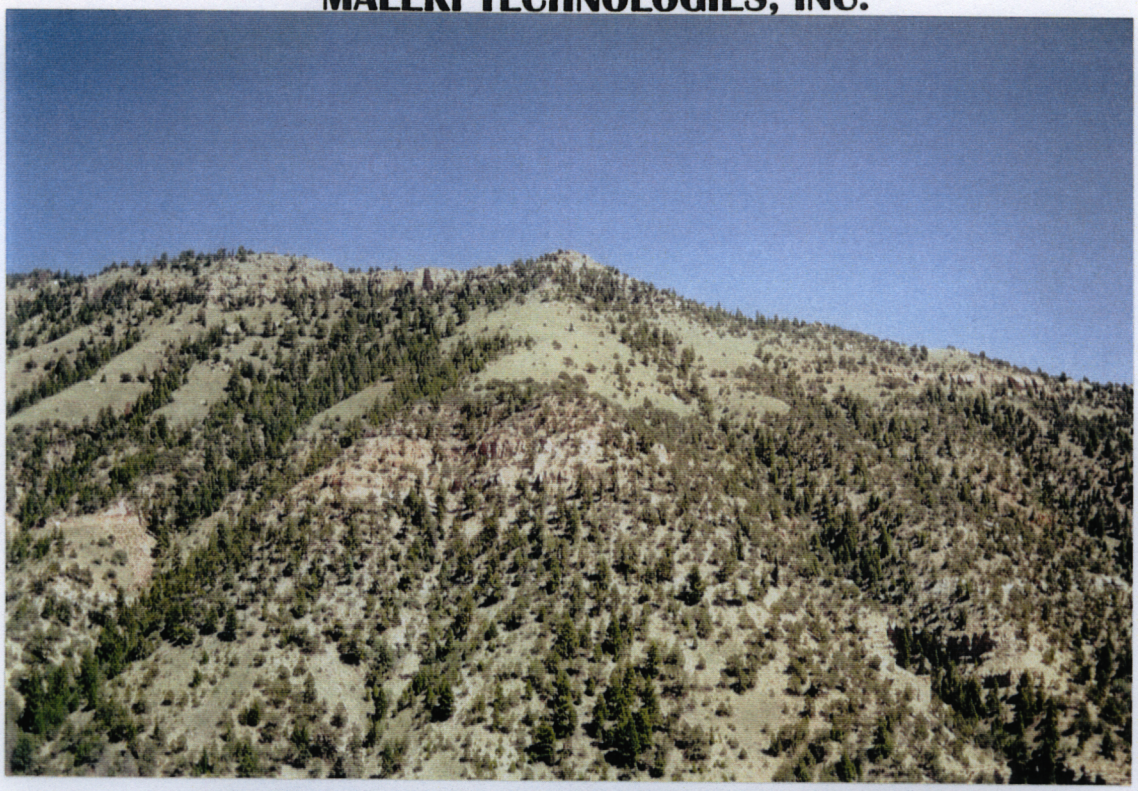

MALEKI TECHNOLOGIES, INC.

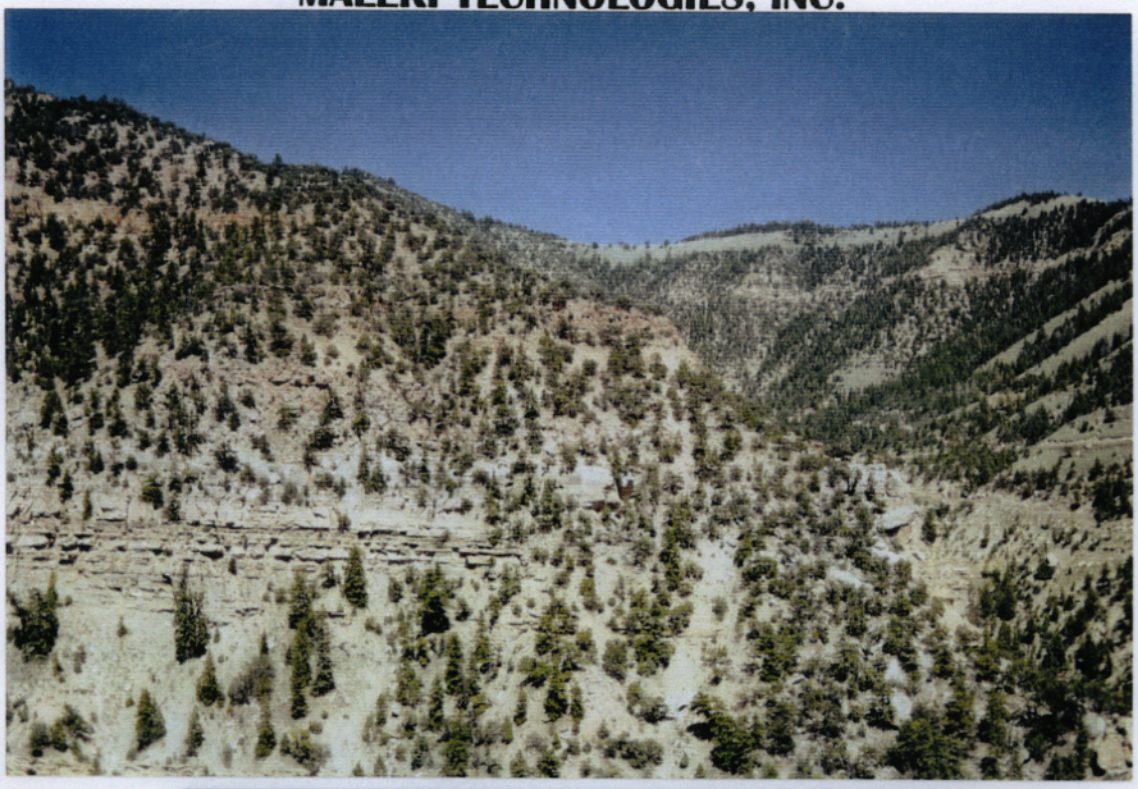

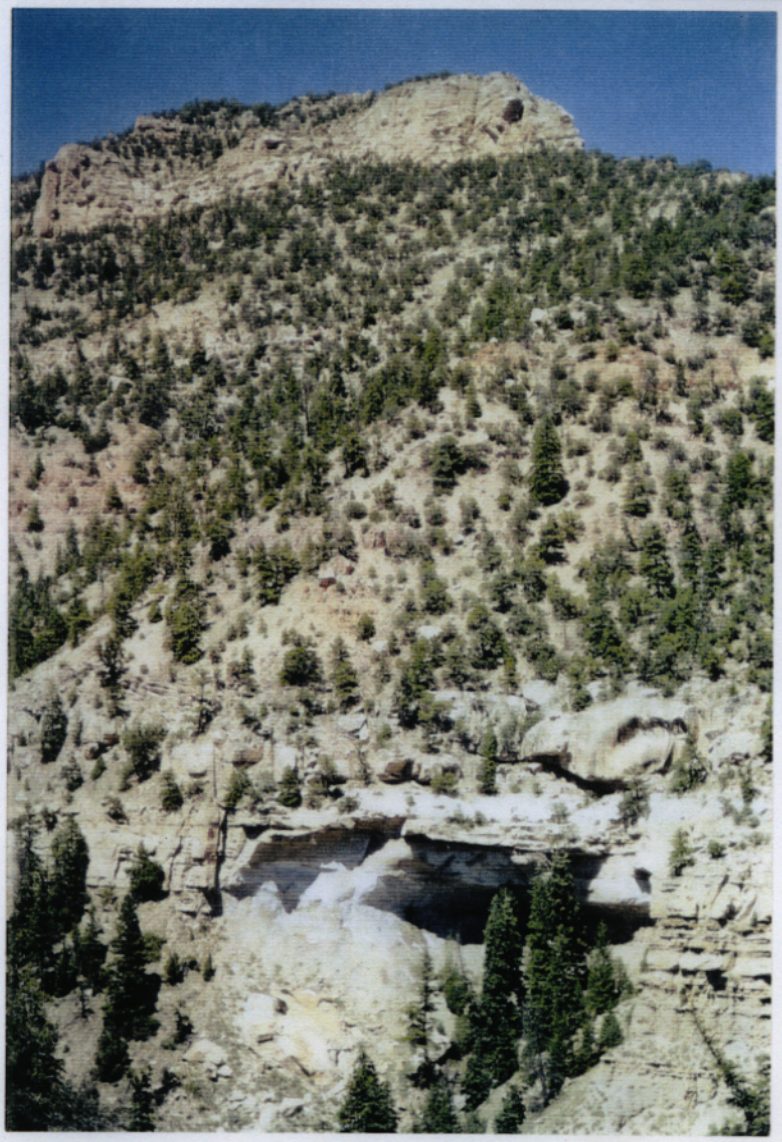

MALEKI TECHNOLOGIES, INC.

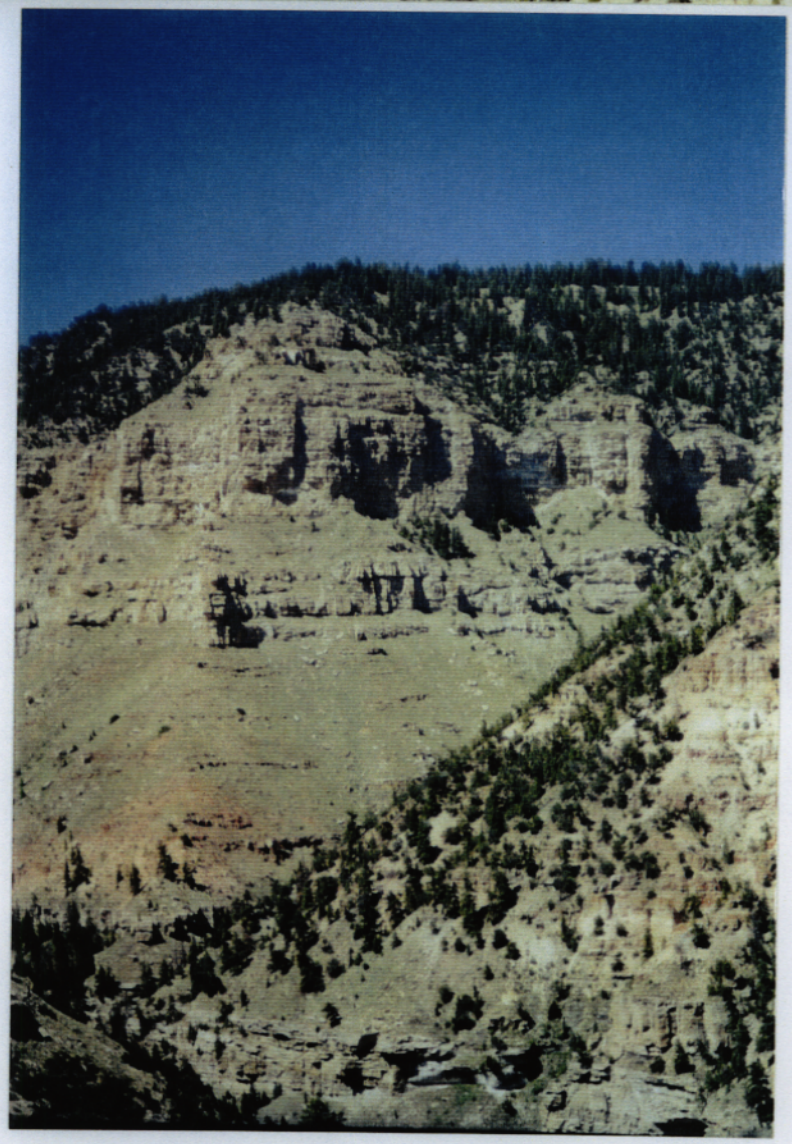

MALEKI TECHNOLOGIES, INC.

MALEKI TECHNOLOGIES, INC.

MALEKI TECHNOLOGIES, INC.

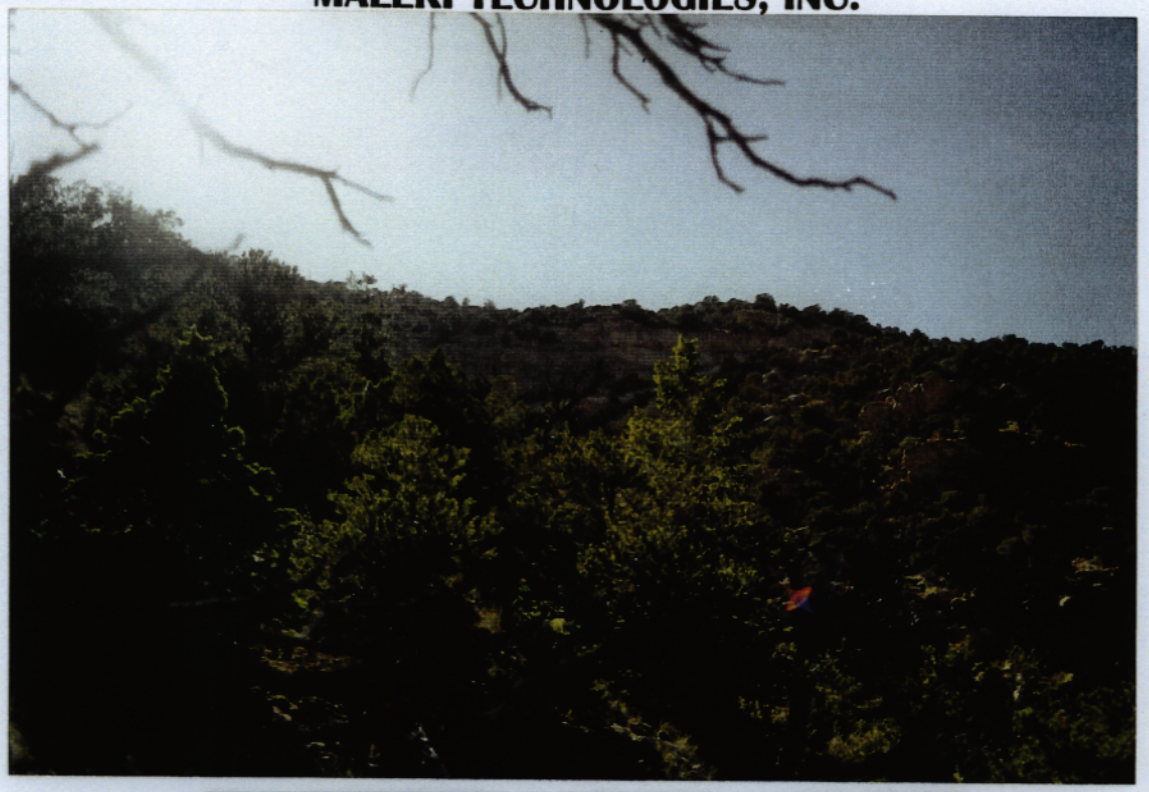

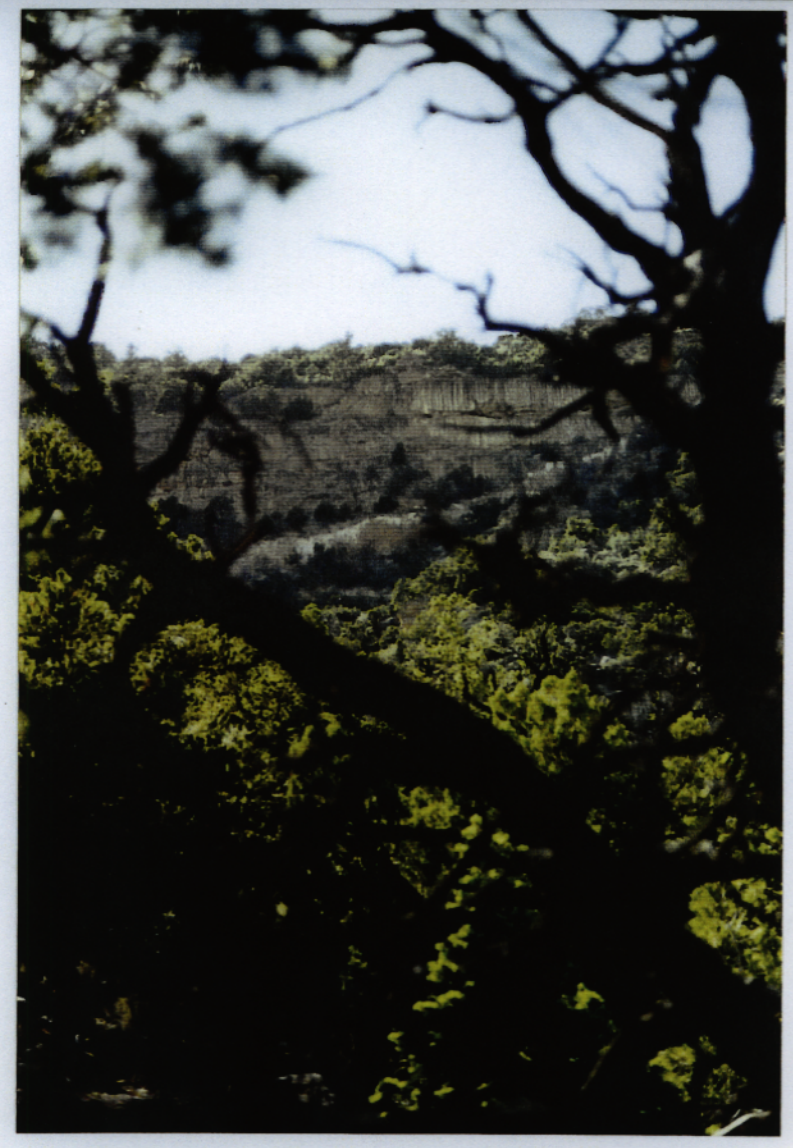

MALEKI TECHNOLOGIES, INC.

MALEKI TECHNOLOGIES, INC.

MALEKI TECHNOLOGIES, INC.

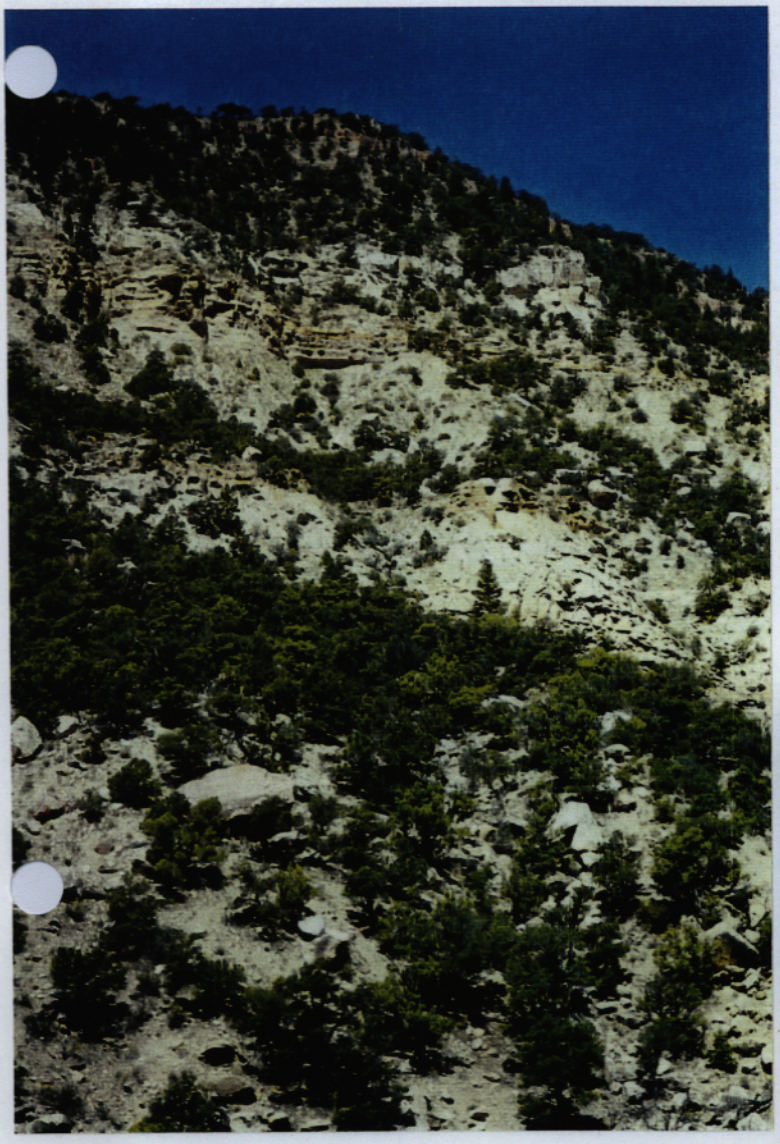

MALEKI TECHNOLOGIES, INC.

MALEKI TECHNOLOGIES, INC.

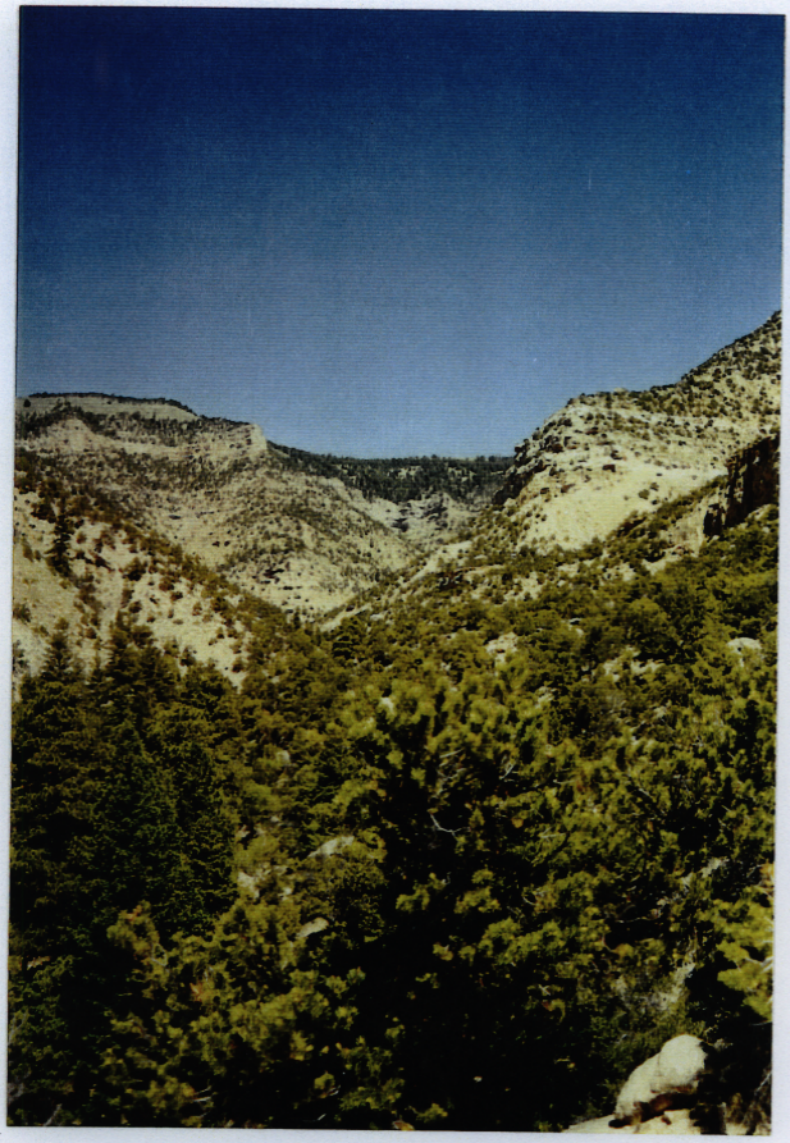

MALEKI TECHNOLOGIES, INC.

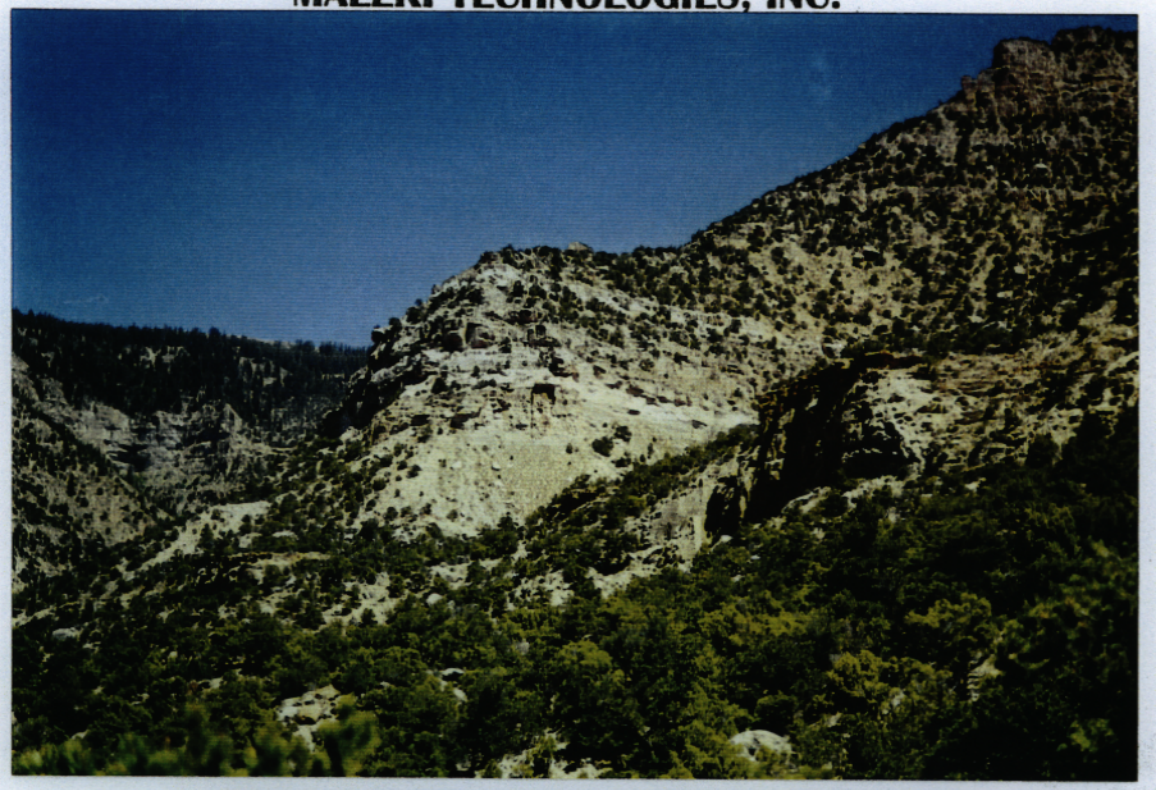

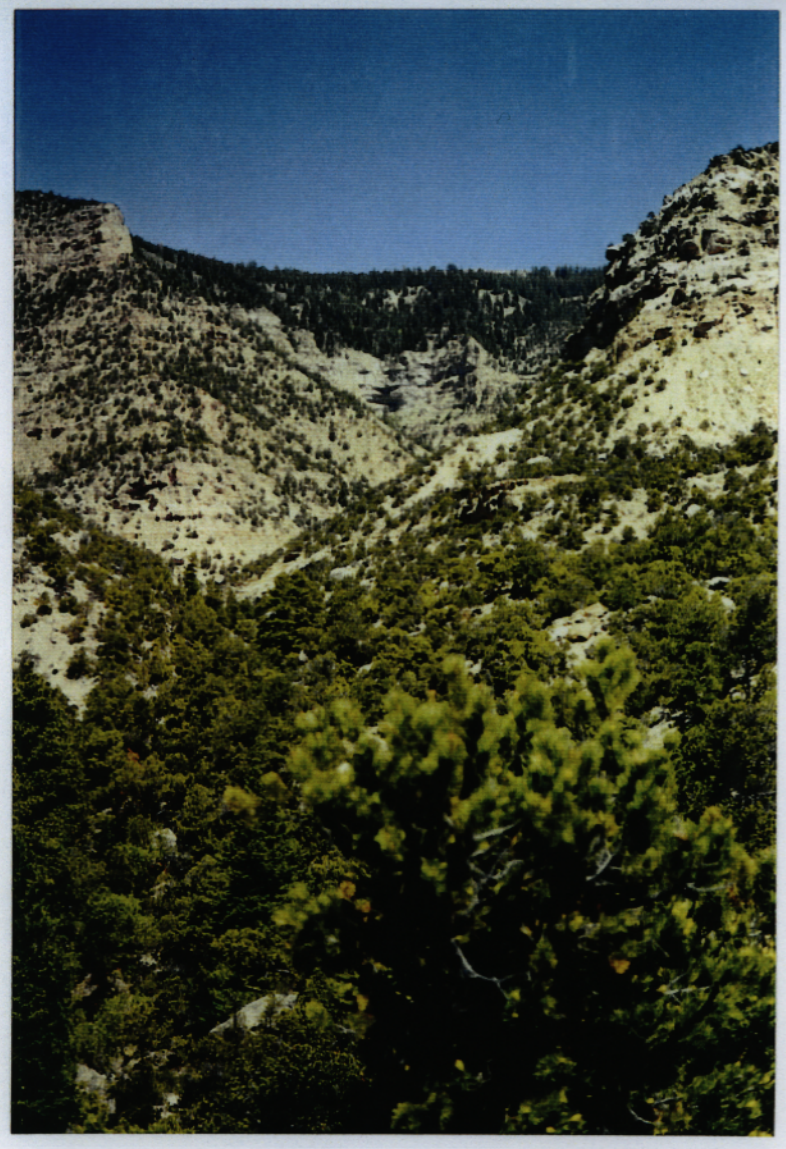

MALEKI TECHNOLOGIES, INC.

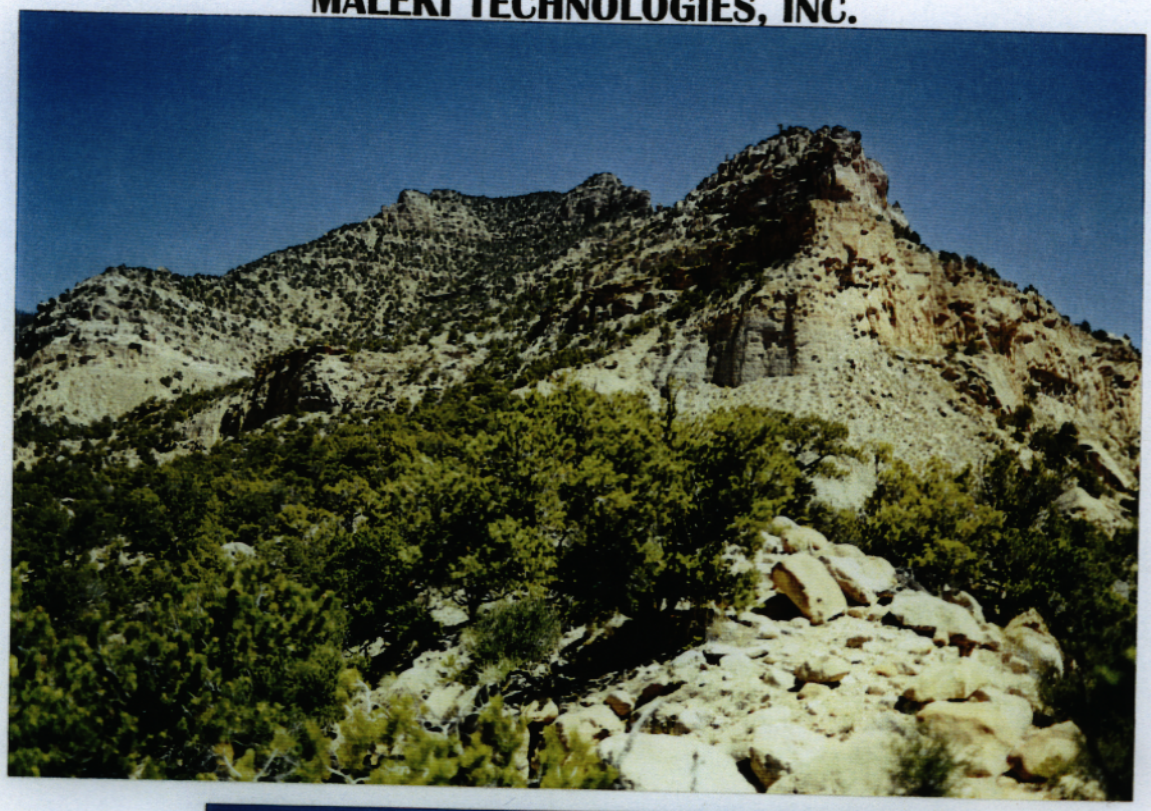

ATTACHMENT C

HISTOGRAM FREQUENCY DIAGRAMS FOR IMPORTANT VARIABLES

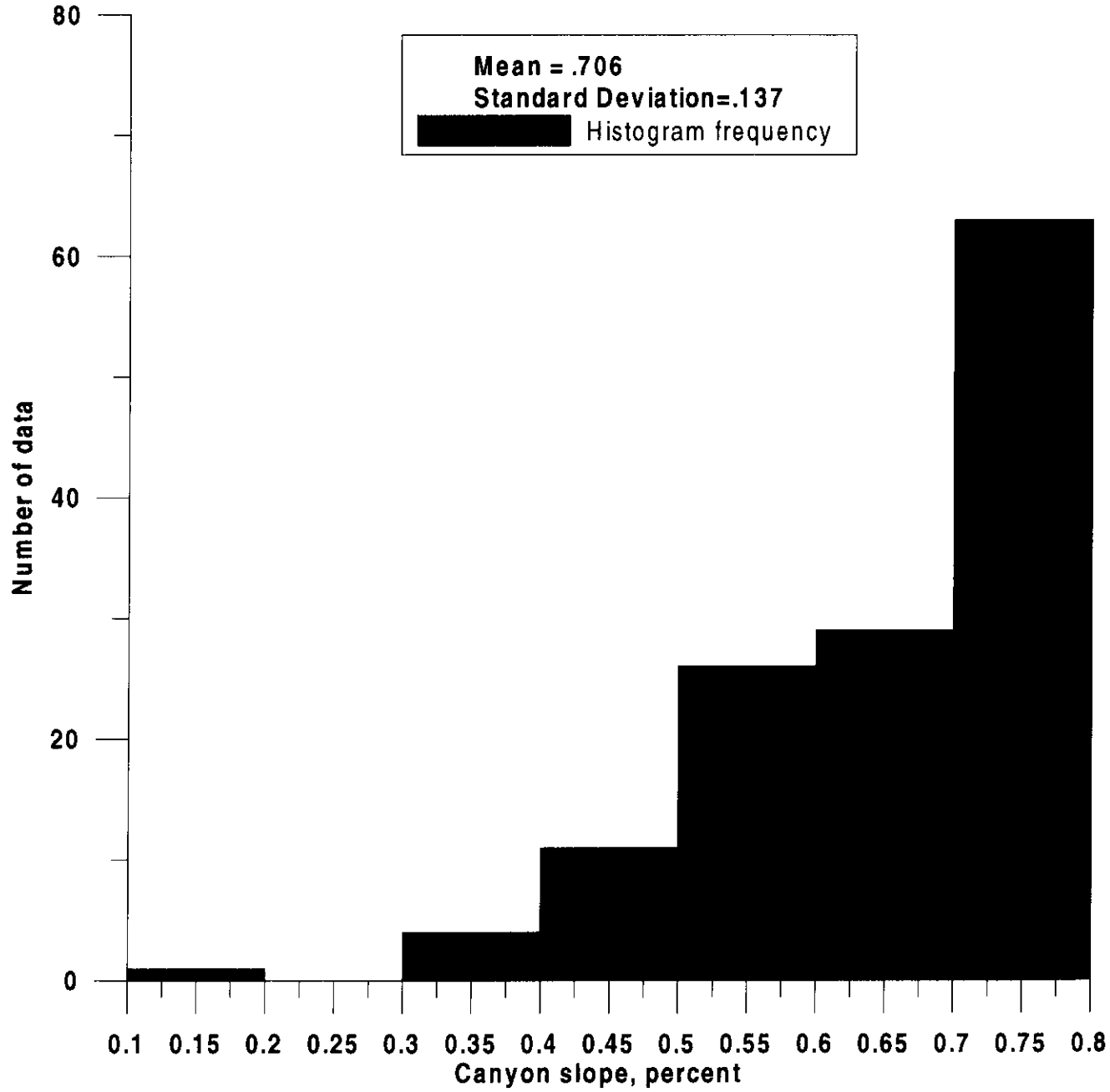
Mean = .706
Standard Deviation=.137
Histogram frequency
Number of data
80
60
40
20
0
0.1
0.15
0.2
0.25
0.3
0.35
0.4
0.45
0.5
0.55
0.6
0.65
0.7
0.75
0.8
Canyon slope, percent

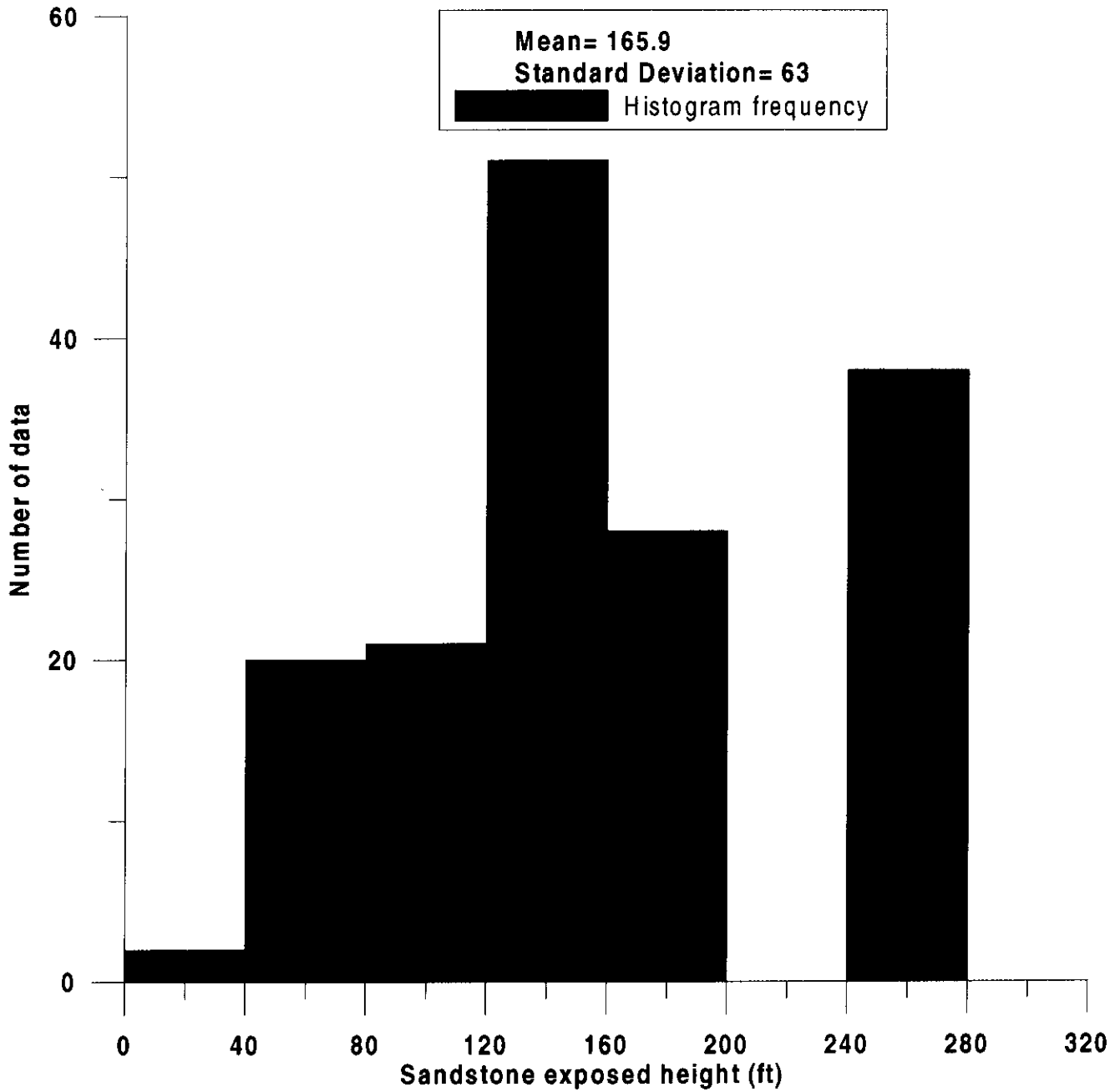
Mean= 165.9
Standard Deviation= 63
Histogram frequency
Number of data
60
40
20
0
0
40
80
120
160
200
240
280
320
Sandstone exposed height (ft)

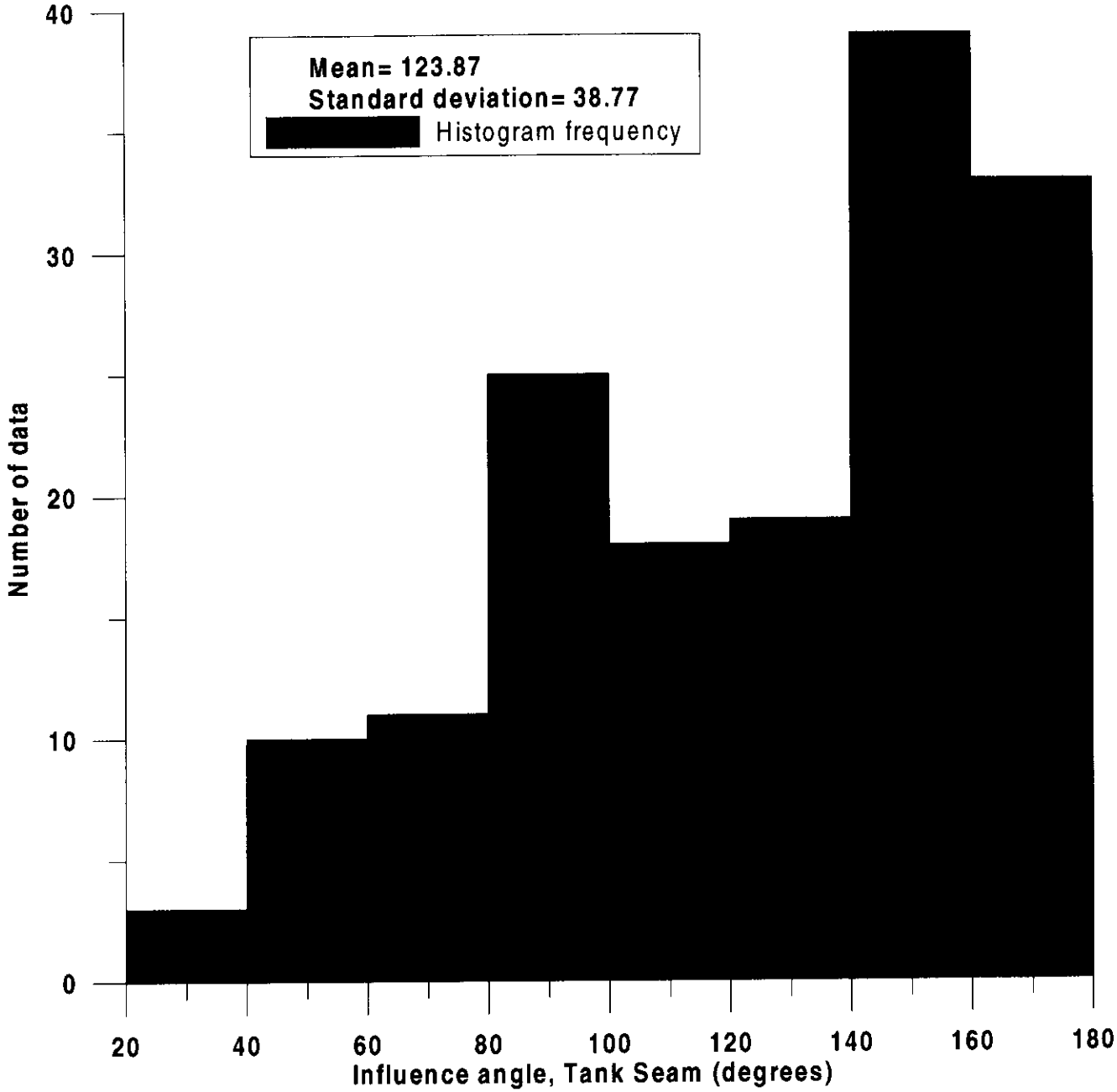
Mean= 123.87
Standard deviation= 38.77
Histogram frequency
Number of data
0
10
20
30
40
20
40
60
80
100
120
140
160
180
Influence angle, Tank Seam (degrees)

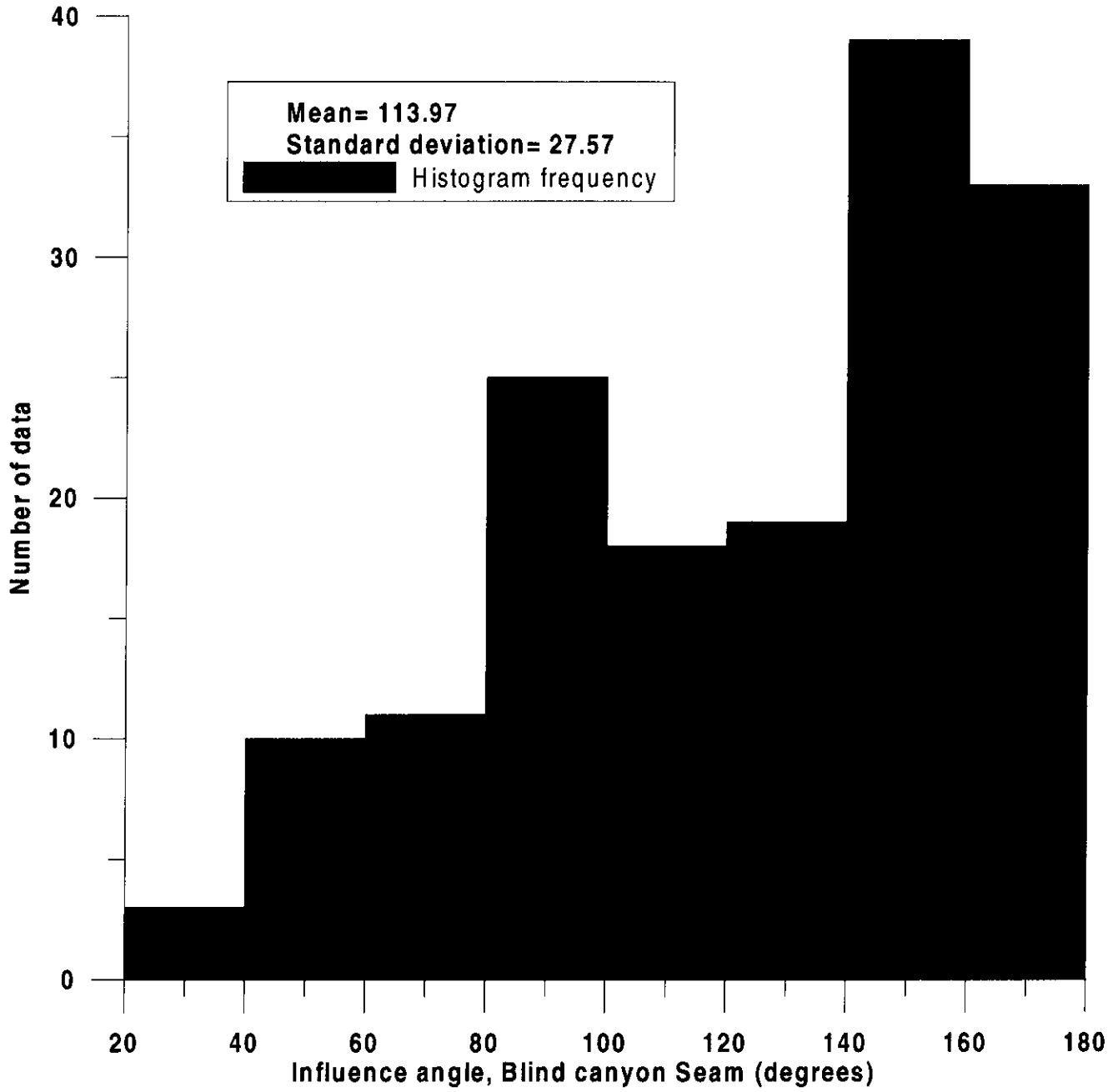
Mean= 113.97
Standard deviation= 27.57
Histogram frequency
Number of data
0
10
20
30
40
20
40
60
80
100
120
140
160
180
Influence angle, Blind canyon Seam (degrees)

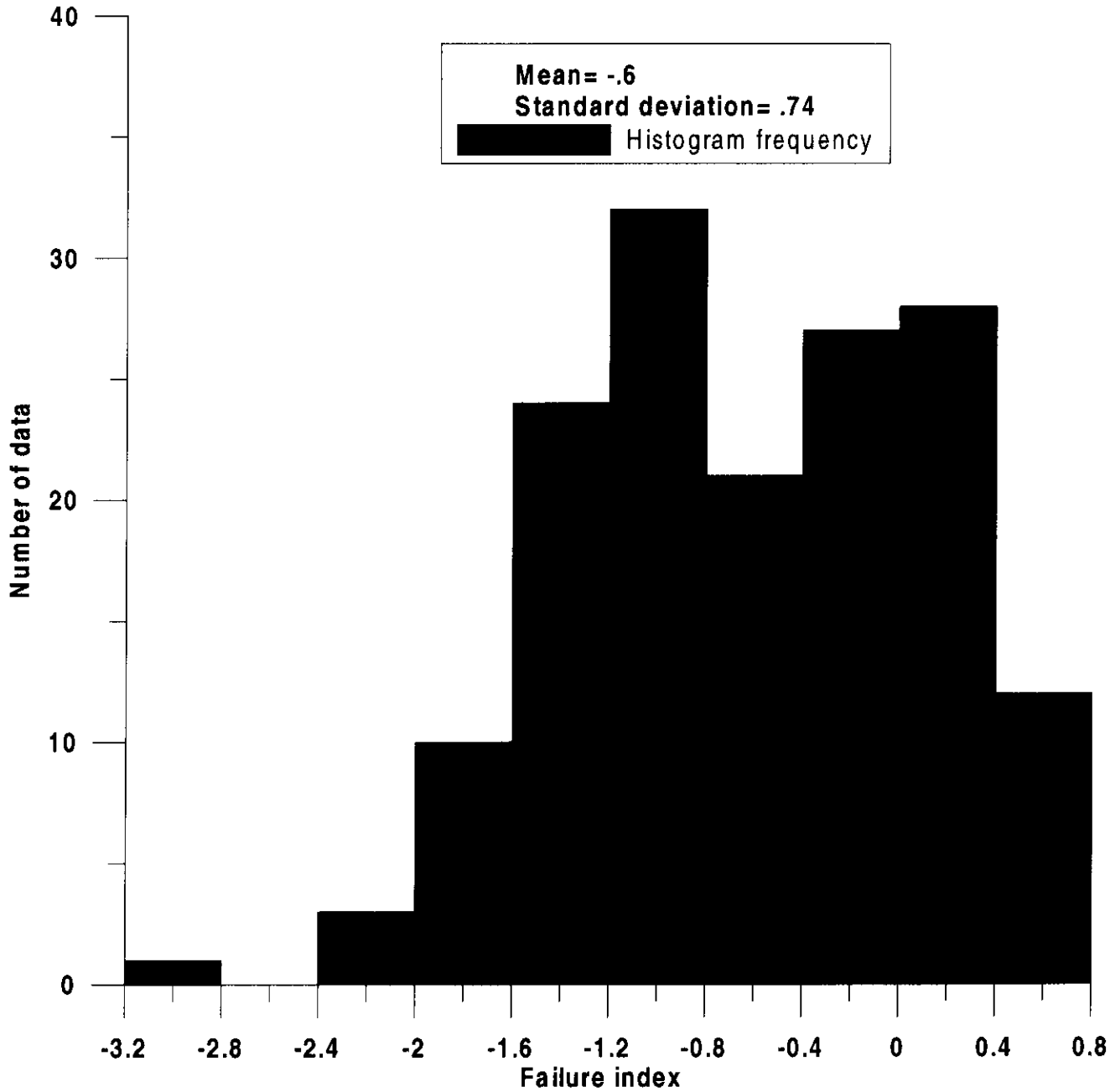
Mean= -.6
Standard deviation= .74
Histogram frequency
Number of data
40
30
20
10
0
-3.2
-2.8
-2.4
-2
-1.6
-1.2
-0.8
-0.4
0
0.4
0.8
Failure index

ATTACHMENT D

PROGRAM OUTPUT FOR ROCK FALL SIMULATIONS

********** CRSP3 **********

COLORADO ROCKFALL SIMULATION PROGRAM

MODELS THE TRAJECTORY OF ROCKS ON IRREGULAR SLOPES
USING SLOPE PROFILE, SURFACE ROUGHNESS, SURFACE MATERIAL PROPERTIES
ROCK SIZE, AND ROCK SHAPE TO PRODUCE A STATISTICAL ANALYSIS OF
ROCKFALL BEHAVIOR ON THE SLOPE

THIS PROGRAM HAS BEEN TESTED AND IS BELIEVED TO BE A RELABLE ENGINEERING TOOL
NO RESPONSIBILITY IS ASSUMED BY THE AUTHOR(S) FOR ANY ERRORS, MISTAKES, OR
MISREPRESENTATIONS THAT MAY OCCUR FROM ANY USE OF THIS PROGRAM

****

BEARWEST.DAT

ROCK STATISTICS

18776 lbs SPHERICAL ROCK 3 ft RADIUS

NUMBER OF CELLS	9
NUMBER OF ROCKS	25
ANALYSIS POSITION	650 ft
INITIAL Y ZONE	8400 ft TO 8560 ft
INITIAL X VELOCITY	1 ft/sec
INITIAL Y VELOCITY	-1 ft/sec

CELL DATA TABLE

BEARWEST.DAT

REMARKS: BEAR CANYON WEST, BACK ANALYSIS

CELL#	SURFACE ROUGHNESS	TANGENTIAL COEFFICIENT	NORM. COEF. RESTITUTION	BEGINNING X,Y	ENDING X,Y
1	5.00	.85	.35	0.0 ,8800.0	350.0 ,8560.0
2	1.00	.87	.37	350.0 ,8560.0	650.0 ,8400.0
3	5.00	.85	.35	650.0 ,8400.0	700.0 ,8240.0
4	5.00	.87	.35	700.0 ,8240.0	800.0 ,8160.0
5	5.00	.82	.33	800.0 ,8160.0	1120.0 ,8000.0
6	5.00	.82	.33	1120.0 ,8000.0	1250.0 ,7920.0
7	5.00	.82	.33	1250.0 ,7920.0	1300.0 ,7840.0
8	5.00	.82	.33	1300.0 ,7840.0	1700.0 ,7600.0
9	5.00	.82	.33	1700.0 ,7600.0	2250.0 ,7440.0

ANALYSIS POINT DATA
BEARWEST.DAT

REMARKS: BEAR CANYON WEST, BACK ANALYSIS

ANALYSIS POINT . . . . . X = 650 , Y =8400
TOTAL ROCKS PASSING ANALYSIS POINT 24

CUMULATIVE PROBABILITY	VELOCITY ft/sec	ENERGY ft - lbs	BOUNCE HEIGHT ft
50%	44.51	822308	0.58
75%	53.44	1108441	7.62
90%	61.47	1365800	13.95
95%	66.29	1520309	17.75
98%	71.70	1693718	22.01
	(NORMAL DISTRIBUTION)		(LOG DISTRIBUTION)

VELOCITY

BOUNCE HEIGHT

ááááááááá

MAXIMUM	64.28	ft/sec
AVERAGE	44.51	ft/sec
MINIMUM	16.20	ft/sec
STANDARD DEVIATION	13.22	ft/sec

ááááááááááááá

MAXIMUM	5.97	ft
AVERAGE	1.68	ft
GEOMETRIC MEAN	0.58	ft
STANDARD DEVIATION	10.42	ft

KINETIC ENERGY
ááááááááááááá

MAXIMUM	1482101	ft - lbs
AVERAGE	822308	ft - lbs
STANDARD DEVIATION	423776	ft - lbs

ANALYSIS POINT BOUNCE HEIGHT DISTRIBUTION

BEARWEST.DAT

```
BOUNCE
HEIGHT ft

  6Ç Ô
  5Ç
  4Ç ÔÔÔ
  3Ç ÔÔÔ
  2Ç ÔÔÔÔ
  1Ç ÔÔÔÔÔÔ
  0Ç ÔÔÔÔÔÔÔ
     0          10         20         30         40         50         60

            FREQUENCY
```

ANALYSIS POINT VELOCITY DISTRIBUTION

BEARWEST.DAT

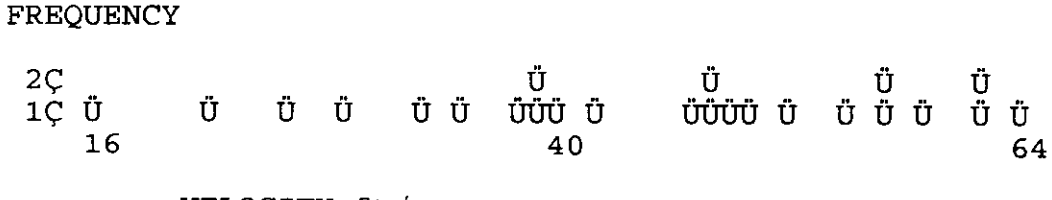

BOUNCE HEIGHT GRAPH

BEARWEST.DAT

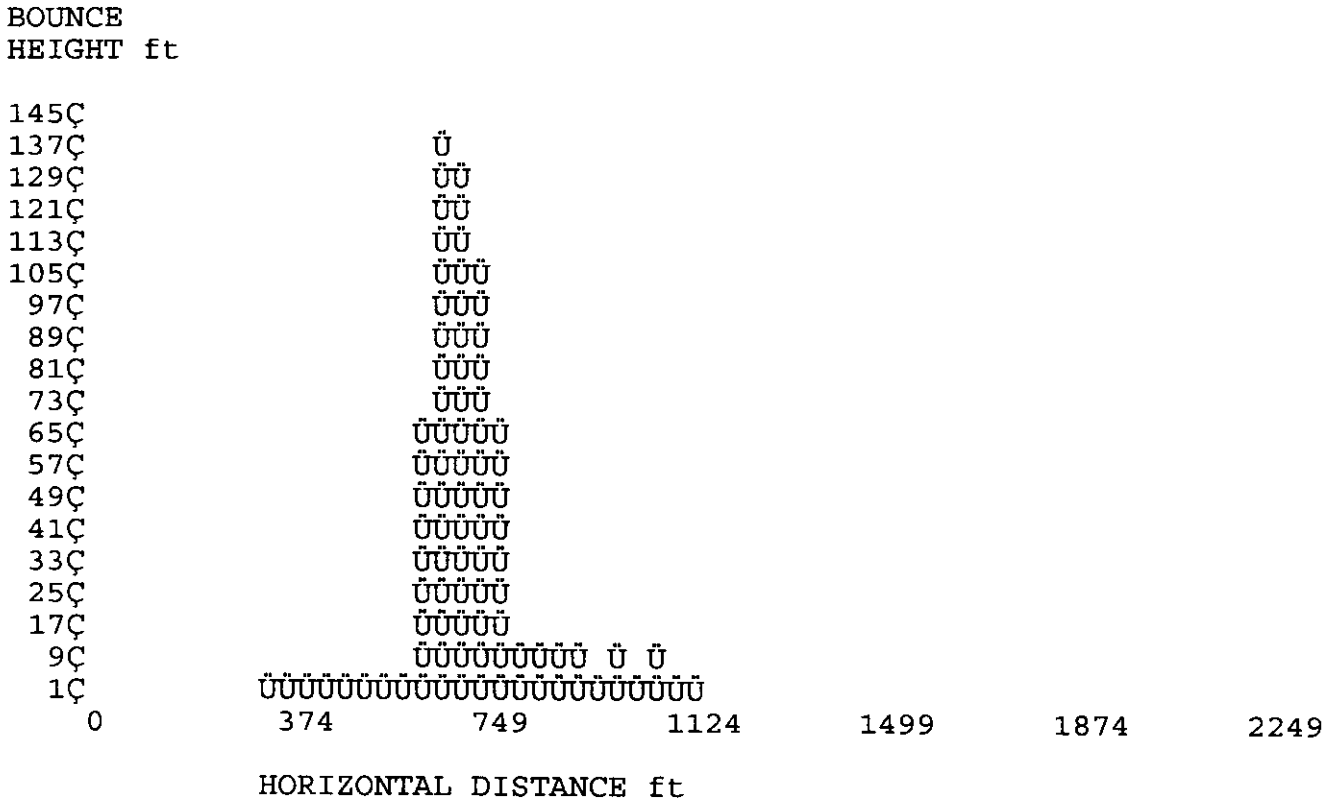

VELOCITY GRAPH
BEARWEST.DAT

VELOCITY ft/sec

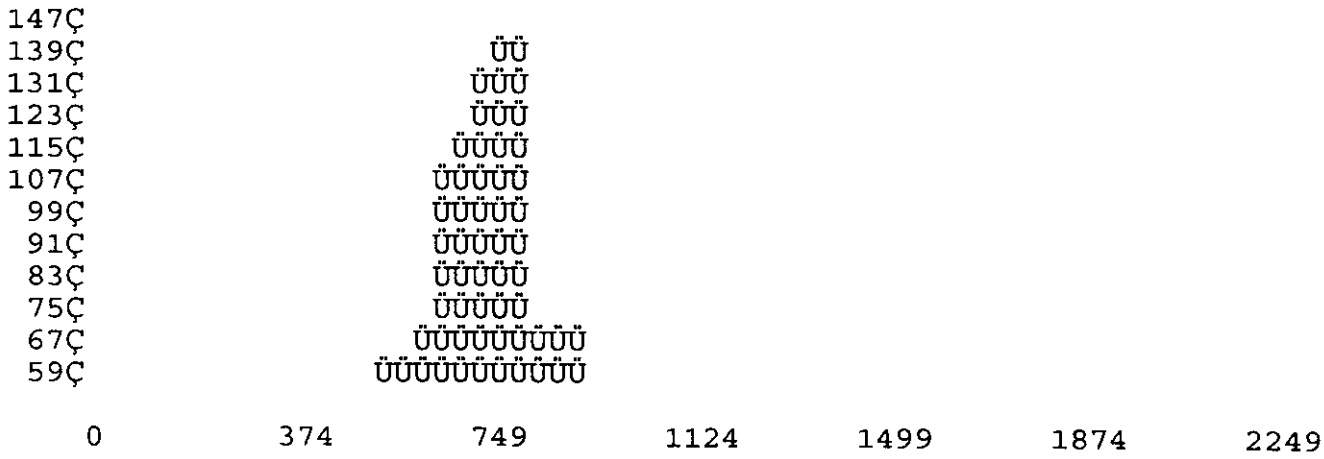

CELL DATA OUTPUT

BEARWEST.DAT

REMARKS: BEAR CANYON WEST, BACK ANALYSIS

DATA COLLECTED AT END OF EACH CELL

CELL #	MAXIMUM VELOCITY (ft/sec)	AVERAGE VELOCITY	STANDARD DEVIATION VELOCITY	AVERAGE BOUNCE HEIGHT (ft)	MAXIMUM BOUNCE HEIGHT (ft)
1	NO ROCKS PASSED POINT				
2	64	44	13.21	1	6
3	97	75	10.50	97	133
4	134	65	41.06	14	53
5	45	35	0.00	5	8
6	NO ROCKS PASSED POINT				
7	NO ROCKS PASSED POINT				
8	NO ROCKS PASSED POINT				
9	NO ROCKS PASSED POINT				

X INTERVAL	ROCKS STOPPED
0 ft TO 10 ft	1
740 ft TO 750 ft	1
810 ft TO 820 ft	1
820 ft TO 830 ft	1
840 ft TO 850 ft	2
850 ft TO 860 ft	1
860 ft TO 870 ft	1
880 ft TO 890 ft	2

910	ft	TO	920	ft	1
920	ft	TO	930	ft	1
940	ft	TO	950	ft	3
960	ft	TO	970	ft	1
970	ft	TO	980	ft	1
980	ft	TO	990	ft	1
1000	ft	TO	1010	ft	1
1030	ft	TO	1040	ft	1
1040	ft	TO	1050	ft	1
1050	ft	TO	1060	ft	1
1080	ft	TO	1090	ft	1
1190	ft	TO	1200	ft	2

********** CRSP3 **********

COLORADO ROCKFALL SIMULATION PROGRAM

MODELS THE TRAJECTORY OF ROCKS ON IRREGULAR SLOPES
USING SLOPE PROFILE, SURFACE ROUGHNESS, SURFACE MATERIAL PROPERTIES
ROCK SIZE, AND ROCK SHAPE TO PRODUCE A STATISTICAL ANALYSIS OF
ROCKFALL BEHAVIOR ON THE SLOPE

THIS PROGRAM HAS BEEN TESTED AND IS BELIEVED TO BE A RELABLE ENGINEERING TOOL
NO RESPONSIBILITY IS ASSUMED BY THE AUTHOR(S) FOR ANY ERRORS, MISTAKES, OR
MISREPRESENTATIONS THAT MAY OCCUR FROM ANY USE OF THIS PROGRAM

****

WHR.DAT

ROCK STATISTICS

18776 lbs SPHERICAL ROCK 3 ft RADIUS

NUMBER OF CELLS	13
NUMBER OF ROCKS	25
ANALYSIS POSITION	800 ft
INITIAL Y ZONE	8160 ft TO 8400 ft
INITIAL X VELOCITY	1 ft/sec
INITIAL Y VELOCITY	-1 ft/sec

CELL DATA TABLE

WHR.DAT

REMARKS: SOUTH WILD HORSE RIDGE, B-B'

CELL#	SURFACE ROUGHNESS	TANGENTIAL COEFFICIENT	NORM. COEF. RESTITUTION	BEGINNING X,Y	ENDING X,Y
1	5.00	.85	.35	0.0 ,8800.0	100.0 ,8780.0
2	5.00	.85	.35	100.0 ,8800.0	300.0 ,8720.0
3	5.00	.85	.35	300.0 ,8720.0	400.0 ,8640.0
4	5.00	.85	.35	400.0 ,8640.0	500.0 ,8560.0
5	5.00	.85	.35	500.0 ,8560.0	600.0 ,8400.0
6	1.00	.87	.37	600.0 ,8400.0	800.0 ,8160.0
7	5.00	.85	.35	800.0 ,8160.0	1050.0 ,8000.0
8	5.00	.87	.35	1050.0 ,8000.0	1350.0 ,7840.0
9	5.00	.82	.33	1350.0 ,7840.0	1600.0 ,7680.0
10	5.00	.82	.33	1600.0 ,7680.0	1800.0 ,7520.0
11	5.00	.82	.33	1800.0 ,7520.0	1820.0 ,7440.0
12	5.00	.82	.33	1820.0 ,7440.0	2000.0 ,7360.0
13	5.00	.82	.33	2000.0 ,7360.0	2300.0 ,7280.0

ANALYSIS POINT DATA
WHR.DAT

REMARKS: SOUTH WILD HORSE RIDGE, B-B'

ANALYSIS POINT . . . . . X = 800 , Y =8160
TOTAL ROCKS PASSING ANALYSIS POINT 24

CUMULATIVE PROBABILITY	VELOCITY ft/sec	ENERGY ft - lbs	BOUNCE HEIGHT ft
50%	64.28	1638737	2.38
75%	77.40	2208965	6.67
90%	89.19	2721851	10.52
95%	96.27	3029768	12.84
98%	104.22	3375352	15.44
	(NORMAL DISTRIBUTION)		(LOG DISTRIBUTION)

VELOCITY		BOUNCE HEIGHT	
MAXIMUM	89.92 ft/sec	MAXIMUM	13.62 ft
AVERAGE	64.28 ft/sec	AVERAGE	4.45 ft
MINIMUM	20.62 ft/sec	GEOMETRIC MEAN	2.38 ft
STANDARD DEVIATION	19.43 ft/sec	STANDARD DEVIATION	6.35 ft

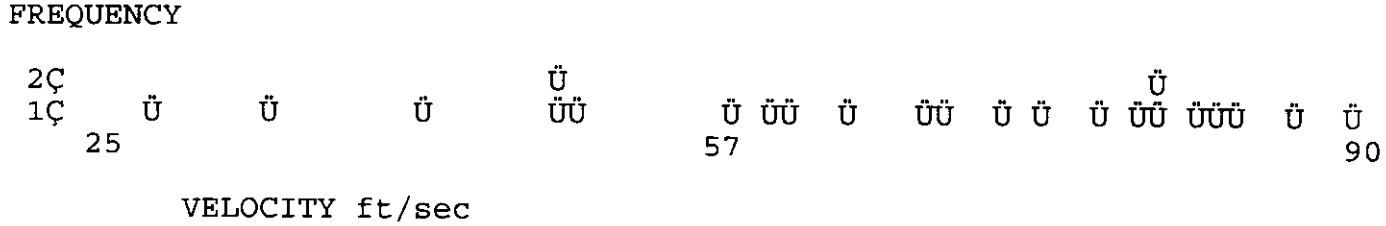

BOUNCE HEIGHT GRAPH

WHR.DAT

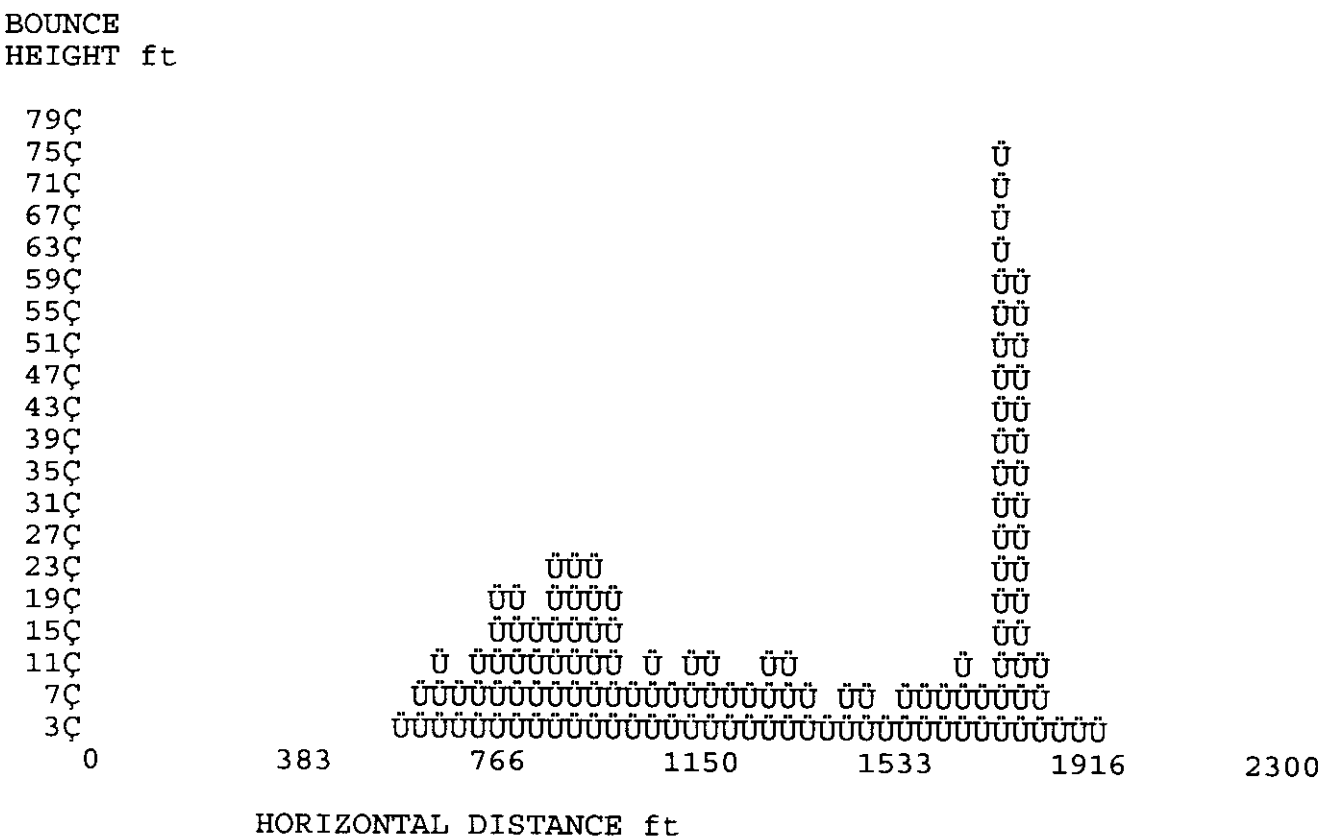

VELOCITY GRAPH
WHR.DAT

VELOCITY ft/sec

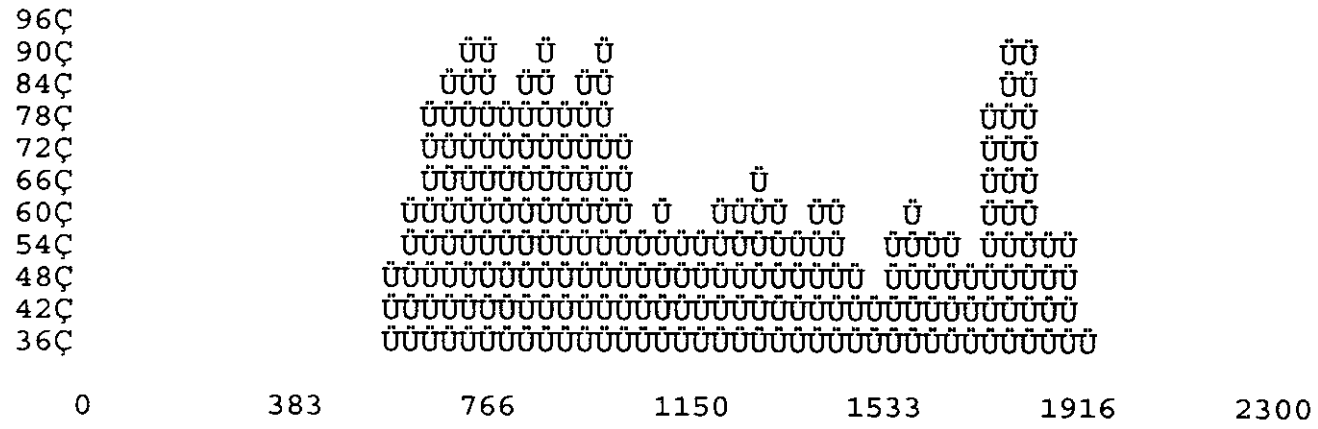

CELL DATA OUTPUT

WHR.DAT

REMARKS: SOUTH WILD HORSE RIDGE, B-B'

DATA COLLECTED AT END OF EACH CELL

CELL #	MAXIMUM VELOCITY (ft/sec)	AVERAGE VELOCITY	STANDARD DEVIATION VELOCITY	AVERAGE BOUNCE HEIGHT (ft)	MAXIMUM BOUNCE HEIGHT (ft)
1	NO ROCKS PASSED POINT				
2	NO ROCKS PASSED POINT				
3	NO ROCKS PASSED POINT				
4	NO ROCKS PASSED POINT				
5	NO ROCKS PASSED POINT				
6	90	64	19.38	4	14
7	72	39	15.02	5	20
8	42	25	11.47	3	6
9	37	22	0.00	2	6
10	46	37	0.00	3	6
11	62	55	0.00	58	74
12	28	28	0.00	7	7
13	NO ROCKS PASSED POINT				

X INTERVAL	ROCKS STOPPED
0 ft TO 10 ft	1
910 ft TO 920 ft	1
970 ft TO 980 ft	1
1010 ft TO 1020 ft	1

1020 ft	TO 1030 ft	1
1050 ft	TO 1060 ft	1
1090 ft	TO 1100 ft	2
1100 ft	TO 1110 ft	1
1120 ft	TO 1130 ft	1
1130 ft	TO 1140 ft	1
1150 ft	TO 1160 ft	3
1170 ft	TO 1180 ft	1
1200 ft	TO 1210 ft	1
1240 ft	TO 1250 ft	1
1270 ft	TO 1280 ft	1
1300 ft	TO 1310 ft	1
1390 ft	TO 1400 ft	1
1450 ft	TO 1460 ft	1
1470 ft	TO 1480 ft	1
1850 ft	TO 1860 ft	1
1970 ft	TO 1980 ft	1
2040 ft	TO 2050 ft	1

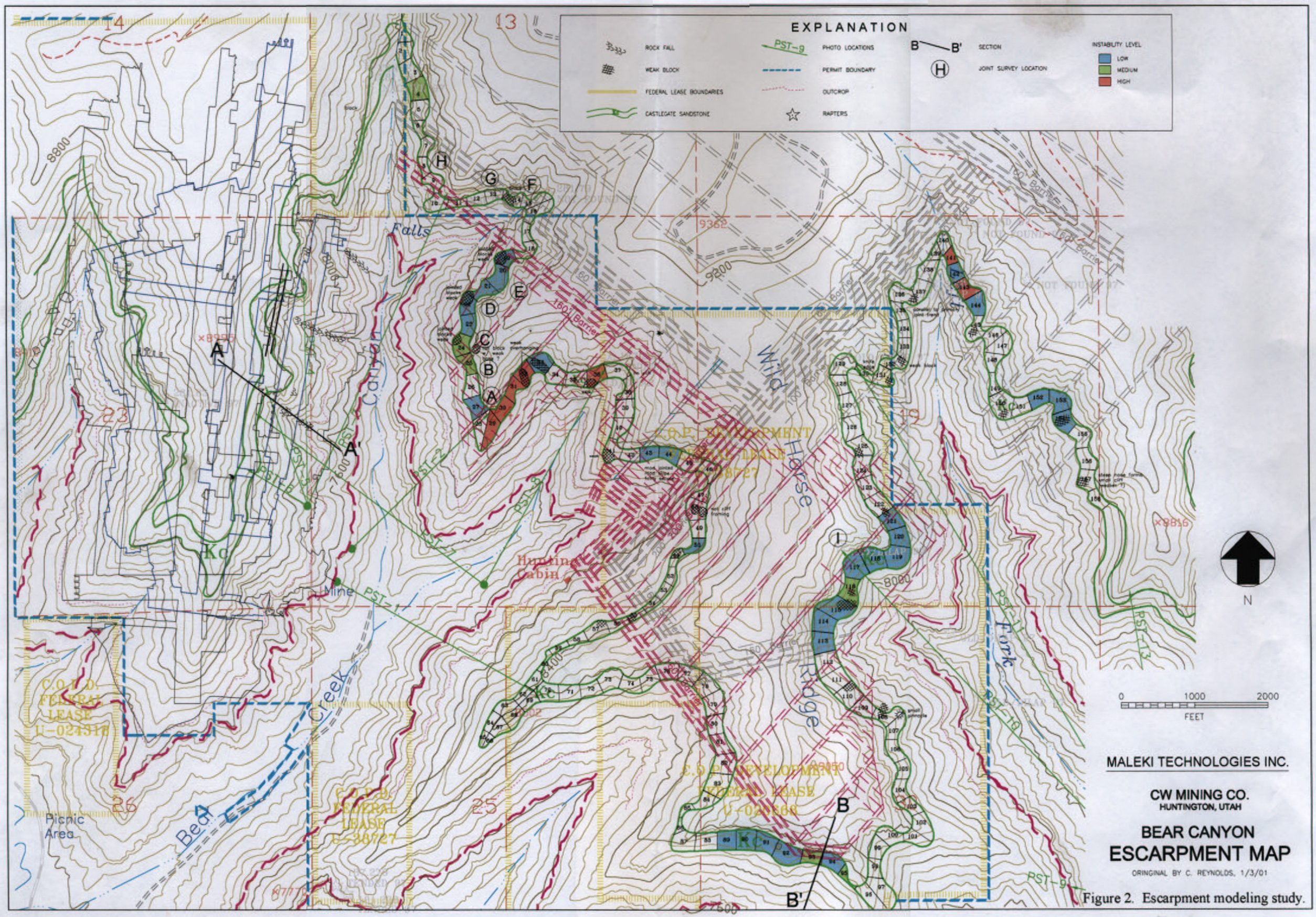

Figure 2. Escarpment modeling study.

CRSP Input File - C:\Program Files\Crsp\A-A'.DAT

Input File Specifications

Units of Measure: U.S.
Total Number of Cells: 9
Analysis Point X-Coordinate 1: 650
Analysis Point X-Coordinate 2: 0
Analysis Point X-Coordinate 3: 0
Initial Y-Top Starting Zone Coordinate: 8560
Initial Y-Base Starting Zone Coordinate: 8400
Remarks:

Cell Data

Cell No.	Surface R.	Tangent C.	Normal C.	Begin X	Begin Y	End X	End Y
1	5	.85	.35	0	8800	350	8560
2	1	.87	.37	350	8560	650	8400
3	5	.85	.35	650	8400	700	8240
4	5	.87	.35	700	8240	800	8160
5	5	.82	.33	800	8160	1120	8000
6	5	.82	.33	1120	8000	1250	7920
7	5	.82	.33	1250	7920	1300	7840
8	5	.82	.33	1300	7840	1700	7600
9	5	.82	.33	1700	7600	2250	7440

C:\Program Files\Crsp\A-A'.DAT Total Rocks Rolled: 25

Spherical Rock: 6-ft dia., 18661-lb

Scale: Each division = 20 feet

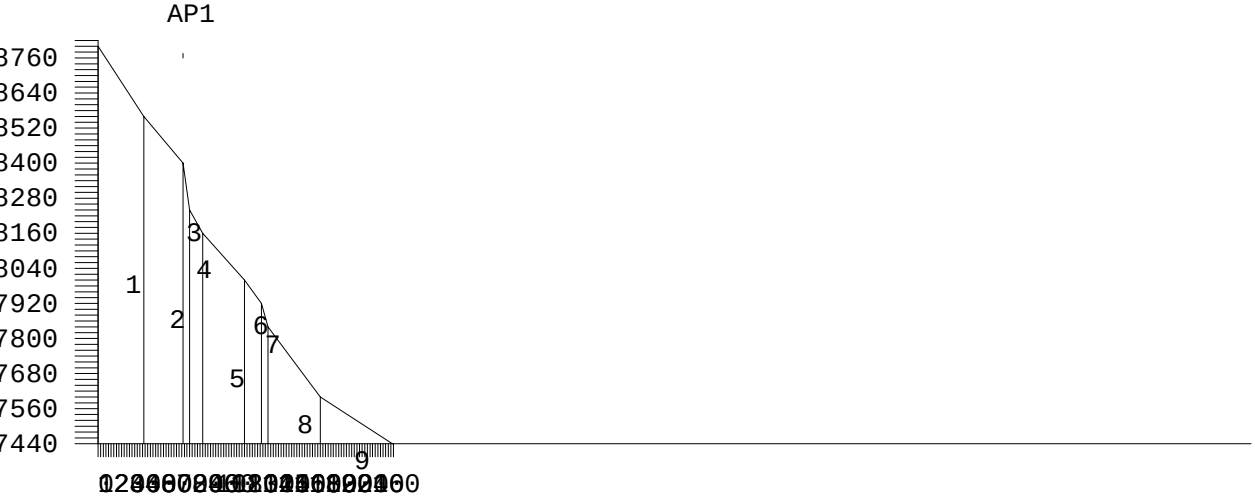

CRSP Analysis Point Data - C:\Program Files\Crsp\A-A'.DAT

Analysis Point 1

Analysis Point 1: X = 650, Y = 8400

Spherical Rock: 6-ft dia., 18661-lb

Total Rocks Passing Analysis Point: 24

Velocity (ft/sec)	Bounce Height (ft)	Kinetic Energy (ft-lb)
Maximum: 64.28	Maximum: 4.63	Maximum: 1473010
Average: 45.19	Average: 1.84	Average: 837192
Minimum: 16.2	G. Mean: .76	Std. Dev.: 434819
Std. Dev.: 13.72	Std. Dev.: 9.73	

CRSP Analysis Point Statistical Analysis - C:\Program Files\Crsp\A-A'.DAT

Analysis Point 1

Analysis Point 1: X = 650, Y = 8400

Spherical Rock: 6-ft dia., 18661-lb

Total Rocks Passing Analysis Point: 24

Cumulative Probability	Velocity (ft/sec)	Energy (ft-lb)	Bounce Height (ft)
50%	45.19	837192	0.76
75%	54.45	1130782	7.33
90%	62.78	1394848	13.24
95%	67.79	1553383	16.79
98%	73.4	1731311	20.78

Note: Velocity and kinetic energy are analyzed assuming a normal distribution.
Bounce height is analyzed assuming a log distribution.

Analysis Point 1 Bounce Height Distribution - C:\Program Files\Crsp\A-A'.DAT

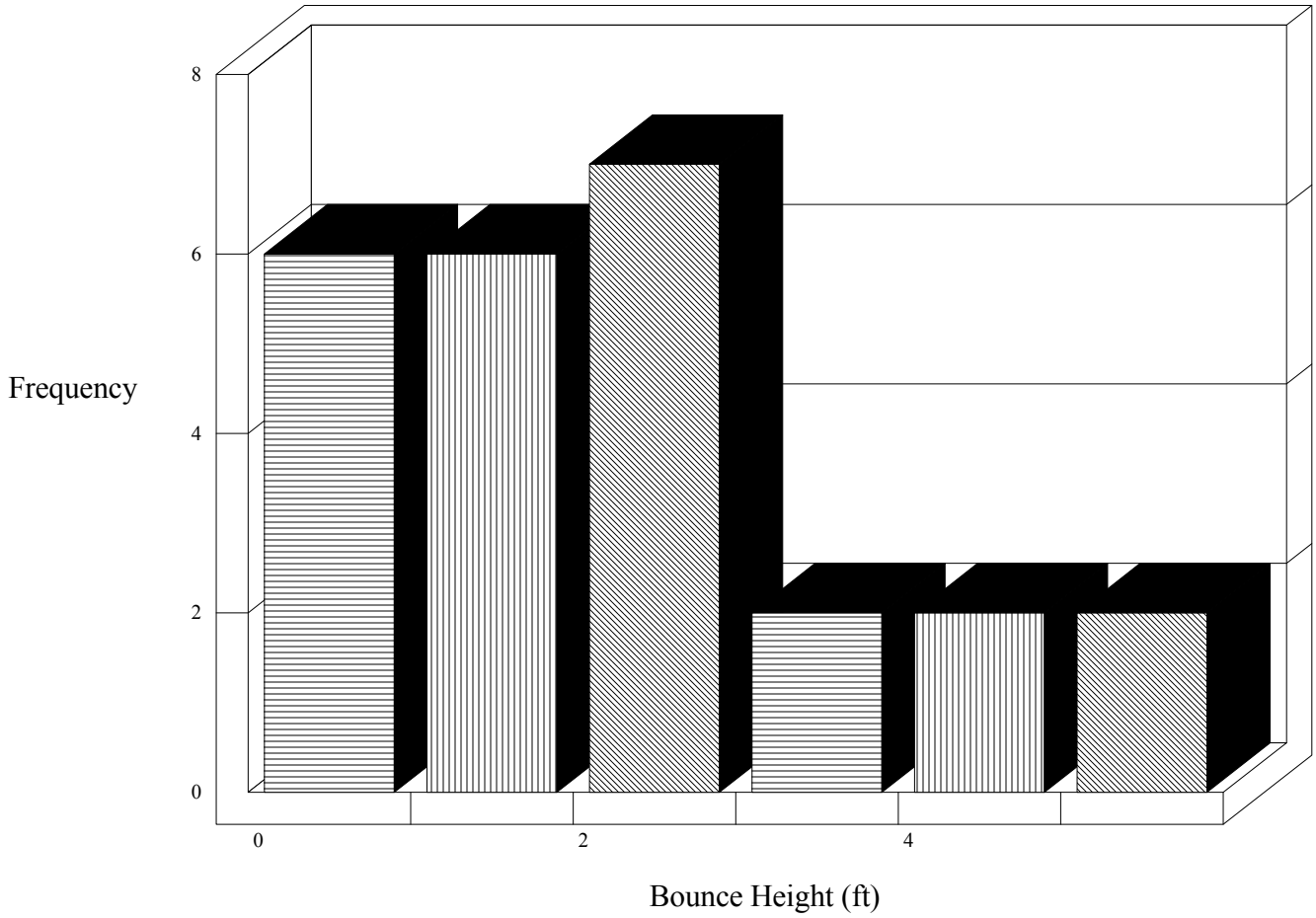

Analysis Point 1 Velocity Distribution - C:\Program Files\Crsp\A-A'.DAT

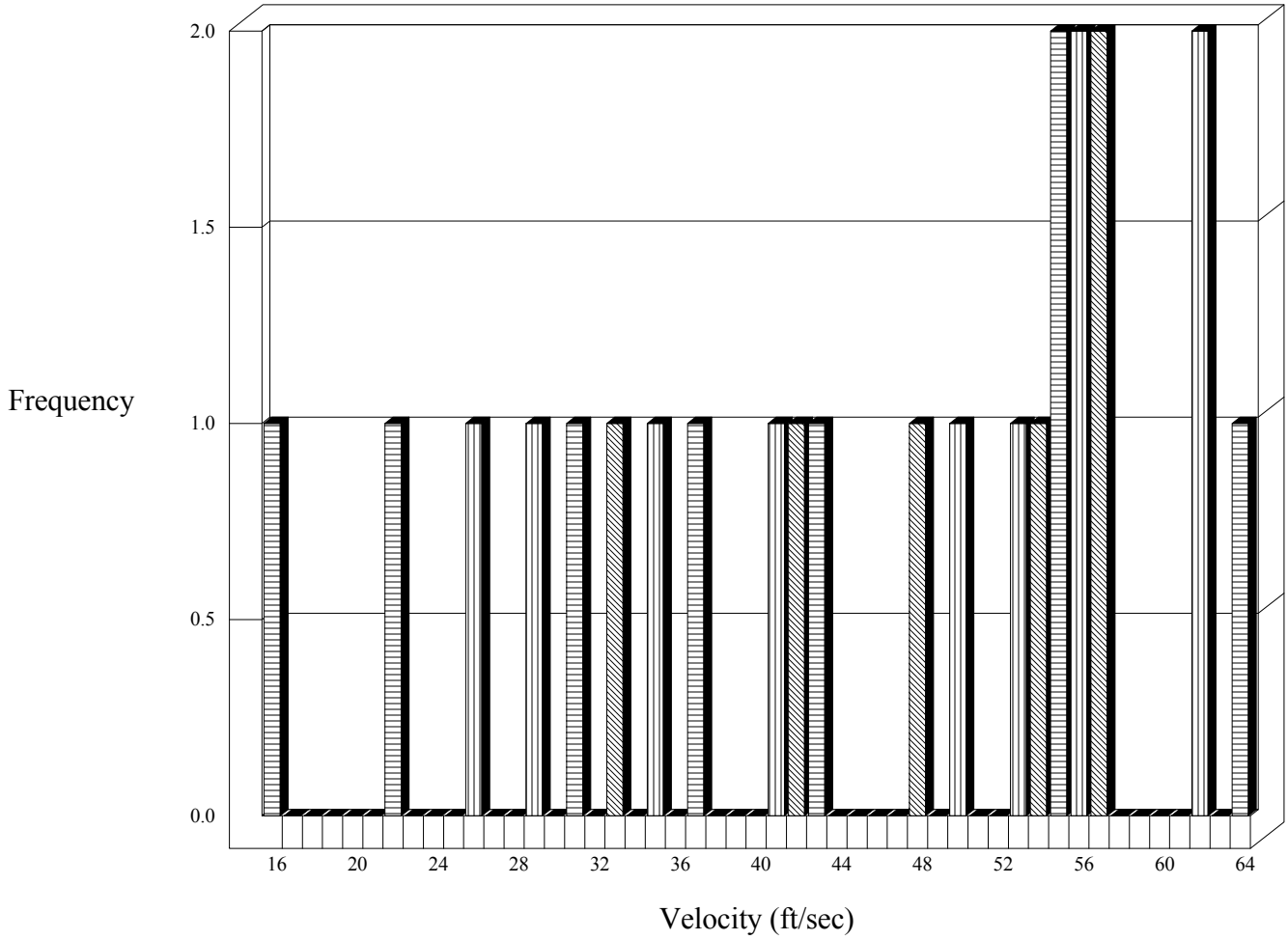

Bounce Height Graph - C:\Program Files\Crsp\A-A'.DAT

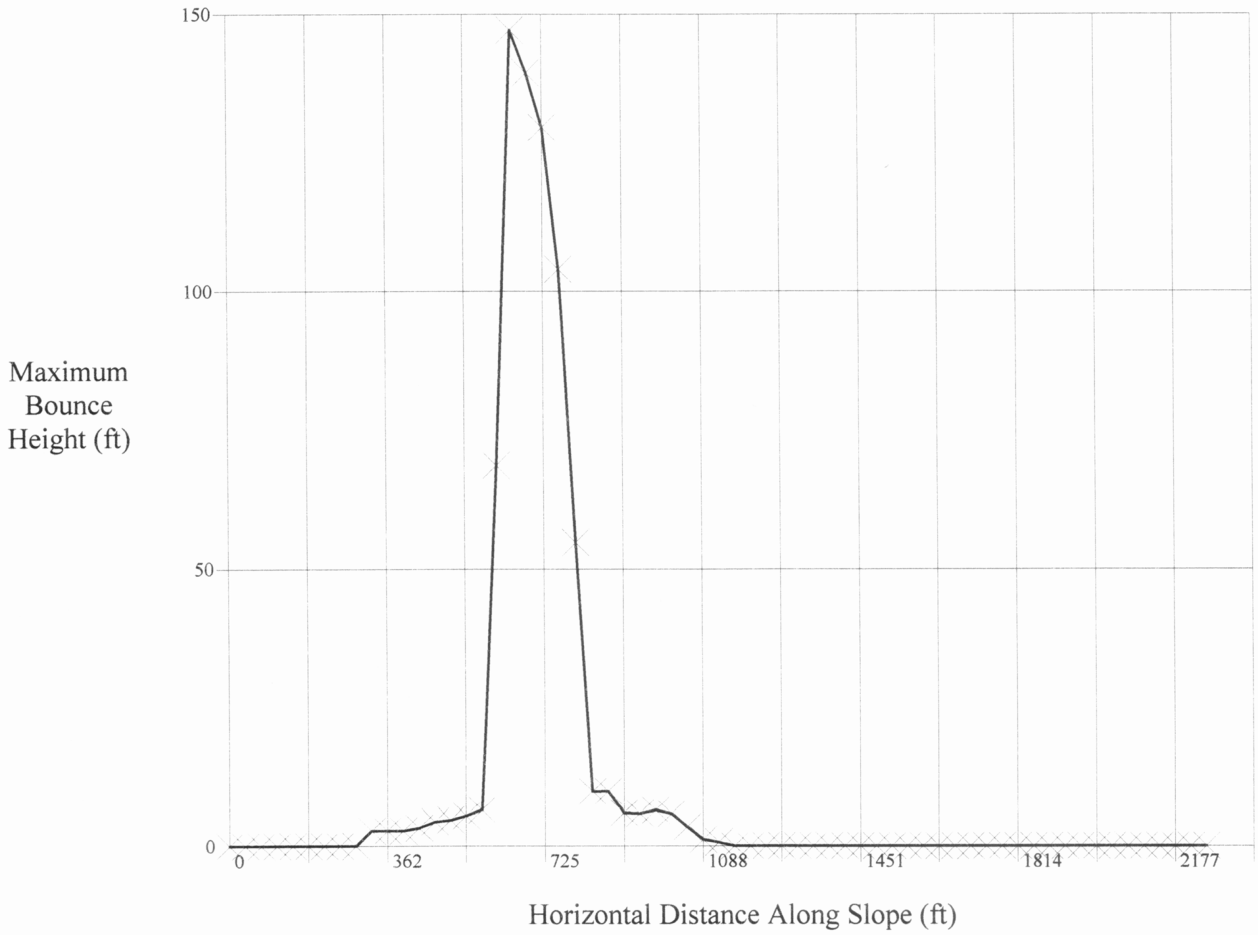

Velocity Graph - C:\Program Files\Crsp\A-A'.DAT

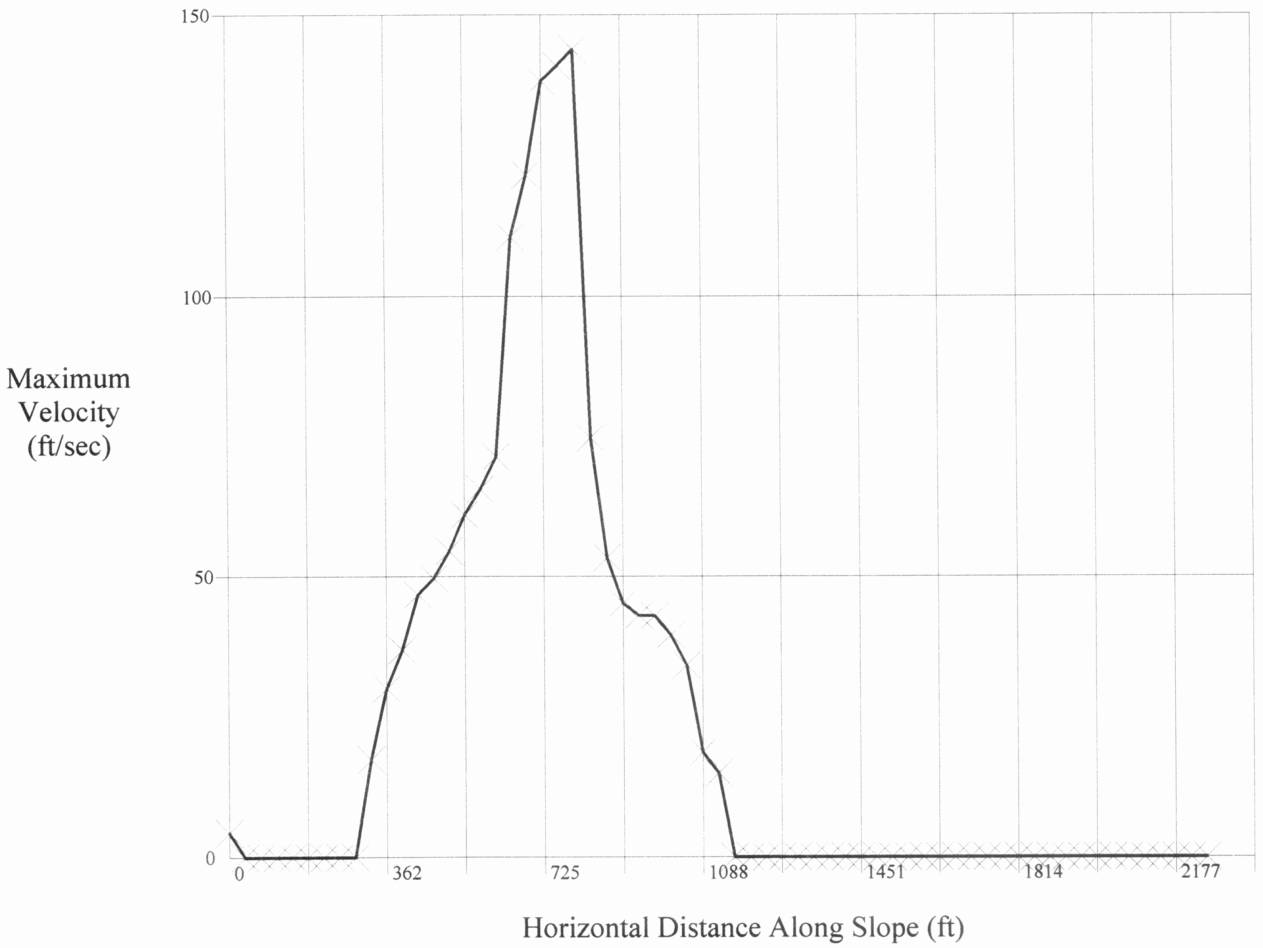

CRSP Data Collected at End of Each Cell - C:\Program Files\Crsp\A-A'.DAT

Velocity Units: ft/sec Bounce Height Units: ft

Cell No.	Max. Velocity	Avg. Velocity	Std. Dev. Velocity	Max. Bounce Ht.	Avg. Bounce Ht.
1	No rocks	past end of cell			
2	62	44	13.69	6	1
3	96	79	9.38	128	92
4	135	58	41.56	50	9
5	39	25	0	2	1
6	37	26	0	4	2
7	68	59	0	33	22
8	27	27	0	2	2
9	No rocks	past end of cell			

CRSP Rocks Stopped Data - C:\Program Files\Crsp\A-A'.DAT

X Interval	Rocks Stopped
0 To 10 ft	1
10 To 20 ft	0
20 To 30 ft	0
30 To 40 ft	0
40 To 50 ft	0
50 To 60 ft	0
60 To 70 ft	0
70 To 80 ft	0
80 To 90 ft	0
90 To 100 ft	0
100 To 110 ft	0
110 To 120 ft	0
120 To 130 ft	0
130 To 140 ft	0
140 To 150 ft	0
150 To 160 ft	0
160 To 170 ft	0
170 To 180 ft	0
180 To 190 ft	0
190 To 200 ft	0
200 To 210 ft	0
210 To 220 ft	0
220 To 230 ft	0
230 To 240 ft	0
240 To 250 ft	0
250 To 260 ft	0
260 To 270 ft	0
270 To 280 ft	0
280 To 290 ft	0
290 To 300 ft	0
300 To 310 ft	0
310 To 320 ft	0
320 To 330 ft	0
330 To 340 ft	0
340 To 350 ft	0
350 To 360 ft	0
360 To 370 ft	0
370 To 380 ft	0
380 To 390 ft	0
390 To 400 ft	0
400 To 410 ft	0
410 To 420 ft	0
420 To 430 ft	0
430 To 440 ft	0

X Interval	Rocks Stopped
440 To 450 ft	0
450 To 460 ft	0
460 To 470 ft	0
470 To 480 ft	0
480 To 490 ft	0
490 To 500 ft	0
500 To 510 ft	0
510 To 520 ft	0
520 To 530 ft	0
530 To 540 ft	0
540 To 550 ft	0
550 To 560 ft	0
560 To 570 ft	0
570 To 580 ft	0
580 To 590 ft	0
590 To 600 ft	0
600 To 610 ft	0
610 To 620 ft	0
620 To 630 ft	0
630 To 640 ft	0
640 To 650 ft	0
650 To 660 ft	0
660 To 670 ft	0
670 To 680 ft	0
680 To 690 ft	0
690 To 700 ft	0
700 To 710 ft	0
710 To 720 ft	0
720 To 730 ft	0
730 To 740 ft	0
740 To 750 ft	0
750 To 760 ft	1
760 To 770 ft	0
770 To 780 ft	0
780 To 790 ft	0
790 To 800 ft	0
800 To 810 ft	2
810 To 820 ft	0
820 To 830 ft	4
830 To 840 ft	0
840 To 850 ft	1
850 To 860 ft	0
860 To 870 ft	0
870 To 880 ft	1
880 To 890 ft	1

X Interval	Rocks Stopped
890 To 900 ft	0
900 To 910 ft	3
910 To 920 ft	1
920 To 930 ft	0
930 To 940 ft	2
940 To 950 ft	1
950 To 960 ft	1
960 To 970 ft	0
970 To 980 ft	1
980 To 990 ft	0
990 To 1000 ft	1
1000 To 1010 ft	1
1010 To 1020 ft	0
1020 To 1030 ft	0
1030 To 1040 ft	0
1040 To 1050 ft	0
1050 To 1060 ft	0
1060 To 1070 ft	0
1070 To 1080 ft	0
1080 To 1090 ft	0
1090 To 1100 ft	0
1100 To 1110 ft	0
1110 To 1120 ft	0
1120 To 1130 ft	1
1130 To 1140 ft	0
1140 To 1150 ft	0
1150 To 1160 ft	0
1160 To 1170 ft	0
1170 To 1180 ft	0
1180 To 1190 ft	0
1190 To 1200 ft	0
1200 To 1210 ft	0
1210 To 1220 ft	0
1220 To 1230 ft	0
1230 To 1240 ft	0
1240 To 1250 ft	0
1250 To 1260 ft	0
1260 To 1270 ft	0
1270 To 1280 ft	0
1280 To 1290 ft	0
1290 To 1300 ft	0
1300 To 1310 ft	0
1310 To 1320 ft	0
1320 To 1330 ft	0
1330 To 1340 ft	0
1340 To 1350 ft	0
1350 To 1360 ft	0
1360 To 1370 ft	0
1370 To 1380 ft	0

CRSP Input File - C:\Program Files\Crsp\B-B'.dat

Input File Specifications

Units of Measure: U.S.
Total Number of Cells: 13
Analysis Point X-Coordinate 1: 800
Analysis Point X-Coordinate 2:
Analysis Point X-Coordinate 3:
Initial Y-Top Starting Zone Coordinate: 8400
Initial Y-Base Starting Zone Coordinate: 8160
Remarks:

Cell Data

Cell No.	Surface R.	Tangent C.	Normal C.	Begin X	Begin Y	End X	End Y
1	5	.85	.35	0	8800	100	8780
2	5	.85	.35	100	8780	300	8720
3	5	.85	.35	300	8720	400	8640
4	5	.85	.35	400	8640	500	8560
5	5	.85	.35	500	8560	600	8400
6	1	.87	.37	600	8400	800	8160
7	5	.85	.35	800	8160	1050	8000
8	5	.87	.35	1050	8000	1350	7840
9	5	.82	.33	1350	7840	1600	7680
10	5	.82	.33	1600	7680	1800	7520
11	5	.82	.33	1800	7520	1820	7440
12	5	.82	.33	1820	7440	2000	7360
13	5	.82	.33	2000	7360	2300	7280

C:\Program Files\Crsp\B-B'.dat Total Rocks Rolled: 25

Spherical Rock: 6-ft dia., 18661-lb

Scale: Each division = 20 feet

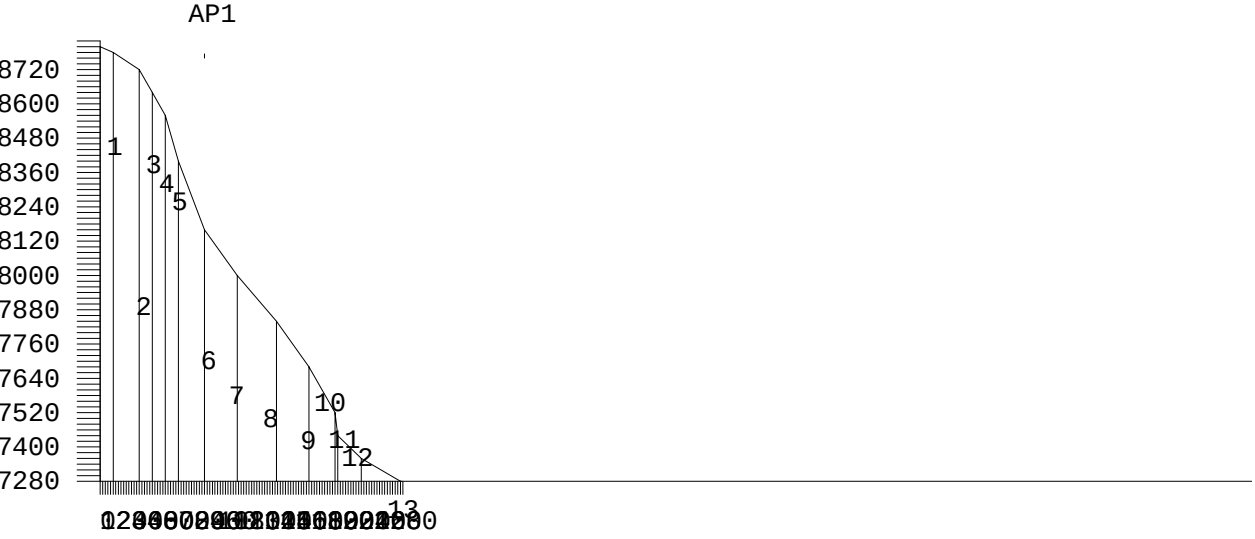

CRSP Analysis Point Data - C:\Program Files\Crsp\B-B'.dat

Analysis Point 1

Analysis Point 1: X = 800, Y = 8160

Spherical Rock: 6-ft dia., 18661-lb

Total Rocks Passing Analysis Point: 24

Velocity (ft/sec)	Bounce Height (ft)	Kinetic Energy (ft-lb)
Maximum: 87.59	Maximum: 18.99	Maximum: 2770052
Average: 61.96	Average: 6.35	Average: 1512508
Minimum: 23.02	G. Mean: 2.79	Std. Dev.: 760375
Std. Dev.: 18.65	Std. Dev.: 8.54	

CRSP Analysis Point Statistical Analysis - C:\Program Files\Crsp\B-B'.dat

Analysis Point 1

Analysis Point 1: X = 800, Y = 8160

Spherical Rock: 6-ft dia., 18661-lb

Total Rocks Passing Analysis Point: 24

Cumulative Probability	Velocity (ft/sec)	Energy (ft-lb)	Bounce Height (ft)
50%	61.96	1512508	2.79
75%	74.55	2025914	8.55
90%	85.88	2487690	13.74
95%	92.68	2764923	16.85
98%	100.32	3076069	20.35

Note: Velocity and kinetic energy are analyzed assuming a normal distribution.
Bounce height is analyzed assuming a log distribution.

Analysis Point 1 Bounce Height Distribution - C:\Program Files\Crsp\B-B'.dat

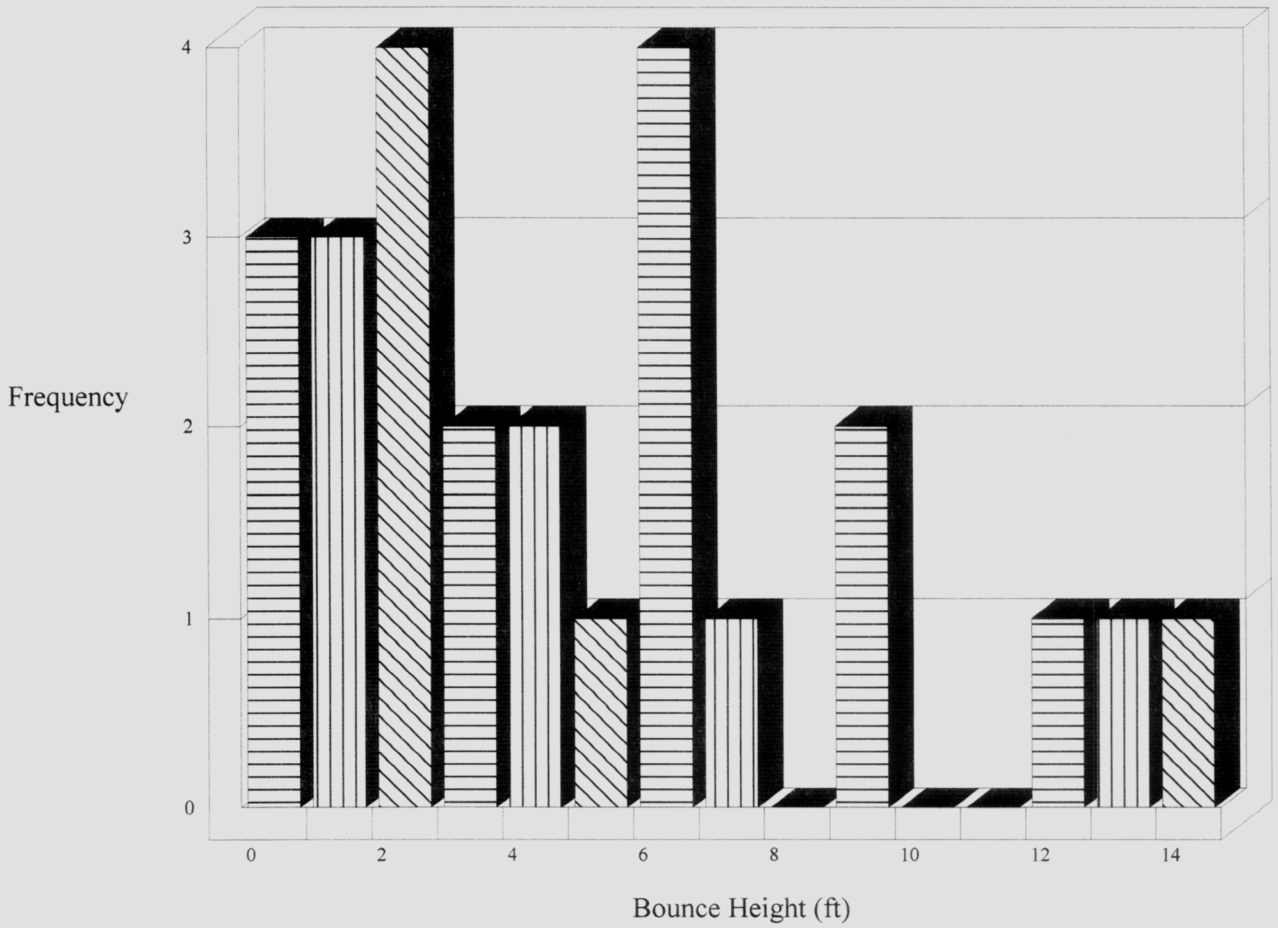

Analysis Point 1 Velocity Distribution - C:\Program Files\Crsp\B-B'.dat

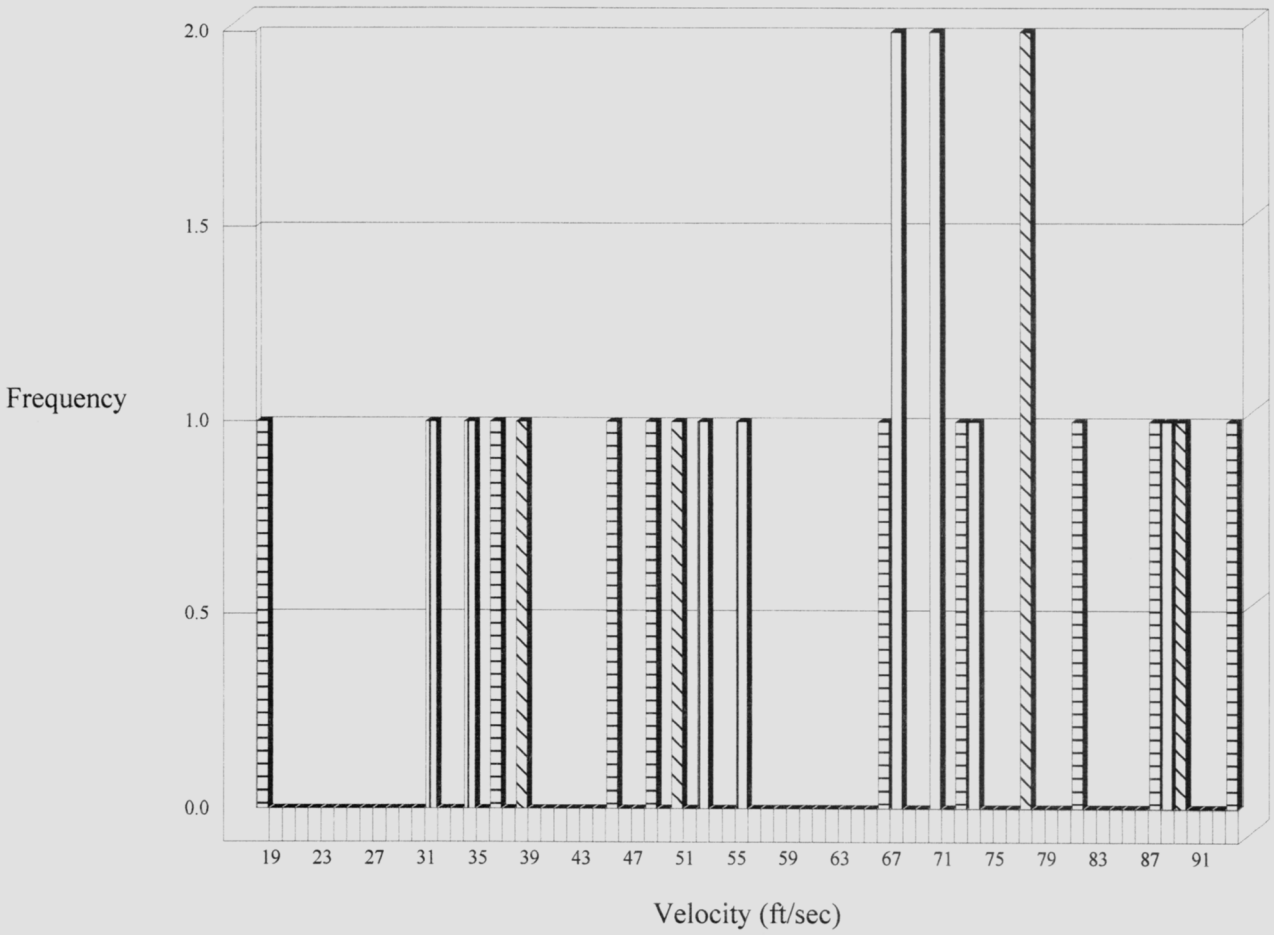

Bounce Height Graph - C:\Program Files\Crsp\B-B'.dat

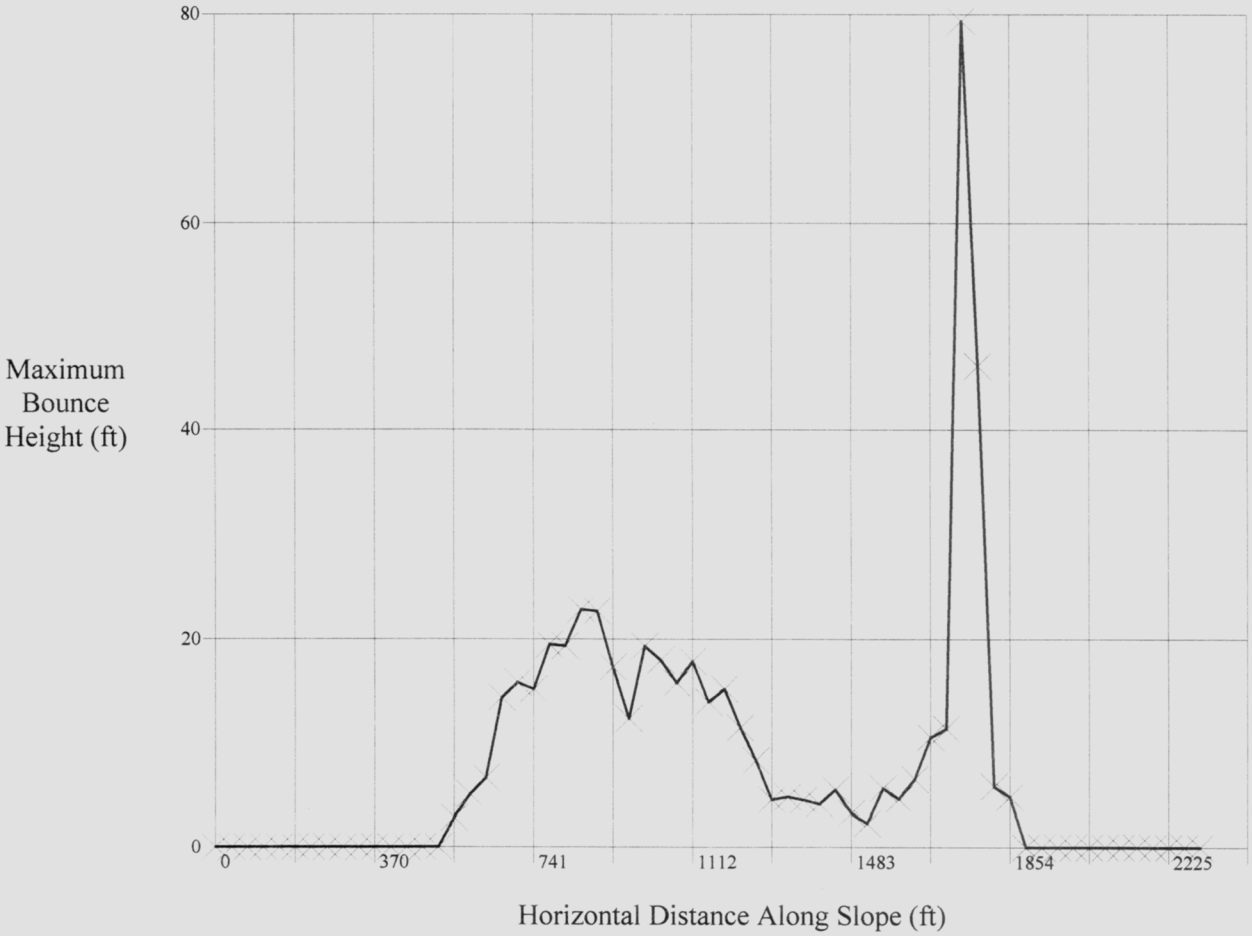

Velocity Graph - C:\Program Files\Crsp\B-B'.dat

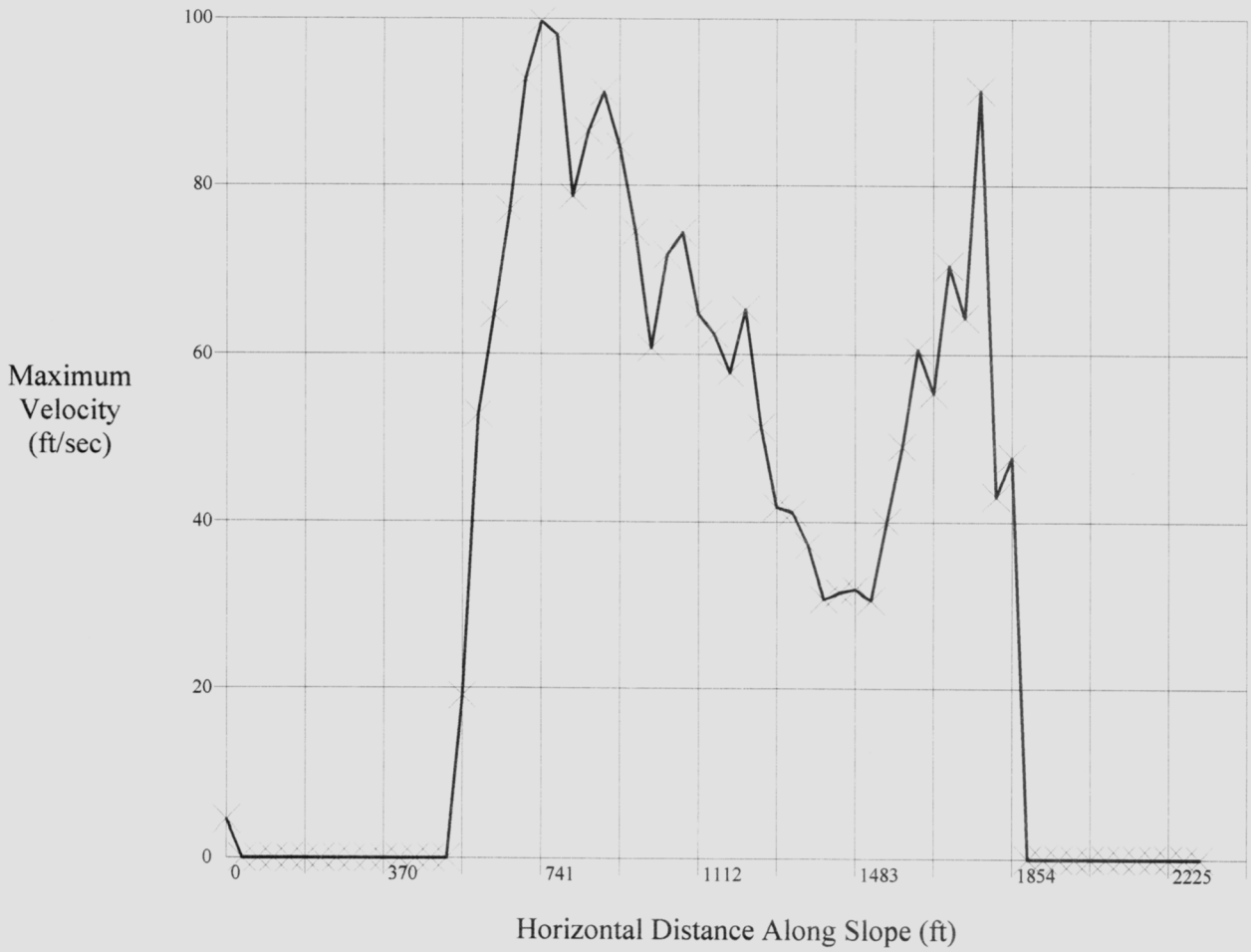

CRSP Data Collected at End of Each Cell - C:\Program Files\Crsp\B-B'.dat

Velocity Units: ft/sec Bounce Height Units: ft

Cell No.	Max. Velocity	Avg. Velocity	Std. Dev. Velocity	Max. Bounce Ht.	Avg. Bounce Ht.
1	No rocks	past end of cell			
2	No rocks	past end of cell			
3	No rocks	past end of cell			
4	No rocks	past end of cell			
5	No rocks	past end of cell			
6	94	63	20.74	14	4
7	52	32	13.15	18	3
8	18	16	0	4	1
9	21	21	0	1	0
10	31	31	0	12	11
11	46	46	0	74	74
12	No rocks	past end of cell			
13	No rocks	past end of cell			

CRSP Rocks Stopped Data - C:\Program Files\Crsp\B-B'.dat

X Interval	Rocks Stopped
0 To 10 ft	1
10 To 20 ft	0
20 To 30 ft	0
30 To 40 ft	0
40 To 50 ft	0
50 To 60 ft	0
60 To 70 ft	0
70 To 80 ft	0
80 To 90 ft	0
90 To 100 ft	0
100 To 110 ft	0
110 To 120 ft	0
120 To 130 ft	0
130 To 140 ft	0
140 To 150 ft	0
150 To 160 ft	0
160 To 170 ft	0
170 To 180 ft	0
180 To 190 ft	0
190 To 200 ft	0
200 To 210 ft	0
210 To 220 ft	0
220 To 230 ft	0
230 To 240 ft	0
240 To 250 ft	0
250 To 260 ft	0
260 To 270 ft	0
270 To 280 ft	0
280 To 290 ft	0
290 To 300 ft	0
300 To 310 ft	0
310 To 320 ft	0
320 To 330 ft	0
330 To 340 ft	0
340 To 350 ft	0
350 To 360 ft	0
360 To 370 ft	0
370 To 380 ft	0
380 To 390 ft	0
390 To 400 ft	0
400 To 410 ft	0
410 To 420 ft	0
420 To 430 ft	0
430 To 440 ft	0

X Interval	Rocks Stopped
440 To 450 ft	0
450 To 460 ft	0
460 To 470 ft	0
470 To 480 ft	0
480 To 490 ft	0
490 To 500 ft	0
500 To 510 ft	0
510 To 520 ft	0
520 To 530 ft	0
530 To 540 ft	0
540 To 550 ft	0
550 To 560 ft	0
560 To 570 ft	0
570 To 580 ft	0
580 To 590 ft	0
590 To 600 ft	0
600 To 610 ft	0
610 To 620 ft	0
620 To 630 ft	0
630 To 640 ft	0
640 To 650 ft	0
650 To 660 ft	0
660 To 670 ft	0
670 To 680 ft	0
680 To 690 ft	0
690 To 700 ft	0
700 To 710 ft	0
710 To 720 ft	0
720 To 730 ft	0
730 To 740 ft	0
740 To 750 ft	0
750 To 760 ft	0
760 To 770 ft	0
770 To 780 ft	0
780 To 790 ft	0
790 To 800 ft	0
800 To 810 ft	0
810 To 820 ft	0
820 To 830 ft	0
830 To 840 ft	0
840 To 850 ft	0
850 To 860 ft	0
860 To 870 ft	0
870 To 880 ft	0
880 To 890 ft	0

X Interval	Rocks Stopped
890 To 900 ft	0
900 To 910 ft	0
910 To 920 ft	1
920 To 930 ft	1
930 To 940 ft	0
940 To 950 ft	0
950 To 960 ft	0
960 To 970 ft	1
970 To 980 ft	0
980 To 990 ft	1
990 To 1000 ft	0
1000 To 1010 ft	0
1010 To 1020 ft	1
1020 To 1030 ft	0
1030 To 1040 ft	1
1040 To 1050 ft	0
1050 To 1060 ft	2
1060 To 1070 ft	0
1070 To 1080 ft	1
1080 To 1090 ft	0
1090 To 1100 ft	0
1100 To 1110 ft	2
1110 To 1120 ft	0
1120 To 1130 ft	2
1130 To 1140 ft	0
1140 To 1150 ft	0
1150 To 1160 ft	0
1160 To 1170 ft	2
1170 To 1180 ft	1
1180 To 1190 ft	0
1190 To 1200 ft	0
1200 To 1210 ft	1
1210 To 1220 ft	0
1220 To 1230 ft	0
1230 To 1240 ft	0
1240 To 1250 ft	0
1250 To 1260 ft	0
1260 To 1270 ft	0
1270 To 1280 ft	1
1280 To 1290 ft	2
1290 To 1300 ft	1
1300 To 1310 ft	0
1310 To 1320 ft	1
1320 To 1330 ft	0
1330 To 1340 ft	0
1340 To 1350 ft	0
1350 To 1360 ft	0
1360 To 1370 ft	0
1370 To 1380 ft	0

CRSP Input File - C:\Program Files\Crsp\C-C'.dat

Input File Specifications

Units of Measure: U.S.
Total Number of Cells: 9
Analysis Point X-Coordinate 1: 200
Analysis Point X-Coordinate 2:
Analysis Point X-Coordinate 3:
Initial Y-Top Starting Zone Coordinate: 8560
Initial Y-Base Starting Zone Coordinate: 8400
Remarks:

Cell Data

Cell No.	Surface R.	Tangent C.	Normal C.	Begin X	Begin Y	End X	End Y
1	5	.85	.35	0	8650	100	8560
2	1	.87	.37	100	8560	200	8400
3	5	.85	.35	200	8400	300	8320
4	5	.87	.35	300	8320	500	8160
5	5	.82	.33	500	8160	650	8080
6	5	.82	.33	650	8080	850	7920
7	5	.82	.33	850	7920	1050	7760
8	5	.82	.33	1050	7760	1480	7600
9	5	.82	.33	1480	7600	1530	7520

C:\Program Files\Crsp\C-C'.dat Total Rocks Rolled: 25

Spherical Rock: 6-ft dia., 18661-lb

Scale: Each division = 20 feet

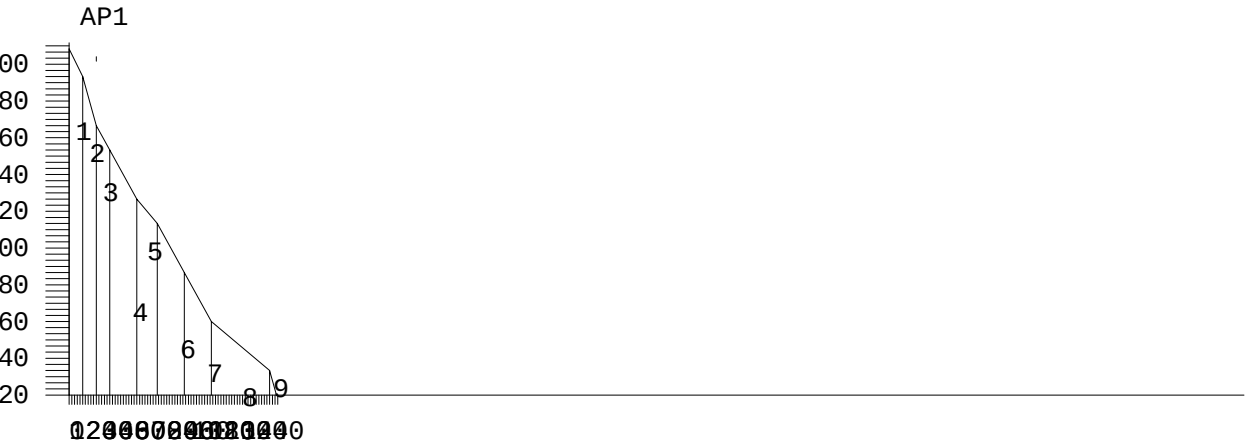

CRSP Analysis Point Data - C:\Program Files\Crsp\C-C'.dat

Analysis Point 1

Analysis Point 1: X = 200, Y = 8400

Spherical Rock: 6-ft dia., 18661-lb

Total Rocks Passing Analysis Point: 24

Velocity (ft/sec)	Bounce Height (ft)	Kinetic Energy (ft-lb)
Maximum: 79.82	Maximum: 17.42	Maximum: 2011921
Average: 54.71	Average: 4.69	Average: 1142518
Minimum: 21.74	G. Mean: 1.89	Std. Dev.: 562001
Std. Dev.: 15.41	Std. Dev.: 7.36	

CRSP Analysis Point Statistical Analysis - C:\Program Files\Crsp\C-C'.dat

Analysis Point 1

Analysis Point 1: X = 200, Y = 8400

Spherical Rock: 6-ft dia., 18661-lb

Total Rocks Passing Analysis Point: 24

Cumulative Probability	Velocity (ft/sec)	Energy (ft-lb)	Bounce Height (ft)
50%	54.71	1142518	1.89
75%	65.11	1521981	6.86
90%	74.46	1863284	11.33
95%	80.08	2068190	14.01
98%	86.39	2298161	17.03

Note: Velocity and kinetic energy are analyzed assuming a normal distribution.
Bounce height is analyzed assuming a log distribution.

Analysis Point 1 Bounce Height Distribution - C:\Program Files\Crsp\C-C'.dat

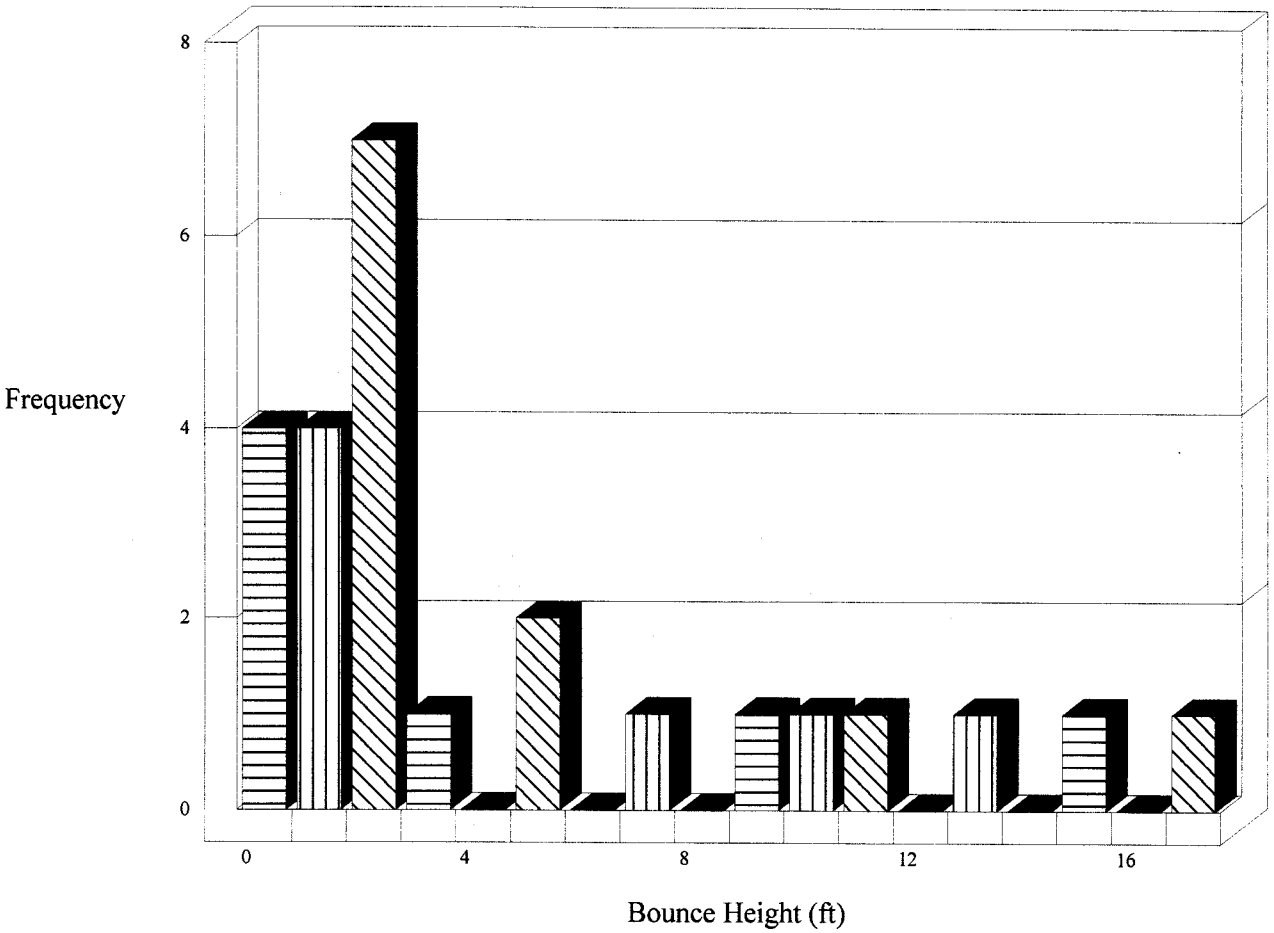

Analysis Point 1 Velocity Distribution - C:\Program Files\Crsp\C-C'.dat

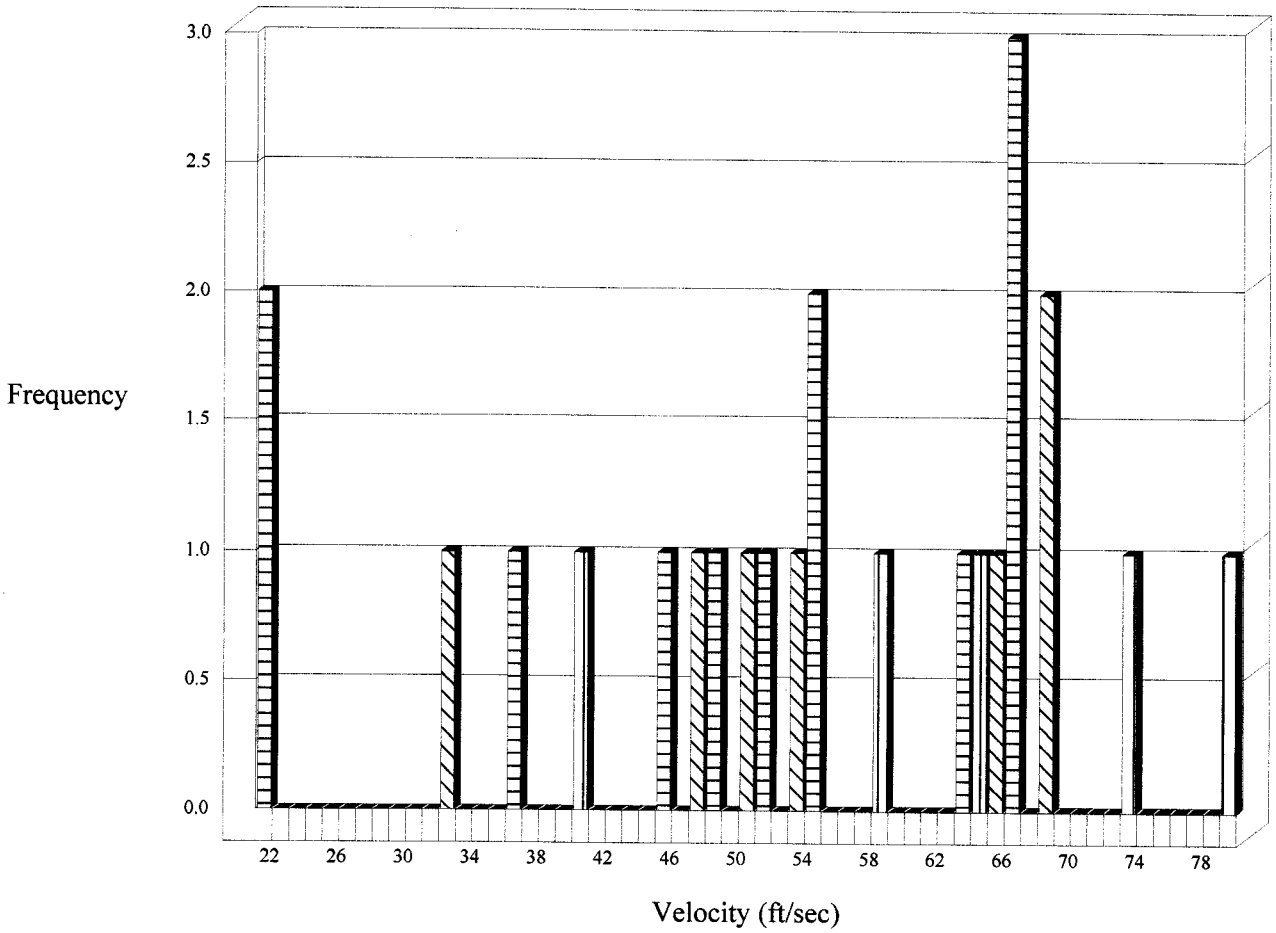

Bounce Height Graph - C:\Program Files\Crsp\C-C'.dat

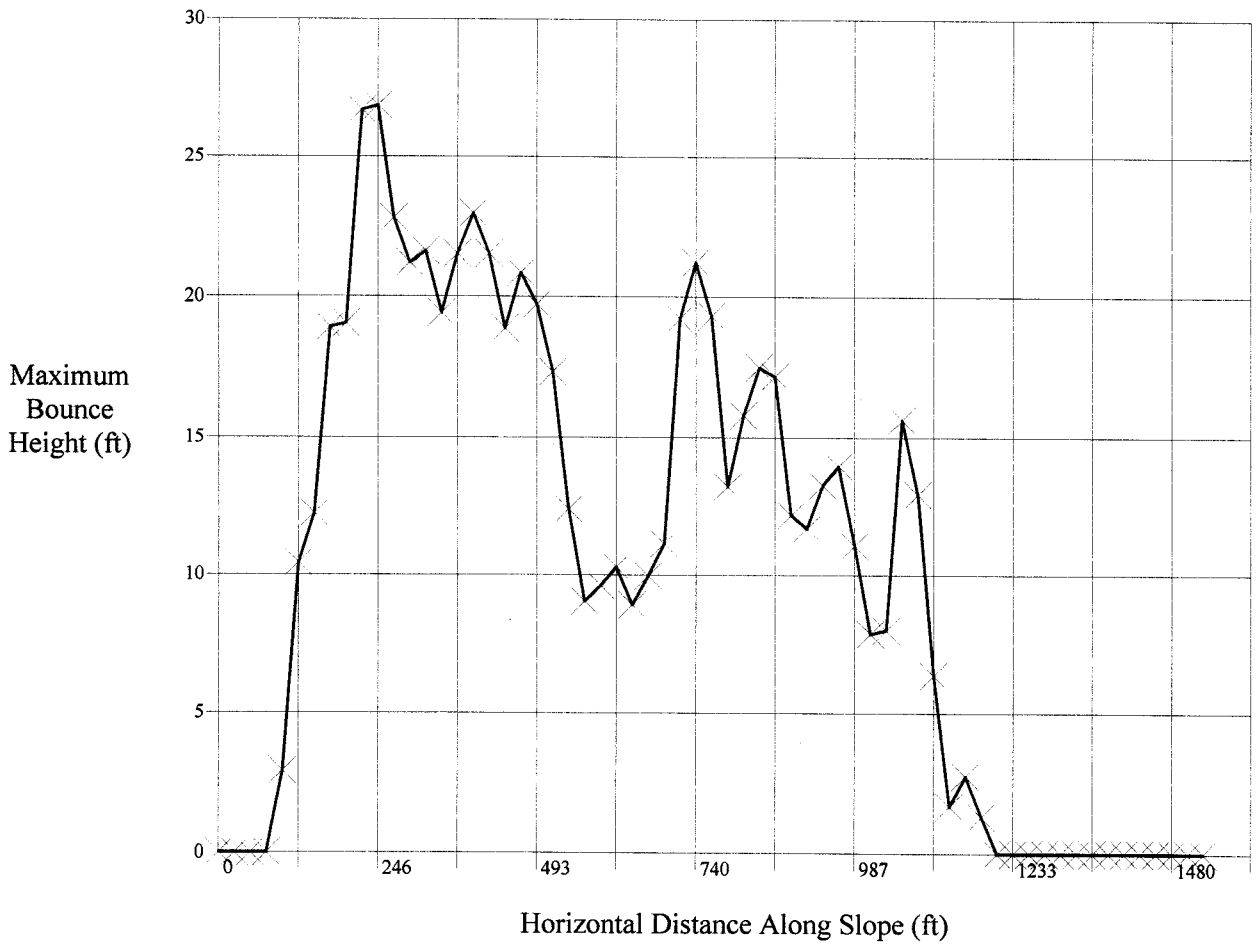

Velocity Graph - C:\Program Files\Crsp\C-C'.dat

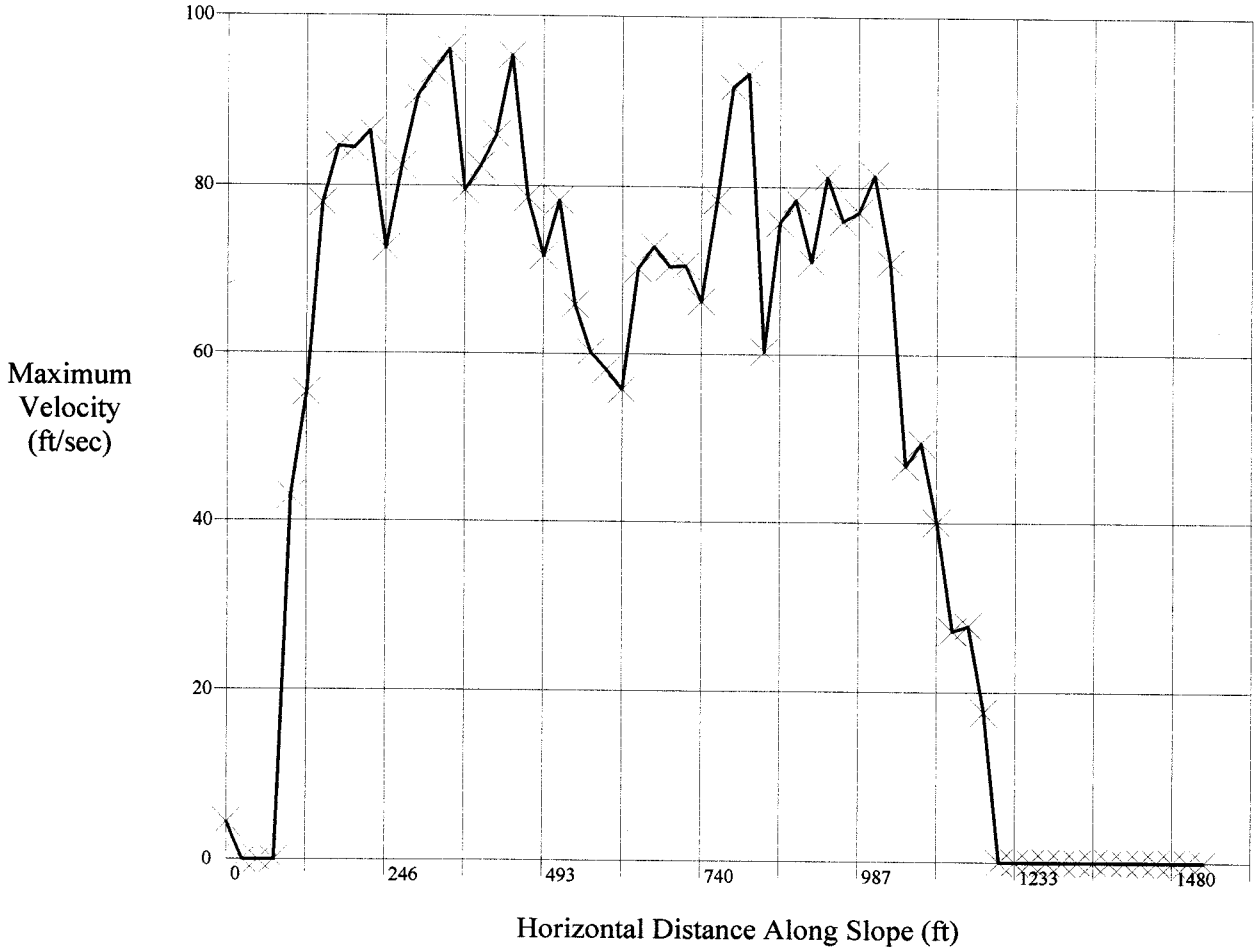

CRSP Data Collected at End of Each Cell - C:\Program Files\Crsp\C-C'.dat

Velocity Units: ft/sec Bounce Height Units: ft

Cell No.	Max. Velocity	Avg. Velocity	Std. Dev. Velocity	Max. Bounce Ht.	Avg. Bounce Ht.
1	No rocks	past end of cell			
2	80	55	15.41	17	4
3	80	45	18.4	16	5
4	63	43	13.95	20	5
5	50	32	12.48	10	3
6	88	45	19.81	11	3
7	79	39	19.54	8	3
8	No rocks	past end of cell			
9	No rocks	past end of cell			

CRSP Rocks Stopped Data - C:\Program Files\Crsp\C-C'.dat

X Interval	Rocks Stopped
0 To 10 ft	1
10 To 20 ft	0
20 To 30 ft	0
30 To 40 ft	0
40 To 50 ft	0
50 To 60 ft	0
60 To 70 ft	0
70 To 80 ft	0
80 To 90 ft	0
90 To 100 ft	0
100 To 110 ft	0
110 To 120 ft	0
120 To 130 ft	0
130 To 140 ft	0
140 To 150 ft	0
150 To 160 ft	0
160 To 170 ft	0
170 To 180 ft	0
180 To 190 ft	0
190 To 200 ft	0
200 To 210 ft	0
210 To 220 ft	0
220 To 230 ft	0
230 To 240 ft	0
240 To 250 ft	0
250 To 260 ft	0
260 To 270 ft	0
270 To 280 ft	0
280 To 290 ft	0
290 To 300 ft	0
300 To 310 ft	0
310 To 320 ft	0
320 To 330 ft	0
330 To 340 ft	0
340 To 350 ft	0
350 To 360 ft	0
360 To 370 ft	0
370 To 380 ft	0
380 To 390 ft	0
390 To 400 ft	0
400 To 410 ft	0
410 To 420 ft	0
420 To 430 ft	0
430 To 440 ft	0

X Interval	Rocks Stopped
440 To 450 ft	0
450 To 460 ft	0
460 To 470 ft	0
470 To 480 ft	0
480 To 490 ft	0
490 To 500 ft	0
500 To 510 ft	0
510 To 520 ft	3
520 To 530 ft	1
530 To 540 ft	0
540 To 550 ft	1
550 To 560 ft	1
560 To 570 ft	1
570 To 580 ft	0
580 To 590 ft	1
590 To 600 ft	1
600 To 610 ft	2
610 To 620 ft	0
620 To 630 ft	2
630 To 640 ft	1
640 To 650 ft	0
650 To 660 ft	0
660 To 670 ft	0
670 To 680 ft	0
680 To 690 ft	0
690 To 700 ft	0
700 To 710 ft	0
710 To 720 ft	0
720 To 730 ft	0
730 To 740 ft	0
740 To 750 ft	0
750 To 760 ft	0
760 To 770 ft	0
770 To 780 ft	0
780 To 790 ft	0
790 To 800 ft	0
800 To 810 ft	0
810 To 820 ft	0
820 To 830 ft	0
830 To 840 ft	0
840 To 850 ft	0
850 To 860 ft	0
860 To 870 ft	0
870 To 880 ft	0
880 To 890 ft	1

X Interval	Rocks Stopped
890 To 900 ft	0
900 To 910 ft	0
910 To 920 ft	0
920 To 930 ft	0
930 To 940 ft	0
940 To 950 ft	0
950 To 960 ft	0
960 To 970 ft	0
970 To 980 ft	0
980 To 990 ft	0
990 To 1000 ft	0
1000 To 1010 ft	0
1010 To 1020 ft	0
1020 To 1030 ft	0
1030 To 1040 ft	0
1040 To 1050 ft	0
1050 To 1060 ft	1
1060 To 1070 ft	0
1070 To 1080 ft	2
1080 To 1090 ft	2
1090 To 1100 ft	2
1100 To 1110 ft	0
1110 To 1120 ft	0
1120 To 1130 ft	0
1130 To 1140 ft	0
1140 To 1150 ft	0
1150 To 1160 ft	1
1160 To 1170 ft	0
1170 To 1180 ft	0
1180 To 1190 ft	0
1190 To 1200 ft	0
1200 To 1210 ft	0
1210 To 1220 ft	0
1220 To 1230 ft	0
1230 To 1240 ft	1
1240 To 1250 ft	0
1250 To 1260 ft	0
1260 To 1270 ft	0
1270 To 1280 ft	0
1280 To 1290 ft	0
1290 To 1300 ft	0
1300 To 1310 ft	0
1310 To 1320 ft	0
1320 To 1330 ft	0
1330 To 1340 ft	0
1340 To 1350 ft	0
1350 To 1360 ft	0
1360 To 1370 ft	0
1370 To 1380 ft	0

CRSP Input File - C:\Program Files\Crsp\D-D'.dat

Input File Specifications

Units of Measure: U.S.
Total Number of Cells: 12
Analysis Point X-Coordinate 1: 500
Analysis Point X-Coordinate 2:
Analysis Point X-Coordinate 3:
Initial Y-Top Starting Zone Coordinate: 8560
Initial Y-Base Starting Zone Coordinate: 8440
Remarks:

Cell Data

Cell No.	Surface R.	Tangent C.	Normal C.	Begin X	Begin Y	End X	End Y
1	5	.85	.35	0	8880	150	8800
2	5	.85	.35	150	8800	250	8720
3	5	.85	.35	250	8720	450	8560
4	1	.87	.37	450	8560	500	8440
5	5	.85	.35	500	8440	600	8320
6	5	.87	.35	600	8320	700	8240
7	5	.87	.35	700	8240	800	8160
8	5	.82	.33	800	8160	1050	8080
9	5	.82	.33	1050	8080	1250	8000
10	5	.82	.33	1250	8000	1450	7920
11	5	.82	.33	1450	7920	1600	7840
12	5	.82	.33	1600	7840	1850	7760

C:\Program Files\Crsp\D-D'.dat Total Rocks Rolled: 25

Spherical Rock: 6-ft dia., 18661-lb

Scale: Each division = 20 feet

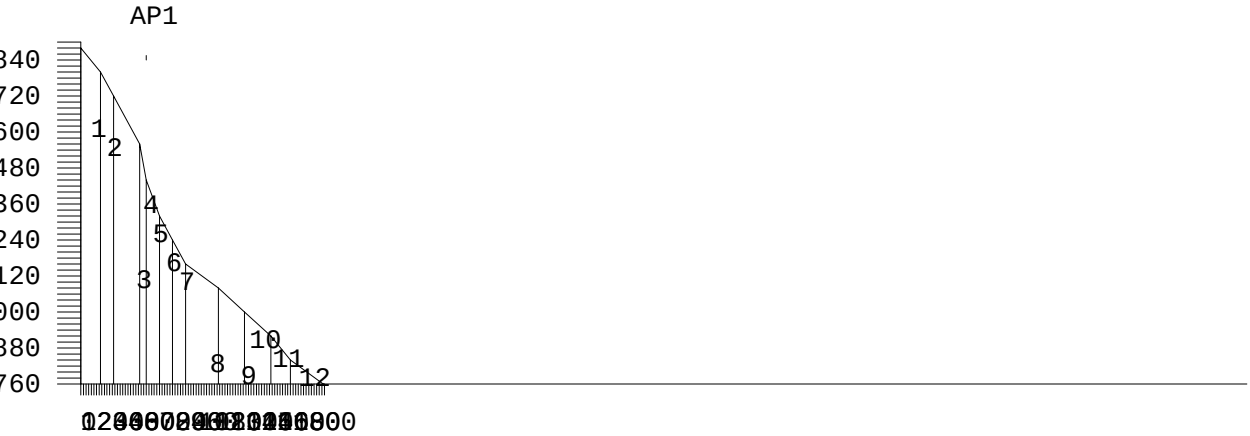

CRSP Analysis Point Data - C:\Program Files\Crsp\D-D'.dat

Analysis Point 1

Analysis Point 1: X = 500, Y = 8440

Spherical Rock: 6-ft dia., 18661-lb

Total Rocks Passing Analysis Point: 24

Velocity (ft/sec)	Bounce Height (ft)	Kinetic Energy (ft-lb)
Maximum: 72.56	Maximum: 20.98	Maximum: 1664681
Average: 48.84	Average: 6.08	Average: 904902
Minimum: 15.78	G. Mean: 3.63	Std. Dev.: 479381
Std. Dev.: 15.07	Std. Dev.: 3.07	

CRSP Analysis Point Statistical Analysis - C:\Program Files\Crsp\D-D'.dat

Analysis Point 1

Analysis Point 1: X = 500, Y = 8440

Spherical Rock: 6-ft dia., 18661-lb

Total Rocks Passing Analysis Point: 24

Cumulative Probability	Velocity (ft/sec)	Energy (ft-lb)	Bounce Height (ft)
50%	48.84	904902	3.63
75%	59.02	1228580	5.7
90%	68.17	1519708	7.56
95%	73.66	1694490	8.68
98%	79.83	1890653	9.94

Note: Velocity and kinetic energy are analyzed assuming a normal distribution.
Bounce height is analyzed assuming a log distribution.

Analysis Point 1 Bounce Height Distribution - C:\Program Files\Crsp\D-D'.dat

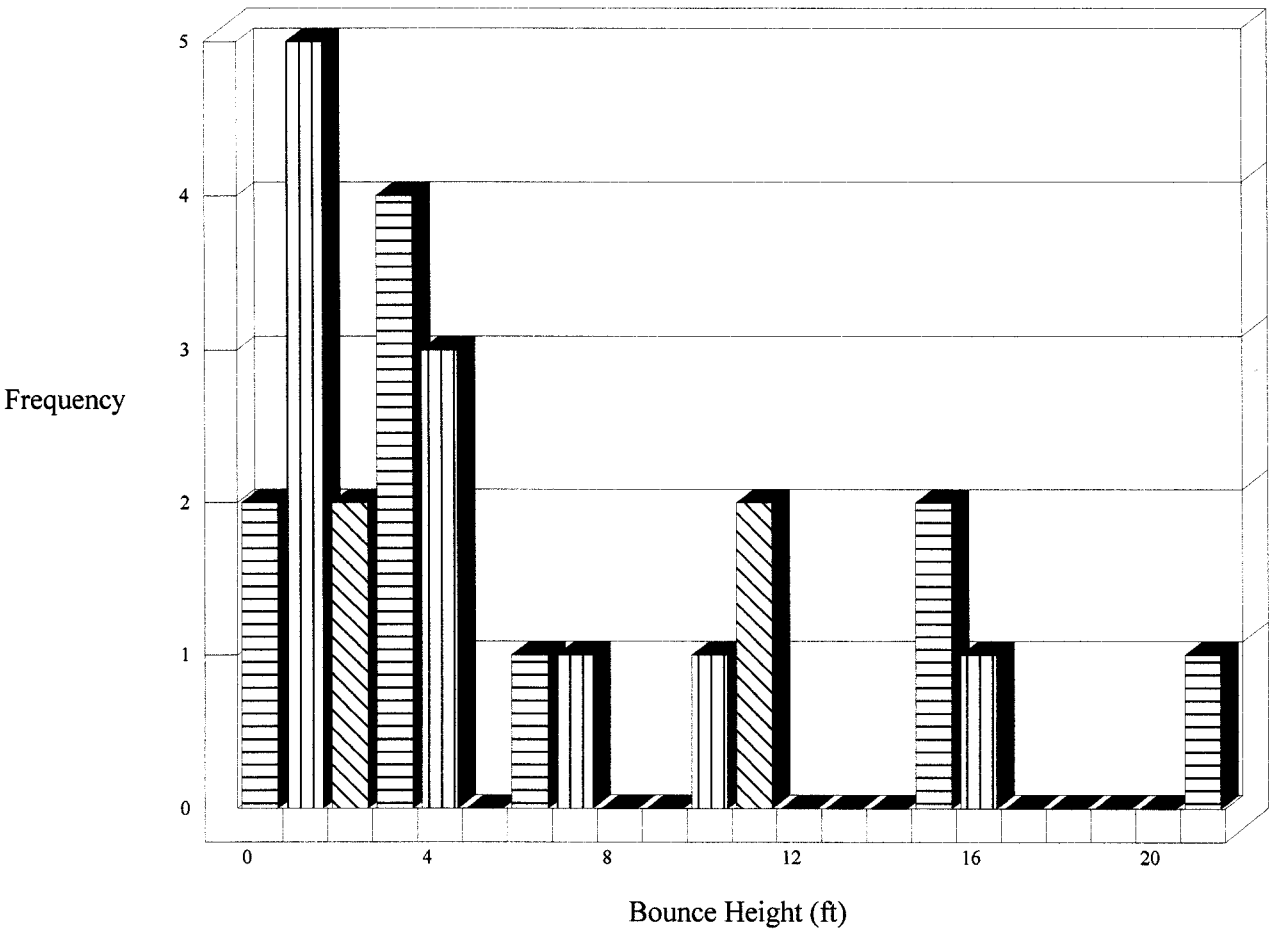

Analysis Point 1 Velocity Distribution - C:\Program Files\Crsp\D-D'.dat

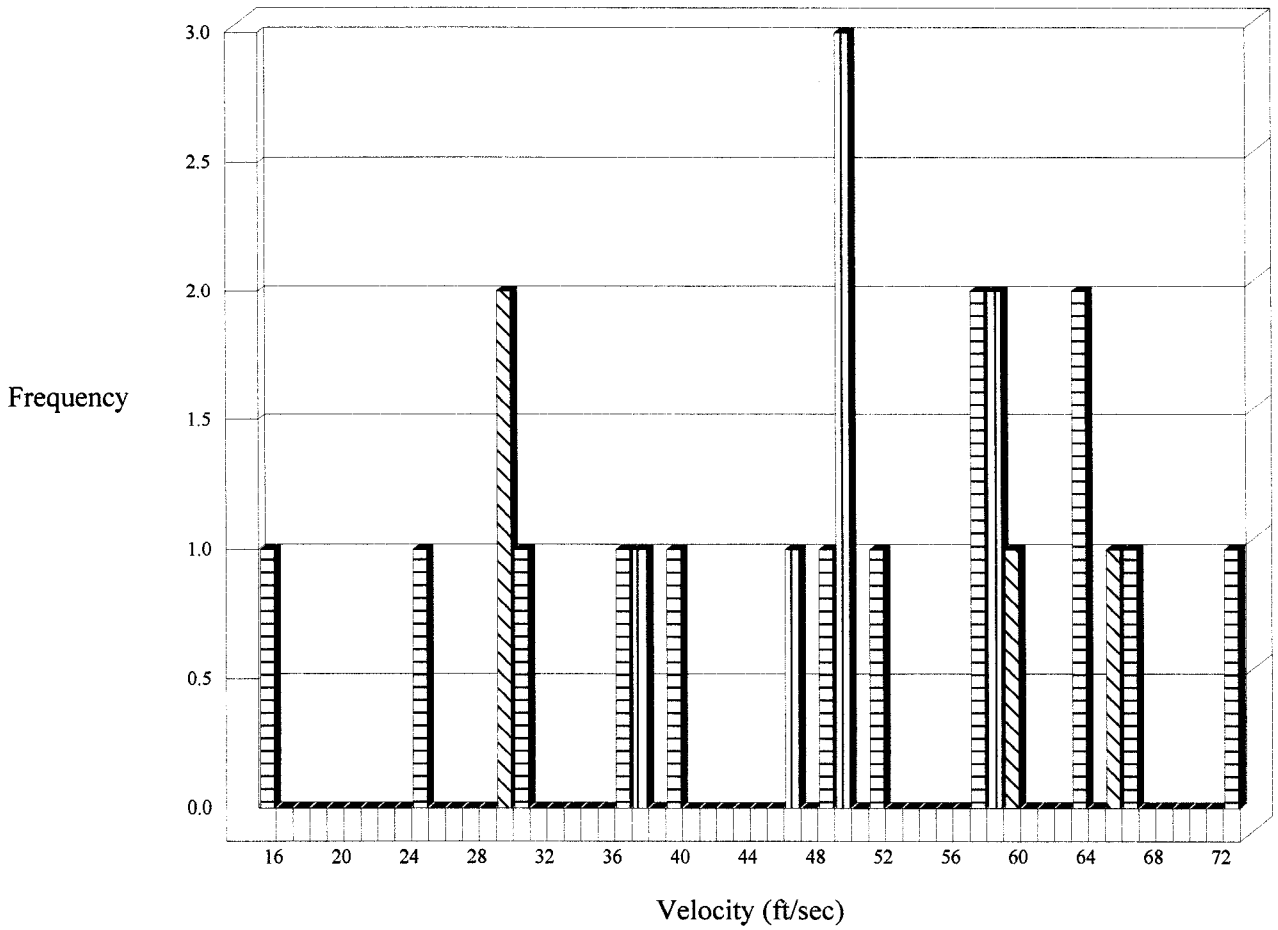

Bounce Height Graph - C:\Program Files\Crsp\D-D'.dat

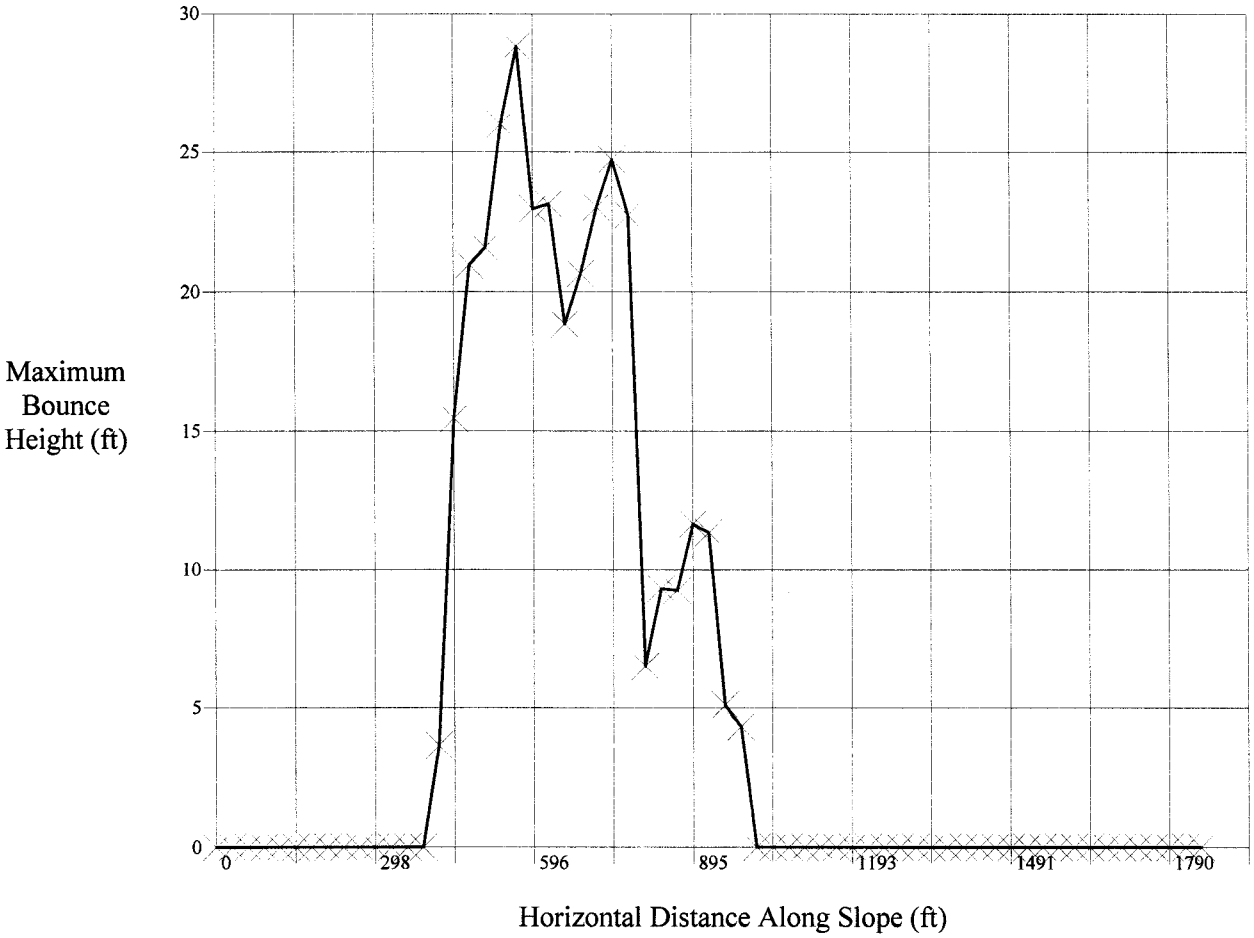

Velocity Graph - C:\Program Files\Crsp\D-D'.dat

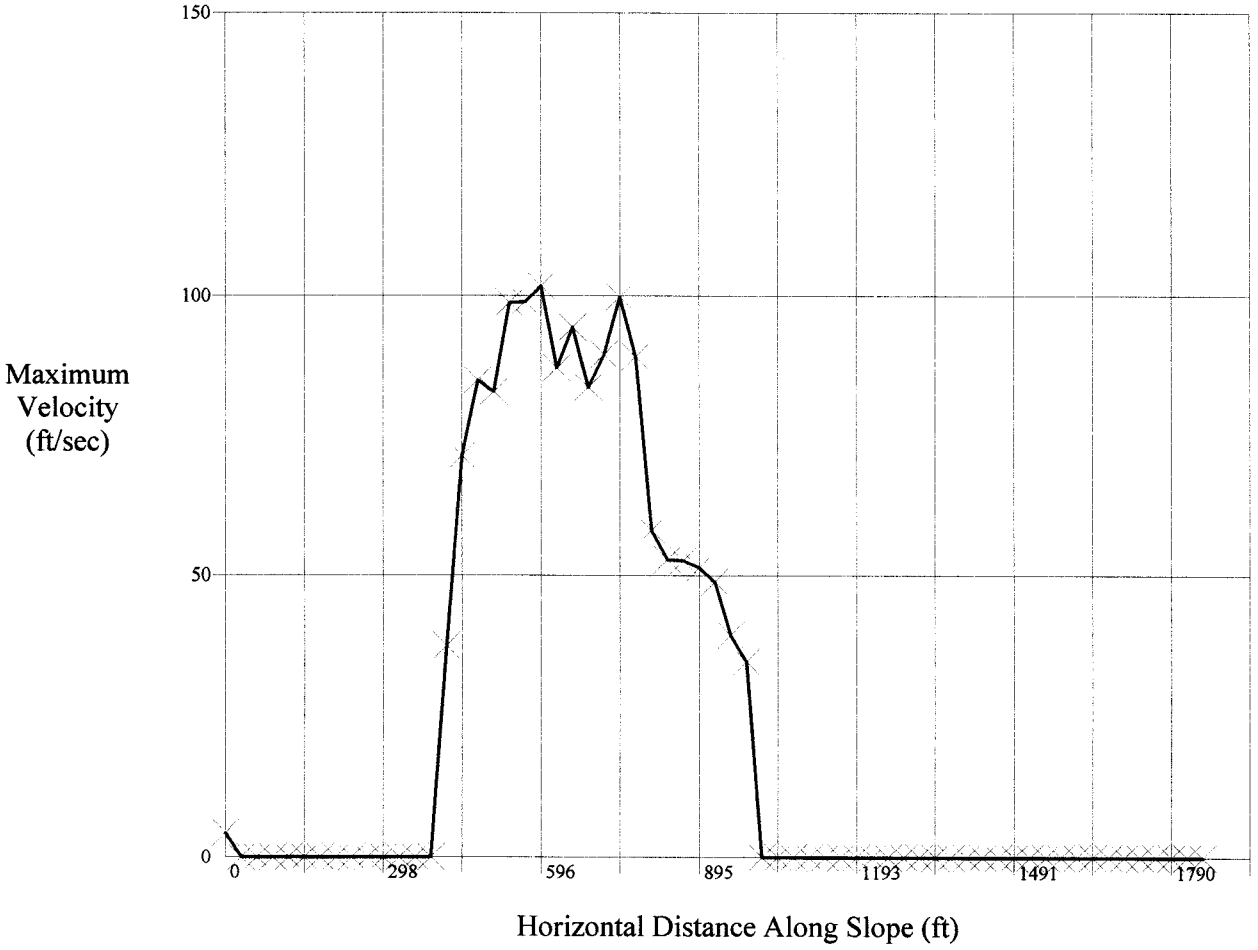

CRSP Data Collected at End of Each Cell - C:\Program Files\Crsp\D-D'.dat

Velocity Units: ft/sec Bounce Height Units: ft

Cell No.	Max. Velocity	Avg. Velocity	Std. Dev. Velocity	Max. Bounce Ht.	Avg. Bounce Ht.
1	No rocks	past end of cell			
2	No rocks	past end of cell			
3	No rocks	past end of cell			
4	73	49	15.07	21	6
5	91	59	16	29	11
6	91	50	20.45	17	6
7	79	46	17.61	23	7
8	No rocks	past end of cell			
9	No rocks	past end of cell			
10	No rocks	past end of cell			
11	No rocks	past end of cell			
12	No rocks	past end of cell			

CRSP Rocks Stopped Data - C:\Program Files\Crsp\D-D'.dat

X Interval	Rocks Stopped
0 To 10 ft	1
10 To 20 ft	0
20 To 30 ft	0
30 To 40 ft	0
40 To 50 ft	0
50 To 60 ft	0
60 To 70 ft	0
70 To 80 ft	0
80 To 90 ft	0
90 To 100 ft	0
100 To 110 ft	0
110 To 120 ft	0
120 To 130 ft	0
130 To 140 ft	0
140 To 150 ft	0
150 To 160 ft	0
160 To 170 ft	0
170 To 180 ft	0
180 To 190 ft	0
190 To 200 ft	0
200 To 210 ft	0
210 To 220 ft	0
220 To 230 ft	0
230 To 240 ft	0
240 To 250 ft	0
250 To 260 ft	0
260 To 270 ft	0
270 To 280 ft	0
280 To 290 ft	0
290 To 300 ft	0
300 To 310 ft	0
310 To 320 ft	0
320 To 330 ft	0
330 To 340 ft	0
340 To 350 ft	0
350 To 360 ft	0
360 To 370 ft	0
370 To 380 ft	0
380 To 390 ft	0
390 To 400 ft	0
400 To 410 ft	0
410 To 420 ft	0
420 To 430 ft	0
430 To 440 ft	0

X Interval	Rocks Stopped
440 To 450 ft	0
450 To 460 ft	0
460 To 470 ft	0
470 To 480 ft	0
480 To 490 ft	0
490 To 500 ft	0
500 To 510 ft	0
510 To 520 ft	0
520 To 530 ft	0
530 To 540 ft	0
540 To 550 ft	0
550 To 560 ft	0
560 To 570 ft	0
570 To 580 ft	0
580 To 590 ft	0
590 To 600 ft	0
600 To 610 ft	0
610 To 620 ft	0
620 To 630 ft	0
630 To 640 ft	0
640 To 650 ft	0
650 To 660 ft	0
660 To 670 ft	0
670 To 680 ft	0
680 To 690 ft	0
690 To 700 ft	0
700 To 710 ft	0
710 To 720 ft	0
720 To 730 ft	0
730 To 740 ft	0
740 To 750 ft	0
750 To 760 ft	0
760 To 770 ft	0
770 To 780 ft	0
780 To 790 ft	0
790 To 800 ft	0
800 To 810 ft	0
810 To 820 ft	3
820 To 830 ft	2
830 To 840 ft	1
840 To 850 ft	0
850 To 860 ft	0
860 To 870 ft	1
870 To 880 ft	2
880 To 890 ft	2

X Interval	Rocks Stopped
890 To 900 ft	0
900 To 910 ft	4
910 To 920 ft	2
920 To 930 ft	2
930 To 940 ft	0
940 To 950 ft	1
950 To 960 ft	0
960 To 970 ft	0
970 To 980 ft	0
980 To 990 ft	2
990 To 1000 ft	0
1000 To 1010 ft	0
1010 To 1020 ft	0
1020 To 1030 ft	1
1030 To 1040 ft	1
1040 To 1050 ft	0
1050 To 1060 ft	0
1060 To 1070 ft	0
1070 To 1080 ft	0
1080 To 1090 ft	0
1090 To 1100 ft	0
1100 To 1110 ft	0
1110 To 1120 ft	0
1120 To 1130 ft	0
1130 To 1140 ft	0
1140 To 1150 ft	0
1150 To 1160 ft	0
1160 To 1170 ft	0
1170 To 1180 ft	0
1180 To 1190 ft	0
1190 To 1200 ft	0
1200 To 1210 ft	0
1210 To 1220 ft	0
1220 To 1230 ft	0
1230 To 1240 ft	0
1240 To 1250 ft	0
1250 To 1260 ft	0
1260 To 1270 ft	0
1270 To 1280 ft	0
1280 To 1290 ft	0
1290 To 1300 ft	0
1300 To 1310 ft	0
1310 To 1320 ft	0
1320 To 1330 ft	0
1330 To 1340 ft	0
1340 To 1350 ft	0
1350 To 1360 ft	0
1360 To 1370 ft	0
1370 To 1380 ft	0

CRSP Input File - C:\Program Files\Crsp\E-E'.dat

Input File Specifications

Units of Measure: U.S.
Total Number of Cells: 8
Analysis Point X-Coordinate 1: 550
Analysis Point X-Coordinate 2:
Analysis Point X-Coordinate 3:
Initial Y-Top Starting Zone Coordinate: 8560
Initial Y-Base Starting Zone Coordinate: 8320
Remarks:

Cell Data

Cell No.	Surface R.	Tangent C.	Normal C.	Begin X	Begin Y	End X	End Y
1	5	.85	.35	0	8880	200	8800
2	5	.85	.35	200	8800	400	8640
3	5	.85	.35	400	8640	500	8560
4	1	.87	.37	500	8560	550	8320
5	5	.85	.35	550	8320	700	8240
6	5	.82	.33	700	8240	800	8160
7	5	.82	.33	800	8160	900	8080
8	5	.82	.33	900	8080	1000	8000

C:\Program Files\Crsp\E-E'.dat Total Rocks Rolled: 25

Spherical Rock: 6-ft dia., 18661-lb

Scale: Each division = 20 feet

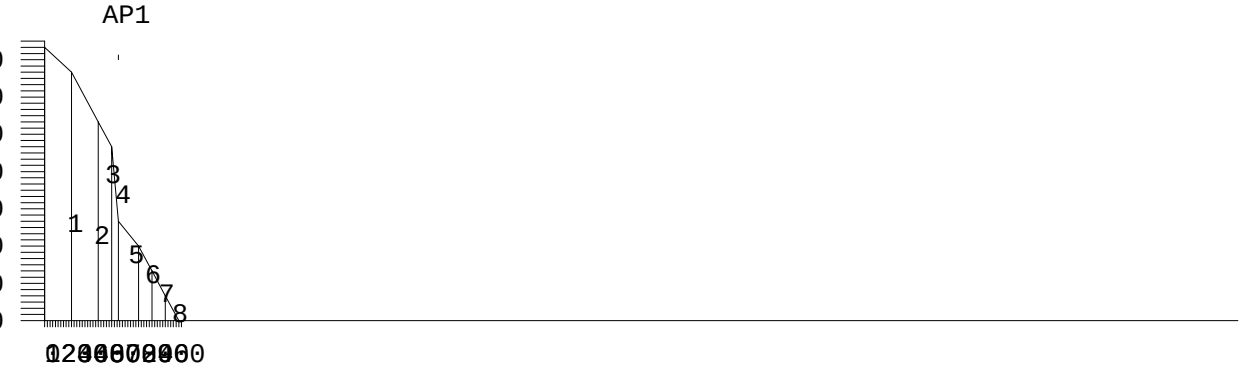

CRSP Analysis Point Data - C:\Program Files\Crsp\E-E'.dat

Analysis Point 1

Analysis Point 1: X = 550, Y = 8320

Spherical Rock: 6-ft dia., 18661-lb

Total Rocks Passing Analysis Point: 24

Velocity (ft/sec)	Bounce Height (ft)	Kinetic Energy (ft-lb)
Maximum: 112.98	Maximum: 68.68	Maximum: 3834550
Average: 64.91	Average: 19.43	Average: 1630396
Minimum: 18.89	G. Mean: 11.07	Std. Dev.: 909983
Std. Dev.: 21	Std. Dev.: 3.51	

CRSP Analysis Point Statistical Analysis - C:\Program Files\Crsp\E-E'.dat

Analysis Point 1

Analysis Point 1: X = 550, Y = 8320

Spherical Rock: 6-ft dia., 18661-lb

Total Rocks Passing Analysis Point: 24

Cumulative Probability	Velocity (ft/sec)	Energy (ft-lb)	Bounce Height (ft)
50%	64.91	1630396	11.07
75%	79.09	2244817	13.44
90%	91.84	2797450	15.57
95%	99.5	3129230	16.85
98%	108.09	3501595	18.28

Note: Velocity and kinetic energy are analyzed assuming a normal distribution.
Bounce height is analyzed assuming a log distribution.

Analysis Point 1 Bounce Height Distribution - C:\Program Files\Crsp\E-E'.dat

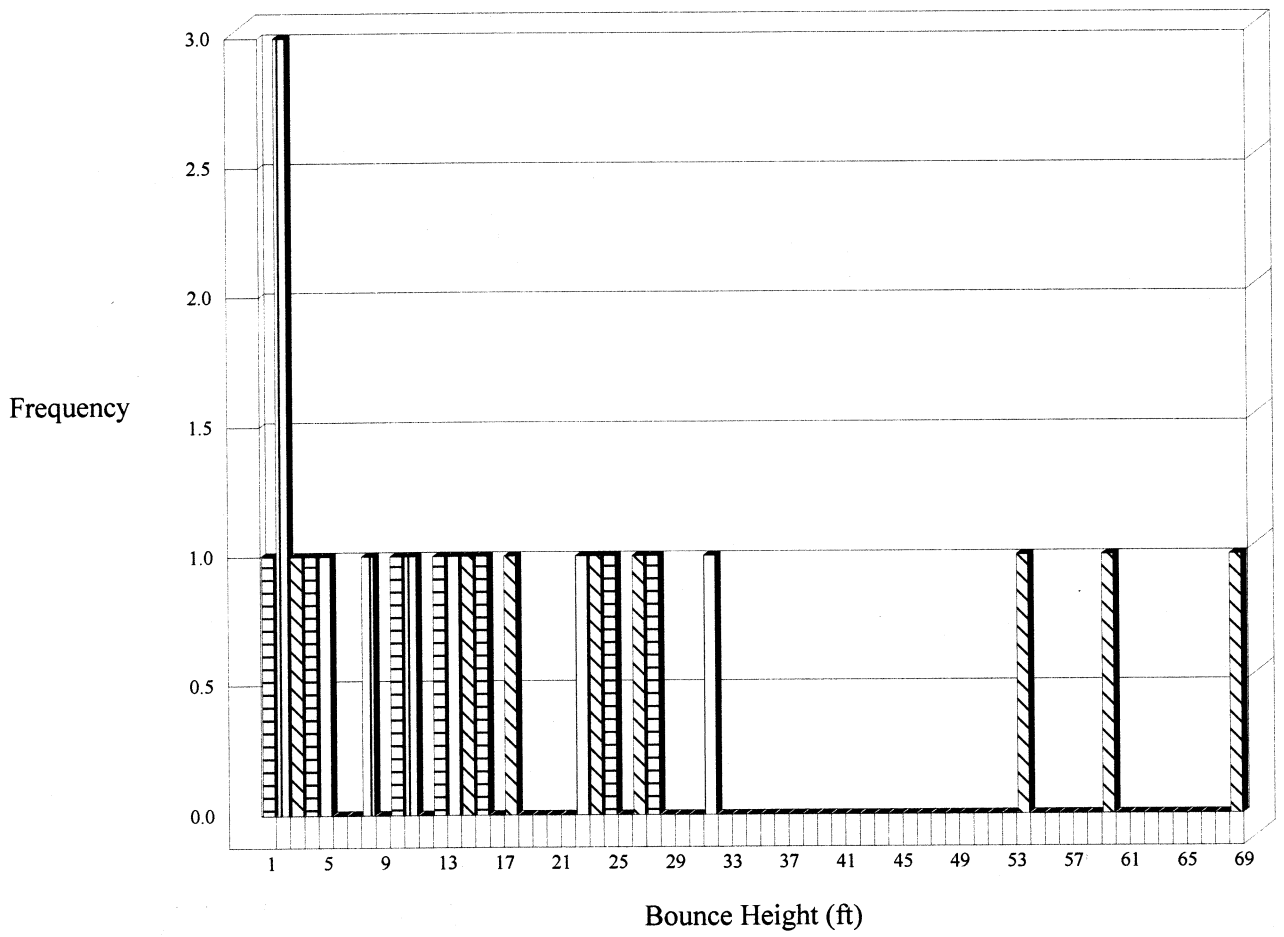

Analysis Point 1 Velocity Distribution - C:\Program Files\Crsp\E-E'.dat

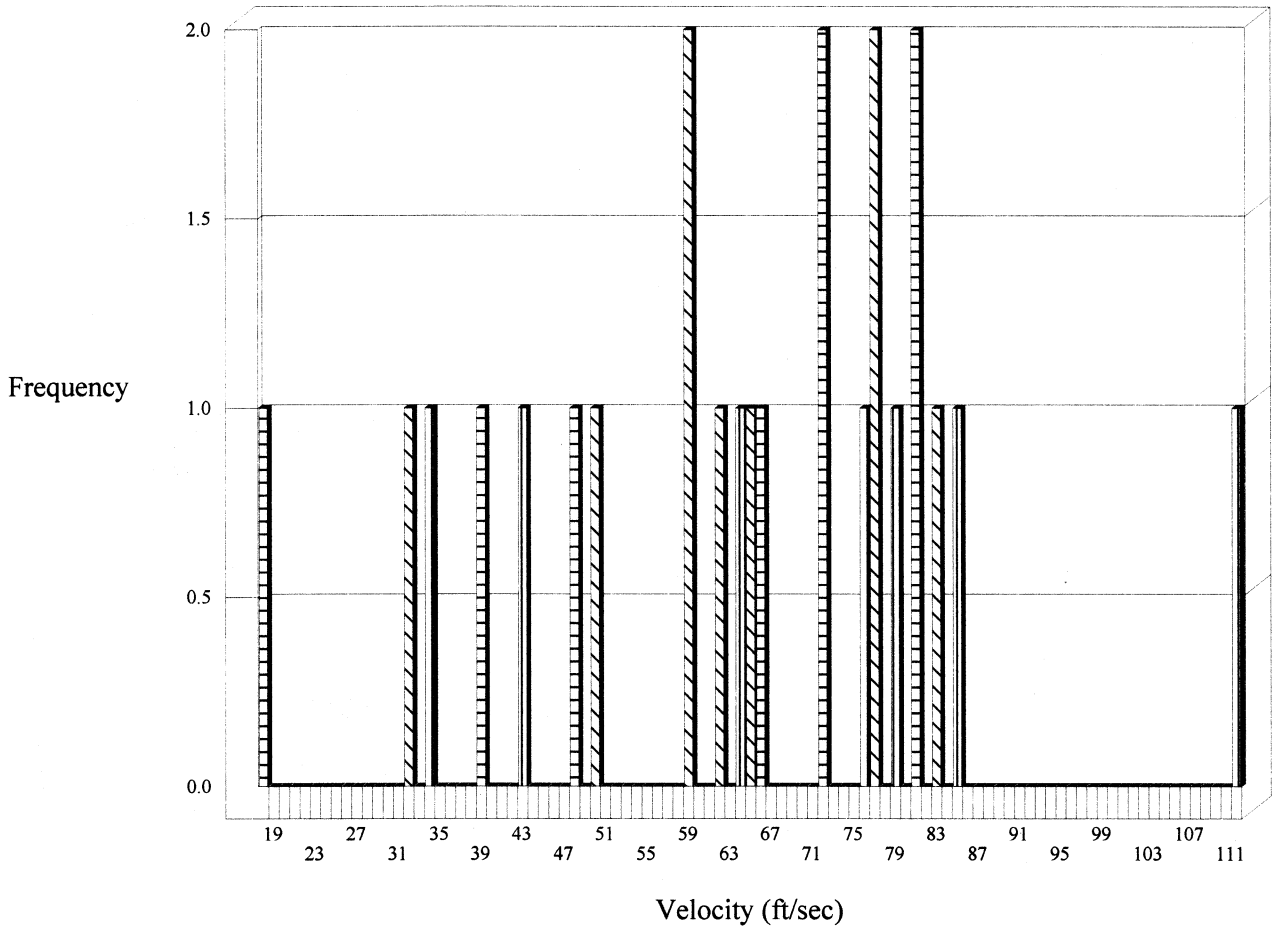

Bounce Height Graph - C:\Program Files\Crsp\E-E'.dat

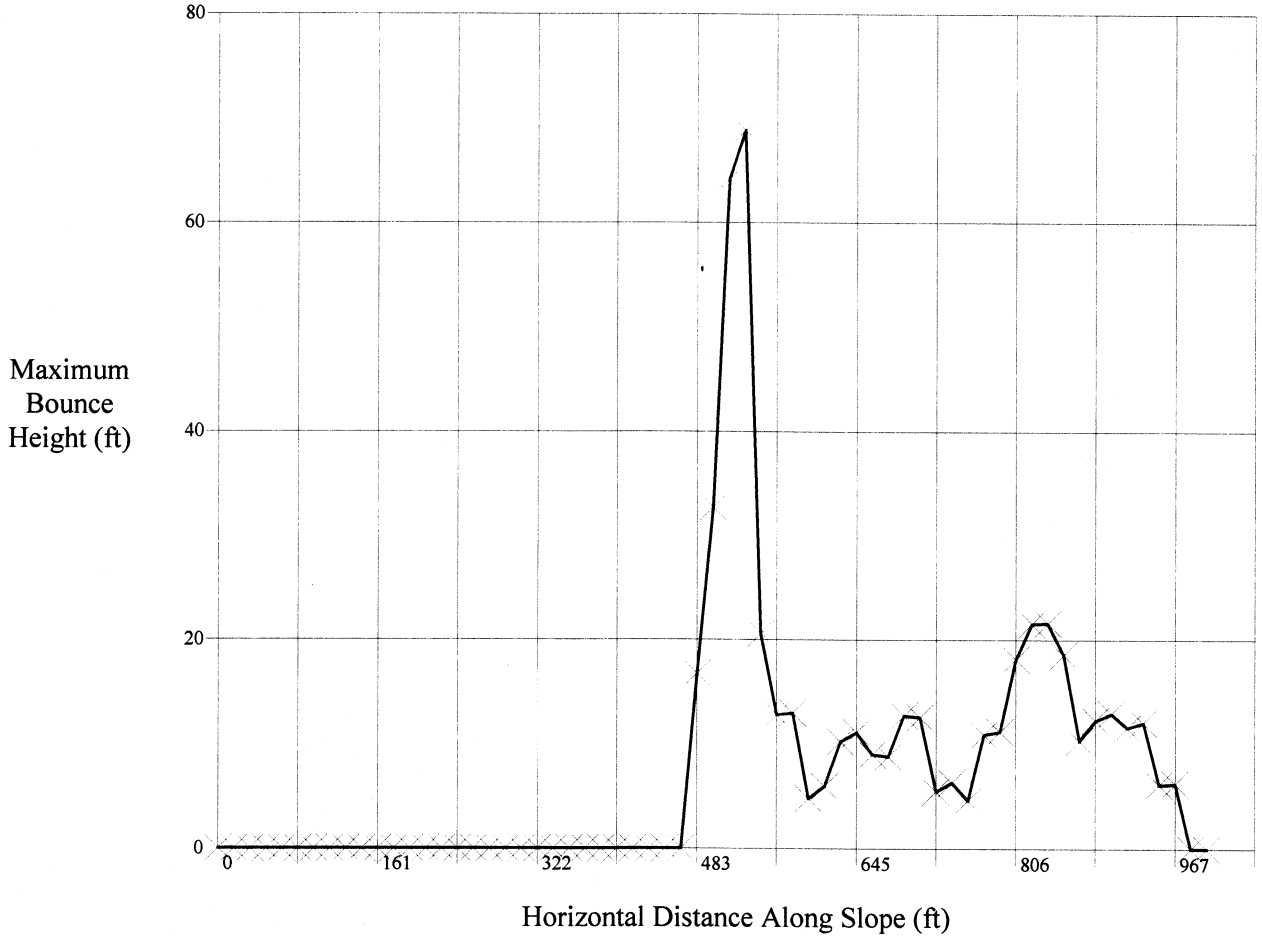

Velocity Graph - C:\Program Files\Crsp\E-E'.dat

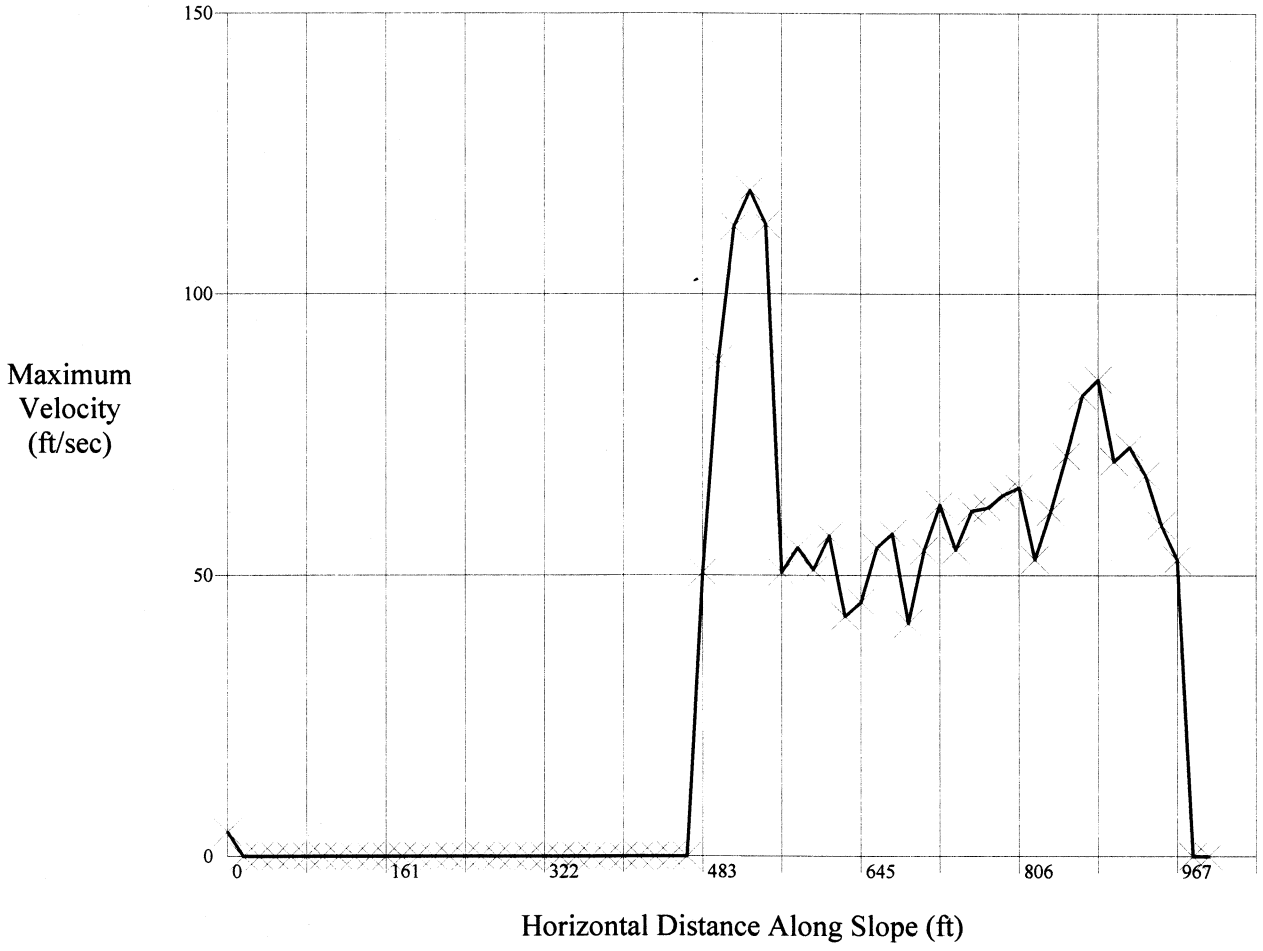

CRSP Data Collected at End of Each Cell - C:\Program Files\Crsp\E-E'.dat

Velocity Units: ft/sec Bounce Height Units: ft

Cell No.	Max. Velocity	Avg. Velocity	Std. Dev. Velocity	Max. Bounce Ht.	Avg. Bounce Ht.
1	No rocks	past end of cell			
2	No rocks	past end of cell			
3	No rocks	past end of cell			
4	113	65	21	69	19
5	55	28	17.13	4	2
6	55	36	11.39	6	3
7	72	51	14.99	12	6
8	52	33	12.88	5	4

CRSP Rocks Stopped Data - C:\Program Files\Crsp\E-E'.dat

X Interval	Rocks Stopped
0 To 10 ft	1
10 To 20 ft	0
20 To 30 ft	0
30 To 40 ft	0
40 To 50 ft	0
50 To 60 ft	0
60 To 70 ft	0
70 To 80 ft	0
80 To 90 ft	0
90 To 100 ft	0
100 To 110 ft	0
110 To 120 ft	0
120 To 130 ft	0
130 To 140 ft	0
140 To 150 ft	0
150 To 160 ft	0
160 To 170 ft	0
170 To 180 ft	0
180 To 190 ft	0
190 To 200 ft	0
200 To 210 ft	0
210 To 220 ft	0
220 To 230 ft	0
230 To 240 ft	0
240 To 250 ft	0
250 To 260 ft	0
260 To 270 ft	0
270 To 280 ft	0
280 To 290 ft	0
290 To 300 ft	0
300 To 310 ft	0
310 To 320 ft	0
320 To 330 ft	0
330 To 340 ft	0
340 To 350 ft	0
350 To 360 ft	0
360 To 370 ft	0
370 To 380 ft	0
380 To 390 ft	0
390 To 400 ft	0
400 To 410 ft	0
410 To 420 ft	0
420 To 430 ft	0
430 To 440 ft	0

X Interval	Rocks Stopped
440 To 450 ft	0
450 To 460 ft	0
460 To 470 ft	0
470 To 480 ft	0
480 To 490 ft	0
490 To 500 ft	0
500 To 510 ft	0
510 To 520 ft	0
520 To 530 ft	0
530 To 540 ft	0
540 To 550 ft	0
550 To 560 ft	5
560 To 570 ft	3
570 To 580 ft	3
580 To 590 ft	1
590 To 600 ft	0
600 To 610 ft	1
610 To 620 ft	0
620 To 630 ft	2
630 To 640 ft	2
640 To 650 ft	0
650 To 660 ft	0
660 To 670 ft	0
670 To 680 ft	1
680 To 690 ft	0
690 To 700 ft	1
700 To 710 ft	0
710 To 720 ft	0
720 To 730 ft	0
730 To 740 ft	0
740 To 750 ft	0
750 To 760 ft	0
760 To 770 ft	0
770 To 780 ft	0
780 To 790 ft	0
790 To 800 ft	0
800 To 810 ft	0
810 To 820 ft	0
820 To 830 ft	0
830 To 840 ft	0
840 To 850 ft	0
850 To 860 ft	0
860 To 870 ft	0
870 To 880 ft	0
880 To 890 ft	0

X Interval	Rocks Stopped
890 To 900 ft	0
900 To 910 ft	0
910 To 920 ft	0
920 To 930 ft	0
930 To 940 ft	0
940 To 950 ft	0
950 To 960 ft	0
960 To 970 ft	0
970 To 980 ft	0
980 To 990 ft	0
990 To 1000 ft	0

PREDICTION OF SURFACE DEFORMATION RESULTING FROM LONGWALL MINING OVER THE BEAR CANYON RESERVE

PREPARED FOR

C.W. MINING COMPANY

HUNTIGTON, UTAH

AUGUST 2006

PREPARED

BY

MALEKI TECHNOLOGIES, INC.

Consulting Mining & Geotechnical Engineers
SOUTH 5608 MAGNOLIA
SPOKANE, WA 99223
(509) 448-7911
maleki.tech@Comcast.net

1.0 INTRODUCTION

This report was prepared at the request of C.W. Mining Company for an evaluation of surface subsidence mechanics and determination of typical deformation expected at the Bear Canyon longwall reserve (figure 1) in the C.W. mining operations, located near Huntington, Utah. The study was initiated in response to a deficiency list prepared by resource specialists of the Utah Division of Oil, Gas, and Mining.

Specific objectives were as follows:

- Description of subsidence mechanisms and angle of draw;
- Description of pillar designs developed by C.W. Mining for the multiple seam reserve in the Bear Canyon Study area,
- Calculation of subsidence profiles over the longwall blocks in both Tank and Hiawatha seams using regional subsidence measurement results, and
- General recommendations for surface subsidence monitoring.

The study area is located adjacent to the permitted areas in the C.W. Mining existing room-and-pillar operations located in the Wasatch Plateau Coal Fields of eastern Utah. Longwall mining has been extensively used in both the Book Cliffs and Wasatch Plateau coal fields since its introduction at the Sunnyside mines during 1960's; it is generally considered an environmentally attractive method to mine coal. It minimizes damage to the surface by permitting gradual subsidence of overburden strata over mined-out areas while at the same time satisfying BLM requirements of maximizing economic recovery of coal resources (Maleki and others 2001).

C.W. Mining is planning to mine coal reserves from the study area using the longwall method mostly in the Tank and Hiawatha seams at a typical depth of 800 to 2,000 ft (two limited panels are also envisioned in the Blind Canyon Seam). Existing mine plans call for extraction of the reserve using an extraction height of 5 to 8 ft within longwall panels. Subsidence calculations (consisting of vertical movements and horizontal strains) were completed for three longwall blocks**,** as illustrated in figure 1.

- Block 1, Tank Seam. For five 500- to-640-ft wide longwall panels retreated from northwest to southeast. Seam thickness varies from 5 to 7.6 ft within this longwall block. We have simulated an average extraction height of 7 ft. This is a conservative and prudent assumption for this study.

- Block 2, Tank Seam. For four 600- to-800-ft wide longwall panels retreated from northwest to southeast. Seam thickness varies from 5 to 8 ft within this longwall block. We have simulated an average extraction height of 7 ft.

- Block 3, Hiawatha Seam. For four 640-ft wide longwall panels retreated from northwest to southeast. Seam thickness varies from 5 to 15 ft within this longwall

block. The extraction height is fixed at 8 ft considering longwall face equipment specifications.

This report is prepared in five sections. After this introduction, the subsidence mechanism is presented in section 2.0, followed in section 3.0 by a description of mining and geologic conditions and subsidence characteristics, including rock mechanics data, subsidence parameters, and a discussion of the conceptual mine layout designs developed by C.W. Mining for multiple seam longwall extraction. Predicted deformation patterns are presented in section 4 using three-dimensional subsidence models. The subsidence monitoring program is reviewed in section 5.

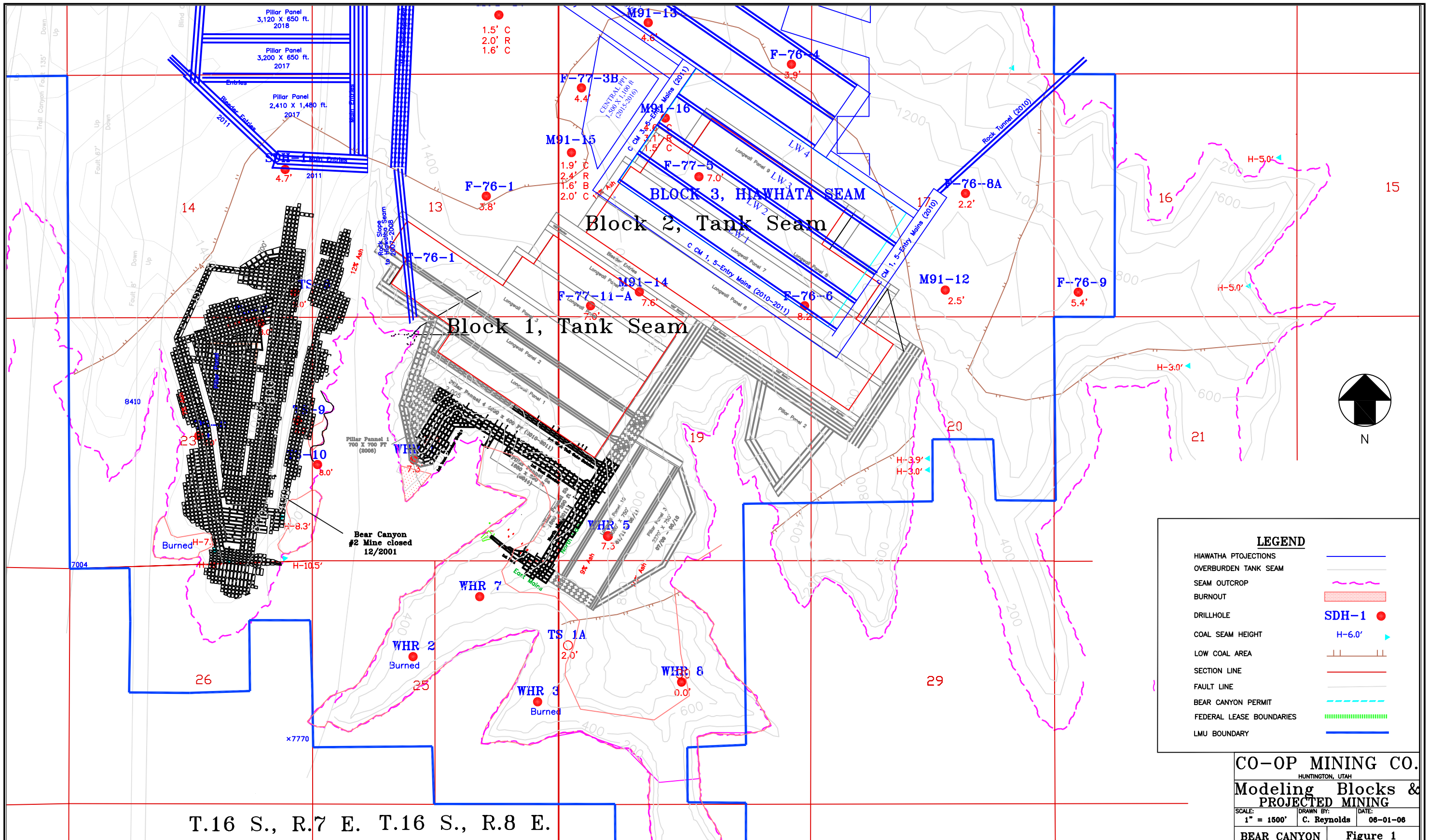

CO-OP MINING CO.
HUNTINGTON, UTAH

Modeling Blocks & PROJECTED MINING

SCALE:	DRAWN BY:	DATE:
1" = 1500'	C. Reynolds	06-01-06

BEAR CANYON | Figure 1

MALEKI TECHNOLOGIES INC.
SPOKANE, WASHINGTON

MINE LAYOUT DESIGN

2.0 SUBSIDENCE MECHANISM

Surface subsidence occurs because of downward rock mass movement caused by the closure and collapse of mined-out excavations. Surface subsidence processes result in both vertical and horizontal displacement of rocks. Two major mechanisms of surface subsidence are associated with mining: formation of sinkholes and creation of troughs.

The type of subsidence mechanism predicted for the study area is the trough-type subsidence. It is characterized by the formation of a relatively smooth basin and is much less damaging than sinkhole subsidence. Sinkholes result from sudden or time-dependent collapse of overburden in localized areas, and these areas can be from several feet to tens of feet in diameter. Based on long-term measurements over the Hanna Basin, Wyoming (Karfakis 1987) and the Colorado Front Range (Matheson and Bliss 1986), researchers have established a relationship between the probabilities of sinkhole subsidence versus overburden depth. A great majority of sinkholes (98% probability) form where depths are less than 160 ft. At typical cover depths of 400 to 2,000 ft over the mains at the longwall project site, the probability of sinkhole occurrence is small, assuming stable "support" pillars.

As longwall operations are initiated in the first panel, roof span increases behind the longwall face until it caves. The roof span varies in mines, but typically ranges from 30 to 200 ft, depending on the strength of the roof rocks. The remaining overburden rocks will remain stable, transferring their load to the face and gate pillars. At some critical face position, the arching and load transfer mechanism collapses, and ground movement expands toward the surface, causing subsidence.

The caving process is associated with fracturing of near-seam strata and settling of overlying rocks. Four zones of movement are associated with subsidence (Peng 1992).

1. *Cave zone—broken and fragmented rocks that fill mined space*. The immediate roof rocks fracture into blocks often controlled by preexisting structure, filling the mined space. Bulking and rotation of individual roof rocks eventually limits the upward growth of failure. The thickness of this zone is estimated to be two to eight times seam thickness, depending on the bulking characteristics of the immediate roof rocks.

2. *Fracture zone—fractured rocks that fail because of shear stresses near the ribs and delamination toward the center of the panel*. This zone is located directly above the cave zone. The strata within this zone move downward, usually in large blocks, but without major rotation, to rest on the caved zone below. The permeability of the rocks is increased within this zone, which is estimated to extend twenty to sixty times seam thickness (Peng 1992) above the mine roof depending on geologic conditions and the strength of the rocks.

3. *Continuous deformation zone—deformation zone from the top of the fractured zone to the surface soils*. The strata flex downward without significant fracturing, gradually settling over the fracture zone. In the absence of soils, this zone extends to the surface,

forming compression zones at the surface to the center of the panel and tension zones at the edge of excavations.

4. *Soil zone*—This zone is an extension of the continuous deformation zone, which, depending on site-specific conditions, generally consists of soils and weathered rocks. Because of the less-brittle nature of soils, tensile cracks associated with transient subsidence may not be detected easily in front of the face and any existing fractures tend to heal quickly. Tensile fractures forming at panel boundaries last longer, but eventually get closed due to caving of fracture walls.

Three subsidence phases are associated with trough subsidence (figure 2).

1. The *subcritical phase* occurs immediately at the beginning when movement is in a small area at the center of the basin.

2. The *critical phase* occurs as the basin area expands when the maximum value of the downward movement is reached at the center. The critical excavation width is generally larger than 1.4 to 1.6 times the overburden thickness and is influenced by position and strength of competent layers within the overburden.

3. The *supercritical phase* occurs as the basin develops a flat bottom. In this phase, the basin area continues to increase with the cave area, but subsidence will remain at the maximum value attained in the critical phase.

Thus, the surface response of longwall mining activity, shown in Figure 2, begins with the subcritical phase, then progresses to the critical phase, and finally, to the supercritical phase. The subsidence process first shows effects on the surface as the upper strata bend, including tension (expansion), which causes near-surface fractures to open up and new ones to be created. Figure 2 shows how the middle portion of the excavation expands as subsidence continues, going through a cycle of, first, tension and then compression, which closes tension cracks. Final subsidence shows an excavation with the middle portions lower in elevation, but back to a near-original state. Areas on the edge of the excavation basin are subjected to tensile strains. Tensile strains are accumulative if the tensile zones overlap during the extraction of side-by-side panels ("transient" subsidence) or superimposed multiple-seam designs. By staggering the position of full extraction boundaries in multiple seams, C.W. Mining has avoided overlapping the tensile zones and thus reduced the potential for surface cracking at final mining boundaries ("permanent" subsidence).

Considering panel width to average overburden depth ratio for the C.W. Mining project area (0.6), these longwall panels are considered to have subcritical widths, and thus the great majority of subsidence is expected during the mining of the second and the third panels. The subsidence process is expected to be mature within 2 years after mining.

Subsidence characteristics for any coal field depends on site-specific geologic conditions and mining practices, including strata competence, geologic structure, topography, extraction height, extraction speed, and mine designs. For instance, rapid changes in topographic

conditions are known to influence both naturally occurring and mining-induced rock mass wasting, including sandstone escarpment failure (Maleki and others 2001). The site-specific subsidence parameters for the Bear Canyon study area are addressed in the following sections using available monitoring results locally and regionally within Utah coal fields.

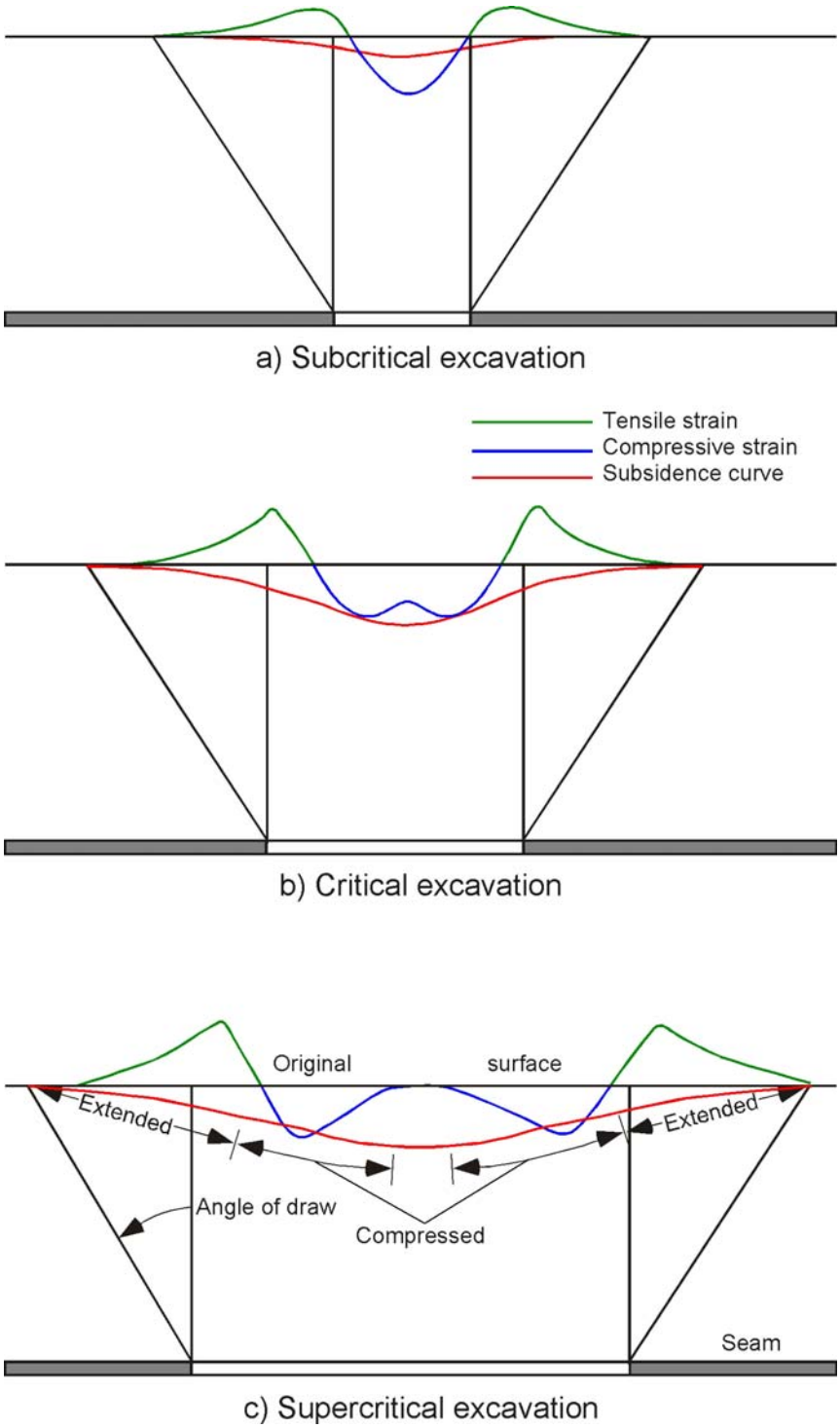

Figure 2. The three phases of subsidence development.

3.0 MINING, GEOLOGIC CONDITIONS AND SUBSIDENCE CHARACTERISTICS

3.1 Conceptual Mine Layout Designs

The C.W. Mining Company, in cooperation with MTI engineering staff, implemented geotechnical studies at both Tank and the Blind Canyon seams during the 1990's to study coal seam behavior and support loading during multiple seam pillar extraction (Maleki and others 1999). These studies consisted of underground and surface mapping, installation and monitoring of geotechnical instruments for the evaluation of Mobile Roof Support, and three-dimensional stress analyses. In addition, during 2001, MTI implemented a preliminary escarpment stability evaluation to assess potential pillaring impacts on the stability of the Castlegate Sandstone escarpments at the Wild Horse Ridge reserve. This study utilized a wealth of data collected over both stable and unstable escarpment areas at the neighboring East Mountain and Trail Mountain mines (Maleki and others 2000, MTI 2001).

As illustrated figure 1, C.W. Mining has oriented the longwall panels N55° W and is planning to use three-entry gateroad systems with 30-ft-wide yield pillars (50 ft center-to-center) and 500- to 800-ft-wide panels. This conceptual mine plan is suitable for permitting purposes and additional stress analyses are planned for finalizing mine designs in multiple-seam bump-prone conditions.

At sufficient deviation of 30° from major joint sets (N15° E and N85° E, MTI 2001), the existing mine orientation is beneficial for stability of development workings because it avoids alignment of joints and mine openings.

From environmental point-of-view, MTI considers this orientation effective in reducing the potential for subsidence-related cracking at the surface. Because at panel boundaries, the subsidence cracks generally form near parallel to longwall face and length (Maleki and others 2006), by misaligning the joints and panel orientation, C.W. Mining increases its chances of limiting the number and length of mining-induced surface fracturing at final mining boundaries.

To control gate pillar bumps, C.W. Mining staff has selected yield pillars to reduce strain energy accumulation within the gate pillars. Pillar size was selected on the basis of successful experience in the neighboring longwall operations in the East Mountain and Trail Mountain.

Based on a comprehensive case study by the USBM in 1980's (Fejes 1985, Dyni 1991, Section 4.2), MTI makes the assertion that the narrow 30-ft-wide yield pillars commonly used in the two-entry Utah reserves crush completely with no influence (or subsidence humps) above the gateroads. Thus the existing layout is also beneficial for reducing surface impacts, although we prefer a two-entry system for coal bump control based on site-specific geotechnical monitoring in the Dugout Canyon Mine (Maleki and others 2003).

3.2 Geology, Rock Strength and Stress Field

The three coal seams of economic interest belong to the Blackhawk Formation which is overlain by the Castlegate Sandstone and underlain by the Star Point Sandstone and the Mancos shale (figure 3). Minable longwall reserves are mostly contained in the Tank and Hiawatha seams with limited reserves also in the Blind Canyon Seam. Tank and Hiawatha seams average 7, and 8 ft in the study area; the Blind Canyon is 7 ft thick. The interburden between the Tank and Hiawatha seams is approximately 300-ft.

The overlying cliff forming Castlegate sandstone is a massive cross-bedded unit. It contains occasional thin, interbeds of shale, pebble conglomerate and mudstone. This unit is 170 to 250 ft thick in the area using the corehole data , however, the actual exposed thickness is locally much lower (as low as 50 ft). The Price River Formation consists of numerous beds of cross-bedded sandstones with occasional interbeds of shale, pebble conglomerate, and mudstone.

The Blackhawk Formation is composed of interbedded deltaic mudstone and siltstone and is less resistant to weathering than the neighboring units. It is characterized by alternating slope and cliff forming units. This unit is approximately 750 ft in thickness.

The Star Point Sandstone consists of thick cliff-forming sandstone units separated by shales. It is light colored and is approximately 350 ft in thickness in the study area. The Mancos shale is a blue-grey color marine shale, approximately 1000 ft thick, and is soft and well weathered.

Jointing patterns were mapped at the Castlegate Sandstone horizon and found similar across the study area (MTI 2001). The joint trends are thought to be generally coincident with jointing found in the overlying Price River and underlying Blackhawk Formations and are consistent with the measurements on the Wasatch Plateau (Maleki 1988, Maleki and others 1999). Joints were typically within a few degrees from vertical.

The most pronounced (primary) joint trend typically ranges between N10° E to N20° E (N15° E average). A less pronounced and secondary joint system trending S80° E to S90° E was also observed. This trend appeared to be generally consistent across the study area.

A third joint set was observed infrequently with a N50° E to N55° E trend. This set was only observed in the east near the Fish Creek Canyon. Spacing on this set is estimated to be greater than 10 feet due to its lack of occurrence or expression.

Apparent joint spacing appears to be controlled by confining stress. In outcrop the primary and secondary joints are more apparent and appear closer spaced at or near the points than in head of drainages. Rocks in place often exhibit jointing at 10 - 15 feet spacing, but more broken rocks nearly always showed closer spaced joints.

Faulting is not expected within the longwall reserves (Reynolds 2006).

Site-specific geologic and rock mechanics data are limited, although MTI has collected large amounts of information from adjacent properties. Figure 4 summarize the mechanical properties of coal measure strata at the neighboring East Mountain, compiled by MTI. Clearly, most overburden rocks are strong and stiff, capable of accumulating large strain energies, which contributes to seismicity.

The researchers from the former USBM and private industry have made a number of stress measurements in mines of Wasatch Plateau, Utah. There are two stress measurements within the close proximity of C.W. Mining operations (figure 5). These measurements confirm that the far-field stress field is unremarkable. The horizontal stress is moderate and is less than 50 percent of the vertical stress magnitude. We anticipate similar stress field at the C.W. Mining operations based on observations of lack of stress-induced stability problems (such as cutters) and an analyses of measurements in the existing reserve (Maleki and others 2000).

3.3 Subsidence Parameters

Subsidence engineering parameters include subsidence factor, angle of draw, angle of critical deformation, and horizontal strain. The subsidence factor is the ratio of maximum measured subsidence to extraction height. Because this ratio depends on excavation width and overburden thickness, it should be measured in supercritical excavations where caving has reached the surface on collapse of the pressure arch.

The angle of draw defines the limit of surface movements beyond the edge of an excavation. It is measured from a vertical line drawn at the panel edge and a line connecting the panel edge to the point of “no” movement on the surface. In practice, the accuracy of surveying equipment defines the point of no movement. This accuracy is usually about 0.1 ft but varies depending on topographic conditions, measurement technique, etc. Angle of critical deformation is similar to the angle of draw, but is measured to a point of critical deformation with respect to existing structures; it is preferred by many practitioners because it avoids the shortfalls connected with the accuracy of surveying equipment. Based on subsidence data from 40 longwall panels, Peng (1992) found that it is 10º less than the angle of draw.

Horizontal strain is the change in horizontal length of the ground divided by the original length of the ground. Positive strain is used here to show tensile strain indicating an increase in the horizontal length of the ground. Compressive strain (negative notation) occurs when the ground is shortened or compressed. Maximum tensile strain is found in supercritical excavation and maximum compressive strain occurs in subcritical excavations. Horizontal strain increases with an increase in extraction height and decreases at greater depths. Surface topography also influences horizontal strain.

The best estimates for the extend and magnitude of subsidence for the C.W. Mining two-seam mining conditions can be obtained by reviewing the results of long-term monitoring in Utah. The USBM implemented a comprehensive subsidence study over the Energy West two-seam longwall reserve from 1978 to 1989. The study monitored surface movements over

four Blind Canyon and six Hiawatha panels. The study addressed angle of draw, subsidence factors for single and multiple-seam mining, and critical width. Similar to the Bear Canyon reserve, the mining area was bounded by faults. Maximum subsidence was 68% to 72% of the extraction height for single and two-seam mining conditions, respectively. This is in general agreement with other measurements in Utah showing a subsidence factor of 70 %. The angle of draw ranged between 25° to 30° for single- and two-seam mining conditions, respectively. This reported maximum angle of draw is higher than average values for the East Mountain (22.5° to 25°, Fejes 1985) but is significantly lower than that reported by the British National Coal Board (NCB 1975).

3.4 Gate Pillar Behavior

Because gate pillar designs may influence surface subsidence, some recent investigations have focused on evaluating subsidence above gate pillars. The Western U.S. measurements show different overburden deformation characteristics influenced by the choice of pillar designs. Based on a comprehensive case study by the USBM in 1980's (Fejes 1985, Dyni 1991, Section 4.2), MTI makes the assertion that the narrow 30-ft-wide yield pillars commonly used in the two-entry Utah reserves crush completely with no influence (or subsidence humps) above the gateroads.

We expect the three-entry yield pillar system at the Bear Canyon Mine to behave similarly in the long-term with no subsidence humps. The exact timing of pillar crushing is uncertain at this time requiring additional stress analyses. However, based on geotechnical measurements in Utah coal fields (Maleki and others 2003), pillar yielding to residual strength can occur quietly rapidly behind the face in moderately deep mines. We expect pillar crushing to be complete after extraction of panels on both sides because of significant convergence at the seam horizon. Site-specific calculations to address ground control issues in the three-entry system are forthcoming and will form the basis for petition to switch to a two-entry system.

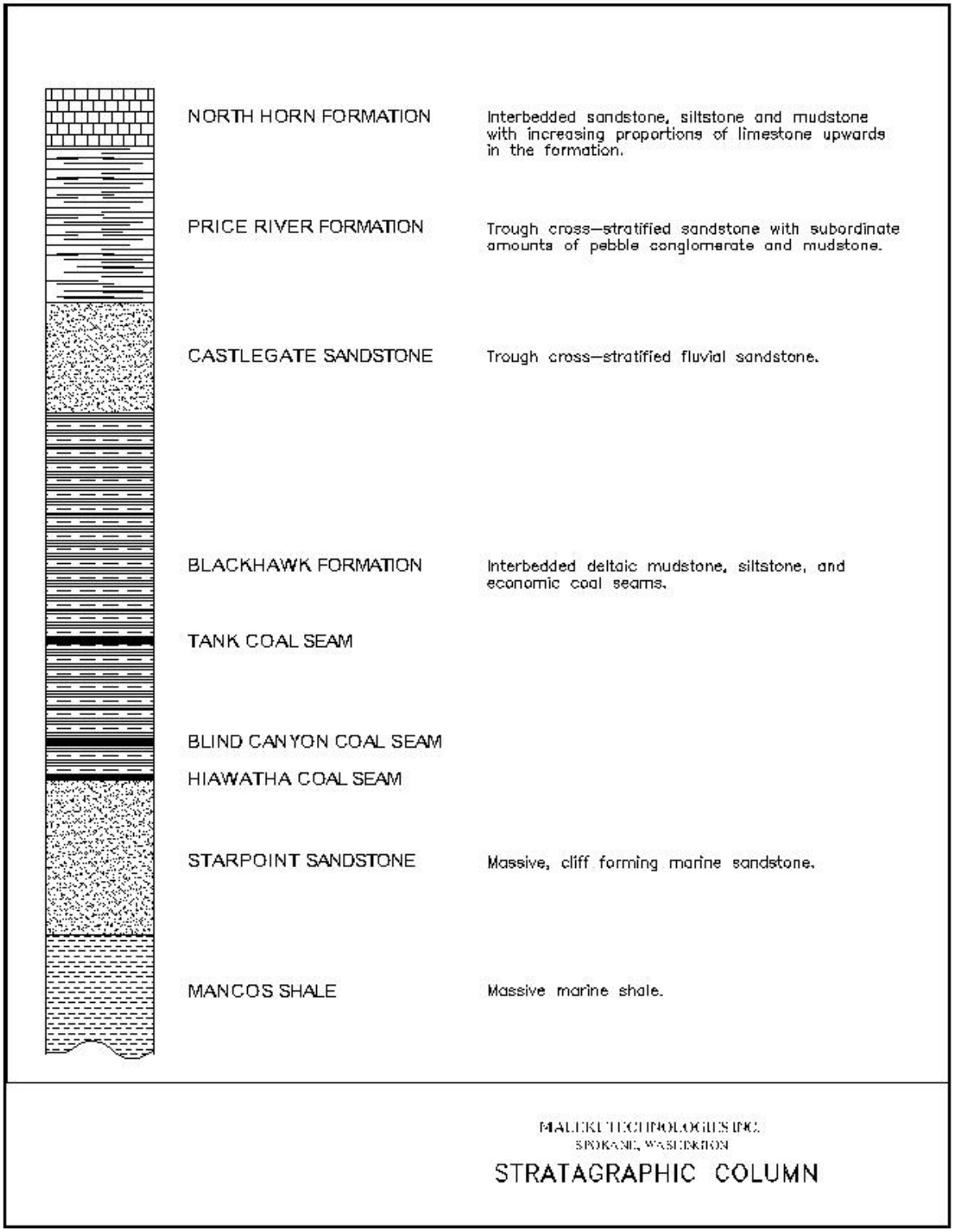

Figure 3. Generalized stratigraphic column.

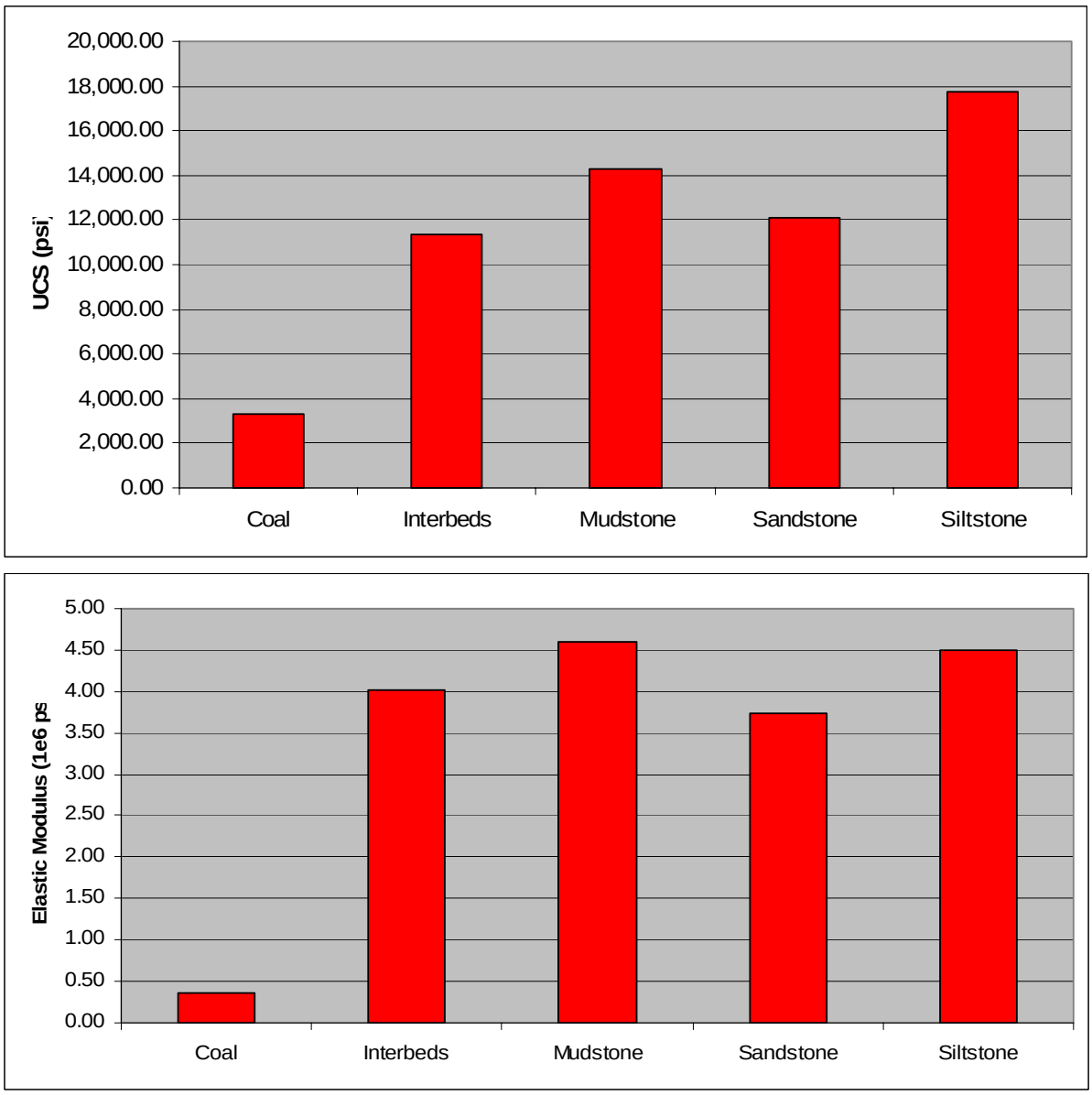

Figure 4. Histogram frequency diagram of uniaxial compressive strength and Young's modulus, regional data compiled by MTI.

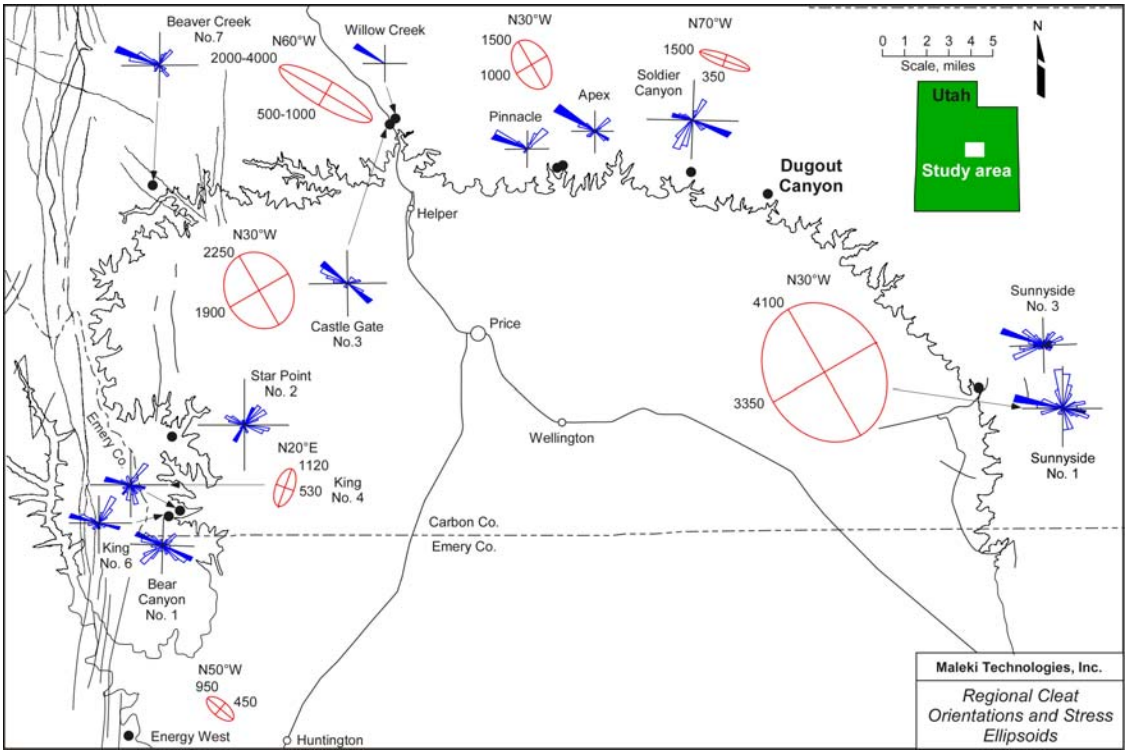

Figure 5. Regional horizontal stress measurements (ellipsoids) and the orientation of cleats in Utah coal fields.

4.0 PREDICTED GROUND MOVEMENTS

4.1 Methodology

Surface subsidence is the readily observable manifestation on the ground surface of the displacement field surrounding the underground portion of the mine. Predicting subsidence magnitude, therefore, constitutes a particular solution of the overall problem of finding the induced displacement field. To study subsidence phenomena and estimate the magnitude of subsidence, a number of empirical, physical, and numerical methods have been used.

Empirical methods, including profile functions, influence functions, and graphical methods were proposed by the British National Coal Board. These methods involve the analysis of existing subsidence from an area to predict future subsidence effects. These methods are based on the mathematical fit of a considerable number of measured subsidence profiles. They apply to geologic conditions in the area where they were developed and require adjustments if they are applied to different strata conditions.

To estimate surface deformation above the proposed longwall panels, we used a three-dimensional influence function method while accounting for site-specific conditions using the subsidence monitoring data from both the neighboring Deer Creek Mine. These methods have become very popular for the prediction of subsidence and surface strains within the last two decades (USBM, 1983; Peng and others 1994; SDPS 2000). They are superior to graphical methods because they can be used to model an entire longwall block while allowing an examination of the sensitivity of results to variations in seam thickness, pillar designs, panel dimensions, and overburden thickness.

These methods rely on the influence of an extracted volume on the displacement components of a remote point on the surface. In the zone calculation method, for example, the circular zone of influence around a point on the ground surface is divided into a number of zones in such a manner that the influence factor of such an area is fixed at a certain value. If the full area of the influence were mined out, the point in question would undergo 100% of maximum possible subsidence. If some portion within the zone of influence were unmined, subsidence would be correspondingly reduced.

Subsidence calculations (consisting of vertical movements, change in surface slopes and strains) were completed for three longwall blocks.

- Block 1, Tank Seam. For five 500- to-640-ft wide longwall panels retreated from northwest to southeast. Seam thickness varies from 5 to 7.6 ft within this longwall block. We have simulated an average extraction height of 7 ft. This is a conservative and prudent assumption for this study.

- Block 2, Tank Seam. For four 600- to-800-ft wide longwall panels retreated from northwest to southeast. Seam thickness varies from 5 to 8 ft within this longwall block. We have simulated an average extraction height of 7 ft.

- Block 3, Hiawatha Seam. For four 640-ft wide longwall panels retreated from northwest to southeast. Seam thickness varies from 5 to 15 ft within this longwall block. The extraction height is fixed at 8 ft considering longwall face equipment specifications (Reynolds 2006).

4.2 Model Calibration

Subsidence predictions were made using a numerical model calibrated with baseline subsidence data from the East Mountain. The long-term surface response to longwall mining in 5E, 6E, 7E and 8E panels was monitored by researchers from the U.S. Bureau of Mines in two phases (figure 6). These panels were mined from May 1974 through January 1983, and subsidence was monitored along five monument lines from September 1979 to June 1983 during phase 1 investigations. Phase 2 results reported by Dyni (1991) include surface response to mining the Hiawatha Seam some 60-ft below extracted 5E through 8E panels in the Blind Canyon Seam.

USBM study reports an average angle of draw of 25 degrees ranging from 16 to 33 degrees, and a final subsidence factor of 67 percent for single-seam mining. Surface effects were described as follows (Fejes 1985):

"*There were no visual surface effects within the subsidence area. The local vegetation were not altered, and no surface fissures were detected……*"

The results of phase 1 monitoring were used to establish modeling parameters. Figures 7 and 8 present a comparison of measured and calculated subsidence along a north-south monument line during the extraction of each four longwall panels and show good agreement. The subsidence factor increased from .35 during the extraction of 6E to 0.67 after the extraction of 8E. Note that yielding gate pillars used in this longwall block, crushed uniformly, showed no humps in the subsidence trough.

The calibrated version of the model was used to make quantitative predictions of the subsidence expected over the Bear Canyon Mine. The similarities in geology and geometry (depth of cover, face width, yielding gate pillars, and mining height) between the monitored area over East Mountain and the neighboring project area justify the use of the back-analyzed parameters for the predictive model.

Some uncertainty exists for predictions made with the model due to variations in geology and mining geometry, including actual mining heights. Precise estimates of subsidence can only be achieved as site-specific data become available, and mine plans are finalized.

4.3 Results

Figure 9 presents expected subsidence pattern after the extraction of each longwall block and figure 10 the combined two-seam subsidence resulting from extraction of blocks 1, 2, and 3 after the completion of mining in the Tank and Hiawatha seams.

Figures 11 and 12 present both subsidence and surface strain profiles along section A passing through the two-seam longwall extraction zone. Additional results are summarized in table 1 including changes in surface slopes.

Table 1. Predicted subsidence parameters for single and two-seam extraction design options.

Block	Average mining height, ft	cover, ft	Maximum subsidence, ft	Maximum tensile strain, ft/ft	Maximum slope, percent
1 Tank	7	1,000	4.9	3.2e-3	.7
2 Tank	7	1,000	4.9	3.2e-3	.7
All combined	8	1,300	10.4	3.2e-3	1

Predicted subsidence varies from approximately4.9 to 10.4 ft for single and two-seam extraction. Using a criterion suggested by Singh and Bhattacharya (1984), tensile strains do not reach levels that could cause localized surface fracturing except at shallow areas (<650-ft cover). This assertion is in agreement with USBM measurements and observations on the East Mountain. The potential for surface fracturing is not higher at the permanent two-seam boundaries because longwall layouts in the Tank and Hiawatha seams are staggered. By not columnizing the longwall extraction areas in multiple seams and by not aligning panel orientation with primary joints, C.W. Mining has reduced the potential for surface fracturing.

Expected surface movement beyond underground mining boundaries varies from 460 ft in block 1 to 750 ft to the northeast where two-seam mining is planned in blocks 2 and 3. Changes in surface slopes are small (approximately one percent).

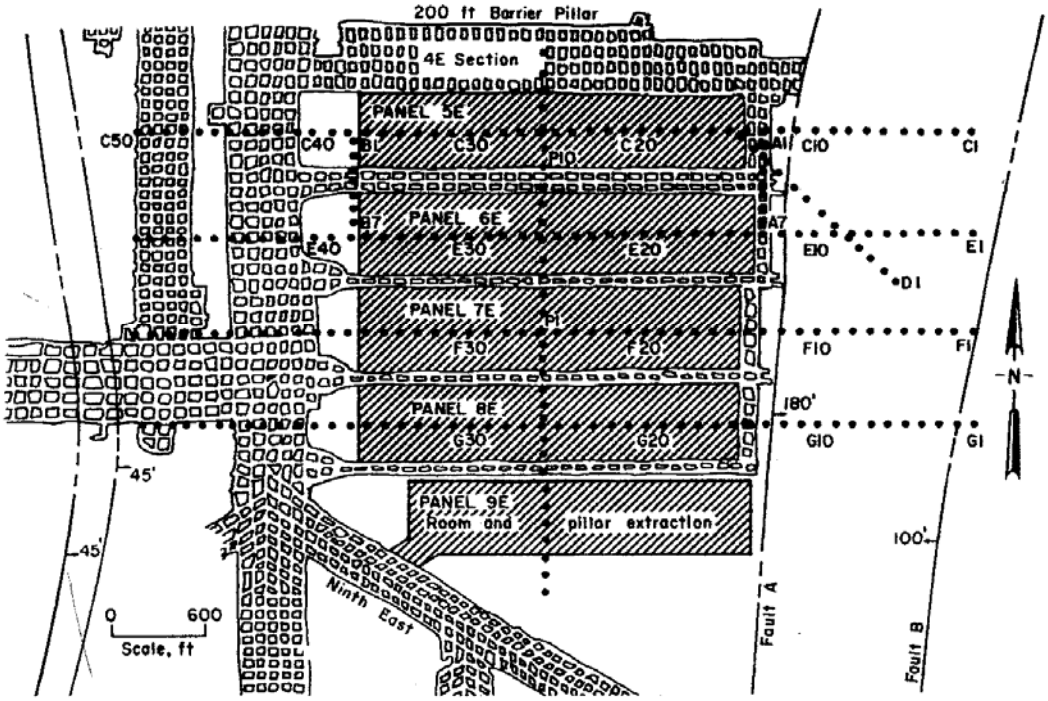

Figure 6. Subsidence monument locations above the USBM study site, East Mountain.

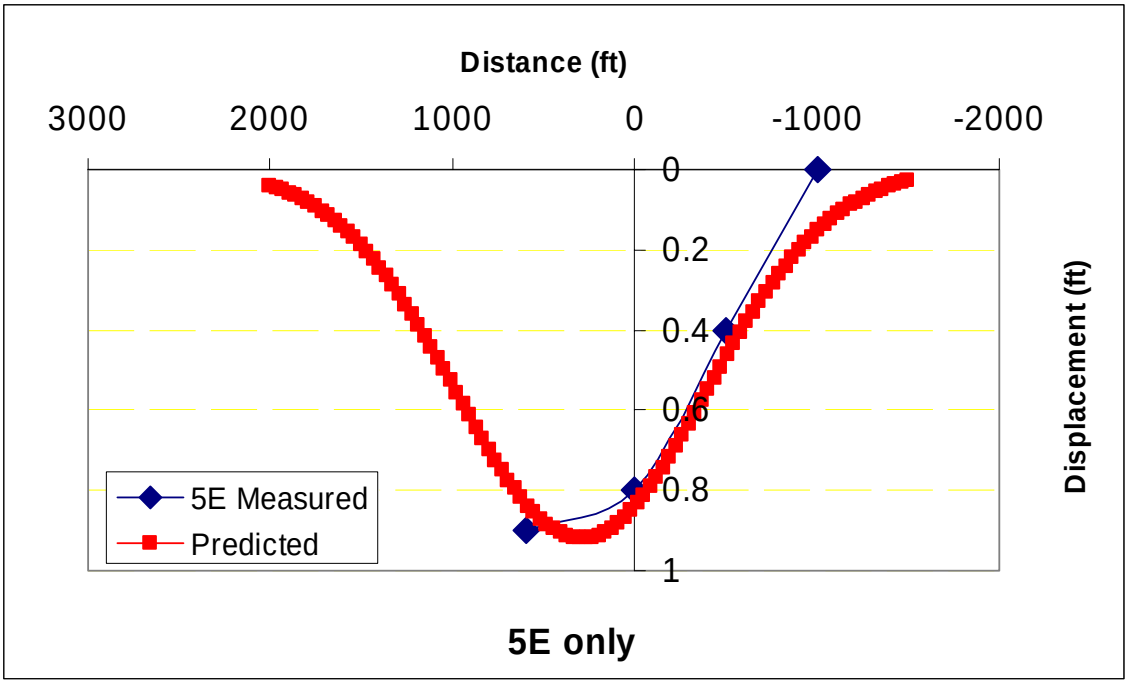

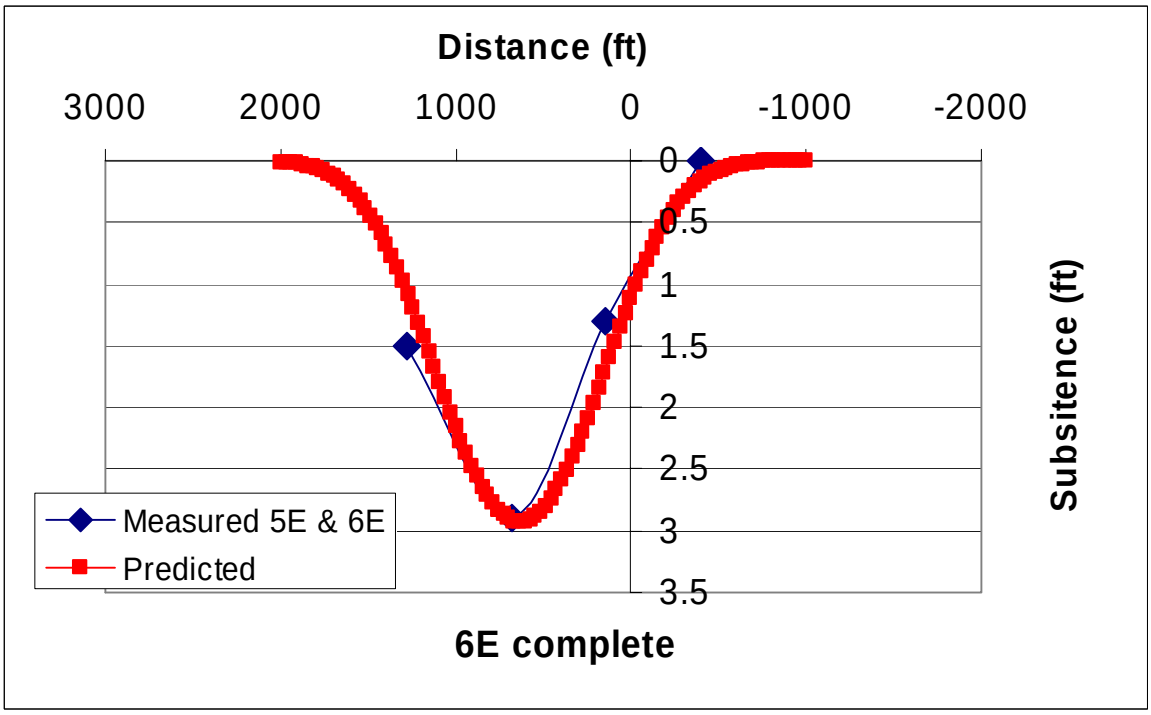

Figure 7. Compared measured and calculated subsidence after extraction of 5E and 6E panels.

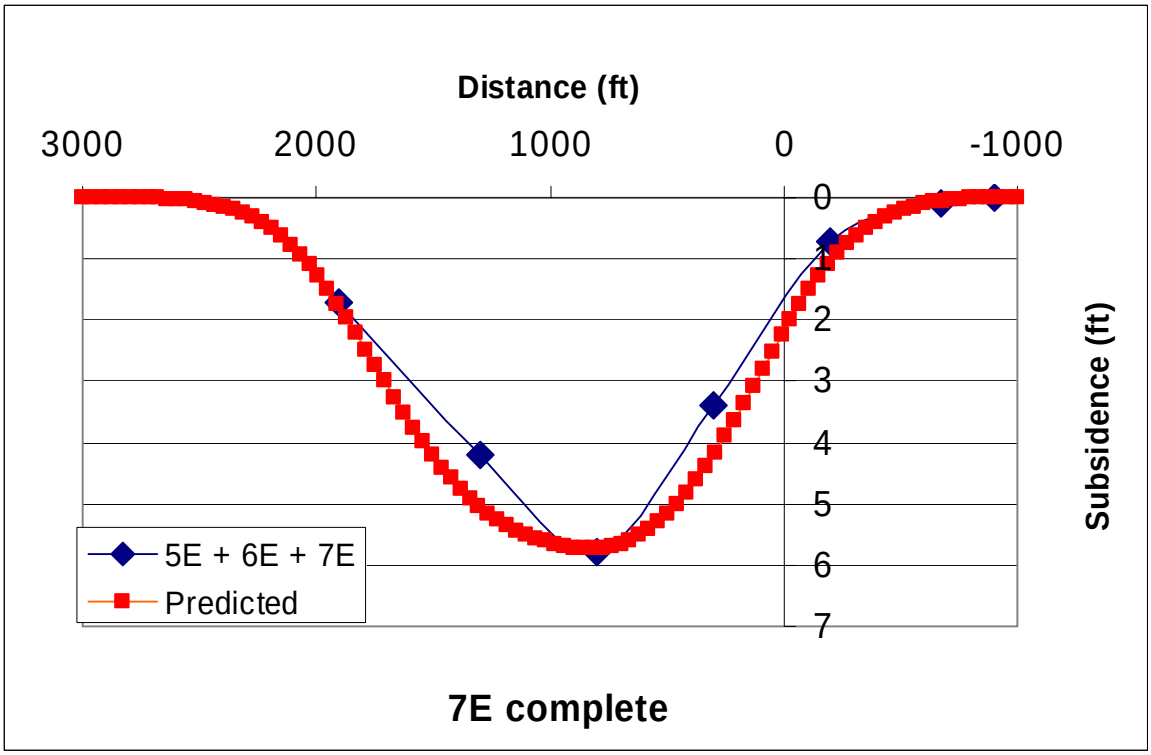

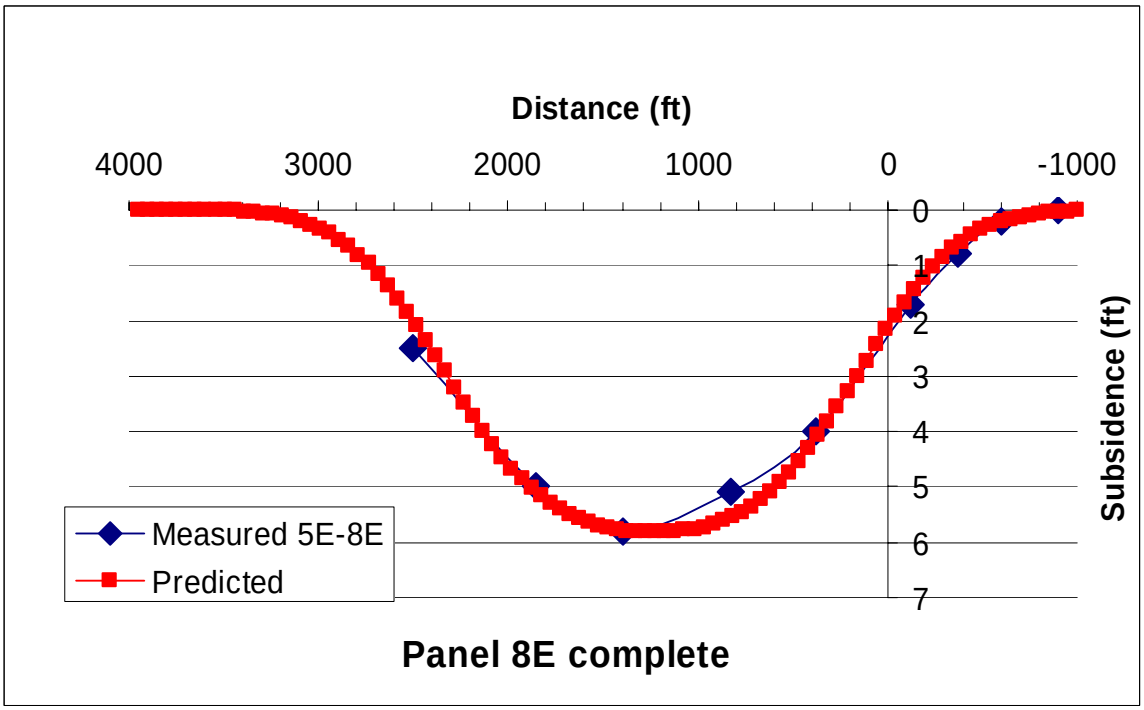

Figure 8. Compared measured and calculated subsidence after extraction of 7E and 8E panels.

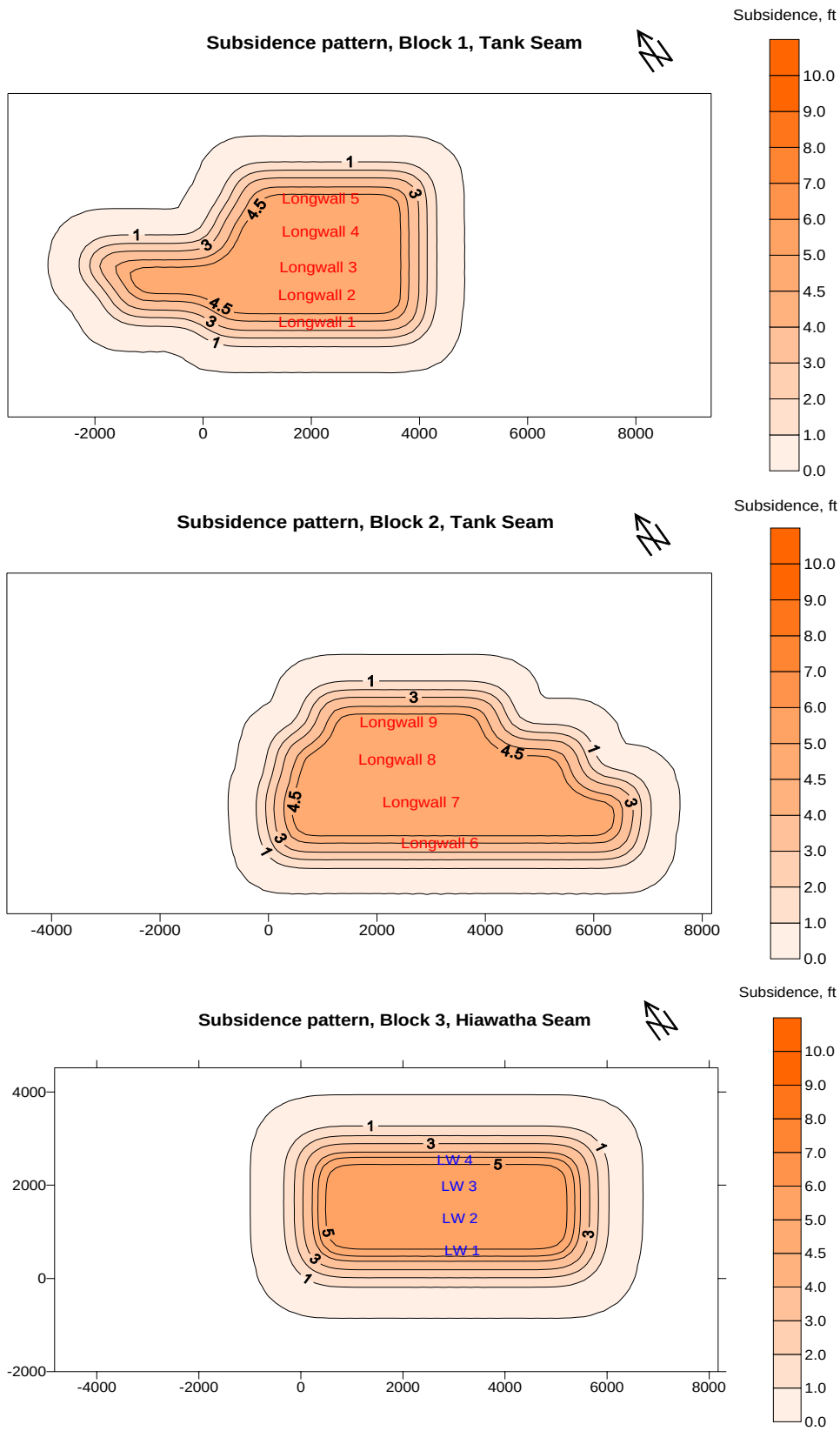

Figure 9. Subsidence pattern over longwall blocks 1, 2 and 3.

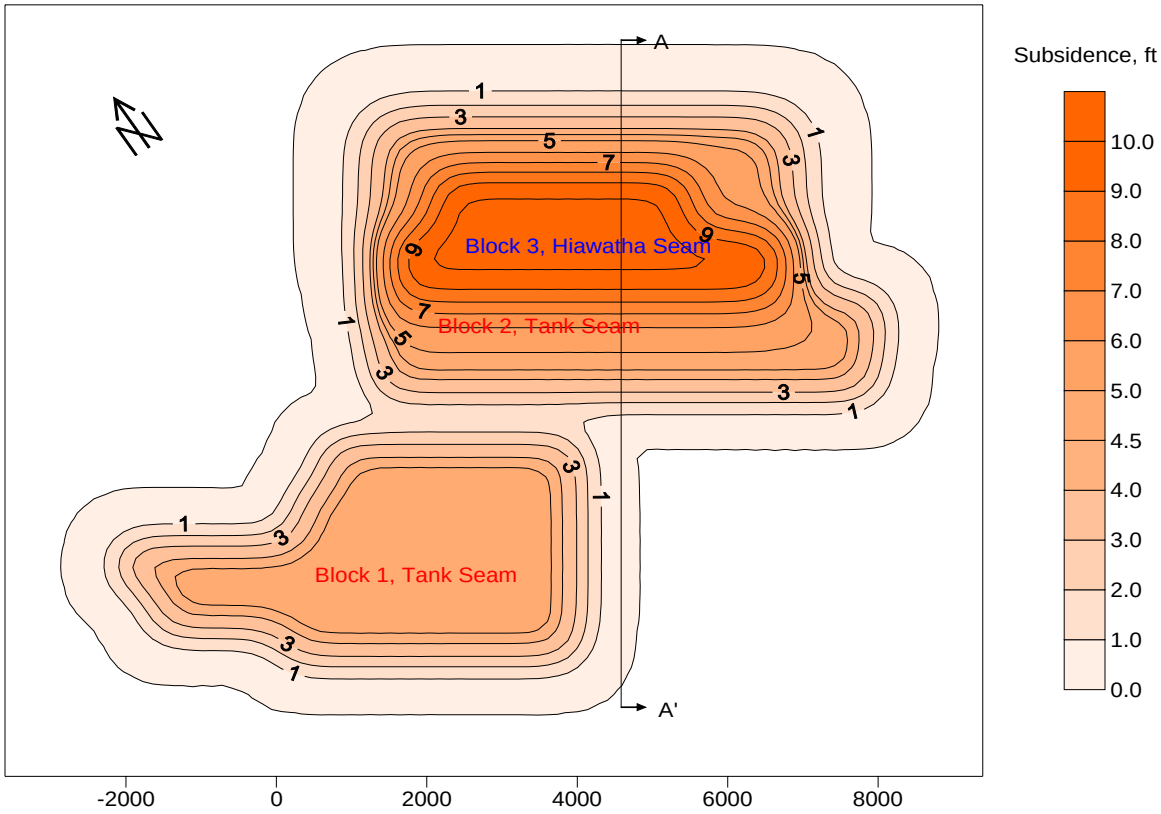

Figure 10. Total subsidence pattern after the extraction of blocks 1 through 3.

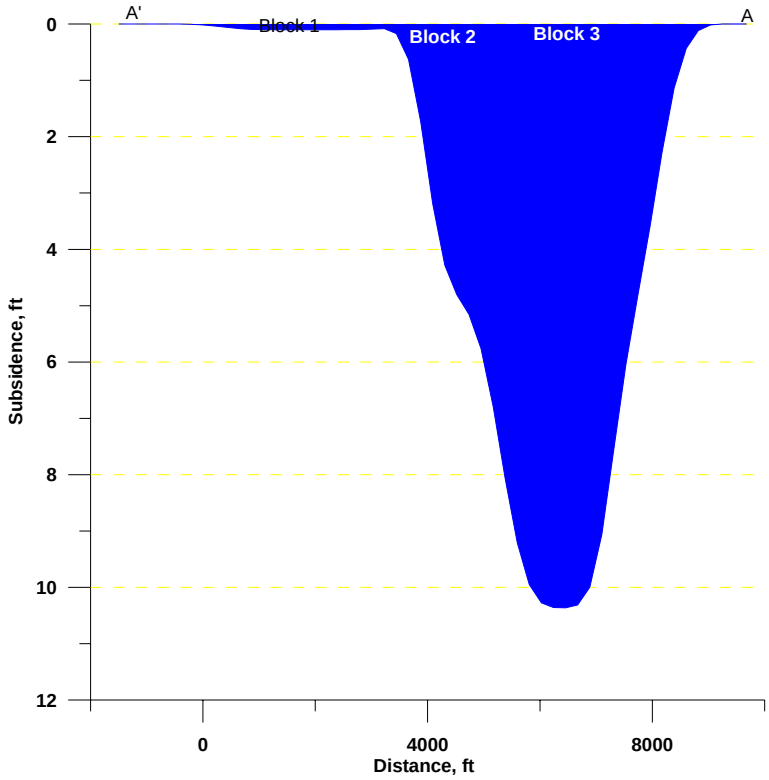

Figure 11. Typical subsidence profile at location A.

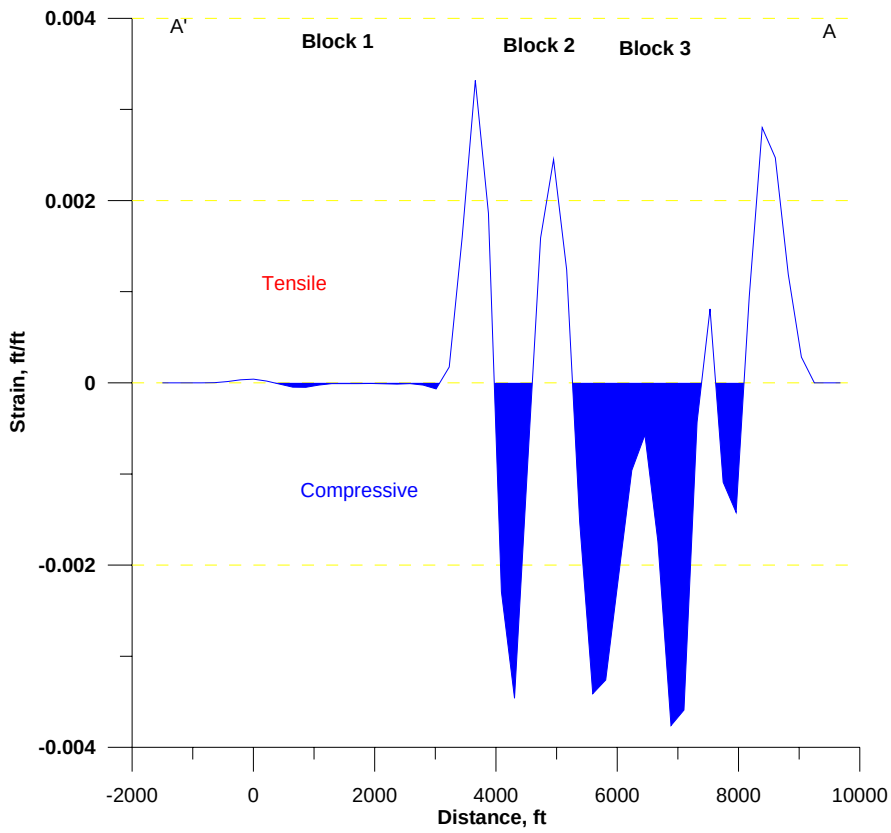

Figure 12. Typical final strain profile at location A.

5.0 MONITORING PROGRAM

A subsidence-monitoring program should be implemented to verify the subsidence predicted in this study and to record any mining-induced damage to surface resources.

Subsidence monuments should be monitored by surveying a monument line across the first longwall block. For verification purposes, it would be desirable to locate the monument line near the center of this block. The monument spacing of 50-ft is recommended over the first longwall panel for detailed comparison to the predictions. The monument spacing may be increased to 250-ft over panels 2 through 5.

From such monitoring, site-specific angle of draw, subsidence factor, and tensile strains can be calculated resulting in predictive subsidence techniques for the Bear Canyon study area. However, the arrangement and location of the monument line or method of survey can vary according to site-specific conditions influenced by topography, roads, etc.

Measurements should include a precision level survey to measure vertical settlement and possibly a steel tape extensometer to measure horizontal strain. GPS methods have recently become available and used in many western U.S. operations successfully. Alternatively, aerial photographic methods used extensively at the neighboring Trail Mountain and East Mountain, may be used.

C.W. Mining has not observed surface cracking above the existing Wild Horse Ridge panels and thus does not foresee the need for detailed monitoring. USBM researchers report very few mining-induced cracks over the East Mountain (Dyni 1991; Fejes 1986). MTI has designed and analyzed surface monitoring programs over Colorado mines (Maleki and others 2006). In some shallow mines, geologic staff conducts an annual crack survey over active longwall panel areas. A visual inspection is deemed sufficient over the deeper mines. The survey data include crack location, orientation, horizontal length, and width. Based on these measurements, MTI recommends a limited monitoring program so that the presence of surface cracks (if any) can be verified.

References

Allgaier F.K. 1994. Surface subsidence over longwall panels in the western United States- Final results at the Deer Creek Mine, Utah. U. S. Bureau of Mines Information Circular 9194, 17 pp.

Dyni, R. C., 1991. Subsidence Resulting from Multiple-Seam Longwall Mining in the Western United States – A Characterization Study. USBM IC 9297.

Fejes, A., 1986, Surface Subsidence Over Longwall Panels in the Western United States, USBM Report of Investigations. IC 9099.

Karfakis, M. 1987. Chimney Subsidence over Abandoned Coal Mines. International Journal of Mining and Geological Engineering, V. 5, pp. 131-134.

MTI 2001, Report prepared by Maleki Technologies, Inc. to C.W. Mining entitled "Modeling of Castlegate Sandstone Escarpment Stability". July 2001, pp 19.

Maleki, H., R. Olson, D. Spillman, and M. Stevenson, 2003. Development of Geotechnical Procedures for the Analysis of Mine Seismicity and Pillar Designs, 22nd International Conference in Ground Control in Mining, Morgantown, WV, 2003.

Maleki, H., R. Heath, and G. Tetreault, 2001. Development of Guidelines for Determination of Maximum Economic Recovery, SME Transactions, Vol. 310, 161 pp.

Peng, S. S., 1992. Surface Subsidence Engineering, SME, 161 pp.

Peng, S. S., and Yi Luo, 1994. Comprehensive and Integrated Subsidence Monitoring, WV University, 64 pp.

SDPS, 2000. Surface Deformation Prediction System, VPI.

USBM 1983. SPASID, A Computer Program for Predicting Ground Movement Due to Underground Mining. USBM contract J02955031.

Maleki H, K. Fleck, C. Semborski and C Pollastro, 2000, Development of a Statistical Technique for Assessing Sandstone Escarpment Stability. 19th. International Conf. On Ground Control, WV university, 2000.

Maleki, H., 1988, Ground Response to Longwall Mining--A Case Study of Two-Entry Yield Pillar Evolution in Weak Rock. CO School of Mines Quarterly, vol. 83, no. 3, 1988.

Maleki, H., J. Owens, W. Howie, 1999, An Overview of Geomechanics Safety Research on Mobile Roof Supports. 17th International System Safety Conference, August 16-21, 1999, Orlando, FL.

Jones R.E. 1994. Investigation of Sandstone Escarpment Stability in the Vicinity of Longwall Mining Operations. M.S. Thesis, Department of Mining Engineering, University of Utah.

Singh, M. M., and S. Bhattacharya. 1984. Proposed criteria for assessing subsidence damage to renewable resource lands, Preprint No., 84-391. Presentation at SME meeting.

Maleki H., C. Stewart, and G. Hunt, 2006. Subsidence Characteristics of Bowie Mines, Colorado, Proceedings of Golden Rocks 2006, 50 years of Rock Mechanics, Colorado School of Mines.

Reynolds, M, 2006, personal communications regarding face support specifications and observed conditions above existing room-and-pillar panels in the Wild Horse Ridge reserve.